University of Zurich[UZH]

Department of Informatics

Artificial Bivalve Burrowing

A dissertation submitted to the Faculty of Economics, Business Administration and Information Technology of the University of Zurich

for the degree of
Doctor of Science (Ph.D.)

by

Daniel Peter Germann

from Jonschwil, Switzerland

Accepted on the recommendation of

Prof. Dr. Rolf Pfeifer
Prof. Øyvind Hammer, Ph.D.
Prof. Phil Husbands, Ph.D.

2013

The Faculty of Economics, Business Administration and Information Technology of the University of Zurich herewith permits the publication of the aforementioned dissertation without expressing any opinion on the views contained therein.

Zurich, September 18, 2013

Head of the Ph.D. program in informatics: Prof. Abraham Bernstein, Ph.D.

Acknowledgements

Many thanks to Rolf Pfeifer for his support, generosity and enthusiasm. For submitting the first SNF (Swiss National Science Foundation) application of the project, their continuing supervision and valuable input, I would like to thank Peter Eggenberger Hotz and Wolfgang Schatz. There are many people who helped me by providing advice, information or critique, in person or by email: Rudolf Füchslin, Juan-Pablo Carbajal, Maik Hadorn, Michael Hautmann and his colleagues from the Palaeontological Institute and Museum of the University of Zurich, Steven M. Stanley, my colleagues from the AILab and others. I would also like to thank Øyvind Hammer and Phil Husbands for reviewing this thesis.

For their hard work, I would like to thank all Bachelor and Master students who contributed to the project: Alexander Gilgen, Katja Dietrich, Pascal Brändli, Christoph Philipp and Thomas Vasileiou. For the supervision of four of these students, I would like to thank Agathe Koller-Hodac from the Hochschule für Technik Rapperswil.

A project of this size involves a lot of administration that would be a lot more tedious without the friendly staff of the AILab and the Department of Informatics. Many thanks to Tamar Tolcachier, Sladjana Ravlija, Claudia Wirth, Claudia Leibundgut, Barbara Jost, Andreas Corti, Beat Rageth, Hanspeter Kunz and Enrico Solcà.

For their technical support I would like to thank Kurt Bösiger, Reto Maier and their team of the physics workshop of the University of Zurich; Florian Jörg, Sandro Ludolini and their team from the LinMot support; Michael Kunz, Kurt Hess, Patrick Bürke, Markus Mattli and colleagues from Hawe Hydratec AG; and Oliver Bruder from the NI support.

Many thanks to the Swiss National Science Foundation (SNF) for their financial support of this research.

Finally, I would like to thank my friends and family for their moral support and encouragement. I thank Tabitha for her patience. And also her impatience.

Abstract

In biological and palaeontological research and related disciplines, analytic methodologies predominate, although synthetic approaches such as sophisticated computer simulations are getting increasing attention. In the field of biomimetics, studying natural organisms and engineering techniques have been combined in a productive and insightful way. While the focus often lies on drawing inspiration from nature to develop creative technical solutions, there is also the other direction, the use of engineering techniques to study natural phenomena.

In this thesis, an experimental setup is described to investigate the burrowing behaviour of bivalves. Applying a synthetic approach, artificial bivalve shells were manufactured using a 3D printer and tested in an underwater sandy environment. The character of the research was exploratory and experimental, investigating different aspects of the burrowing process and testing existing hypotheses about the function of shell features.

The experiments showed that the influence of the sediment dynamics is underestimated in the literature. On the other hand, the influence of the surface sculpture was smaller than anticipated based on various studies describing their function in the burrowing process. Size and pulling force played a major role, however the increase in burrowing performance by larger forces (muscles) was quite balanced with the decrease in burrowing performance due to bigger shells. The influence of water expulsion was found to be sensitive to different situations and was not as clearly increasing burrowing performance as expected.

A main idea of the project was to suggest a synthetic approach not only to emulate the burrowing process but also the morphological evolution of bivalves. The setup may thus serve as an integrated tool to perform systematic studies of bivalve functional shell morphology and how it may have been shaped by evolutionary pressure. This is a novel approach in the field of palaeontology. We performed the first ever experiment evolving physical bivalve shell shapes.

The major drawback of the built setup was the lack of a satisfying method to control the sediment state before burrowing experiments. Technical improvements and a simple linear correction of the data alleviated this issue. Although the repeatability of the experiments was restricted due to the sediment fluctuations, significant results could be achieved.

Despite the limitations of this first setup, we believe that the presented approach has a large potential for biomimetic and palaeontological research. In particular, we see the following main advantages: (1) using artificially generated and 3D printed shapes, not only shell morphologies existing in nature but any conceivable morphology can be studied, (2) using a technical setup as opposed to observing real bivalves, the influence of single parameters can be systematically tested and the results can be quantified using different sensors, (3) the functional morphology of fossil species can be tested in action, adding an new method to palaeontological research, (4) applying artificial evolution may be a powerful tool to develop optimal burrowing morphologies and motion patterns and to study how evolutionary constraints shaped the functional morphology.

Many ideas developed or applied in this project are of general value for interdisciplinary research and especially for the application of a synthetic methodology in the field of palaeontology.

As technologies – such as 3D printers – and computational models improve, integrated systems as the one described in this thesis will open up new possibilities for testing functional morphologies, exploring morphospaces and simulating the morphological evolution of organisms.

Zusammenfassung

In Biologie, Paläontologie und verwandten Disziplinen werden für die Forschung vorwiegend analytische Methoden verwendet, auch wenn synthetische Ansätze wie komplexe Computersimulationen immer häufiger Anwendung finden. In der Bionik führt die Kombination von Technik und Biologie sowohl zu neuen biologischen Erkenntnissen als auch zu neuen technischen Anwendungen. Oft liegt der Schwerpunkt auf der Entwicklung neuartiger technischer Lösungen nach dem Vorbild der Natur, aber es ist auch sinnvoll, die andere Richtung zu betrachten, nämlich den Gebrauch von technischen Methoden, um natürliche Phänomene besser zu verstehen.

In dieser Doktorarbeit wird eine Experimentanordnung beschrieben, die verwendet wurde, um das Grabeverhalten von Muscheln zu untersuchen. Es wurde ein synthetischer Ansatz angewendet indem künstliche Muschelschalen mit einem 3D-Drucker hergestellt und in einem mit Sand und Wasser gefüllten Aquarium getestet wurden. Der Charakter dieser Arbeit war experimentell und darauf ausgerichtet, verschiedene Aspekte des Grabeprozesses zu untersuchen und bestehende Erkenntnisse über den genauen Grabevorgang und die Funktionsmorphologie von Muscheln zu testen.

Die Experimente zeigten auf, dass die dynamischen Vorgänge während des Grabens in der Fachliteratur im Vergleich zu statischen Eigenschaften wie Sandkorngrösse unterschätzt werden. Auf der anderen Seite war der Einfluss der Oberflächenstruktur der Schale kleiner als angenommen. Viele Studien legen einen positiven Einfluss der Oberflächenstruktur auf die Grabeeffizienz nahe. Schalengrösse und Zugkraft hatten wie erwartet einen grossen Effekt. Wenn berücksichtigt wird, dass grössere Muscheln auch grössere Muskeln haben und damit grössere Zugkräfte erzeugen können zeigt sich allerdings, dass sich diese Effekte praktisch die Waage halten. Der Einfluss von zwischen den Schalenhälften hinausgepresstem Wasser war situationsabhängig und erhöhte die Grabeeffizienz nicht so stark wie erwartet.

Eine Hauptidee des Projets bestand darin, den synthetischen Ansatz nicht nur auf das nachahmen des Grabeprozesses anzuwenden, sondern auch auf die Evolution der Schalenmorphologie. Die Anlage kann als ganzheitliches System dienen, um systematisch die funktionelle Schalenmorphologie zu studieren, und wie evolutionärer Druck diese geformt haben könnte. Dies entspricht einem neuartigen Ansatz in der Paläontologie. Mit der Anlage wurde das weltweit erste Experiment durchgeführt, das künstliche physische Muschelformen evolvierte.

Die grösste Beschränkung der Anlage lag darin, dass keine zufriedenstellende Methode gefunden wurde, um das Sediment vor jedem Experiment in einen einheitlichen Grundzustand zu versetzen. Mit technischen Verbesserungen der Anlage und mit einem linearen Modell zur nachträglichen Korrektur von Daten konnte diese Beschränkung zwar abgeschwächt aber nicht ganz vermieden werden. Die Wiederholbarkeit von Experimenten war daher durch die Fluktuationen im Sediment limitiert. Es konnten aber dennoch signifikante Resultate erzeugt werden.

Trotz der Mängel dieses ersten Prototyps sind wir davon überzeugt, dass der beschriebene Ansatz in bionischer und paläontologischer Forschung ein grosses Potenzial hat. Insbesondere

hat er folgende Vorteile: (1) durch das Herstellen von künstlichen 3D-gedruckten Schalen können nicht nur in der Natur vorkommende Formen, sondern auch beliebige künstliche Formen untersucht werden, (2) in einer technischen Anlage können systematisch einzelne Parameter verändert und die daraus entstehenden Effekte gemessen werden, (3) die Funktionsmorphologie von fossilen Muscheln kann zusätzlich zu bisherigen Methoden der Paläontologie "in Aktion" getestet werden, (4) die Verwendung künstlicher Evolution ist ein mächtiges Werkzeug um optimale Grabeformen zu erzeugen und den Einfluss verschiedener Randbedingungen während der Evolution der Schalenform zu studieren.

Im Rahmen dieses Projekts erarbeitete Ideen könnten auch in anderen interdisziplinären Forschungsprojekten Anwendung finden, die einen synthetischen Ansatz auf biologische oder paläontologische Fragen anwenden. Mit immer besser und billiger werdenden Technologien wie 3D-Druckern eröffnen kombinierte Anlagen wie die hier beschriebene neue Möglichkeiten, die funktionelle Morphologie von Organismen und deren Evolution zu untersuchen.

Contents

List of Figures

List of Tables

Chapter 1

Introduction

Bivalves constitute about a ninth of the known fossil record (Amler et al., 2000). Recent and fossil species exhibit a large variety of different shell morphologies (Seilacher, 1984; Stanley, 1968, 1977). The wide distribution of burrowing bivalves may be due to their increased protection within the sediment and to the occupation of new ecological niches inaccessible to other animals (Stanley, 1968).

Trueman (1966) found that most bivalves use the same kind of motion pattern to bury themselves. The shell and the foot, a tongue-like expansion of the soft body, alternate in anchoring the bivalve in the sediment, while the other part is moved forward. The shell is moved by muscle contraction in a rocking manner.

There is a large body of literature providing morphometric analyses of the bivalve shell, associations of species to different habitats, and phylogenetic investigations connecting recent and fossil species. Also, the functional morphology of the shell has been studied extensively. It is assumed that the overall shell shape, its surface sculpture, e.g. concentric or radial ridges, and the burrowing motion pattern play an important role in burrowing (Savazzi and Huazhang, 1994; Seilacher, 1984; Stanley, 1969, 1975b).

However, studies using living bivalves are difficult and thus many findings remain qualitative or speculative. Studies on the burrowing dynamics, generalizations of functional principles to non-existent morphologies or on the association of fossil species to habitats and motion patterns have been absent or limited.

In the research presented in this thesis, we therefore applied a synthetic approach to investigate bivalve burrowing. A robotic platform was built to simulate the burrowing process. A large number of different shell morphologies were manufactured and tested in terms of their burrowing performance using well established geometrical models of bivalve shells and a 3D printer. 3D printers are becoming affordable and open up new possibilities to study functional morphology. We performed the first ever artificial evolution of a physical bivalve shell shape. The simulation of not only physical processes but also evolution can be a powerful tool for studying the functional morphology of animals since it allows to investigate evolutionary pressure exerted by the environment.

The synthetic approach has been increasingly productive in fields such as biomimetics, biorobotics and artificial life (Langton, 1989; Webb, 2000). Also the emulation of evolution has proved both insightful and useful in many areas (Bäck, 1997; Fogel, 1998). Evolutionary algorithms have been used to optimize technical systems (Bentley, 1999; Rechenberg, 1973, 2000) or to evolve controllers of robots (Floreano et al., 2008). Also morphologies of artificial organisms have been evolved in software (Bongard and Pfeifer, 2003; Eggenberger Hotz, 1997, 2003; Sims, 1994) or, as manufacturing processes become faster and cheaper, hardware (Lipson and Pollack, 2000).

Most biomimetic research has two aspects: (a) to draw inspiration from nature to build better

technical artefacts and (b) to use a synthetic approach to better understand natural phenomena and organisms. Often the focus lies on the first aspect, especially in the case of artificial evolution, which is often used as a bio-inspired optimization tool. In this thesis we focus on the second aspect and suggest to expand the synthetic methodology by using evolutionary algorithms to study the evolutionary pressure on the functional morphology of organisms such as burrowing bivalves.

It is technically difficult to closely mimic living bivalves, especially their soft parts. We therefore used simple rigid shell models that were moved in a rocking manner by an external actuation system. The focus lay on comparing different shell morphologies and motion patterns among each other rather than trying to authentically mimic specific natural species. First results show, that the setup can be used to investigate questions of biological relevance.

Bivalves were chosen for these studies for several reasons. First, suitable mathematical models of bivalve shell morphology already exist. Second, the behaviour of bivalves is simple compared to other organisms. Third, the main locomotion behaviour of many bivalves is burrowing, and in contrast to other animals, they do not use a complicated system of multiple movable body parts or the secretion of mucus to burrow. Fourth, bivalves have a rich fossil record, which facilitates the reconstruction of their morphological evolution. And fifth, a large range of shells with different shapes and sculptures is easily available.

The methodology and the goals of this research are highly interdisciplinary. While the phenomenon of interest is always bivalve burrowing, both the methods and the research questions concern different fields. To develop the setup, the synthetic approach (artificial life/intelligence, engineering), a shell growth model (palaeontology) and evolutionary algorithms (artificial intelligence) were combined. The research questions stem from biology (biomechanics, functional morphology, locomotion), palaeontology (evolution of the shell morphology, habitat and behaviour of fossil bivalves), physics (dynamics of granular media, burrowing in general), biomimetics (locomoting robots) and embodied artificial intelligence (emergence of complex behaviour from agent-environment interaction).

The character of this research is exploratory and experimental. It is exploratory, because in contrast to observing living bivalves, building and testing artificial bivalves is novel. Also, because of uncertainties in the behaviour of the sediment and technical possibilities to build artificial bivalves, the best method is still unclear. It is experimental, because we suggest to use the platform to experimentally test biological and palaeontological hypotheses that cannot be investigated by analytical methods and observations of natural bivalves. Using the setup, correlations between shell morphology, sediment type, burrowing motion and burrowing performance may be quantified and thus offer evidence to test those hypotheses.

Only two other studies applying a synthetic approach to bivalve burrowing are known to the author: the work by Stanley (1975a, 1977) and by Winter et al. (2012). However, both use models that are pushed into the sediment, while we used a pulling mechanism. Moreover, we were the first to apply evolutionary algorithms to evolve physical shell morphologies. The combination of evolutionary algorithms and 3D printers is quite new (Lipson and Pollack, 2000) but will certainly become more popular in the future.

The synthetic methodology is not widely used in palaeontology yet. We believe that there is a large potential in this combination. First, building experimental platforms to test the functional morphology of fossil species generates insights that are not accessible using only analytic and observational methods. Second, expanding biomimetics from extant organisms to the whole evolutionary history opens a rich solution space that so far has not been exploited. Third, while evolutionary algorithms have proven very useful as optimization techniques, we suggest that the other direction may be just as fruitful, i.e. using synthetic evolutionary systems to investigate evolutionary pressure that shaped the functional morphology of an organism.

While other types of locomotion such as walking, flying or swimming have been intensely

studied in biomimetic research, our study adds locomotion through granular media. This is difficult terrain that has not been studied well yet. Possible applications include automatic burrowing devices for anchoring ships and platforms.

This project was structured around a set of research questions and associated hypotheses as listed below. The task of building the setup was formulated as a research question as well. The other research questions and hypotheses are essentially a summary of the correlations of bivalve shell morphology, burrowing motion, sediment and burrowing performance described in the literature that have not been tested yet using a synthetic methodology. The answers we found to the questions are discussed in chapter 3.

Research Question 1. *Can we build a scientific setup mimicking bivalve burrowing?*

Hypothesis 1.1. *Burrowing is possible* using the built setup. We can induce a rocking burrowing motion of the shell. The shell penetrates the sediment resulting in a difference between initial and final position.

Hypothesis 1.2. We can measure (quantify) the *burrowing performance*. See section 2.1.4 for possible definitions of "burrowing performance".

Hypothesis 1.3. The measured performance for a configuration (a given environment, shell morphology and motion pattern) is *reproducible*. The same configuration always leads to the same burrowing performance.

Hypothesis 1.4. We can measure *significant differences* between different configurations.

Hypothesis 1.5. The measured effects are due to *general properties* of bivalve burrowing, and not due to the particular technical characteristics of the setup.

Research Question 2. *How does shell morphology influence burrowing performance?*

Hypothesis 2.1. Shell *size* (scale) inversely correlates with burrowing performance. Smaller shells have a higher relative burrowing performance (relative to their body length) due to smaller sediment resistance.

Hypothesis 2.2. The overall shell *shape* has an effect on burrowing performance.

Hypothesis 2.3. *Surface sculpture* has an effect on burrowing performance.

Research Question 3. *How does the burrowing motion pattern influence burrowing performance?*

Hypothesis 3.1. The *Step size* and the location and direction of the *pulling cables* have an effect on burrowing performance.

Hypothesis 3.2. The *timing* of the rocking motion has an effect on burrowing performance.

Hypothesis 3.3. *Water expulsion* correlates with burrowing performance.

Research Question 4. *How does the sediment type influence burrowing performance?*

Hypothesis 4.1. The *sculpture amplitude* maximizing burrowing performance is proportional to the sediment grain size.

Research Question 5. *How did evolutionary pressure shape the functional shell morphology?*

Hypothesis 5.1. The setup can be used to evolve optimal shell morphologies, i.e. the burrowing performance (fitness) of individuals increases over time (with generation index).

Hypothesis 5.2. There are jumps in the fitness curve that can be associated with innovations in functional shell morphology.

Hypothesis 5.3. Evolved shell morphologies exhibit features associated with natural bivalves, such as a streamlined shape, a blunt anterior shell area, commarginal ridges or elongation.

This thesis is based on the published or submitted articles reprinted in chapters A–F. The publications contain descriptions of the built setup and provide the results and discussions of the performed experiments. They are chronologically ordered and reflect the development of ideas, the building and improvement of the setup, and the execution of experiments simulating the burrowing process and later also evolution. Additional methods and materials and results previously unpublished are described in chapters G and H. The contents of the remaining chapters are as follows:

Chapter 2 Here, background information is given about bivalves, their shell morphology and burrowing behaviour, and ecological niche, i.e. the sandy sediment of oceans, lakes and rivers. Also biomimetics and (artificial) evolution are described.

Chapter 3 This chapter is an overall discussion, summarizing and interpreting all results published in the articles in chapters A–F. It is partly based on the research questions and hypotheses given in the introduction.

Chapter A (published) Here, the main ideas of the project were first described and published in a palaeontological context.

Chapter B (published) This chapter presents the first complete experimental setup. The principle stayed the same until the end of the project. The main difference to later experiments was that here, position control instead of force control was used, i.e. the trajectories of the shells were fixed while the pulling forces were measured.

Chapter C (published) In this chapter, first results generated using the first setup are described. They partially already used force control, where the pulling forces were fixed and the burrowing depth was measured as burrowing performance.

Chapter D (published) This chapter summarizes the project in a general way.

Chapter E (submitted) This is a thorough discussion of the final setup. We introduce a modular approach for the shells such that only the valves have to be manufactured by the 3D printer and the central part containing a mechanism for water expulsion can be re-used. Results about the influence of shell morphology, sediment and controller type are presented.

Chapter F (submitted) In this chapter, an experiment for evolving shell morphologies is described. The used geometrical model of the shells, its parameters and the evolutionary algorithm are explained in detail.

Chapter G This chapter provides more detailed information about the setup and its components. It covers technical details, such as sediment standardization techniques, and abandoned solutions not mentioned in previous publications.

Chapter H Here, additional results are described that are not covered in the other chapters, mainly concerning the effects of the burrowing motion pattern. Two of the experiments again used an evolutionary algorithm.

Chapter 2

Background

2.1 On Bivalves

The organisms investigated throughout this thesis are bivalves (bivalvia) which are a class belonging to the mollusca. We are only concerned with burrowing species, since the phenomenon of interest is the burrowing process. In this chapter the anatomy, shell morphology, the burrowing behaviour and the (morphological) evolution of burrowing bivalves is described.

2.1.1 Anatomy

The soft body of a bivalve is protected by two calcite or aragonite valves that are connected by a hinge called ligament. The anatomy (Amler et al., 2000; Cox, 1971) of the soft parts is shown in Figure 2.1. Burrowing bivalves are often laterally symmetric and have a large tongue-like expansion, the foot, which is used for burrowing. A combination of muscles and hydraulic pressure of the haemolymph (blood) allows the foot to extend, retract, expand, shrink and probe into the sediment (Trueman, 1966). The valves are closed by two adductor muscles, their attachment location is visible as an adductor scar at the inside of the valve surfaces. The attachment location of the retractor muscles is often adjacent to that of the adductor muscles. The mantle envelopes the soft body and stretches beyond it to the shell edge. At the pallial line parallel to the shell edge, it is attached to the valves. The valves are opened passively by the ligament. Some burrowing species additionally (or only, if a ligament is missing) press water into the mantle cavity, i.e. the space between the mantle lobes, to separate the valves (Ziegler, 1983, p. 317).

Gills are situated at both sides of the foot and are supplied by fresh water through a pair of siphons, one inhaling, one exhaling. The length of the siphons usually corresponds to the burrowing depth and the size of the pallial sinus, an indentation of the pallial line that marks the space to which the siphons can be retracted in most species. Most bivalves are suspension feeders, i.e. they suck nutrients through the siphons and transport them from the gills to the mouth (Amler et al., 2000).

To reproduce, bivalves eject their sperm into the water exhaled from the siphons. After fertilization, bivalve larvae live suspended in the water as part of the plankton. From a dorsal point that is later called umbo, the shell starts to grow in commarginal growth lines similar to the growth rings of a tree. As the bivalve ages, new layers of calcium carbonate are accumulated along the ventral shell edge by cells in the mantle edge (Amler et al., 2000).

Bivalves have three pairs of ganglia, two close to both adductor muscles and one in the foot. They have senses to perceive gravity and chemical conditions like salinity and pH level. Some

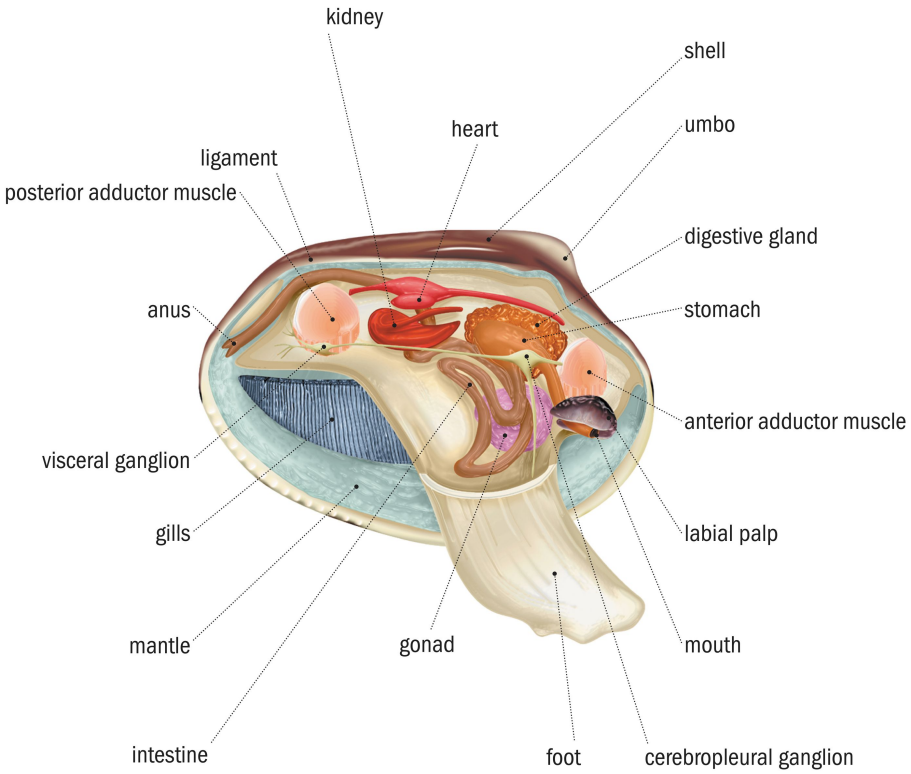

Figure 2.1: Bivalve anatomy. Most relevant for burrowing are the foot and the shell. The valves are closed by the anterior and posterior adductor muscles and passively opened by the ligament. Reproduced with the permission of QA International, www.ikonet.com from the book "The Visual Dictionary". © QA International, 2003. All rights reserved.

bivalves have primitive eyes, but usually not those burrowing into the sediment (Amler et al., 2000).

Most relevant for burrowing are the foot and the shell. Bivalve species show a large variety in shell shapes, surface structures and colour patterns. It is assumed that the shell features have a function and tend to enhance burrowing efficiency.

2.1.2 Shell Morphology

While the discipline of palaeontology has been studied for centuries, computational methods have recently changed the way (functional) morphologies are analysed (Adams et al., 2004; Bennett, 2013). Among other possibilities, the analysis using landmarks, i.e. salient features of the morphology, has been increasingly popular (Adams et al., 2004; Bookstein, 1997; Crampton, 1995; Dryden and Mardia, 1998).

Bivalve shells, like the shells of the related gastropods (snails and slugs) have a convoluted shape. One of the first attempts to mathematically model this shape was done by Raup and Michelson (1965), who also introduced the term "theoretical morphology". Since then, many different approaches have been suggested, but most of them are based on a simple growth process that produces a sequence of closed curves of increasing size that travel along a three-dimensional helicospiral (Fowler et al., 1992; Hammer and Bucher, 2005; Okamoto, 1988). Only a few parameters are needed to generate realistic virtual shell shapes. The geometrical model used in this study is described in detail in chapter F.

From the morphological parameters, a theoretical morphospace can be constructed, i.e. a multidimensional space where the dimensions correspond to the parameters and each individual shape is represented as a point. Following McGhee (1999), there are two aspects to theoretical morphology: (1) The mathematical simulation of organic morphologies using either (a) geometrical models with as few parameters as possible or (b) actual biological morphogenesis and (2) the analysis of existent and inexistent (in nature) specimens and the area they occupy in the morphospace. The mathematical growth models for shells follow the logic of 1a, models for 1b may be based on genetic regulatory networks (GRN Eggenberger Hotz, 1997). McGhee identified three phases of analysis using theoretical morphospaces (point 2 above): (a) the construction of a theoretical morphospace of hypothetical yet potentially existent morphologies, (b) the examination of the distribution of existent form in the morphospace to determine which forms are common, rare or nonexistent in nature, (c) the functional analysis of both existent and nonexistent form to determine whether the distribution of existent form is indeed of adaptive significance.

Evolution can be seen as a trajectory through a morphospace. A representation of the shell by morphological parameters is therefore well suited for evolutionary experiments, where the parameters of the functional morphology are optimized with respect to a fitness function measuring e.g. burrowing performance. Such an experiment and its results are reported in chapter F.

The surface of bivalve shells is often sculptured and features different kinds of ridges or other structures. This sculpture may be modelled together with the overall shape, e.g. by adding high frequency ripples to the aperture curve to produce radial ridges. Frequencies may be analysed using an elliptic Fourier analysis (Crampton, 1995). Another simple approach is to separate the two main spatial frequencies and to add the sculpture in a second step to the overall shape. In our study, we followed the second approach and added the sculpture using profile curves to generate radial and commarginal ridges (see chapter F). Other possibilities allowing to generate more sophisticated sculptures would be a reaction-diffusion system (Turing, 1952) following the approach by Meinhardt (2003); Meinhardt and Klingler (1987), or again a genetic regulatory network.

2.1.3 Environment

Bivalves burrow into different kinds of sediments, from mud (*Cardium*, *Mya*, Cox 1971; Ziegler 1983) over sand (*Venus*, Ziegler 1983) to coarse sand (*Donax*, *Solenids*, Ziegler 1983). The burrowing depth varies considerably between species but also between individuals (Stanley, 1970). The association of bivalve species to habitats (different sediment types) and living modes (burrowing behaviour, position within the sediment) is well documented (Alexander et al., 1993; Cox, 1971; Ziegler, 1983).

While the literature focuses on static properties of the habitats such as grain size, granular media exhibit highly complex dynamics that are not yet well understood (Du et al., 1995; Jaeger and Nagel, 1992; Li et al., 2009, 2013; Losert et al., 2000; Ren et al., 2011; Sassa et al., 2011; Umbanhowar and Goldman, 2010; Yu and Behringer, 2005). While sediment behaves similar to a fluid in a loosened state, because the grains freely move in the water, it comes close to a solid in a compacted state, because the grains lock each other. Mutual locking of grains is also called jamming (To et al., 2001). Impulses applied to parts of the sediment propagate along touching grains in so-called "force chains". The compaction of the sediment can be influenced by different factors, such as currents or suction, which can increase the hardness of the sediment by a factor of 20-50 (Sassa et al., 2011). Computer simulations of granular media are discussed in section 3.2.3.

2.1.4 Burrowing Behaviour

In addition to their hard shells, burrowing bivalves seek to protect themselves within the sediment. In particular, there are the following reasons for burrowing: protection against predators, sunlight (beach), currents; the sediment acts as buffer ameliorating thermal, salinity, pH, and other environmental extremes; minimization of desiccation (drying-out) (Sassa et al., 2011; Watters, 1993).

To reach their living position, bivalves have to locomote through the granular soil. In order to burrow themselves into the sediment, bivalves use a two-anchor system. The shell and the foot alternate in anchoring the bivalve in the sediment, while the other is pushed or pulled forward. The dynamics of this process were first described in greater detail by Trueman (1966). He identified the motion sequence described in Figure 2.2 which is called the "burrowing sequence". This motion sequence is applied by virtually all bivalves. They are also able to adapt their burrowing motion to the properties of the sediment (Sassa et al., 2011).

It has been known for several decades that bivalves use water expulsion by valve contraction to liquefy the surrounding sediment (Trueman, 1966). Winter et al. (2012) documented in more detail how *Ensis directus* employs this localized fluidization to reduce energy consumption needed for burrowing. It even reduces the energy for burrowing from a quadratic to a linear function of burrowing depth. The timing has to be such that the shell moves down deeper into the sediment before the liquefied sediment can collapse by a landslide.

In nature, burrowing depths of a few up to a few dozen centimetres are common, corresponding to partial burial or a burrowing depth of up to around 3 body lengths. Values for deep burial mentioned in the literature range from 30 to 70 cm (Amler et al., 2000; Cox, 1971; Holland and Dean, 1977; Ziegler, 1983). In extreme cases over one metre may be possible (McMillin, 1924). The maximal retractor pulling force lies around 10 N for *Ensis* (Trueman, 1967), the water expulsion pressure at 0.1 bar (Trueman, 1967, p. 459). The expulsion duration of the water ejection can be up to several seconds (*Mya*, Checa and Cadée 1997). 3–20 burrowing steps are usually performed (Stanley, 1970; Trueman, 1967; Ziegler, 1983). Burrowing times may differ greatly, common values are between a few seconds and 1–2 min, with increasing pauses between burrowing steps (McLachlan et al., 1995; Sassa et al., 2011; Ziegler, 1983); but in some cases, burrowing may take up to 105 min (*Ruditapes philippinarum*, Sassa et al. 2011, p. 4). The step size for *Ensis directus* is

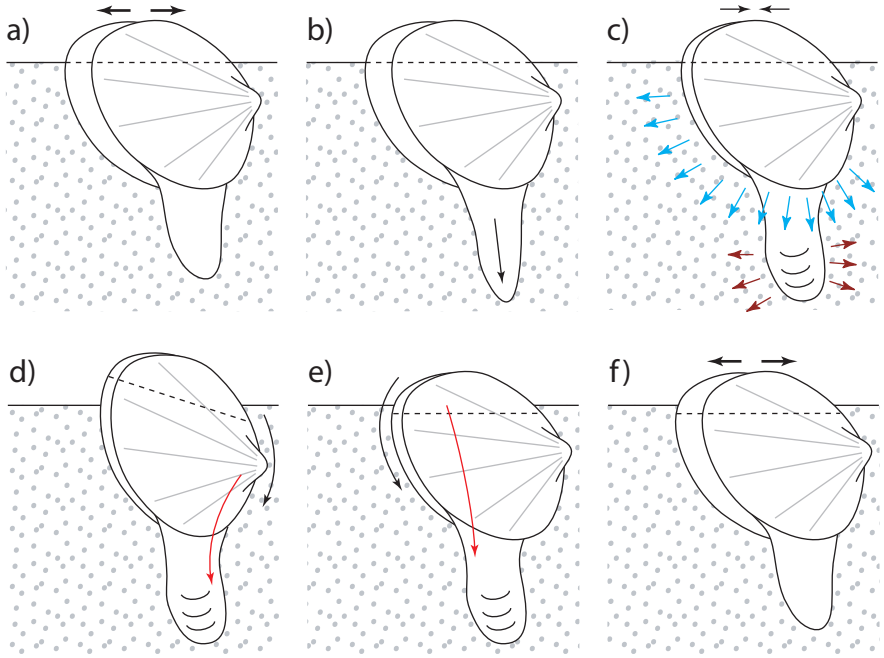

Figure 2.2: The *burrowing sequence* for bivalves as described by Trueman (1966). (a) The clam is in erect position, partially burrowed in the sediment. The valves are open to anchor the shell, i.e. to prevent back-slippage. (b) The foot probes deeper into the sediment. (c) The adductor muscles contract, partially closing the shell. The water expelled from the cavity liquefies the surrounding sediment to reduce the resistance to penetration. From the soft body inside the shell, blood is pressed into the foot, which is inflated and serves as a new anchor. (d) The anterior retractor muscle (red arrow) pulls the front side of the bivalve towards the foot, leading to a rotation of the shell (black arrow). (e) In the same way, the posterior retractor muscle rotates the shell back into the erect position. (f) The two rotations around different rotation axes led to a net downward translation, as illustrated by the dashed line. The valves open again to allow for another burrowing cycle starting at (a). Reprinted from Koller-Hodac et al. (2010), ©2010 IEEE.

1 cm (Trueman, 1967). The body density ranges from $1.04\ \mathrm{g/cm^3}$ to $2.10\ \mathrm{g/cm^3}$ (McLachlan et al., 1995, p. 147).

There is an extensive literature on how bivalve morphology, burrowing motion and sediment type correlate (Stanley, 1975b). Stanley found that ridges at a right angle to the burrowing direction are advantageous and used with rocking motions covering a small angle, while v-shaped ridges are also possible, leading to larger rotation angles (Stanley, 1969). He also found that: knobs help burrowing, but only in fine sand; ridges help more in fine than in coarse sand, a prosogyrous overall shape helps burrowing (more than sculpture); both anterior and lateral ridges help burrowing (Stanley, 1977). Savazzi and Huazhang (1994) summarized that the sculpture amplitude increases with sediment grain size, that the profile of the sculpture should be asymmetric and the gentle slope should be facing the burrowing direction. Other adaptations include becoming more streamlined and elongated (Seilacher, 1984; Watters, 1993), reducing back-slippage and forward friction using terrace-shaped commarginal ridges (Savazzi and Huazhang, 1994; Seilacher, 1984), by using discordant ridges (Stanley, 1969), by adjusting the sculpture to the sediment type (Alexander et al., 1993; de la Huz et al., 2002; Nel et al., 2001).

There are several possibilities to measure the burrowing performance of bivalves. Values that are commonly measured and known for many species include the burrowing depth and the burrowing time. From these two, an average burrowing speed may be computed. Since during the burrowing process, the size of the burrowing steps tends to decrease and the pause until another step is executed tends to increase, burrowing speed may also be measured by fitting a saturating function, e.g. $\tanh$ to the burrowing curve.

A popular parameter to measure burrowing performance was introduced by Stanley (1970). It is called burrowing rate index B.R.I. and defined as:

$$\mathtt{BRI} = \frac{\sqrt[3]{\mathtt{mass\ [g]}}}{\mathtt{burrowing\ time\ [s]}} \times 100.$$

Stanley (1970) found that there is a linear relationship between the length and the burrowing time of *Donax denticulatus*. He then generalized from length to the third root of mass. The B.R.I. is approximately constant throughout the size range of a species (Stanley, 1970) and is therefore characteristic for it. Stanley called bivalves with a B.R.I. ≤ 0.09 "very slow", those with a B.R.I. between 0.6 and 1 "moderately rapid" and those with a B.R.I. ≥ 6 "very rapid". Rapid burrowers such as *Donax* (Sassa et al., 2011), living on beaches reach B.R.I.s between 2 and 17 (McLachlan et al., 1995).

One may also want to measure how much energy is needed for burrowing. For *Ensis directus*, Winter et al. (2012) estimated, based on Trueman (1967), an energy consumption of 0.21 J/cm.

2.1.5 Evolution

Bivalves constitute about a ninth of the known fossil record (Amler et al., 2000). While bivalves had been around since the Ordovician, their major radiation happened during the Mesozoic and Cenozoic Eras, probably due to mantle fusion and siphon formation and thus the ability to occupy habitats deeper within the sediment (Stanley, 1968, 1975b).

Seilacher (1984) identified several ways in which evolution is restricted and coined the field of constructional morphology. He also analysed the repeated transitions of bivalve species from hard to soft substrates and back. Bivalves originated in invertebrates that lived on hard substrate. They moved to soft substrate as "primary soft-bottom dwellers". Some species returned to the hard substrate and eventually went back to the soft substrate ("secondary soft-bottom dwellers"). The variation of the latter ones is much higher. The transition from hard to soft substrate resulted in fast and drastic morphological changes. In burrowing bivalves evolutionary within-habitat

trends in shell morphology were limited to minor modifications that improved the burrowing function.

Since extinct taxa cannot be observed any more, function has to be derived from their structure, i.e. morphological features. There are two methods to do this (Thomason, 1997). The phylogenetic method infers function by identifying homologous features of extant and extinct taxa and then analysing them by studying the living specimens (Stanley, 1970). However, the function is not dependent on a structure based on its homology to other taxa, but rather because of the mechanical properties of the structure itself. The second method to infer function from structure is called the paradigm method (Rudwick, 1964). A paradigm structure is a structure predicted from an abstract mechanical model developed based on the hypothesized function of the structure. After developing and comparing different paradigm structures, the function is inferred that belongs to the paradigm structure that best matches the found fossil structure. Rudwick commented this with the words

> "Consequently the range of our functional inferences about fossils is limited not by the range of adaptations that happen to be possessed by organisms at present alive, but by the range of our understanding of the problems of engineering." (Rudwick, 1964, p. 33)

In his seminal work in the field of functional morphology, Arnold (1983) established the view that the mapping from morphology to fitness should be divided into a mapping from morphology to performance (e.g. at a particular task) and a mapping from performance to fitness. Ideally, fitness should be defined as the number of offspring surviving to an age corresponding to that of the parents (Arnold, 1983, p. 355-356). In our work, we only consider the functional morphology of bivalves for burrowing in soft substrates. We do not consider non-burrowing bivalve species, nor physical or behavioural characteristics not related to burrowing. In nature, the fitness of bivalves does obviously not only depend on burrowing performance, but also on other factors such as metabolism, environmental influences, reproduction, interaction with other species etc. In the context of this thesis, we use the terms fitness, (burrowing) performance and (burrowing) efficiency as synonyms.

2.2 On Biomimetics

The idea of biomimetics, i.e. the emulation of living systems using machines, is very old. However, the methodology connected to it, the synthetic approach or "understanding by building" has not been widely adopted in biology-related fields until in recent decades, enabled by computers and improved manufacturing methods. It is now widely used in fields such as artificial life (Langton, 1989, 1995), artificial intelligence (Pfeifer and Scheier, 2001) and biorobotics (Webb, 2000). In artificial intelligence, the embodiment turn has led researchers to recognize that to fully understand intelligent or complex behaviour, robots have to be built (Pfeifer et al., 2007a,b). The keyword "embodiment" refers to the idea that in order to understand behaviour, not only the controller, but also the whole body morphology and its interaction with the environment have to be examined. The real world exhibits some properties like nonlinearities, noise and time pressure that are hard to simulate, therefore it is important to always verify software simulations and build real robots.

2.2.1 Biomimetics

Biology itself is largely perceived as an analytic discipline. Scientists investigate natural systems like animals or plants by observation, measurement and analysis. In biomimetics, inspiration

from biology is used for designing surprisingly simple or efficient solutions for engineering or architectural problems, i.e. the focus often lies on drawing inspiration from nature for building better technical devices. However, there is also research stressing the other direction, i.e. using a synthetic approach to better understand natural phenomena.

Usually, biomimetics is concerned with recent nature, i.e. organisms living today. However, it is at least conceivable to expand biomimetics to the whole evolutionary history. This would open a much larger "solution space". But of course, it is more difficult to analyse the functional morphology of extinct species (see section 2.2.3). One instance of such a project is "Pterodrone", where robots inspired by Pterodactyls (flying dinosaurs) were built (Chatterjee et al., 2010). On the other hand, the application of a synthetic approach in palaeontology is not common though it may have increased recently.

Pfeifer and Scheier (2001) described the three constituents principle for robots. It states that to design a robot, three constituents need to be considered: (1) the ecological niche, (2) the desired behaviours and tasks and (3) the design of the robot itself. In this research, these are all well identified as: (1) sandy sediment, (2) burrowing and (3) bivalve morphology. A similar conception is described by Webb (2000). While we first focused on point 3, because it was considered the most complex and difficult part, finally we had more results on the difficulty to control the sediment to be able to perform reproducible results than on the functional morphology of bivalves.

2.2.2 Locomotion

Probably the main characteristic that separates animals from other living systems is their ability to move. The variety of strategies to locomote is as high as the variety of different habitats on the planet (Dickinson, 2000).

Appreciating the importance of locomotion behaviour, there are many biomimetic projects mimicking different locomotion mechanisms of different animals. From biped, quadruped and hexapod walking (Anderson et al., 2005; Brooks, 1989; Clark et al., 2001; Floyd et al., 2006; Kevin C. Galloway et al., 2010; Niiyama et al., 2007; Zhou and Bi, 2012) over climbing (Clark et al., 2007; Jusufi et al., 2008; Saunders et al., 2006; Tin Lun Lam and Yangsheng Xu, 2011; Trimmer et al., 2006) and flying (Peterson et al., 2011; Wood, 2007) to swimming (Chu et al., 2012; Ziegler et al., 2006) and locomoting soft robots (Lin et al., 2011; Shepherd et al., 2011; Yuk et al., 2011).

Granular media (see section 2.1.3) are another type of habitat and pose special difficulties because of their high frictional resistance and complex dynamics (Bekker, 1960; Nedderman, 1992). Both walking on and (undulatory) locomotion through dry or underwater granular soils has recently been investigated Ding et al. (2012); Gravish et al. (2013); Jung (2010); Li et al. (2009, 2013); Maladen et al. (2011); Mazouchova et al. (2013).

Two examples of bivalve burrowing robots are known to the author. Stanley (1975b) performed experiments based on a machine which was manually actuated using rods and weights. He produced a cast of a specimen of *Mercenaria mercenaria* that had a blunt anterior area and tested it in real sediment. By comparing the burrowing performance to a second model where he had altered the shape to display a sharper front edge, he could explain the advantage of the blunt anterior region of this particular species. He later used the same method to investigate *Trigonia* (Stanley, 1977).

More recently, a bivalve burrowing robot called RoboClam was built at MIT (Jung et al., 2011; Winter et al., 2010, 2012). The robot was inspired by the elongated and fast burrowing bivalve family *Ensis*. Pneumatically actuated, it could laterally move its valves and was pushed from above into the sediment.

2.2.3 Artificial Evolution

Not only the emulation of the mechanics of natural organisms but also of their evolution has proved both insightful and useful in many areas (Bäck, 1997; Fogel, 2000, 1998). Evolutionary algorithms have been used to optimize technical systems (Rechenberg, 1973, 2000) or other designs (Bentley, 1999).

Despite the power of evolution to generate creative solutions (Bentley, 1999), the use of artificial evolution in robotics is not straightforward (Webb, 2000). Often it is used to evolve controllers of fixed robots (Floreano et al., 2008; Husbands, 1998; Nolfi and Floreano, 2000). Also morphologies of artificial organisms have been evolved in software (Eggenberger Hotz, 1997, 2003; Sims, 1994) or, as manufacturing processes became faster and cheaper, hardware (Lipson and Pollack, 2000). However, it is agreed that more integrated and natural approaches have a large potential, such as the co-evolution of morphology and control (Bongard, 2010; Pfeifer and Scheier, 2001; Pfeifer et al., 2007b) or morphological changes during evolution or development (Bongard, 2011).

2.3 Outlook

In this study, we applied a synthetic approach to investigate bivalve burrowing and the morphological evolution of bivalve shells. The setup developed and built to do the experiments is described in chapters A–G, the results are described in chapters B–H. The next chapter provides an overall discussion of the research questions in the introduction based on the results in the mentioned chapters.

Chapter 3

Discussion

The goal of this study was to investigate the phenomenon of interest, the burrowing behaviour of bivalves, using a synthetic approach. The functional morphology of the shell, the burrowing pattern and their evolution were studied in an artificial setup.

The setup did work insofar as different burrowing depths could be measured for different configurations. It did also produce unexpected results that raised new questions. On the other hand, it was often difficult to separate the influence of the sediment state from the influence of the morphology or burrowing pattern.

The setup was built to mimic bivalve burrowing. However, while some parameters matched the natural equivalents, other properties of the setup differed considerably (see numbers in section 2.1.4).

Parameters matching the natural equivalents were step size, step duration and overall burrowing time. The shell and grain sizes were within the range of natural figures though above average. This was due to technical reasons such as printer resolution. The sand used in the setup was well rounded, similar to that of natural habitats. However, environmental influences like other objects in the sediment or currents were absent in our setup. The mass and density distribution of the whole bivalve and our counterpart differed considerably. While the density of the printed ABS shells was slightly lower than that of water, the density of the central stainless steel disc was about eight times that of water. In natural bivalves, the body density is around that of water, while the shell density is between 2.5 and 3 times that of water. The attachment locations of the cables were outside the ventral edge, while in natural bivalves, the retractor muscles are attached between the valves, close to the valve adductors. The largest discrepancy was probably between the natural and emulated pulling forces. While the retractor muscles of bivalves apply forces around 10 N (Trueman, 1967), the motors in our setup applied forces up to around 200 N.

Due to the differences between natural bivalves and our setup, we could not directly compare the measured values to real bivalves. We did therefore always compare different configurations tested with our setup to one another. Rather than making statements about particular bivalve species, general conclusions about bivalve-like burrowing may be made.

The simulation of natural phenomena can usually be done in two ways: using a physical setup or a computer simulation. It had always been clear that a physical setup had to be built to realistically simulate bivalve burrowing. The reason was not only that a real setup does automatically provide the full complex physics of granular media, but also that one of the goals of the project was to explore the effects of the details of the burrowing process in the first place. In order to implement a computer simulation, the relevant dynamics would have had to be known in advance. As a complement to the setup, however, a computer simulation would have been useful; but difficulties connected to computer simulations of granular media as described in section 3.2.3 led to the decision to abandon the efforts to implement one.

3.1 Artificial Bivalve Burrowing

This section contains a discussion of the research questions and hypotheses introduced in the introduction. For this purpose, results from chapters H and A–F are summarized.

Research Question 1. *Can we build a scientific setup mimicking bivalve burrowing?*

> **Hypothesis 1.1.** *Burrowing is possible* using the built setup. We can induce a rocking burrowing motion of the shell. The shell penetrates the sediment resulting in a difference between initial and final position.

This goal was achieved using the built setup. Several hundred burrowing experiments were performed. Despite the large pulling forces of up to $200\ \mathrm{N}$, the larger shells (ca. $10\ \mathrm{cm}$) could only be buried partly. Smaller shells reached a depth (distance sediment surface to bottom-most shell part) between one and two times their own size. Depending on the lag parameter, the shells did all exhibit a rocking burrowing motion.

> **Hypothesis 1.2.** We can measure (quantify) the *burrowing performance*. See section 2.1.4 for possible definitions of "burrowing performance".

The internal position sensors of the linear motors measured the slider position very precisely ($\ll 1\ \mathrm{mm}$). This indirect measurement of the burrowing depth was used in most experiments as burrowing performance. Due to the deformation of the setup structure and the cables, the true burrowing depth deviated from this measurement by about 6% (section H.1).

It is not obvious how to compute the energy consumed by the setup for burrowing, especially when considering water expulsion. When computing mechanical energy from the measured forces and displacement, we found a value about 4–8 times larger than in natural bivalves (section H.1).

The burrowing rate index B.R.I. (section 2.1.4) for the shells used in our experiments was around 14-24, since most valves had a mass between $82\ \mathrm{g}$ (B-smooth, cf. chapter E) and $161\ \mathrm{g}$ (BB-radial2) and one burrowing run usually took 25–$30\ \mathrm{s}$. According to the ranking by Stanley (1970), the shells we used would therefore be qualified as "very rapid". But of course there is no biological meaning in this comparison, because the density of our shells was higher than that of natural bivalves and the burrowing time was artificially fixed.

Because the control program used a fixed time schedule of successive burrowing steps (see figure G.6), and thus the burrowing time was a constant given parameter, we did not use any burrowing performance measure related to burrowing time, such as speed.

> **Hypothesis 1.3.** The measured performance for a configuration (a given environment, shell morphology and motion pattern) is *reproducible*. The same configuration always leads to the same burrowing performance.

This hypothesis could only be partially fulfilled by the setup. While the motor controllers, the static parts of the setup and the shell models could be kept constant for a series of experiments, it was difficult to standardize the state of the sediment. By technical improvements, e.g. using steel cables instead of fishing lines for pulling the shells, events like string bursts and the following disturbance of the sediment to replace the strings could be avoided. However, there was usually a gradual compaction through a series of experiments that could not be avoided. In some evaluations, we therefore used a linear model of the drift to correct the burrowing depths. Experiments that were repeated after some time, e.g. several days and several experiment series later, did not exactly match the results of the first instance due to the incessant change of the sediment state. The difference was in the order of magnitude of the differences that also the shell morphology or

motion pattern induced. However, within one experiment series and using the linear correction we could measure consistent burrowing depths.

Hypothesis 1.4. We can measure *significant differences* between different configurations.

Within one burrowing series, most of the differences between configurations were highly significant (according to the computed p-values). However, also events in the sediment led to significant changes of burrowing performance from one burrowing run to the next. Therefore, extra care had to be taken to attribute significant differences to the correct cause: a difference in the shell morphology or motion pattern (according to the purpose of the experiment) or a difference in the sediment state.

Hypothesis 1.5. The measured effects are due to *general properties* of bivalve burrowing, and not due to the particular technical characteristics of the setup.

We tested for wall effects in the sediment and characteristics of the controllers in experiments reported in chapter E. No artefact caused by these two effects could be found. A difference in burrowing performance caused by the friction between the cables and the sand was found in the experiments with varying attachment location, see below. We did not test for further artefacts.

Research Question 2. *How does shell morphology influence burrowing performance?*

This question was tackled by generating, printing and testing different shell morphologies. Using the 3D printer, about 30 shells were printed (with additional 60 shells for the morphological evolution experiment). The shapes were then compared to each other using a constant burrowing pattern.

Hypothesis 2.1. Shell *size* (scale) inversely correlates with burrowing performance. For the same shell size, pulling force correlates with burrowing performance.

In our experiments, smaller shells consistently reached larger burrowing depths than bigger shells and in the results shown in section H.3.2, the burrowing performance linearly increased with pulling force. The basic relations formulated in the hypothesis were therefore supported by the experiments.

More interesting is the question how shell size and pulling force relate to each other. Since it can be assumed that in natural bivalves, muscle size and strength increase together with shell size, one may ask if additional size increases burrowing performance due to increased force or if it decreases burrowing performance due to increased resistance. In chapter E we investigated this trade-off and found that bigger shells tended to reach larger absolute depths while smaller shells tended to reach larger depths relative to their body length.

Hypothesis 2.2. The overall shell *shape* has an effect on burrowing performance.

In chapter E we described the results of a comparison between different shapes of the same volume. While the bivalve shape was clearly better at reaching larger absolute depths than a sphere, disc or wedge, the result was reversed when considering relative depth. The evolutionary experiment reported in chapter F showed clearly that there were differences between different overall shell shapes.

Hypothesis 2.3. *Surface sculpture* has an effect on burrowing performance.

There are many results in the literature suggesting that different kinds of surface sculpture increase burrowing performance. However, in our setup, sculptured shells tended to decrease burrowing performance, see chapters C, E and F.

Research Question 3. *How does the burrowing motion pattern influence burrowing performance?*

This question was investigated by testing the same shell in experiments of varying burrowing motion patterns. The pattern was changed by setting the parameters of the control program, by using different locations to attach the cables to the shells and by switching on and off the water expulsion mechanism.

> **Hypothesis 3.1.** The *Step size* and the location and direction of the *pulling cables* have an effect on burrowing performance.

Larger step sizes tended to increase burrowing performance (sections H.3.4 and H.4.1). It was found that distant attachment locations and uncrossed cables increased burrowing performance (sections H.3.3 and H.4.1). However, in both cases – crossed strings vs. uncrossed strings and moving the attachment arms – the configuration with cables moving more vertically through the sand performed better. A measurement of the different friction of the cables in the sand showed that the difference between cables pulled vertically and cables pulled at an angle to the bottom plate was comparable to the earlier findings. This suggests that the difference in burrowing performance was due to these friction properties and not to different attachment locations. Thus our results do not support the hypothesis that the attachment location plays an important role.

> **Hypothesis 3.2.** The *timing* of the rocking motion has an effect on burrowing performance.

According to the results in section H.3.5, a time lag between the motors does not have a positive effect on burrowing performance. However, the results were not entirely consistent and should be repeated. That a small lag may be beneficial was also supported by the evolutionary experiment 1 (section H.4.1), where the lag decayed to 0 over the generations. If this result is confirmed, it would mean that synchronously pulling with both retractor muscles and thus doubling the pulling force compared to one retractor muscle is better than adding a lag to create a rocking motion. Since many bivalves do use a rocking motion, more experiments should be performed to resolve this issue. In particular, the rocking motion should be tested in combination with different surface sculptures and sediment types.

> **Hypothesis 3.3.** *Water expulsion* correlates with burrowing performance.

We did not find any clear relationship between water expulsion duration and burrowing performance. An analysis of many different experiments that involved tests with and without water expulsion showed no difference (chapter E). On the other hand, the evolutionary experiment reported in section H.4.1 resulted in an almost uninterrupted water expulsion, suggesting this was the most relevant parameter to optimize burrowing performance. Water expulsion also had the highest correlation with the fitness (burrowing depth). Of course, a constant water expulsion would not be possible in natural bivalves, because water has to first re-enter the mantle cavity, before it can be expelled again.

A possible explanation for the inconsistent results may be that water expulsion interacted with the memory effect in the sediment, increasing the fluctuations. Also, in our setup, we could only simulate a part of the water expulsion effect. Natural bivalves expel water by contracting the valves. This does not only move water from the mantle cavity into the surrounding sediment but also makes room for loosened sediment because the valves recede from their widened anchoring position. The water expulsion mechanism in our setup only ejected water into the surrounding sediment without reducing the volume occupied by the shell, and did thus only capture a partial effect.

Research Question 4. *How does the sediment type influence burrowing performance?*

Hypothesis 4.1. The *sculpture amplitude* maximizing burrowing performance is proportional to the sediment grain size.

We did not test different types of sand for practical reasons. It was a large effort to exchange the sediment and the water in the setup. Also, we were concerned that smaller grains might damage the setup, e.g. by entering the holes of the water expulsion channels.

Research Question 5. *How did evolutionary pressure shape the functional shell morphology?*

One of the main goals of the study was to perform evolutionary experiments. The built setup was developed not only as a device to simulate bivalve burrowing but also as an integrated system to analyse the evolution of the functional shell morphology and the burrowing motion pattern of bivalves. Three larger evolutionary experiments were performed, two optimizing the motion pattern (evolutionary experiment 1 and 2, section H.4) and one optimizing the shell morphology (chapter F). For all experiments, an evolution strategy was used (Schwefel, 1995) and the mutation rate was adapted by inheriting it along with the morphological or motion parameters.

Hypothesis 5.1. The setup can be used to evolve optimal shell morphologies, i.e. the burrowing performance (fitness) of individuals increases over time (with generation index).

Performing evolutionary experiments technically worked. However, due to the insufficient control of the sediment state, it was not always possible to consistently increase the fitness over generations. The increasing compactness of the sediment counteracted the effect of optimizing the shell morphology or burrowing pattern. To a certain extent, the drift in the sediment may be corrected, as described in chapter F. However, an unambiguous correction vector would require an impracticably high number of repetitions that would further increase the time necessary to perform the experiments.

In evolutionary experiment 1 (section H.4.1), the parameter ranges were covered to a reasonable degree and the mutation rate increased and then decreased, showing the desirable pattern of an adaptive mutation rate in an evolutionary experiment. On the other hand, in the morphological evolution experiment (chapter F), the mutation rate decreased from the beginning and most parameters stayed almost constant. This was due to a suboptimal mapping of genomes to shell morphologies which involved a large portion of invalid shells.

Hypothesis 5.2. There are jumps in the fitness curve that can be associated with innovations in functional shell morphology.

In the performed experiments, there were no marked jumps that could be associated to particular morphological features. The most prominent jumps of burrowing depth were generally always due to events in the sediment.

Hypothesis 5.3. Evolved shell morphologies exhibit features associated with natural bivalves, such as a streamlined shape, a blunt anterior shell area, commarginal ridges or elongation.

Many of the resulting morphological features and parameters of the motion pattern were surprising and did not correspond to the natural case. However, it is precisely the purpose of the setup to identify these discrepancies and to improve the system accordingly. Each discrepancy potentially sheds light on a particular aspect of bivalve burrowing. In our research we did the first generation of evolutionary experiment. Following this iterative approach of performing experiments, comparing the results to the natural case and improving the setup may be very productive and should be continued.

In the morphological evolution, shells emerged with a short vertical dimension such that they

did only occupy the top sediment layers, where the resistance to penetration was smaller. We did not anticipate this, although with hindsight, the result can be easily explained. Considering the result, we may suspect that animals that want to overcome the resistance of the sediment that increases fast with burrowing depth, have to develop a method to loosen it e.g. using repeated volume expansion and reduction, which was missing in our setup.

Another interesting result was that in evolution 1 (section H.4.1), the burrowing cycles became shorter, i.e. the burrowing became faster over the generations. This is surprising because the fitness function did not reward fast burrowing at all, but only a large burrowing depth. By increasing the relative duration of the water expulsion, the speed indirectly grew. This kind of non-obvious evolutionary pressure may also be present in natural bivalves. Winter et al. (2012) mentioned that *Ensis directus* moves deeper into the sediment before the area of the fluidized sediment collapses, i.e. timing is important to take advantage of the fluidization. It may therefore be that burrowing speed is driven more by a fast collapse of the fluidization than by predators.

Evolution 2 (section H.4.2) did not produce significant correlations of parameters and fitness or burrowing depth. One reason may be the small number of generations, which was only 10. We stopped the experiment at that point because of practical reasons. Because the number of steps was very large, usually between 40 and 60, the experiments took a long time. Another reason for the insignificant results may have been the fitness function. In this experiment it was not designed to measure burrowing depth but burrowing efficiency defined as the ratio of burrowing depth and consumed energy. It is certainly reasonable to include consumed energy in the fitness function. However, it is more difficult to compute energy. For this experiment it was computed by integrating force along the travelled path through the sediment. The contribution of depth to energy was found to dominate the fitness, such that larger depths were not rewarded.

The interpretation of the results of the evolutionary experiments is difficult because of the small number of generations and the small population sizes. After a revision of the setup, the experiments should be repeated to see if all of them lead to the same final optimal morphology or burrowing motion.

3.2 Limitations

Our setup was the first one to combine models of bivalve shells with an external actuation mechanism based on pulling cables. Because of the exploratory nature of the setup and the experiments, there are a number of drawbacks that need to be improved in future research.

3.2.1 Discrepancy between the setup and natural bivalves

Differences between parameters of the setup and of natural bivalves have already been described above. While certain elements of the setup like the 3D-printed shell shapes or the induced rocking motion corresponded well to natural bivalves, other elements were entirely missing. The setup contained shell models consisting of a rigid one-piece object, while bivalves move their valves and use their soft foot for burrowing. The setup was restricted to mimic the shell morphology, the rocking motion and water ejected into the sediment without an associated valve adduction.

The burrowing performance measure we usually used to compare bivalves was burrowing depth. However, it is not entirely clear if there actually is a pressure on natural bivalves to dig as deep as possible (see also chapter E). It may be that other criteria such as burrowing speed, or counteracting buoyancy or currents is more important. It would actually be possible to use our setup to investigate this question by testing different fitness functions and comparing the resulting optimized morphologies to natural bivalves.

3.2.2 Threats to validity

The largest effect endangering the validity of the results was the memory effect in the sediment. We were not able to implement a satisfying standardization technique to control the sediment before experiments. See chapters E and F for a more detailed description of this issue.

We tested for artefacts introduced to the burrowing process by the setup. These artefacts would measure properties of the particular setup instead of general properties of bivalve-like burrowing. Wall effects of the sediment compartment were discussed in chapter E, different controller policies in section G.2 and chapter E and angle dependent friction of the cables in section 3.1.

Due to the large amount of resources needed to perform evolutionary experiments, we stopped after 10-20 generations. To get reliable results, a larger number of generations should be performed, and the experiments should be repeated using different initial populations. For comparison, in the examples of evolutionary experiments in hardware mentioned by Rechenberg (2000), between 27 and 2400 generations were generated, with several hundred being a typical value. In our case, this would only be practicable if the whole burrowing experiment could be automated, including sediment standardization, retrieval of the shell from the sediment and maintaining a standardized initial position and orientation.

3.2.3 Computer Simulations of Granular Media

When applying a synthetic approach, it is considered good practice to investigate a phenomenon of interest both by computer simulations and physical experiments. The advantages of each approach can thus be combined. Computer simulations need less resources, are safe, and fast. Especially when performing artificial evolution, it is desirable to do as much of it as possible in software, since only a fast process allows large population sizes and a high number of generations. A disadvantage of computer simulations is that they may miss essential properties of the physical world, because every element of the simulation has to be explicitly programmed. Physical experiments, on the other hand, provide complex real dynamics for free and are in this sense more realistic. But they usually need much more resources and can often only be partially automated, resulting in a high personal and temporal effort.

Since we had planned to perform evolutionary experiments from the beginning, we started to experiment with software simulations of the bivalve burrowing process. We planned to profit from the parallel development of a computer simulation and a physical setup. The setup should be used to calibrate and to verify the results of the simulation. The simulation could have been used as a fast replacement for real experiments, allowing for extensive evolutionary experiments in software. On the other hand, simulations could have served as exploratory studies to find interesting effects that then could be tested using the physical setup. However, due to the reasons below, we finally did not implement and use a computer simulation of bivalve burrowing.

Approaches to develop simulations of a phenomenon of interest may be divided in two categories: top-down and bottom-up. The top-down approach is often used in physics. The first simulation is made as simple and abstract as possible and should capture the most important effect. If its predictions are supported by the evidence, it is successively refined to capture more details of the process. In a bottom-up approach, a simulation is started at the finest granularity and more complex behaviour is composed from these components. This approach may be more popular in biology.

As described in section 2.1.3, granular media exhibit complex dynamics. Since the purpose of the study was to investigate details of the interaction of shell morphology, such as surface ridges, with sediment grains and water, we decided to follow a bottom-up approach. There is a large number of software packages able to simulate rigid bodies or fluids. However, none of

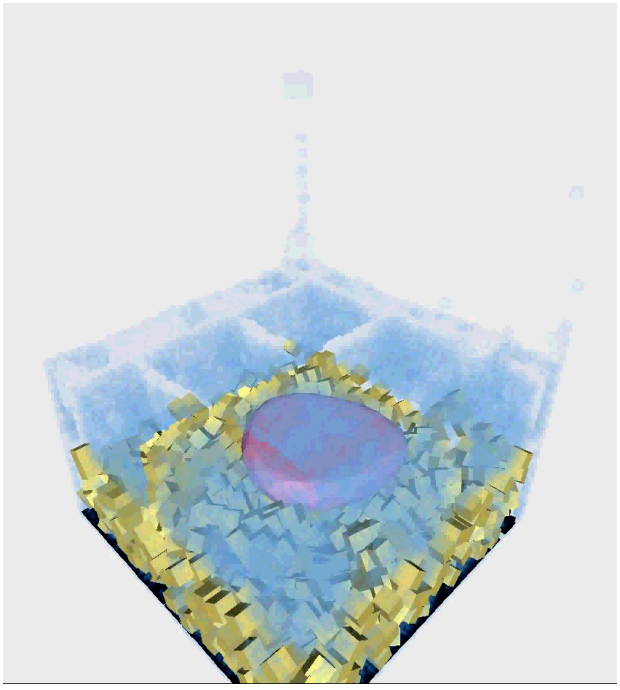

Figure 3.1: Simulation screenshot.

them naturally supports granular materials with their particular dynamics (e.g. as proposed by Herrmann, 1992; Oliveira and Stewart, 2012). Sand has to be simulated using particles or a large number of rigid bodies. We decided to test the PhysX SDK, because it is hardware accelerated and therefore potentially allows a larger number of particles (Nvidia Corporation, 2010). We implemented a simulation using simple rigid bodies such as spheres or cubes to represent sand grains and a fluid to represent water, see Figure 3.1. The water tank was implemented using half-spaces. The simulation worked for large sand grains. However, when reducing the size of the grains to get more realistic results, the simulation was not numerically stable any more. Within the limits of the project it was not possible to further pursue the implementation of a computer simulation of the bivalve burrowing process. The focus was laid on developing the experimental setup.

3.3 Future Work

Since this study was exploratory and experimental, it may be continued in many directions. The setup may be technically improved to make experiments faster, more automated, more reliable and better documented with richer sensory data. The generation of shell morphology could be improved by employing more sophisticated models or even ontogenetic simulations that are able to create, e.g., skew ridges. More (evolutionary) experiments may be performed, e.g. to test ambiguous results of this study, to reproduce findings in the literature generated by analytic methods, or to evolve optimal burrowing morphologies for different fitness functions.

3.3.1 Setup improvements

Future research using a similar setup as the one described here should try to avoid the limitations described in section 3.2.

Several methods to standardize the sediment state before each burrowing run were tested (section G.3.1). Since none of them led to satisfactory results, we suggest as an alternative method an automated procedure consisting of two stages: (a) loosening of the sediment: pump high pressure water into the sediment, e.g. through a lattice in the bottom plate, and (b) compacting the sediment: vibrate the whole sediment compartment laterally modulating the frequency from low to high. Step (a) is necessary to resolve any residual structure from previous interactions, e.g. jammed regions, within the sediment. Using a rake to do this as described in section G.3.1 did non cover the whole sediment compartment and therefore just replaced one structure by another. If a more compacted initial state is desired, as it most probably occurs in natural settings, step (b) should be applied with frequency, amplitude and duration adapted to produce the best results. This should again be done with the whole sediment compartment. According to our experience, shaking the compartment should be the best method to increase sediment compaction in a homogeneous way (Nadler et al., 2011).

To be able to test higher forces and to reduce the discrepancy between the externally measured slider positions and the actual shell position, the static structure of the setup should be strengthened such that it is not deformed by the high tension in the cables.

The geometric model could be enhanced using a Meinhardt-type reaction-diffusion system (Meinhardt and Klingler, 1987) to produce the sculpture. Thus, also skew sculpture and more complex patterns would be possible. If appropriate, a more sophisticated ontogenetic simulation involving a genetic regulatory network (GRN) may be used (Eggenberger Hotz, 1997) to generate the sculpture or the whole shell morphology.

3.3.2 Richer sensory feedback

The setup did only contain position sensors in the linear motors and force sensors inserted between the slider ends and the attached cables. To achieve more direct and complete measurements of the trajectory of the shell, we experimented with different alternative sensors. This included an IMU within the shell (Vasileiou, 2012 (unpublished), force sensors within the shell (Brändli, 2009), and a visual 2D motion tracking system (Brändli, 2009). Although all these attempts were helpful, we did not find a solution suited as a standard procedure to record the results of experiments. The IMU system and the internal force sensors were relatively big, leading to a shell that could only partially penetrate the sediment. Visual tracking was difficult because the shell vanished within the sediment and because dust in the water obstructed the view. Even if the water was clear in the beginning, shell-grain and grain-grain interactions abraded dust over time and raised it into the water. Also, traces of the chemicals used to remove the support material from the 3D-printed shells accumulated in the water and produced small dust flakes.

Possibly one of these methods could be improved to obtain richer data from experiments, like a complete 3D trajectory of the shell. Such data could be visualized by an animation and thus help to understand and communicate the burrowing process.

3.3.3 Additional experiments

The improved setup could be used to investigate open questions in biology, palaeontology and biorobotics. Different fossil bivalve shapes could be scanned, reproduced and tested in the setup to compare their performance or to associate them with a sediment type. Using an evolutionary algorithm, an optimal burrowing motion could be evolved for a given shape. Computed

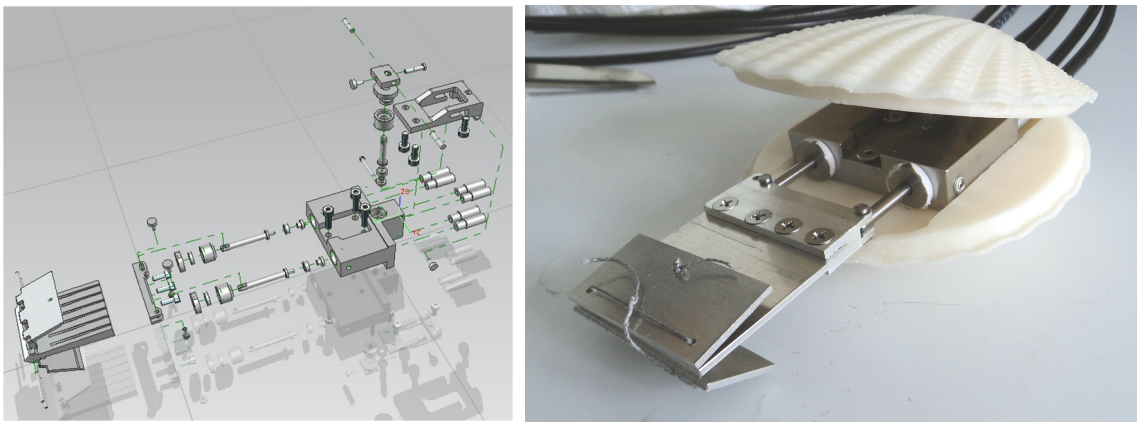

(a) (b)

Figure 3.2: Hydraulic bivalve. (a) Exploded view of the cylinder block and all its components. Reprinted from Brändli (2009). (b) Picture of the assembled hydraulic bivalve.

tomography (CT) scanning of recent and fossil shells and subsequent printing on the 3D printer is feasible as verified by scanning one valve of *Cardium pseudolima* and printing it. Features could be reproduced with a resolution of about $0.5\ \mathrm{mm}$.

The parameters defining shell morphology and motion pattern can both be controlled. It would therefore be possible to perform evolutionary experiments changing only one type of parameter or both at the same time. Thus, the co-evolution of morphology and motion control in an organism could be investigated.

3.3.4 Hydraulic setup

The setup described so far was used for all experiments reported in this thesis. However, due to the limitations of the previous setup, a second, completely independent hydraulic setup was designed and built. Unfortunately, it was never put into operation.

The purpose of the hydraulic setup was to deal with some of the limitations of the previous setup by implementing a more sophisticated simulation of the burrowing process that more closely mimics the burrowing sequence of bivalves (Figure 2.2). This included adding an artificial foot and a hinge to open and close the valves. The shell therefore had four degrees of freedom: open and close the valves, inflate and shrink the foot and expanding and retracting the foot using an anterior and a posterior cylinder. The major differences compared to the previous setup were: (a) the actuation was done hydraulically, (vs. electromagnetic linear motors), (b) the bivalve was "mechanically autonomous", i.e. the actuation was provided by the motion of the bivalve itself, (vs. external motors pulling the bivalve), (c) the valves could be opened and closed, (d) the bivalve featured an artificial foot. Thus, the hydraulic setup incorporated the two anchors that bivalves use for burrowing. This means that the mechanical parts used for propulsion through the sediment were all included in the bivalve, while only the pressured oil, i.e. the energy supply, had to be provided from outside. In the previous setup, anchoring had not been possible and the shell was held in place by the tension in the cables.

Bivalve shells were generated and printed using the same method as described in section G.1.1. Instead of bayonet couplings different attachment structures were used to attach the valves to the inner hydraulic structure as shown in Figure 3.2.

The first prototype of the foot was a hook with movable arms, as shown in Figure 3.2. A second test version was cast from silicone and could be inflated through a tube. For the hydraulic system, we chose oil instead of water or air. A hydraulic system functioning with water would have been too expensive and susceptible and an admixture would have been necessary to add lubricating characteristics to the water. Air would have generated buoyancy and is compressible.

To finish the setup, the control circuitry and the control program have to be implemented. It would then be interesting to test the setup and, if it works properly, to compare the results to the previous findings. In particular, the following points should be considered: (a) comparison between external and internal actuation, e.g. without connection to cables, back-slippage may become an issue, (b) comparison between water expulsion by squirting water through a perforated tube at the shell edge and by closing the valves, (c) benefits of the artificial foot.

To produce significant results with the hydraulic setup, it would also be necessary to consider the improvements described above, e.g. a better standardization technique to control the sediment state.

3.4 Conclusion

An entirely synthetic approach was followed by constructing a setup mimicking bivalve shell models and the rocking burrowing motion. Together with evolutionary algorithms, an integrated platform was built to investigate the functional morphology and morphological evolution of the shell of burrowing bivalves.

The main findings are that the state of the sediment plays a far more important role than expected and also than described in the literature. In the literature, the focus lies on the bivalve itself, the sediment type and correlations of the shell morphology to static properties of the sediment (like grain size). Shell size and pulling force have a relevant influence, as expected, while the effect of the surface sculpture is negligible. This is in contrast to the literature as well. Water expulsion tends to have a positive effect, but the results are not conclusive in our experiments. The dynamics of granular media are still not well understood. As long as there are no reliable and detailed computer simulations available, only physical experiments can deliver realistic results.

The built setup was the first of its kind. The two other approaches known to the authors used a pushing mechanism and either casts of real shells or abstracted metallic shells (Stanley, 1975b; Winter et al., 2012). We were also the first to artificially evolve physical bivalve shell morphologies. Because it was a prototype, our setup had several limitations, the most critical one being the difficulty to control the sediment.

Nevertheless, we believe the ideas connected to our approach have a large potential for palaeontological research and also other disciplines. The main ideas are: 1) By applying a synthetic approach, palaeontological questions may be tackled that are difficult to answer using analytic methods, e.g. finding a burrowing motion pattern fitting to a given fossil shape. Morphological and other parameters can be precisely controlled and the results quantified using internal and external sensors. 2) Technical advances such as cheap 3D printers open new possibilities to build experimental setups to study functional morphologies. 3) Using artificial evolution, not only physical processes like burrowing, but also evolutionary pressure shaping the morphology of organisms may be investigated, adding trajectories to the static points in a morphospace. 4) Because the approach is synthetic, results can be generalized to a higher degree. It is possible to not only study nature as it is but also as it could be (Langton, 1989). Morphologies from the entire morphospace can be tested, by using different fitness functions in artificial evolution, different evolutionary pressures and their effect on morphology may be investigated. 5) By controlling morphological and motion parameters, an integrated system can be built that does not only evolve controllers to fixed robots, as is usually done in evolutionary robotics, but that is able to

co-evolve morphology and motion pattern.

The research presented here is basic research. However, a better understanding of locomotion through granular media may have several potential applications. Automatic burrowing devices may be used to anchor ships or platforms in sandy sediments. Difficult terrain often contains granular material, also on land. Robots able to move through such terrain may be useful for different tasks, even extraterrestrial exploration, e.g. on Mars (Huntsberger et al., 2007; Zacny et al., April 15-18, 2012). A two-anchor method to locomote may also be applicable in other situations, such as motion through human tissue in medical contexts.

Bibliography

Adams, D. C., Rohlf, F. J., and Slice, D. E. Geometric morphometrics: Ten years of progress following the " revolution". *Italian Journal of Zoology*, 71(1):5–16, 2004. URL http://www.informaworld.com/openurl?genre=article&doi=10.1080/11250000409356545&magic=crossref.

Alexander, R. R., Stanton, R. J. J., and Dodd, J. R. Influence of sediment grain size on the burrowing of bivalves; correlation with distribution and stratigraphic persistence of selected neogene clams. *Palaios*, 8(3):289–303, 1993.

Amler, M., Fischer, R., and Schröder-Rogalla, N. *Muscheln*, volume 5 of *Haeckel-Bücherei*. Enke im Georg Thieme-Verlag, Stuttgart, 2000. ISBN 3-13-118391-8.

Anderson, S., Wisse, M., Atkeson, C., Hodgins, J., Zeglin, G., and Moyer, B. Powered bipeds based on passive dynamic principles. In *5th IEEE-RAS International Conference on Humanoid Robots, 2005*, pages 110–116, 2005. doi: 10.1109/ICHR.2005.1573554.

Arnold, S. J. Morphology, performance and fitness. *Integrative and Comparative Biology*, 23(2): 347–361, 1983. ISSN 1540-7063. doi: 10.1093/icb/23.2.347.

Bäck, T. *Handbook of evolutionary computation*. Oxford University Press, New York, 1997. ISBN 0750303921.

Bekker, M. G. *Off-the-road locomotion; Research and development in terramechanics*. University of Michigan Press, Ann Arbor, 1960. ISBN 9780472041428.

Bennett, V. Patterns in palaeontology : Old shapes, new tricks – the study of fossil patterns in palaeontology. *Palaeontology Online*, 3(3):1–10, 2013.

Bentley, P. J. *Evolutionary design by computers*. Morgan Kaufmann Publishers, San Francisco, CA, 1999. ISBN 978-1558606050.

Bongard, J. The utility of evolving simulated robot morphology increases with task complexity for object manipulation. *Artificial Life*, 16(3):201–223, 2010. ISSN 1064-5462. doi: 10.1162/artl.2010.Bongard.024.

Bongard, J. Morphological change in machines accelerates the evolution of robust behavior. *Proceedings of the National Academy of Sciences*, 2011. ISSN 0027-8424. doi: 10.1073/pnas.1015390108.

Bongard, J. C. and Pfeifer, R. Evolving complete agents using artificial ontogeny. In *In Morpho-functional Machines: The New Species (Designing Embodied Intelligence*, pages 237–258. Springer-Verlag, 2003.

Bookstein, F. L. *Morphometric tools for landmark data: Geometry and biology*. Cambridge University Press, Cambridge, repr. edition, 1997. ISBN 9780521585989.

Brändli, P. *Muschelroboter*. PhD thesis, Hochschule für Technik Rapperswil (HSR), Rapperswil, Switzerland, 2009.

Brooks, R. A. A robot that walks; emergent behaviors from a carefully evolved network. *Neural Computation*, 1(2):253–262, 1989. ISSN 0899-7667. doi: 10.1162/neco.1989.1.2.253.

Carl Stahl Technocables. URL http://www.carlstahl-technocables.de/home.html.

Chatterjee, S., Roberts, B., and Lind, R. Pterodrone: a pterodactyl-inspired unmanned air vehicle that flies, walks, climbs, and sails. In Brebbia, C. A. and Carpi, A., editors, *Design and nature V*, volume 138 of *WIT transactions on ecology and the environment*. WIT, Southampton, 2010. ISBN 1845644549.

Checa, A. G. and Cadée, G. C. Hydraulic burrowing in the bivalve mya arenaria linnaeus (myoidea) and associated ligamental adaptations. *Journal of Molluscan Studies*, 63(2):157–171, 1997. doi: 10.1093/mollus/63.2.157. URL http://mollus.oxfordjournals.org/content/63/2/157.full.pdf#page=1&view=FitH.

Chu, W.-S., Lee, K.-T., Song, S.-H., Han, M.-W., Lee, J.-Y., Kim, H.-S., Kim, M.-S., Park, Y.-J., Cho, K.-J., and Ahn, S.-H. Review of biomimetic underwater robots using smart actuators. *International Journal of Precision Engineering and Manufacturing*, 13(7):1281–1292, 2012. ISSN 2234-7593. doi: 10.1007/s12541-012-0171-7.

Clark, J., Cham, J., Bailey, S., Froehlich, E., Nahata, P., Full, R., and Cutkosky, M. Biomimetic design and fabrication of a hexapedal running robot. In *Robotics and Automation, 2001. Proceedings 2001 ICRA. IEEE International Conference on*, volume 4, pages 3643–3649 vol.4, 2001. doi: 10.1109/ROBOT.2001.933183.

Clark, J., Goldman, D., Lin, P., Lynch, G., Chen, T., Komsuoglu, H., Full, R., and Koditschek, D. Design of a bio-inspired dynamical vertical climbing robot. In *Proceedings of Robotics: Science and Systems*, Atlanta, GA, USA, 2007.

Cox, L. *Mollusca 6: Bivalvia*, volume Part N of *Treatise on invertebrate paleontology*. Geological Society of America, Boulder, Colorado, USA, 1971. ISBN 0-8137-3026-0.

Crampton, J. S. Elliptic fourier shape analysis of fossil bivalves: some practical considerations. *Lethaia*, 28(2):179–186, 1995. ISSN 0024-1164. doi: 10.1111/j.1502-3931.1995.tb01611.x.

de la Huz, R., Lastra, M., and López, J. The influence of sediment grain size on burrowing, growth and metabolism of donax trunculus l. (bivalvia: Donacidae). *Journal of Sea Research*, 47(2):85–95, 2002. ISSN 13851101. doi: 10.1016/S1385-1101(02)00108-9.

Dickinson, M. H. How animals move: An integrative view. *Science*, 288(5463):100–106, 2000. ISSN 0036-8075. doi: 10.1126/science.288.5463.100.

Dimension 3D printer. URL http://www.stratasys.com.

Ding, Y., Sharpe, S. S., Masse, A., Goldman, D. I., and Levin, S. A. Mechanics of undulatory swimming in a frictional fluid. *PLoS Computational Biology*, 8(12):e1002810, 2012. ISSN 1553-7358. doi: 10.1371/journal.pcbi.1002810.

Dryden, I. L. and Mardia, K. *Statistical shape analysis*. Wiley series in probability and statistics. Wiley & sons, Chichester, 1998. ISBN 978-0471958161.

Du, Y., Li, H., and Kadanoff, L. P. Breakdown of hydrodynamics in a one-dimensional system of inelastic particles. *Phys. Rev. Lett.*, 74(8):1268–1271, 1995. doi: 10.1103/PhysRevLett.74.1268. URL http://link.aps.org/doi/10.1103/PhysRevLett.74.1268.

Eggenberger Hotz, P. Evolving morphologies of simulated 3d organisms based on differential gene expression. In *ECAL - European Conference on Artificial Life*, pages 205–213. MIT Press, 1997.

Eggenberger Hotz, P. Genome-physics interaction as a new concept to reduce the number of genetic parameters in artificial evolution. In *IEEE Congress on Evolutionary Computation, CEC '03*, pages 191–198. IEEE, 2003. ISBN 0-7803-7804-0. doi: 10.1109/CEC.2003.1299574.

Floreano, D., Husbands, P., and Nolfi, S. Evolutionary robotics. In Siciliano, B. and Khatib, O., editors, *Springer handbook of robotics*. Springer, Berlin, 2008. ISBN 978-3-540-23957-4.

Floyd, S., Keegan, T., Palmisano, J., and Sitti, M. A novel water running robot inspired by basilisk lizards. In *Intelligent Robots and Systems, 2006 IEEE/RSJ International Conference on*, pages 5430–5436, 2006. doi: 10.1109/IROS.2006.282111.

Fogel, D. What is evolutionary computation? *IEEE Spectrum*, 37(2):26, 28–32, 2000. doi: 10.1109/6.819926.

Fogel, D. B. *Evolutionary Computation: The Fossil Record*. Wiley-IEEE Press, 1 edition, 1998. ISBN 0780334817.

Fowler, D. R., Meinhardt, H., and Prusinkiewicz, P. Modeling seashells. In Catmull, E. E. and McCormick, B. H., editors, *SIGGRAPH '92 conference proceedings*, volume 26.1992,2 of *Computer graphics*, pages 379–387, New York, 1992. ACM Press. ISBN 0201515857.

Gravish, N., Monaenkova, D., Goodisman, M. A. D., and Goldman, D. I. Climbing, falling, and jamming during ant locomotion in confined environments. *Proceedings of the National Academy of Sciences*, 2013. ISSN 0027-8424. doi: 10.1073/pnas.1302428110.

Hammer, Ø. and Bucher, H. Models for the morphogenesis of the molluscan shell. *Lethaia*, 38(2):111–122, 2005. ISSN 0024-1164.

Herrmann, H. J. Simulation of granular media. *Physica A*, 191:263–276, 1992.

Holland, A. F. and Dean, J. M. The biology of the stout razor clam tagelus plebeius: I. animal-sediment rlationships, feeding mechanism, and community biology. *Chesapeake Science*, 18(1):58, 1977. ISSN 00093262. doi: 10.2307/1350364.

Huntsberger, T., Stroupe, A., Aghazarian, H., Garrett, M., Younse, P., and Powell, M. Tressa: Teamed robots for exploration and science on steep areas. *JOURNAL OF FIELD ROBOTICS*, 24(11-12):1015–1031, 2007. ISSN 1556-4959. doi: 10.1002/rob.20219.

Husbands, P. *Evolutionary robotics: First European workshop, EvoRobot98, Paris, France, April 16-17, 1998 / proceedings*, volume 1468 of *Lecture notes in computer science*. Springer, Berlin, 1998. ISBN 978-3-540-64957-1. URL http://sfx.ethz.ch/sfx_locater?sid=ALEPH:EBI01&issn=0302-9743&volume=1468.

Jaeger, H. M. and Nagel, S. R. Physics of the granular state. *Science*, 255(5051):1523–1531, 1992. ISSN 0036-8075. doi: 10.1126/science.255.5051.1523.

Jung, S. Caenorhabditis elegans swimming in a saturated particulate system. *Physics of Fluids*, 22(3):031903, 2010. ISSN 10706631. doi: 10.1063/1.3359611.

Jung, S., Winter, A. G., and Hosoi, A. Dynamics of digging in wet soil. *International Journal of Non-Linear Mechanics*, 46(4):602–606, 2011. ISSN 00207462. doi: 10.1016/j.ijnonlinmec.2010.11.007.

Jusufi, A., Goldman, D. I., Revzen, S., and Full, R. J. From the cover: Active tails enhance arboreal acrobatics in geckos. *Proceedings of the National Academy of Sciences*, 105(11):4215–4219, 2008. ISSN 0027-8424. doi: 10.1073/pnas.0711944105.

Kevin C. Galloway, G. C. Haynes, B. Deniz Ilhan, Aaron M. Johnson, Ryan Knopf, Goran Lynch, Benjamin Plotnick, Mackenzie White, and D. E. Koditschek. X-rhex: A highly mobile hexapedal robot for sensorimotor tasks, 2010.

Koller-Hodac, A., Germann, D. P., Gilgen, A., Dietrich, K., Hadorn, M., Schatz, W., and Eggenberger Hotz, P. Actuated bivalve robot: Study of the burrowing locomotion in sediment. In *IEEE International Conference on Robotics and Automation (ICRA), 2010*, pages 1209–1214, Piscataway, NJ, 2010. IEEE. ISBN 9781424450381.

Langton, C. G. *Artificial life: The proceedings of an Interdisciplinary Workshop on the Synthesis and Simulation of Living Systems held september, 1987, in Los Alamos, New Mexico*, volume 6 of *Santa Fe Institute studies in the sciences of complexity. Proceedings*. Addison-Wesley, Redwood City Calif, 1989. ISBN 0201093464.

Langton, C. G. *Artificial life: An overview*. Complex adaptive systems. MIT Press, Cambridge, 1995. ISBN 9780262121897.

Li, C., Umbanhowar, P. B., Komsuoglu, H., Koditschek, D. E., and Goldman, D. I. From the cover: Sensitive dependence of the motion of a legged robot on granular media. *Proceedings of the National Academy of Sciences*, 106(9):3029–3034, 2009. ISSN 0027-8424. doi: 10.1073/pnas.0809095106.

Li, C., Zhang, T., and Goldman, D. I. A terradynamics of legged locomotion on granular media. *Science*, 339(6126):1408–1412, 2013. ISSN 0036-8075. doi: 10.1126/science.1229163.

Lin, H.-T., Leisk, G. G., and Trimmer, B. Goqbot: a caterpillar-inspired soft-bodied rolling robot. *Bioinspiration & Biomimetics*, 6(2):026007, 2011. ISSN 1748-3182. doi: 10.1088/1748-3182/6/2/026007.

LinMot. URL http://www.linmot.com/.

Lipson, H. and Pollack, J. B. Automatic design and manufacture of robotic lifeforms. *Nature*, 406 (6799):974–978, 2000. ISSN 00280836. doi: 10.1038/35023115.

Losert, W., Géminard, J.-C., Nasuno, S., and Gollub, J. Mechanisms for slow strengthening in granular materials. *Physical Review E*, 61(4):4060–4068, 2000. ISSN 1063-651X. doi: 10.1103/PhysRevE.61.4060.

Maladen, R. D., Ding, Y., Umbanhowar, P. B., Kamor, A., and Goldman, D. I. Mechanical models of sandfish locomotion reveal principles of high performance subsurface sand-swimming. *Journal of The Royal Society Interface*, 8(62):1332–1345, 2011. ISSN 1742-5689. doi: 10.1098/rsif.2010.0678.

Mazouchova, N., Umbanhowar, P. B., and Goldman, D. I. Flipper-driven terrestrial locomotion of a sea turtle-inspired robot. *Bioinspiration & Biomimetics*, 8(2):026007, 2013. ISSN 1748-3182. doi: 10.1088/1748-3182/8/2/026007.

McGhee, G. R. *Theoretical morphology: The concept and its applications*. Perspectives in paleobiology and earth history. Columbia Univ. Press, New York, USA, 1999. ISBN 0231106173.

McLachlan, A., Jaramillo, E., Defeo, O., Dugan, J., Ruyck, and Coetzee, P. Adaptations of bivalves to different beach types. *Journal of Experimental Marine Biology and Ecology*, 187(2):147–160, 1995. ISSN 0022-0981. doi: 10.1016/0022-0981(94)00176-E. URL http://www.sciencedirect.com/science/article/pii/002209819400176E.

McMillin, H. C. *The Life-history and Growth of the Razor Clam*. F. M. Lamborn, public printer, 1924. URL http://books.google.ch/books?id=PcIrAQAAMAAJ.

Meinhardt, H. *The algorithmic beauty of sea shells*. The virtual laboratory. Springer, Berlin, 3 edition, 2003. ISBN 9783540440109.

Meinhardt, H. and Klingler, M. A model for pattern formation on the shells of molluscs. *Journal of Theoretical Biology*, 126(1):63–89, 1987.

Nadler, S., Bonnefoy, O., Chaix, J.-M., Thomas, G., and Gelet, J.-L. Parametric study of horizontally vibrated grain packings. *The European Physical Journal E*, 34(7):1–10, 2011. ISSN 1292-8941. doi: 10.1140/epje/i2011-11066-y. URL http://dx.doi.org/10.1140/epje/i2011-11066-y.

National Instruments compactDAQ. URL http://www.ni.com/data-acquisition/compactdaq/.

National Instruments LabView. URL http://www.ni.com/labview.

Nedderman, R. *Statics and kinematics of granular materials*. Cambridge University Press, Cambridge, 1992. ISBN 978-0521404358. URL http://sfx.ethz.ch/sfx_locater?sid=ALEPH:EBI01&genre=book&isbn=9780521404358.

Nel, R., McLachlan, A., and Winter, D. P. E. The effect of grain size on the burrowing of two donax species. *Journal of Experimental Marine Biology and Ecology*, 265(2):219–238, 2001. ISSN 0022-0981. doi: 10.1016/S0022-0981(01)00335-5. URL http://www.sciencedirect.com/science/article/pii/S0022098101003355.

Niiyama, R., Nagakubo, A., and Kuniyoshi, Y. Mowgli: A bipedal jumping and landing robot with an artificial musculoskeletal system. In *Robotics and Automation, 2007 IEEE International Conference on*, pages 2546–2551, 2007. doi: 10.1109/ROBOT.2007.363848.

Nolfi, S. and Floreano, D. *Evolutionary robotics: The biology, intelligence, and technology of self-organizing machines*. Intelligent robots and autonomous agents. MIT Press, Cambridge, Massachusetts, 2000. ISBN 9780262640565.

Nvidia Corporation. Physx sdk, 2010. URL http://www.geforce.com/hardware/technology/physx.

Okamoto, T. Analysis of heteromorph ammonoids by differential geometry. *Palaeontology*, 31: 35–52, 1988.

Oliveira, S. and Stewart, D. E. Physically accurate granular flow simulation. *Procedia Computer Science*, 9(0):286–291, 2012. ISSN 1877-0509. doi: 10.1016/j.procs.2012.04.030. URL http://www.sciencedirect.com/science/article/pii/S1877050912001512.

Peterson, K., Birkmeyer, P., Dudley, R., and Fearing, R. S. A wing-assisted running robot and implications for avian flight evolution. *Bioinspiration & Biomimetics*, 6(4):046008, 2011. ISSN 1748-3182. doi: 10.1088/1748-3182/6/4/046008.

Pfeifer, R. and Scheier, C. *Understanding intelligence*. A Bradford book. MIT Press, Cambridge, 1. mit press paperback edition, 2001. ISBN 9780262161817.

Pfeifer, R., Bongard, J., and Grand, S. How the body shapes the way we think: A new view of intelligence, 2007a. URL http://site.ebrary.com/lib/academiccompletetitles/home.action.

Pfeifer, R., Lungarella, M., and Iida, F. Self-organization, embodiment, and biologically inspired robotics. *Science*, 318(5853):1088–1093, 2007b. ISSN 0036-8075. doi: 10.1126/science.1145803.

PhysX SDK. URL https://developer.nvidia.com/physx.

Qt. URL http://qt.digia.com/Product/.

Rapala Sufix Advanced Superline. URL http://www.rapala.com.

Raup, D. M. and Michelson, A. Theoretical morphology of the coiled shell. *Science*, 147(3663): 1294–1295, 1965. ISSN 0036-8075. doi: 10.1126/science.147.3663.1294.

Rechenberg, I. *Evolutionsstrategie: Optimierung technischer Systeme nach Prinzipien der biologischen Evolution*, volume 15 of *Problemata*. Frommann-Holzboog, Stuttgart-Bad Cannstatt, 1973. ISBN 3772803733.

Rechenberg, I. Case studies in evolutionary experimentation and computation. *Computer Methods in Applied Mechanics and Engineering*, 186(2-4):125–140, 2000. ISSN 00457825. doi: 10.1016/S0045-7825(99)00381-3.

Ren, J., Dijksman, J. A., and Behringer, R. P. Linear shear in a model granular system. *Chaos: An Interdisciplinary Journal of Nonlinear Science*, 21(4):041105, 2011. ISSN 10541500. doi: 10.1063/1.3664407.

Rudwick, M. J. S. The inference of function from structure in fossils. *The British Journal for the Philosophy of Science*, 15(57):27–40, 1964.

Sassa, S., Watabe, Y., Yang, S., Kuwae, T., and Thrush, S. Burrowing criteria and burrowing mode adjustment in bivalves to varying geoenvironmental conditions in intertidal flats and beaches. *PLoS ONE*, 6(9):e25041, 2011. ISSN 1932-6203. doi: 10.1371/journal.pone.0025041.

Saunders, A., Goldman, D. I., Full, R. J., Buehler, M., Gerhart, G. R., Shoemaker, C. M., and Gage, D. W. <title>the rise climbing robot: body and leg design</title>. In *Defense and Security Symposium*, SPIE Proceedings, pages 623017–623017–13. SPIE, 2006. doi: 10.1117/12.666150.

Savazzi, E. and Huazhang, P. A. Experiments on the frictional properties of terrace sculptures. *Lethaia*, 27(4):325–336, 1994. ISSN 0024-1164. doi: 10.1111/j.1502-3931.1994.tb01583.x.

Schwefel, H.-P. *Evolution and optimum seeking*. Sixth-generation computer technology series. Wiley, New York, 1995. ISBN 978-0471571483.

Seilacher, A. Constructional morphology of bivalves: Evolutionary pathways in primary versus secondary soft-bottom dwellers. *Palaeontology*, 27:207–237, 1984. URL http://palaeontology.palass-pubs.org/pdf/Vol%2027/Pages%20207-237.pdf.

Shepherd, R. F., Ilievski, F., Choi, W., Morin, S. A., Stokes, A. A., Mazzeo, A. D., Chen, X., Wang, M., and Whitesides, G. M. From the cover: Multigait soft robot. *Proceedings of the National Academy of Sciences*, 108(51):20400–20403, 2011. ISSN 0027-8424. doi: 10.1073/pnas.1116564108.

Sims, K. Evolving 3d morphology and behavior by competition. *Artificial Life*, 1(4):353–372, 1994. ISSN 1064-5462. doi: 10.1162/artl.1994.1.4.353.

Stanley, S. M. Post-paleozoic adaptive radiation of infaunal bivalve molluscs: A consequence of mantle fusion and siphon formation. *Journal of Paleontology*, 42(1):214–229, 1968. ISSN 00223360. URL http://www.jstor.org/stable/1302143.

Stanley, S. M. Bivalve mollusk burrowing aided by discordant shell ornamentation. *Science*, 166 (3905):634–635, 1969. ISSN 0036-8075. doi: 10.1126/science.166.3905.634.

Stanley, S. M. *Relation of shell form to life habits of the Bivalvia (Mollusca)*, volume 125 of *Memoir / The Geological Society of America*. The Geological Society of America, Boulder, Colorado, USA, 1970. ISBN 05854216.

Stanley, S. M. Why clams have the shape they have: An experimental analysis of burrowing. *Paleobiology*, 1(1):48–58, 1975a.

Stanley, S. M. Adaptive themes in the evolution of the bivalvia (mollusca). *Annual Review of Earth and Planetary Sciences*, 3(1):361–385, 1975b. ISSN 0084-6597. doi: 10.1146/annurev.ea.03.050175.002045.

Stanley, S. M. Coadaptation in the trigoniidae, a remarkable family of burrowing bivalves. *Palaeontology*, 20:869–899, 1977.

Thomason, J. *Functional morphology in vertebrate paleontology*. Cambridge University Press, Cambridge, New York, 1 edition, 1997. ISBN 978-0521629218.

Tin Lun Lam and Yangsheng Xu. Climbing strategy for a flexible tree climbing robot #x2014;treebot. *Robotics, IEEE Transactions on*, 27(6):1107–1117, 2011. ISSN 1552-3098. doi: 10.1109/TRO.2011.2162273.

To, K., Lai, P.-Y., and Pak, H. Jamming of granular flow in a two-dimensional hopper. *Physical Review Letters*, 86(1):71–74, 2001. ISSN 0031-9007. doi: 10.1103/PhysRevLett.86.71.

Trimmer, B., Takesian, A., Sweet, B., Rogers, C., Hake, D., and Rogers, D. Caterpillar locomotion: A new model for soft-bodied climbing and burrowing robots. In *7th Int. Symp. Technology and the Mine Problem*, 2006.

Trueman, E. R. Bivalve mollusks: Fluid dynamics of burrowing. *Science*, 152(3721):523–525, 1966. ISSN 0036-8075. doi: 10.1126/science.152.3721.523.

Trueman, E. R. The dynamics of burrowing in ensis (bivalvia). *Proceedings of the Royal Society of London. Series B, Biological Sciences*, 166(1005):p 459–476, 1967. ISSN 00804649. URL http://www.jstor.org/stable/75643.

Turing, A. M. The chemical basis of morphogenesis. *Philosophical Transactions of the Royal Society B: Biological Sciences*, 237(641):37–72, 1952. ISSN 0962-8436. doi: 10.1098/rstb.1952.0012.

Umbanhowar, P. and Goldman, D. I. Granular impact and the critical packing state. *Physical Review E*, 82(1), 2010. ISSN 1063-651X. doi: 10.1103/PhysRevE.82.010301.

Vasileiou, T. *Recording the 2D trajectory of a bivalve robot using an IMU (inertial measurement unit)*. PhD thesis, University of Zurich, Zürich, Switzerland, 2012 (unpublished).

Watters, G. T. Some aspects of the functional morphology of the shell of infaunal bivalves (mollusca). *Malacologia*, 35(2):315–342, 1993.

Webb, B. What does robotics offer animal behaviour? *Animal Behaviour*, 60(5):545–558, 2000. ISSN 00033472. doi: 10.1006/anbe.2000.1514.

Winter, A. G., Hosoi, A. E., Slocum, A. H., and Deits, R. L. H. The design and testing of roboclam: A machine used to investigate and optimize razor clam-inspired burrowing mechanisms for engineering applications. In *Proceedings of the ASME International Design Engineering Technical Conferences and Computers and Information in Engineering Conference - 2009*, pages 721–726, New York, NY, 2010. ASME. ISBN 9780791849040.

Winter, A. G., Deits, R. L. H., and Hosoi, A. E. Localized fluidization burrowing mechanics of ensis directus. *Journal of Experimental Biology*, 215(12):2072–2080, 2012. ISSN 0022-0949. doi: 10.1242/jeb.058172.

Wood, R. Liftoff of a 60mg flapping-wing mav. In *Intelligent Robots and Systems, 2007. IROS 2007. IEEE/RSJ International Conference on*, pages 1889–1894, 2007. doi: 10.1109/IROS.2007.4399502.

Yu, P. and Behringer, R. P. Granular friction: A slider experiment. *Chaos: An Interdisciplinary Journal of Nonlinear Science*, 15(4):041102, 2005. ISSN 10541500. doi: 10.1063/1.2130689.

Yuk, H., Kim, D., Lee, H., Jo, S., and Shin, J. H. Shape memory alloy-based small crawling robots inspired by c. elegans. *Bioinspiration & Biomimetics*, 6(4):046002, 2011. ISSN 1748-3182. doi: 10.1088/1748-3182/6/4/046002.

Zacny, K., Malla, R. B., Binienda, W., Li, C., Ding, Y., Gravish, N., Maladen, R. D., Masse, A., Umbanhowar, P. B., Komsuoglu, H., Koditschek, D. E., and Goldman, D. I. Toward a terramechanics for bio-inspired locomotion in granular environments. In *Thirteenth ASCE Aerospace Division Conference on Engineering, Science, Construction, and Operations in Challenging Environments, and the 5th NASA/ASCE Workshop On Granular Materials in Space Exploration*, pages 264–273, April 15-18, 2012. doi: 10.1061/9780784412190.031.

Zhou, X. and Bi, S. A survey of bio-inspired compliant legged robot designs. *Bioinspiration & Biomimetics*, 7(4):041001, 2012. ISSN 1748-3182. doi: 10.1088/1748-3182/7/4/041001.

Ziegler, B. *Spezielle Paläontologie: Protisten, Spongien und Coelenteraten, Mollusken*, volume 2/3 of *Einführung in die Paläobiologie / Bernhard Ziegler*. Schweizerbart'sche Verlagsbuchhandlung, Stuttgart, 1 edition, 1983. ISBN 3-510-65036-0.

Ziegler, M., Iida, F., and Pfeifer, R. Cheap underwater locomotion: Roles of morphological properties and behavioral diversity. In *9th Int. Conference on Climbing and Walking Robots*, virtual, 2006.

Appendix A

Correlation between morphology, behaviour and habitat – bivalve burrowing in simulation and robotics

Reprinted from:

Daniel Germann, Wolfgang Schatz, Maik Hadorn, Andreas Fischer and Peter Eggenberger Hotz, *Correlation between morphology, behaviour and habitat – bivalve burrowing in simulation and robotics*, Abstracts of the 6th Swiss Geoscience Meeting, 2008, Pages 123-124.

Correlation between morphology, behaviour and habitat – bivalve burrowing in simulation and robotics

Germann Daniel*, Schatz Wolfgang**, Hadorn Maik*, Fischer Andreas* & Eggenberger Hotz Peter*

*University of Zurich, Department of Informatics, Artificial Intelligence Laboratory, Andreasstrasse 15, CH-8050 Zurich (germann@ifi.uzh.ch)
**University of Lucerne, Pfistergasse 20, CH-6003 Lucerne

Bivalves show a large diversity of shell shapes and sculptures during their long history of evolutionary adaptations to different modes of life. The comparatively dense fossil record of bivalves, the well-defined morphological space and the quite complete picture of bivalvian phylogeny offer basis for an analysis of general evolutionary processes. However, while the fossil record conveys information about the shape and the habitat of bivalves, the interpretation of the functional morphology, locomotion and changes in shell shape is generally vague, as fossils represent only discrete states in the morphological space and suffer from the preservational bias. Thus, the purpose of this project is to extend the knowledge about the evolution of bivalves and their adaptations to burrowing using both a computer simulation and a burrowing robot. The simulation will cover the dynamics of burrowing as well as the evolution in morphology and behaviour, reconstructing a trajectory in the morphological space and analysing the processes inducing these state-shifts.

There already exist mathematical models of sea shells (e.g. Raup & Michelson 1965), models of granular media (e.g. van Wachem & Almstedt 2003), burrowing robots and simulations of artificial evolution, but they have never been combined. Our simulation consists of (i) models of recent, fossil and artificial bivalve morphospecies, (ii) a model of a granular medium including the physical interactions with the shell, (iii) an implementation of the burrowing sequence (cf. Trueman 1966) and (iv) an artificial evolutionary system. The artificial evolution may change parameters controlling the behaviour or the morphology of the bivalves. Using a computer simulation allows an efficient and systematic analysis of the burrowing efficiency by changing just a single parameter at a time.

The virtual shell models are converted into physical objects using a 3D-printer (Fig. 1). As a starting point for the physical experiments, finally leading to a self-sufficient burrowing robot, we will attach the shell to two rods simulating the rocking locomotion of the bivalve during the burrowing process (cf. Stanley 1975). In further steps, the opening and closing of the valves and finally an artificial foot probing into the sediment will be added to complete the robot. The data provided by the robot is used to calibrate the simulation and to assess the coherence of the model and the physical reality. After testing the biological significance of the simulation, we will explore the functional correlations between the shell shapes and sculptures, the burrowing behaviour and the sediment type.

As shown in earlier examples (Hadorn et al. 2004), a close collaboration between palaeontology and evolutionary computation/robotics can return profit for both scientific fields. A possible application of this research may be a tool for palaeontologists to link shell forms and the mode of life of fossil bivalves in a more sophisticated way. The simulation can be used to perform experiments with evolution, to identify functional constraints, to find explanations for aberrant and extinct shell forms and even to create and test shell forms that have never existed. By investigating the functionality not only of recent but also of fossil shells, the field of bionics could be remarkably extended. In industry, the robot might serve as a prototype for autonomous burrowing robots or removable and fixed anchorage of man-made structures in soft sediments.

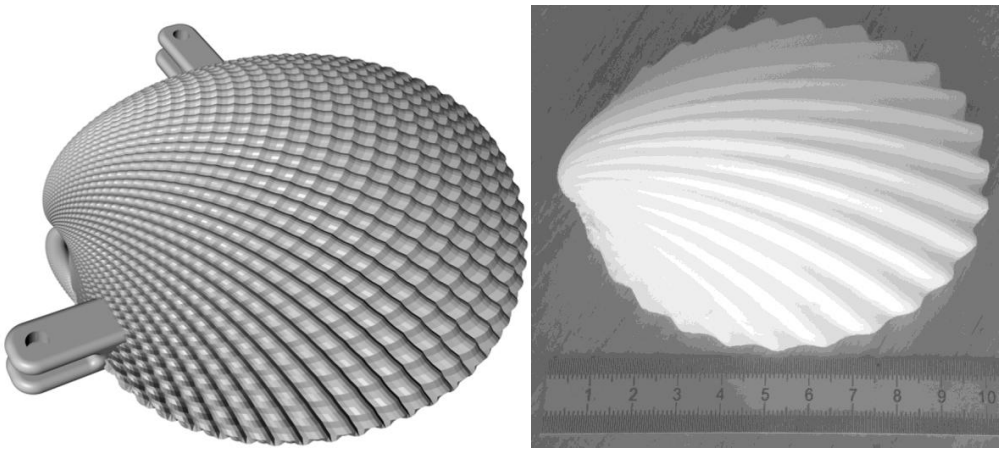

Figure 1. Left: An artificial shell generated by the simulation software with added sockets for the rods. Right: Photo of a valve printed by the 3D-printer (scale in centimetres).

This work is part of the Swiss National Foundation project no. 113934.

REFERENCES

Hadorn, M., Schatz, W. & Eggenberger Hotz, P. 2004: Were Adam and Eve Ediacarans? – A possible sexual dimorphism in Dickinsonia costata, Abstracts of the 2nd Swiss Geoscience Meeting.

Raup, D. & Michelson, A. 1965: Theoretical morphology of the coiled shell, Science, 147, 1294-1295.

Stanley, S. 1975: Why clams have the shape they have; an experimental analysis of burrowing, Paleobiology, 1, 48-58.

Trueman, E. 1966: Bivalve mollusks: Fluid dynamics of burrowing, Science, 152, 523-525.

van Wachem, B. & Almstedt A. 2003: Methods for multiphase computational fluid dynamics, Chemical Engineering Journal, 96, 81-98.

Retracing the Evolution of Bivalves in Simulation and Robotics

University of Zurich

Correlating Morphology, Behaviour and Habitat in the Context of Evolution Using a Computer Simulation and Robots

ai lab
Artificial Intelligence Laboratory

Daniel Germann, Wolfgang Schatz, Maik Hadorn, Andreas Fischer & Peter Eggenberger Hotz

Abstract

We combine for the first time mathematical models of bivavles, physical simulations of sedimentary structures, artificial evolution and robotics to investigate the influence of bivalve morphology on the burrowing process and the morphological change of bivalves during evolution. The resulting modelling system may support palaeontologists in understanding the bivalvian evolution in a more sophisticated way and lead to innovations in bionics and engineering.

Background

Bivalves show a large diversity of shell shapes and sculptures during their long history of evolutionary adaptations to different modes of life. While the fossil record conveys information about the shape and the habitat of bivalves, the interpretation of the functional morphology and its change during evolution is generally vague, as fossils represent only discrete states in the morphological space and suffer from the preservational bias.

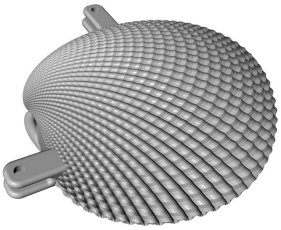

Figure 1: Based on virtual shells 3D plastic models are generated and tested for their burrowing efficiency (see Fig. 3b).

Methods

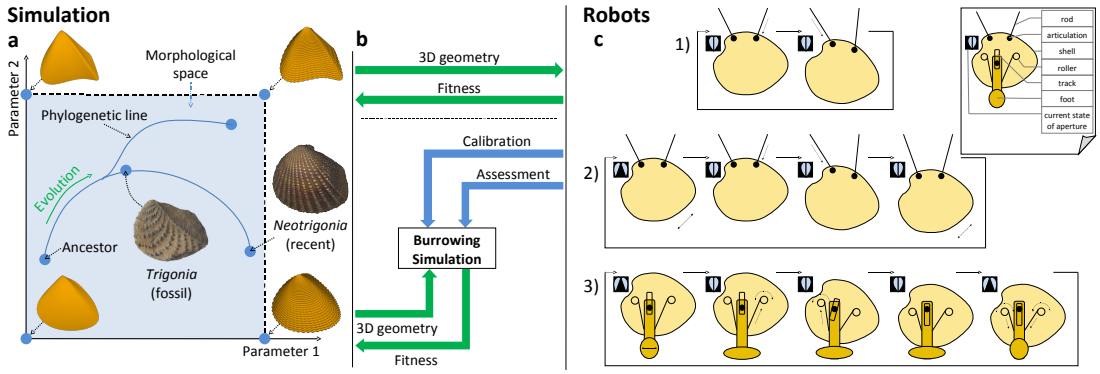

Figure 2: Overview of the system consisting of a computer simulation and robots.
(a) Recent, fossil and artificial bivalves can be located in a morphological space defined by parameters controlling a mathematical growth model of the shells (see e.g. Raup & Michelson 1965). Phylogenetic lines are identified with trajectories through the morphological space. The simulation can reproduce the morphology at any point, thus reconstructing the evolution between fossils. Artificial evolution can control the change in parameters and therefore explain the processes that induce the state-shifts in the morphological space.
(b) The evolutionary process includes the selection of morphologies based on a fitness value that is computed as the burrowing performance of a moving bivalve. The performance is either measured from a real burrowing robot or determined using a physical simulation of the burrowing process. The burrowing simulation comprises a model of a granular medium (e.g. van Wachem & Almstedt 2003) and its physical interactions with the shell. The behaviour of the bivavles is implemented as the burrowing sequence (cf. Trueman 1966) and can also be controlled by artificial evolution. The data produced by the robots are used to calibrate the physical burrowing simulation and to assess its biological significance.
(c) In order to build a bivalve robot, the virtual shells are converted into real objects using a 3D printer (dimension bst 768). By converting small populations of virtual shells into real robots, measuring their performances and feeding these fitness values back to the simulation, artificial evolution can be done in hardware. The steps towards an autonomously burrowing robot are the following: (1) Building an artificial shell, actuated externally by rods that induce the rocking motion bivalves use during burrowing (cf. Stanley 1975). (2) Adding a mechanism for opening and closing the shell. (3) Replacing the external actuation by an artificial foot.

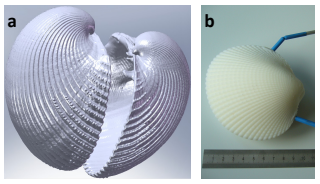

Figure 3: (a) Model of a recent morphospecies: shell surface reconstructed from a computed tomography (CT) scan of a specimen of *Cardium pseudolima*.
(b) Photograph of a plastic model implementing the virtual model shown in Fig. 1 and illustrating stage 1 in Fig. 2c.

Discussion

As shown in earlier examples (Hadorn et al. 2004), a close collaboration between palaeontology and evolutionary computation/robotics can return profit for both scientific fields. This research proposes a system performing artificial evolution based on functional bivalve morphology both in simulation and robotics. It may assist palaeontologists in interpreting fossil bivalves including aberrant and extinct shell forms, even allowing to create and test shell forms that have never existed. By investigating not only recent but also fossil shells, the field of bionics could be remarkably extended. In industry, autonomously burrowing robots might serve as a prototype for removable and fixed anchorage of man-made structures in soft sediments.

REFERENCES
Hadorn, M., Schatz, W. & Eggenberger Hotz, P. 2004: Were Adam and Eve Ediacarans? – A possible sexual dimorphism in Dickinsonia costata, Abstracts of the 2nd Swiss Geoscience Meeting.
Raup, D. & Michelson, A. 1965: Theoretical morphology of the coiled shell, Science, 147, 1294-1295.
Stanley, S. 1975: Why clams have the shape they have; an experimental analysis of burrowing, Paleobiology, 1, 48-58.
Trueman, E. 1966: Bivalve mollusks: Fluid dynamics of burrowing, Science, 152, 523-525.
van Wachem, B. & Almstedt A. 2003: Methods for multiphase computational fluid dynamics, Chemical Engineering Journal, 96, 81-98.

Daniel Germann [1], Wolfgang Schatz [2], Maik Hadorn [1], Andreas Fischer [1] & Peter Eggenberger Hotz [1,3]

[1] University of Zurich, Department of Informatics, Artificial Intelligence Laboratory, Andreasstrasse 15, CH-8050 Zurich, Switzerland
[2] University of Lucerne, Pfistergasse 20, CH-6003 Lucerne, Switzerland
[3] University of Southern Denmark , The Maersk Mc-Kinney Moller Institute for Production Technology, Niels Bohrs Alle, DK-5230 Odense M, Denmark

This work is part of the Swiss National Foundation project no. 113934.

Appendix B

Actuated Bivalve Robot – Study of the Burrowing Locomotion in Sediment

Reprinted from:

Agathe Koller-Hodac; Daniel P. Germann, Alexander Gilgen, Katja Dietrich, Maik Hadorn, Wolfgang Schatz, Peter Eggenberger Hotz, *Actuated bivalve robot study of the burrowing locomotion in sediment*, 2010 IEEE International Conference on Robotics and Automation (ICRA), pp.1209,1214, 3-7 May 2010. doi: 10.1109/ROBOT.2010.5509329, http://ieeexplore.ieee.org/stamp/stamp.jsp?tp=&arnumber=5509329&isnumber=5509124

Actuated Bivalve Robot
Study of the Burrowing Locomotion in Sediment

Agathe Koller-Hodac, Daniel P. Germann, Alexander Gilgen, Katja Dietrich,
Maik Hadorn, Wolfgang Schatz and Peter Eggenberger Hotz

Abstract— **This paper presents the design and control of an actuated bivalve robot, which has been developed to study the burrowing locomotion of bivalves in sediment. The setup consists of a tank filled with sand and water, plastic models of bivalve shells capable of expelling water and an external actuation mechanism simulating the rocking burrowing motion typically used by these animals. The realistic shell shapes have been realized using three-dimensional plotting techniques allowing testing influences of different shell shapes and surface structures (sculptures) on the burrowing efficiency.**

Based on the experimental setup, the burrowing process has been reproduced. The results show that this setup can be used to identify correlations in the burrowing process. Further experimental work will investigate the influence of factors such as shell shape and sculpture or the motion sequence on the burrowing performance.

Keywords: biorobotics; biomimetics; burrowing locomotion; bivalves

I. INTRODUCTION

Bivalves have been part of the animal world for a long period of time and are well adapted to their particular mode of life. Our focus lies on their locomotion behavior, which in many cases consists of burrowing into the sediment for protection against predators and other environmental factors. This behavior provides an excellent instance of a well defined and well studied process suited to test novel methodological approaches. In our project, we pursue an "understanding by building" approach, as we built a robotic experimental setup to investigate bivalve burrowing without using living animals. The total control of the morphology and actuation of the artificial bivalves allows a systematic examination of the burrowing process by varying single parameters. We intend to use the constructed platform to shed light on correlations of morphology, motion and sediment and thus better understand the link between morphology and functionality.

There are several reasons why clams are used to study correlations between morphology and behavior. First, suitable mathematical models of bivalve shell morphology already exist. Second, the mechanical behavior of bivalves, which mainly consists of burrowing into the sediment, is simple when compared to other organisms. Third, in contrast to other animals, bivalves do not use a complicated system of multiple movable body parts or the secretion of mucus to burrow. Such complex dynamics would be much harder to simulate. And fourth, a large range of shells with different shapes and sculptures is easily available.

It is technically difficult to get close to living bivalves. Therefore we lay our focus on comparing robots among each other while systematically varying parameters instead of trying to authentically mimic specific species or individuals. The built platform is able to burrow artificial bivalves into the sediment using a simple, externally actuated shell model. The correlation between burrowing efficiency, shape, sculpture and size can be established.

A further goal is to understand the burrowing process so that energy saving sequences can be defined to dig and anchor objects in sediment for sea applications. A study analyzing real bivalve behavior in sediment shows that the surrounding sediment is fluidized through the opening and closing of shells [1]. It appears essential to mimic the natural behavior and liquidize the soil during digging in order to reduce the soil resistance.

In this paper, the design and control of the bivalve robot is described. An experimental apparatus based on an aquarium tank containing water and sediment is presented. The experimental setup allows simulating the burrowing locomotion in sediment. Experimental results illustrate the characteristics of burrowing locomotion for digging into substrates. The discussion describes the biological relevance of the platform and in the future work section, we explain which additional functionalities will be integrated into the setup and which further experiments will be performed to identify correlations between morphology and burrowing performance.

II. RELATED WORK

A. Bivalve Shape

The soft body of bivalves is enveloped by two valves which are dorsally connected and pushed open by an elastic ligament. The valves of burrowing clams are closed by usually two adductor muscles. The part inside the shell not

This work is funded by the Swiss National Science Foundation as project no. 113934 "From Morphology to Functionality – Development and Application of a Bivalve Burrowing Simulation".

A. Koller-Hodac, A. Gilgen and K. Dietrich are with the Institute for Laboratory Technology, University of Applied Sciences Rapperswil, Oberseestrasse 10, 8640 Rapperswil, Switzerland {akoller|agilgen|kdietric}@hsr.ch

D. Germann and M. Hadorn are with the Artificial Intelligence Laboratory, Department of Informatics, University of Zurich, Andreasstrasse 15, 8050 Zurich, Switzerland {germann|hadorn}@ifi.uzh.ch

P. Eggenberger Hotz is with the Mærsk-McKinney-Møller Institute, University of Southern Denmark 5230, Odense, Campusvej 55, Denmark eggen@mmmi.sdu.dk

W. Schatz is with the Academic Services Centre, University of Lucerne, Pfistergasse 20, 6000 Luzern, Switzerland wolfgang.schatz@unilu.ch

W. Schatz and P. Eggenberger Hotz contributed equally to this work.

Correspondence should be addressed to D. Germann.

occupied by the animal body is called the mantle cavity. A part of the soft body called foot protrudes ventrally from the shell and plays a major role in the burrowing process. Depending on the species, the shell sculptures have characteristic structures such as concentric ridges. It has been discovered that the shell features have a function and tend to enhance burrowing efficiency [2] [3].

Bivalve shells, as the shells of the related gastropods (snails) have a convoluted shape. One of the first attempts to mathematically model this shape was done by Raup [4] in 1965, where he also introduced the term "theoretical morphology". Since then, many different approaches have been suggested, but most of them are based on a simple growth process that produces a sequence of aperture curves of increasing size that travel along a three-dimensional helicospiral (see also [5], [6], [7], [8], [9], [10]). Only a few parameters are needed to generate realistic virtual shell shapes.

B. Bivalve Burrowing

In order to burrow themselves into the sediment, bivalves use a two-anchor system. The shell and a part of the soft body called foot alternate in anchoring the bivalve in the sediment, while the other is pushed or pulled forward. Anchoring is done by increasing the size: the shells are opened, the foot swells under blood pressure. The dynamics of this process were first described in greater detail by Trueman [1]. He identified the motion sequence described in fig. 1 which is called the "burrowing sequence". He observed the behavior of littoral bivalves making films through the glass of an aquarium tank.

In natural bivalves, valve adduction happens in about 0.1 s, immediately followed by the anterior and posterior pedal retraction. After the relaxing of the adductor muscles to reopen the valves and a rest period, the next burrowing cycle begins. With increasing depth, the rest period tends to become longer and the depth increase per burrowing cycle smaller. Small and rapid burrowers reach their living position in just a few seconds (e.g. *Donax denticulatus* in 3 to 11 s). Shallow burrowers live only 1 to 3 cm below the sediment surface, whereas deep burrowers move to a depth of 20 cm and more (up to 100 cm). In particular cases (e.g. *Divaricella quadrisulcata*), this is more than ten times the body size. [11]

It was recognized early on that the morphology of the shell and foot have a large impact on the burrowing performance. A notable physical experiment was performed in 1975 by Stanley [12]. He produced a cast of a specimen of *Mercenaria mercenaria* that has a blunt anterior area and tested it in real sediment. He simulated the rocking burrowing motion by manually and alternately pushing two rods attached to the shell. By comparing the burrowing performance to a second model where he had altered the shape to display a sharper front edge, he could explain the advantage of the blunt anterior region of this particular species.

Bivalve morphologies suitable for efficient burrowing and correlations between morphology, burrowing motion and sediment have already been detected. Stanley found that

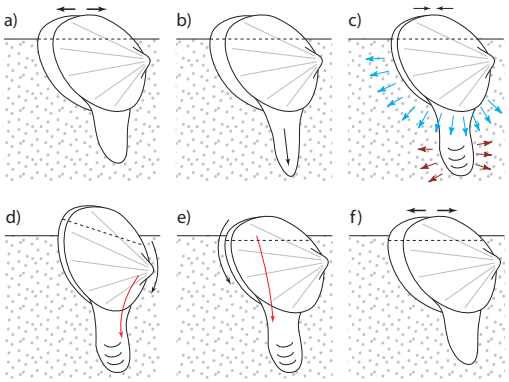

Fig. 1. The *burrowing sequence* for bivalves as described by Trueman [1]. (a) The clam is in erect position, partially burrowed in the sediment. The valves are open to anchor the shell, i.e. to prevent back-slippage. (b) The foot probes deeper into the sediment. (c) The adductor muscles contract, partially closing the shell. The water expelled from the cavity liquefies the surrounding sediment to reduce the resistance to penetration. From the soft body inside the shell, blood is pressed into the foot, which is inflated and serves as a new anchor. (d) The anterior retractor muscle (red arrow) pulls the front side of the bivalve towards the foot, leading to a rotation of the shell (black arrow). (e) In the same way, the posterior retractor muscle rotates the shell back into the erect position. (f) The two rotations around different rotation axes led to a net downward translation, as illustrated by the dashed line. The valves open again to allow for another burrowing cycle starting at (a).

ridges at a right angle to the burrowing direction are advantageous and used with rocking motions covering a small angle, while v-shaped ridges are also possible, leading to larger rotation angles [13]. Savazzi [14] summarizes that the sculpture amplitude increases with sediment grain size, that the profile of the sculpture should be asymmetric and the gentle slope should be facing the burrowing direction. Using our experimental setup, we intend to verify these and similar findings and generate new ones.

C. Burrowing Robots

Although there have been a few burrowing robots, most of them are conceived of as applications in a bionics context. An interesting approach is the RoboClam from the Hatsopoulous Microfluidics Laboratory at MIT (Massachusetts Institute of Technology) which mimics the behavior of the razor clam to perform anchoring operations [15] [16]. The project focuses on the *Ensis* clam genus, an elongate species by which the shell digs into sediment without rocking motion. The robot is actuated using pneumatic pistons which apply forces to push the razor clam into the sediment. The efficiency of clam digging has been demonstrated in comparison to standard anchoring techniques.

Another example of a burrowing robot is a soft-bodied climbing system named Softbot [17]. This robot is not inspired from bivalves but from caterpillars, that are capable to crawl and burrow into confined spaces.

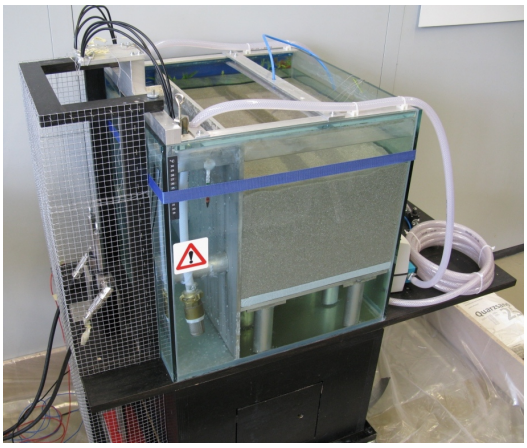

Fig. 2. The experimental setup consisting of an actuation mechanism (left), a tank filled with sediment and water (middle) and a hydraulic system for water expulsion (right).

III. METHODS AND MATERIALS

Figure 2 shows the complete experimental apparatus, which has been realized to investigate the burrowing behavior of bivalves in sediment. It consists of three main parts: (1) an aquarium tank, (2) an actuation mechanism and (3) a hydraulic system. The aquarium with the dimensions of 60×60×60 cm (216 ℓ) is filled with sediment and water. Since the sediment is deposited onto a bottom plate, it can be exchanged to investigate the influence of sediment characteristics on the burrowing process. The tank has been filled with normal tap water and some anti-algae solution. The first experiments were done with a simple unwashed sand with grain sizes between 0 and 4 mm. Later and future experiments were or will be conducted with a well-rounded quartz sand with grain sizes between 0.7 and 1.2 mm, which falls in the category of coarse to very coarse sand. After being placed at the interface between water and sediment, the bivalve robot can perform its burrowing motion in sediment. A number of parameters determining the morphology and behavior of the robot bivalves can be varied, including the overall shell shape, the amount and shape of radial and commarginal sculpture and the operation timing during the burrowing cycle.

A. Robot Bivalve Shells

It is well recognized in malacological research that the shell morphology has a major impact on the burrowing performance. To study the relationships between physical morphology and burrowing efficiency, a dedicated software tool has been developed in order to generate different complex forms of virtual shells. The program uses a mathematical model similar to the one described in [5]. To print the generated model on a 3D printer, it has to be transformed from an open surface into a closed solid. This has been achieved by closing both sides of the tubular mesh with disk-like patches. The patch closing the aperture is either flat or manually designed by a computer aided design (CAD) program. The former allows gluing two parts together to produce a one-piece shell, while the latter may be used to equip the shell with an attachment site that fits to the inner structure of a more complicated robot. The final result is a closed triangle mesh that is stored in STL format and can be directly sent to the 3D printer.

Fig. 3. Left: Real bivalve shell (*Cardium pseudolima*). Right: A similar shell, artificially generated and realized with a 3D plotter.

A *dimension® bst 768* 3D printer [18] and its *CatalystEx* software has been used to print the shells. The shells are printed in solid mode to avoid the plastic from absorbing too much water. The resolution of the printer is about 0.5 mm. Available bivalve specimen can be scanned by computed tomography to get virtual geometrical models of their shells. This approach allows the fabrication of one-piece shells as well as thin-walled half-shells. They have an outside geometry close to real bivalves but can also include robotic components in the inner cavity. Figure 3 depicts both a specimen of *Cardium pseudolima* and a shell model realized by 3D plotting.

B. Burrowing Motion

According to the burrowing sequence described in [1], the downward digging and the rocking along the longitudinal axis have been implemented in the bivalve robot. Linear electrical motors integrated into the setup provide a flexible actuation solution to perform digging operations.

As shown in Figure 4, bivalve shells are pulled downward using two strings which are actuated externally by LinMot motors. These two linear actuators (called left and right motors) are synchronized to obtain the rocking down-motion of the bivalve. Motor parameters such as rocking step resolution and time can be varied. Force and position are monitored using the control unit of the motors. Pulling forces up to 200 N and a maximum stroke of 66 cm can be obtained with this configuration.

The system control has been implemented in the motor control box using LinMot-Talk [19]. Based on PID position controllers, a response time of 10 ms and a positioning accuracy of 30 µm have been achieved, which is sufficient for reproducing the burrowing motion.

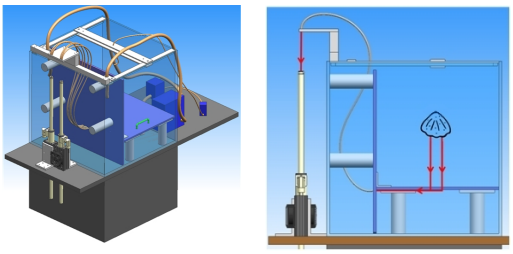

Fig. 4. Two schematic drawings of the bivalve model, the tank and the actuation mechanism. The red arrows show the track of the strings that are attached to the shell and to two linear motors that pull the bivalve into the sediment. The strings are deviated to avoid cutting the glass bottom of the tank. To reduce the friction on the string, it only runs through the sand right below the shell. After passing through a hole in the horizontal plate, it is led through water and a cable casing.

C. Burrowing Efficiency

To perform a comparison between several burrowing strategies for a given species, it is particularly relevant to define a parameter called burrowing efficiency which indicates the mechanical energy E_{mech} required to reach a defined burrowing depth in sediment. The necessary energy shall be kept as low as possible to obtain an optimized burrowing locomotion.

$$E_{mech} = F_d v t_d \tag{1}$$

The burrowing efficiency, given in Equation 1, depends on three parameters: the pulling force F_d, the average speed v and the digging time t_d. As introduced by Trueman [2], the bivalve mass shall be considered to compare the burrowing efficiency among bivalves of varying sizes. Therefore, the burrowing efficiency parameter $E_{mech,s}$ includes a shell body mass parameter m_s and is represented by Equation 2.

$$E_{mech,s} = \frac{F_d}{m_s} v t_d \tag{2}$$

D. Water Expulsion

Vertical digging of an object into sediment under water requires extremely large forces so that the necessary energy to reach a digging depth in soil increases drastically. It has been observed early on that real bivalves use water expulsion combined with rocking motion to fluidize sediment and therefore facilitate the digging process.

Water expulsion has been simulated using a hydraulic pump which is connected to the bivalve. Perforated tubing has been inserted into the shells to allow water expulsion along the bivalve edge. The water pressure p is regulated between 0.1 and 1.0 bar by a pressure regulation valve. The membrane pump generates a volume flow Q between 0.5 and 3.0 ℓ/min. A two-position two-way valve is integrated into the liquid path to block the liquid flow when closed. The valve command signal is generated by the controller of the electrical motors. The hydraulic parameters have been set so that the amount of water expelled per cycle corresponds to the volume expelled from the mantle cavity during the closing of the shells. For energy comparison, the hydraulic energy E_{hydr} required for water expulsion must be added to the mechanical energy E_{mech} supplied for the rocking motion. The total energy E_t required for burial is given by Equation 3.

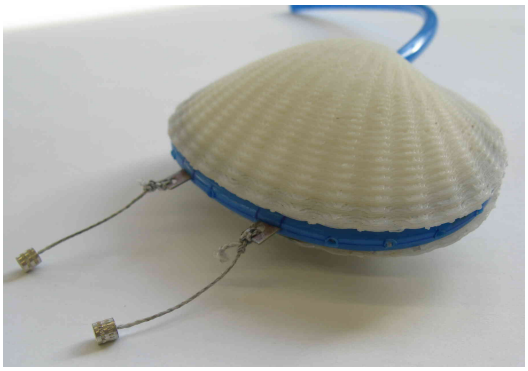

Fig. 5. Burrowing robot design including water expulsion mechanism. A plastic shell includes a peripheral rubber tube with holes to emit water. The tube is connected to the hydraulic pump placed next to the tank.

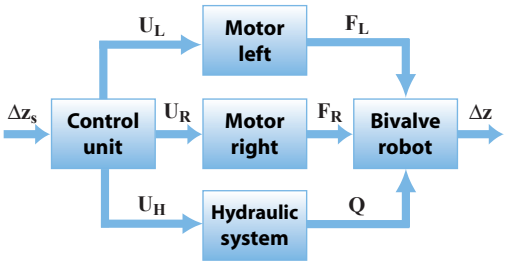

Fig. 6. Control Scheme for the bivalve robot. The control unit generates commands to the linear motors and the hydraulic system to obtain the burrowing motion.

$$E_t = E_{mech} + E_{hydr} \tag{3}$$

where E_{hydr} depends on the volume flow and the hydraulic pressure.

The Figure 6 illustrates the control scheme. The control unit is in charge of the synchronization between rocking motion and water expulsion in order to reach a defined depth Δz_s. The command unit generates control voltages U_R and U_L to the motor amplifiers as well as on/off commands U_H to the hydraulic valve. The motors generate alternate forces F_R and F_L to pull down the bivalve robot. The water flows through the robot when the hydraulic valve is opened.

IV. RESULTS

Several burrowing sequences have been tested experimentally. After the robot has been brought to the sediment surface, the burrowing process has been started. Under the

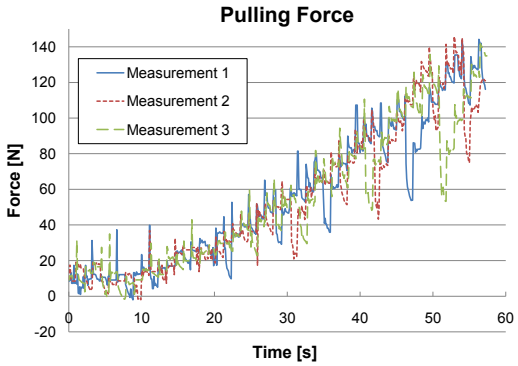

Fig. 7. Measured digging force generated by linear motors to pull the bivalve robot into sediment. The graph shows the results of three successive runs of the same burrowing experiment. For each run, the force applied by the left (posterior) motor is plotted against time. During this burrowing period, the shell was pulled 10 cm into the sediment by regular steps of 2 mm. The force measurements are fairly repeatable even if environmental conditions cannot be completely identical from one experiment to another.

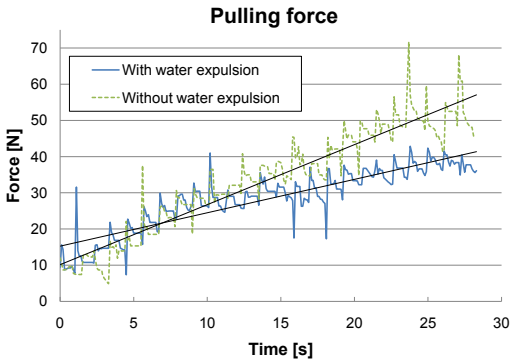

Fig. 8. Comparison of force profiles for a burrowing motion when water is expelled or not from the bivalve shells. The water was ejected through a perforated tube along the commissure of the two valves. For these experiments, the pump was operated at full capacity. During the whole period, the shell was pulled 5 cm into the sediment. At the beginning, there was no noticeable difference, but after about 10 s, water expulsion reduced the necessary force to pull the shell deeper into the sediment. The linear trendlines are plotted for lucidity, the intersection is of no known significance.

assumption that the strings do not deform, the information about force and position provided by the motor control unit are good indicators about the burrowing efficiency of the bivalve robot.

A. Burrowing Motion

Repeated measurements on the pulling forces F_R and F_L generated by the motors have shown that these forces increase almost linearly with the digging depth Δz measured from the sediment surface. Although initial conditions for each experiment cannot be completely identical due to sediment's sinking effects, the force measurements are fairly repeatable, as illustrated on Figure 7. The pulling forces increase slowly in the first 10 mm in sediment because only a small part of the bivalve is covered by sand. Since the forces generated by the right and left motors are similar, only the force of the left motor (simulating the posterior retractor muscle) is represented for a better graph readout.

By performing displacement steps of 2 mm every 1.1 s, alternately with the left and right motors, the bivalve reaches a depth of 100 mm in about 57 s. Force values between 0 and 144 N have been measured during a burrowing sequence. Measured short force peaks can be explained by inhomogeneities and density variations in the substrate. The closed-loop position control system leads to significant force deviations along the path, depending on whether the bivalve is in contact with compacted or loose sediment.

B. Water Expulsion

To investigate the impact of sediment fluidization on the burrowing efficiency, several experiments have been performed with and without water expulsion. To prevent a motor overload, these measurements can be done only for a reduced depth in sediment.

Figure 8 illustrates the forces necessary to pull downward the burrowing robot into sediment. In the initial phase, the required forces are fairly similar since the bivalve is located at the boundary between water and sediment. After the transition phase, a significant force reduction is observed if water expulsion is active. When the bivalve robot digs into the sediment to a final depth of 50 mm, the required force has been reduced by a factor of 1.7. Since the bivalve robot is position controlled, water expulsion has no influence on the digging time but improves the burrowing efficiency by a factor of 1.7.

V. DISCUSSION

A. Proposed Approach

This paper describes the design and realization of an experimental setup to investigate the burrowing locomotion of bivalves. This apparatus consists of bivalve shells generated using geometric growth models and realized as plastic objects by a 3D printer, a tank providing an underwater sandy environment and an external actuation system. Current results have shown that artificial clams can be burrowed and that the setup allows collecting very useful data about the burrowing process and the influence of different factors such as overall shape, sculpture, burrowing parameters and water expulsion.

B. Biological Relevance

During the burrowing process, bivalves press water out of the mantle cavity and into the surrounding sediment. This is done by quick contractions of the adductor muscles to partially close the shell. Since this was discovered, it has been assumed that the resulting loosening of the sediment reduces the resistance to penetration. It could be shown

experimentally that the rocking motion combined to sediment fluidization enables significant energy savings for digging operations.

A major criterion for the usefulness of the proposed setup is its ability to authentically mimic biological bivalve morphology and burrowing behavior. The closeness to nature is limited by several technical restrictions.

(a) The current geometric model allows only radial and com-marginal sculptures and mixtures of the two (leading to a coffered pattern). It is not possible to generate skew, asymmetric or locally varying sculptures. (b) The size of the printed shells lies in the upper range of natural shell sizes (about 10 cm). This is partly due to the limited printer resolution. Consequently, we use sand with grain sizes slightly above average (0 to 4 mm and 0.7 to 1.2 mm). But it cannot be expected that all the relevant physical processes scale to the used magnitude. (c) The density distribution of an artificial bivalve made of ABS (acrylonitrile butadiene styrene) shells and inner metal parts is different from a natural bivalve consisting of calcite/aragonite and organic material. (d) The rotation axes during the burrowing sequence depend on the attachment location of the muscles/strings. While the muscles of living bivalves work on contact points dorsally inside the shell, the strings in our setup are tied to a metal part ventrally protruding from the shell. (e) All soft body parts including the foot are currently missing.

VI. FUTURE WORK

Ongoing experiments consist in testing different shell shapes in order to understand their role in the burrowing locomotion. A more sophisticated geometric model that allows skew sculpture will allow testing a larger variety of different shells. The influence of sediment has also to be further investigated. In particular, the influence of grain size on the burrowing performance is to be analyzed in correlation with the shell morphology.

The final goal is to develop an autonomously burrowing robot including an anchoring foot to mimic the bivalve behavior. In a first step, the water expulsion mechanism using rubber tubes will be replaced by and compared to an artificial bivalve with shells that can be opened and closed. In a seconds step, a mechanically autonomous burrowing robot will be realized by adding an artificial foot made from soft material.

VII. ACKNOWLEDGMENTS

Many thanks to Rolf Pfeifer, Ruedi Füchslin, Marc Ziegler and the other members of the AIlab for their support. We also would like to thank the Swiss National Science Foundation for their financial support.

REFERENCES

[1] E.R. Trueman, Bivalve Mollusks: Fluid Dynamics of Burrowing, Science, New Series, Vol. 152, No. 3721, pp. 523-525, 1966.
[2] E.R. Trueman, A.R. Brand and P. Davis, The dynamics of burrowing of some common littoral bivalves, Journal of Experimental Biology, Vol. 44, pp. 469-492, 1966.
[3] A. Seilacher, Constructional Morphology of Bivalves – Evolutionary Pathways in Primary Versus Secondary Soft-Bottom Dwellers, Palaeontology, Vol. 27, pp. 207-237, 1984.
[4] D. Raup and A. Michelson, Theoretical Morphology of the Coiled Shell, Science, Vol. 147, pp. 1294-1295, 1965.
[5] D.R. Fowler, H. Meinhardt and P. Prusinkiewicz, Modeling seashells, Computer Graphics, Vol. 26, pp. 379-387, 1992.
[6] O. Hammer and H. Bucher, Models for the morphogenesis of the molluscan shell, Lethaia, Vol. 38, pp. 111-122, 2005.
[7] M.B. Cortie, Models for mollusk shell shape, South African Journal of Sicence, Vol. 85, pp. 454-460, 1989.
[8] C. Illert, Formulation and solution of the classical seashell problem. 2. Tubular 3-dimensional seashell surfaces, Nuovo Cimento della Societa Italiana Di Fisica D, Vol. 11, pp. 761-780, 1989.
[9] T. Okamoto, Analysis of Heteromorph Ammonoids by Differential Geometry, Palaeontology, Vol. 31, pp. 35-52, Part 1, 1988.
[10] E. Savazzi, C++ classes for theoretical shell morphology. Computers and Geosciences, Vol. 19, pp. 931-964, 1993.
[11] S.M. Stanley, Shell Form and Life habits in the Bivalvia (Mollusca), Memoirs of the Geological Society of America, Vol. 125, 1970.
[12] S.M. Stanley, Why clams have the shape they have: an experimental analysis of burrowing, Paleobiology, Vol. 1, No. 1, pp. 48-58, 1975.
[13] S.M. Stanley, Bivalve Mollusk Burrowing Aided by Discordant Shell Ornamentation, Science, Vol. 166, pp. 634-635, 1969.
[14] E. Savazzi and H. Pan, Experiments on the frictional properties of terrace sculptures, Lethaia, Vol. 27, pp. 325-336, 1994.
[15] A.G. Winter, A.E. Hosoi, A.H. Slocum and R.L.H. Deits, The Design and Testing of RoboClam: A Machine Used to Investigate and Optimize Razor Clam-Inspired Burrowing Mechanisms for Engineering Applications, Proceedings of the ASME 2009 International Design Engineering Technical Conferences & Computers and Information in Engineering Conference, IDETC/CIE, 2009.
[16] E.R. Trueman, Dynamics of Burrowing in Ensis (Bivalvia), Proceedings of the Royal Society of London Series B – Biological Sciences, Vol. 166, Issue 1005, pp. 459-&, 1967.
[17] B. A. Trimmer, A. E. Takesian, B. M. Sweet, C.B. Rogers, D. C. Hake and D. J. Rogers, Caterpillar locomotion, a new model for soft-bodied climbing and burrowing robots, Proceedings of the 7th International Symposium on Technology and the Mine Problem, Monterey, CA May 2-5, 2006.
[18] Dimension® http://www.dimensionprinting.com/.
[19] LinMot® http://www.linmot.com/.

Appendix C

Bivalve burrowing robots: correlating shell morphology and movement pattern with burrowing efficiency

Reprinted from:

Daniel P. Germann, Wolfgang Schatz and Peter Eggenberger Hotz, *Bivalve burrowing robots: correlating shell morphology and movement pattern with burrowing efficiency*, Design and Nature V, WIT Transactions on Ecology and the Environment, Vol 138, pp. 389-402, June, 2010.

Bivalve Burrowing Robots – Correlating Shell Morphology and Movement Pattern with Burrowing Efficiency

D. P. Germann, W. Schatz and P. Eggenberger Hotz
Artificial Intelligence Laboratory, University of Zurich, Switzerland;
Academic Services Centre, University of Lucerne, Switzerland;
Mærsk-McKinney-Møller Institute, University of Southern Denmark, Denmark

Abstract

This work examines correlations between functional morphology and behaviour in the instance of the burrowing locomotion of bivalves. A comparatively simple and assessable behaviour and a rich fossil record documenting the evolutionary adaptations in morphology make these animals adequate for investigation. In this paper a robotic setup to simulate the burrowing behaviour of bivalves is presented. Models of both natural bivalve shell shapes and artificially designed shapes are pulled into sediment in the rocking modality these animals typically use. Different shapes, motion patterns and a water expulsion mechanism are evaluated and compared in terms of burrowing performance. The results presented here and further experiments using the (improved) platform may shed light on how bivalves burrow, how features of functional morphology evolved and how efficient automatic burrowing devices may be constructed.
Keywords: biorobotics, biomimetics, underwater robots, functional morphology, burrowing locomotion, shell morphology, bivalves, artificial evolution

1 Introduction

This work pursues a synthetic ("understanding by building") rather than an analytic approach for understanding functional morphology and its influence

on behaviour in the case of bivalves. Biomimetic research usually focuses on using nature as inspiration to solve technical problems in a novel and elegant way and build useful applications. The approach taken here is the opposite one, as engineering and the building of a robotic experiment setup are used to tackle concrete questions of bivalve burrowing and general questions of the correlation of functional morphology and behaviour. As it is technically difficult to closely mimic natural bivalves, the built artificial ones are compared among themselves. This can be done systematically, as the shapes are generated in the computer by mathematical models and turned into physical objects by a 3D printer. This allows total control over the morphology and the separation of the effect of single parameters.

Bivalves have been extensively studied in a biological, ecological and palaeontological context. They make up a considerable part of the entire fossil record. The animals consist of a soft body enclosed by two valves that are opened passively by the joint between them (the ligament) and closed actively by usually two strong adductor muscles. Burrowing bivalves have a tongue-like muscular extension of their soft body that is called foot. It can protrude out of the shell and is important for the burrowing process.

Raup [1] (1965) was among the first to geometrically model the bivalve shell. Bivalve shells (like the shells of snails) can be generated by sweeping a circular aperture curve along a 3D helicospiral (see, e.g., Fowler [2] and Hammer [3]). The spiral is logarithmic and the aperture scaled up along the path, creating the characteristic convoluted shape.

In order to burrow themselves into the sediment, bivalves use a two-anchor system. The dynamics of burrowing were first described in greater detail by Trueman [4]. He identified the motion sequence described in figure 1.

It was recognised early on that the morphology of the shell and foot have a large impact on the burrowing performance. A notable physical experiment was performed in 1975 by Stanley [5]. He produced a cast of a specimen of *Mercenaria mercenaria* that has a blunt anterior area and tested it in real sediment. By comparing the burrowing performance to a second model where he had altered the shape to display a sharper front edge, he could explain the advantage of the blunt anterior region of this particular species.

Stanley [6] also found that ridges at a right angle to the burrowing direction are advantageous and used with rocking motions covering a small angle, while v-shaped ridges are also possible, leading to larger rotation angles. Savazzi [7] summarises that the sculpture (surface structure) amplitude increases with sediment grain size, that the sculpture profile should be asymmetric and the gentle slope facing the burrowing direction.

There has been a variety of different burrowing robots. Most of them are conceived of as applications in a bionics context and not as means to tackle biological questions. Recently, a bivalve burrowing robot called RoboClam and inspired by the fast burrowing bivalve family *Ensis* was built at MIT (Winter [8]). Another example of a burrowing robot is given by Trimmer [9].

In Koller-Hodac [10], we described in detail the basic setup used also

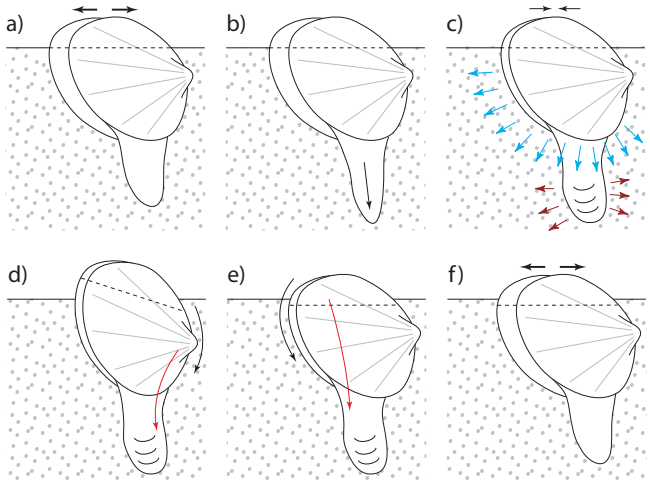

Figure 1: The *burrowing sequence* for bivalves as described by Trueman [4]. (a) The clam is in erect position (sagittal plane vertical), partially burrowed in the sediment. The valves are open to anchor the shell, i.e. to prevent back-slippage. (b) The foot probes deeper into the sediment. (c) The adductor muscles contract, partially closing the shell. The water expelled from the cavity liqefies the surrounding sediment to reduce the resistance to penetration. From the soft body inside the shell, blood is pressed into the foot, which is inflated and serves as a new anchor. (d) The anterior retractor muscle (red arrow) pulls the front side of the bivalve towards the foot, leading to a rotation of the shell (black arrow). (e) In the same way, the posterior retractor muscle rotates the shell back into the erect position. (f) The two rotations around different rotation axes led to a net downward translation, as illustrated by the dashed line. In a recreation phase, the valves open again to allow for another burrowing cycle starting at (a).

for this work and reported first test results. Differences were measured in performance depending on whether water expulsion was used or not.

2 Methods and Materials

2.1 Tank

The burrowing experiments were performed in a cubic glass tank with a content of 216 ℓ. It is filled with normal tap water and a well-rounded quartz sand with grain sizes between 0.7 and 1.2 mm. A structure mainly built from aluminium plates keeps the sand in a restricted area of the tank to facilitate maintenance. See figure 2 for a picture of the tank.

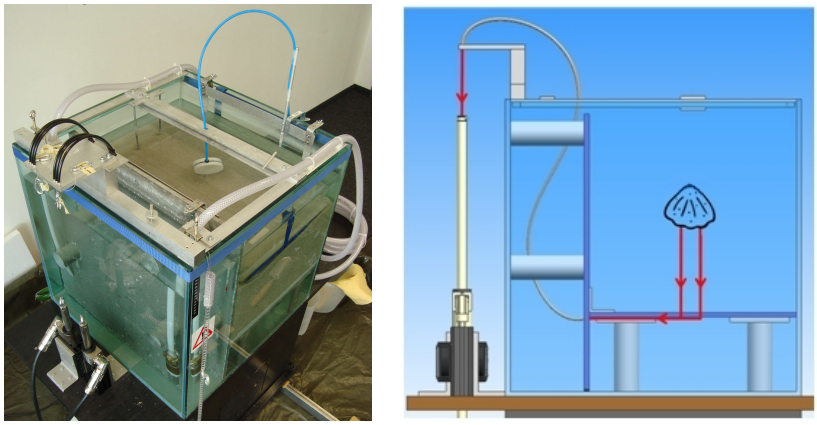

Figure 2: (left) The experimental burrowing setup. (right) A schematic drawing of the bivalve model, the tank and the actuation mechanism. The red arrows show the track of the strings that are attached to the shell and to two linear motors that pull the bivalve into the sediment. The strings are deviated to avoid cutting the glass bottom of the tank.

2.2 Shell Models

It would be possible to use real shells to perform physical experiments, but for our work we artificially generate them using mathematical models in the computer. This procedure has several advantages: (1) We exert total control on the morphology of the shells. The exact geometry is always known, which simplifies comparison. (2) We can potentially generate any shell form, even if they do not exist in nature. This gives the possibility to experimentally analyse the whole theoretical morphospace of bivalves by systematically varying the parameters. (3) Shells can be produced in larger quantities. This does not only allow replacing broken shells by another copy, increasing the degree of reproducibility, but also gives rise to the possibility of performing evolutionary robotics experiments later.

The program uses a mathematical model similar to the one described in the introduction, where an aperture curve is swept along a 3D helicospiral. Every shell consists of an overall shape and a higher frequency surface sculpture. The sculpture is added to the surface by shifting its points in normal direction. The main parameters for shell generation are the aperture curve, the scaling factor from one to the next growth step, and the sculpture profiles in radial and commarginal direction. The curves are in our case represented using NURBS (non-uniform rational basis splines) in order to give a large flexibility in generating different shell shapes.

The generated shell geometries are turned into ABS plastic models using a dimension® 3D printer [11] and its CatalystEx software. The shells are

printed in solid mode to avoid the plastic from absorbing too much water. The resolution of the printer is about 0.5 mm.

Two plastic valves produced by the printer are then glued together. Two short strings ending with screw couplings allow easy attachment and detachment to the actuation system (see figure 3).

2.3 Actuation

Following the burrowing sequence described by Trueman [4], a rocking downward motion is applied to the shell. The external actuation mechanism consists of two linear motors that are installed vertically beside the tank and connected to the models by strings deviated to pull them into the sediment from below (see figure 2 (right)). To mimic the rocking motion of bivalves during burrowing, the motors are pulling alternately. The motors thus simulate the retractor muscles of real bivalves that are part of the foot and pull the shell deeper into the sediment. The right motor is connected to the front (anterior) part of the shell and thus representing the anterior retractor muscle. The left motor simulates the hind (posterior) retractor muscle. In the current setup, an artificial foot is missing. We use two LinMot® linear motors [12] with the following characteristics: stroke max.: 660 mm, peak force: 206 N, force constant: 25.8 N/A, max. velocity: 2.6 m/s, position repeatability: ±0.01 mm.

2.4 Water Expulsion

The water expulsion that living bivalves use for liquefying the sediment and that is induced by closing the valves is simulated in our setup by ejecting water through the holes in a peripheral rubber tube. A pump produces a permanent water pressure that is released by a valve activated by the controllers of the linear motors.

2.5 Control

The linear motors are controlled by the software LinMot® Talk. To synchronise the motor motion with the water expulsion, the commands for the water valve are integrated into the controller programs of the motors. A burrowing run contains the following command sequence for the right motor: (a) Go to the starting position and pause. (b) Open the valve for water expulsion and close it again after 100 ms. (c) Pull the shell one step further into the sediment. (d) Pause. (e) Repeat starting at (b). The controller of the left motor does not contain commands for the water expulsion valves, but otherwise executes the same command sequence, offset by a certain time lag. During the pause in (a), the shell is manually put in an erect position above the sediment surface. The size of the burrowing steps in (c) was usually set to a value of 5 or 8 mm.

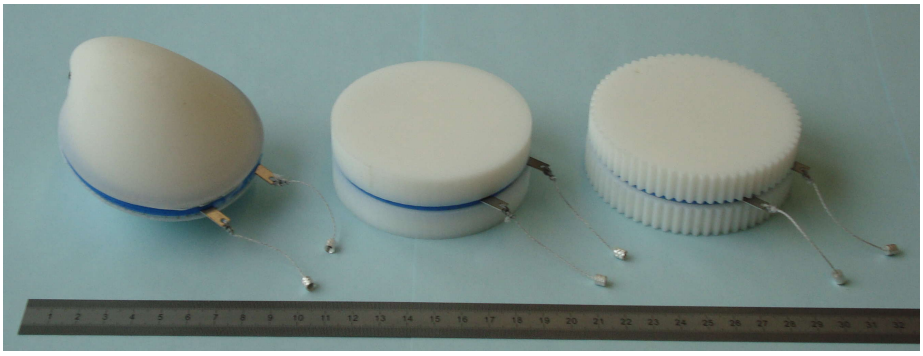

Figure 3: Plastic shells with a peripheral rubber tube (blue) with holes to emit water. The two strings with screw couplings allow easy attachment and detachment of the shell. The picture shows the three shells compared in the results section (from left): smooth bivalve shape, smooth disk shape and ridged disk shape.

Following the standard way of programming the linear motors, the first kind of controller used position commands to prescribe a burrowing motion that was precisely followed. As this leads to the same burrowing depth for all bivalve models, the force curve was analysed instead. Larger pulling forces for the same motion pattern imply a less efficient shape.

A second kind of controller was implemented to better reflect the biological reality. The force for pulling the shell into the sediment was restricted. This allowed for the possibility of a deviation of the actual position from the programmed target position when the penetration resistance was too large.

2.6 Experiments

Using the described setup, several systematic experiments were performed. Many parameters determining the morphology and behaviour of the robot bivalves can be varied, including the overall shell shape, the amount and shape of radial and commarginal sculpture and the timing of the elements of the burrowing cycle. So far, only parameters with a supposedly larger effect have been analysed, namely the overall shape, peripheral ridges, water expulsion and pulling angle.

10 to 20 identical burrowing runs were executed immediately one after the other for one experiment. In order to change only one factor from experiment to experiment, the initial conditions before each burrowing run had to be standardised. In the case of the sediment, a rake was moved to a certain depth and up through the sand to loosen the compacted state from the last run. The sediment height and planarity was established by dragging a metal slat over beams attached to the tank walls.

To judge the performance of a particular morphology or burrowing pattern, we consider burrowing depth and the energy used for burrowing most important. Energy cannot be measured directly easily, so we use force. The linear motors provide internal sensors for both position and force (current), therefore we use them to record data about the burrowing performance. The data is logged by LabView [13] and evaluated using Matlab [14].

3 Results

This section will summarise the results of the experiments. Several sources of error (see discussion) led to fluctuations and made it hard to produce significant results. In all experiments, the right motor had to exert a larger force or moved to a lesser depth than the left motor. This may be due to a slightly shorter right string. Force values are consequently only compared for either of the motors but not between the motors. In comparisons we consider morphologies or configurations to be "better" if they lead to a larger burrowing depth or to smaller pulling forces.

3.1 Data

As the strings are always straight, the position of the motor sliders is taken to reflect the burrowing depth. The force exerted by the motors is proportional to the current, so we compute the force necessary for burrowing by multiplying the force by the motor specific force factor and adding the weight of the sliders, as the motors are placed vertically. These computations are already done by LabView. The resulting data record for a single burrowing experiment consists of a series of triplets (t_i, f_i, x_i), i.e. time, force and position, respectively. Usually, 20 ms are used as measurement time intervals, values between 10 and 100 ms are possible. The sensors sometimes produce faulty values (values outside the range of physically possible values). We filter the data as follows: invalid positions are replaced by the linear interpolation between the next valid neighbouring values; we cannot drop these values entirely, because the number of data points has to be consistent with the other data sets for further evaluation; extreme values like burrowing depths, however do not change by this procedure. Invalid forces are replaced by `NaN` and ignored for the evaluation. Gaps in the time sequence are completed by the same means (linear interpolation and inserting `NaN`). The average fractions of invalid data are roughly 2% for positions and 5% for forces. Gaps make up 3% of the data.

3.2 Comparison of Shapes

Until now, we mainly tested the three disk-related shapes shown in figure 3, i.e. a smooth bivalve shape, a smooth disk shape and a ridged disk shape (shaped like a cogwheel). The diameter of the disks and of the aperture of the

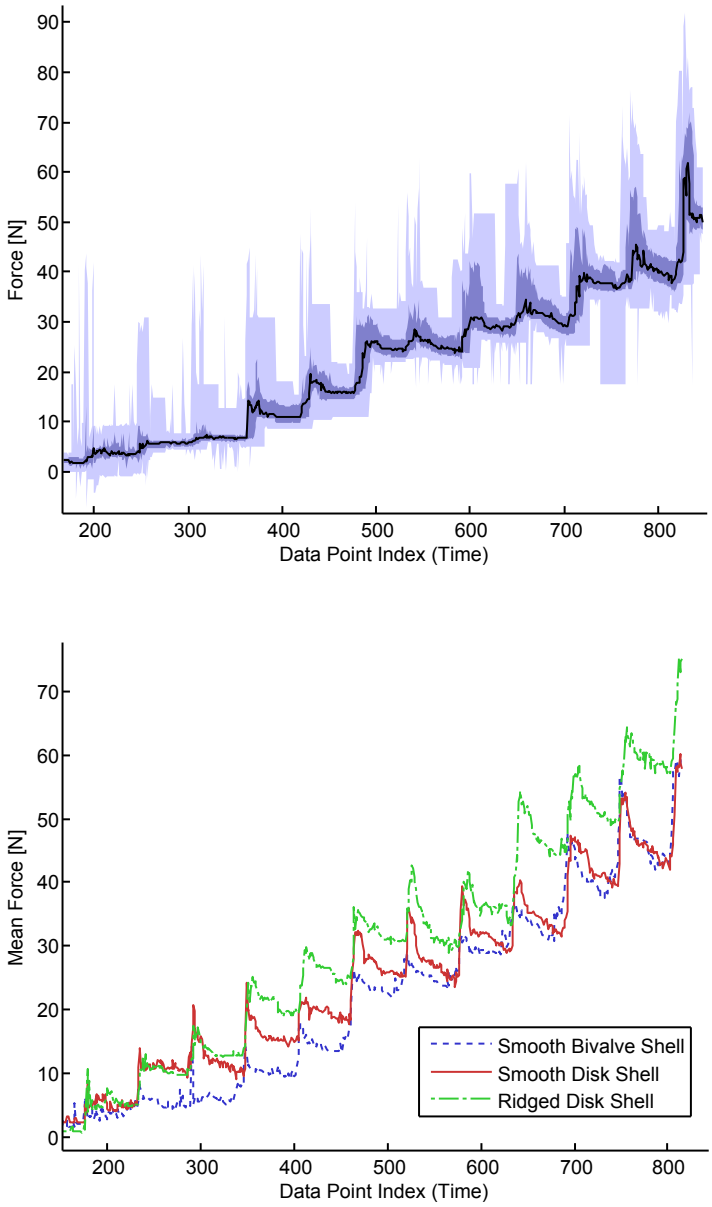

Figure 4: (Top) The pulling force of the right motor for the smooth disk shell, water expulsion deactivated. Shown is the median (black), the 25% and 75% (dark blue) and the 2.5% and 97.5% quantiles. (Bottom) The mean pulling forces exerted by the right motors for the three shapes, water expulsion activated. Each curve is computed from 20 burrowing experiments. A curve has roughly the shape of a step function with 12 steps that correspond to the burrowing cycles.

bivalve shape are equal. Also, the masses are almost the same. Differences in burrowing performance of the three models should therefore reflect the differences in shape. The bivalve shape does not represent any particular living species. It is artificially designed to be similar to the disk shapes but is generated using the shell generation method described earlier. The wavelength of the ridges of one of the disk shells is 4 mm, the peak-to-peak amplitude 2 mm.

Using the position control program, the pulling forces shown in figure 4 were measured. The top graph shows the pulling force applied during one burrowing run. As the model is pulled deeper into the sediment, the force increases. The periodic steps in the curve correspond to the burrowing cycles. The bottom graph in figure 4 shows the mean force curves for the three different shapes. The error margins are similar to the top chart but were omitted for better readability. The ridged shell consistently performed worst, the bivalve shape tended to be better than the smooth disk shape.

3.3 Water Expulsion

Figure 5 (top) shows a boxplot of the burrowing depths reached with different configurations and the force control program. As already mentioned, there is a difference between the depth reached by the left and the right motor. Additionally, the burrowing runs using water expulsion usually penetrate deeper. The effect is not always present, but positive if it is. In the bivalve case it seems to be rather significant, while in the disk case in this graph, there is only a small difference.

3.4 Pulling Angle

In bivalve burrowing, the rotation angle induced by the retractor muscles is often adjusted to the sculpture and influences burrowing performance. By altering the pulling direction of the strings, we can change the amount of rotation in our setup. Therefore we tested two different configurations. The setting provides three different pairs of strings of which we used the outmost one, where the holes in the bottom plate are at a distance of 112 mm. In the second configuration, the same string pair was used in a crossed way, i.e. the shell was rotated around the vertical axis by 180°. In the uncrossed setting, the strings pull the anterior attachment site forward at an angle of 8° to the vertical line, in the crossed setting they pull it backward at 14°. As the second setting implies a more tangential pulling direction, it leads to a bigger rotation.

See figure 5 (bottom) for a comparison of the two configurations. Figure 6, however, shows that the ranking is not constant throughout the burrowing process.

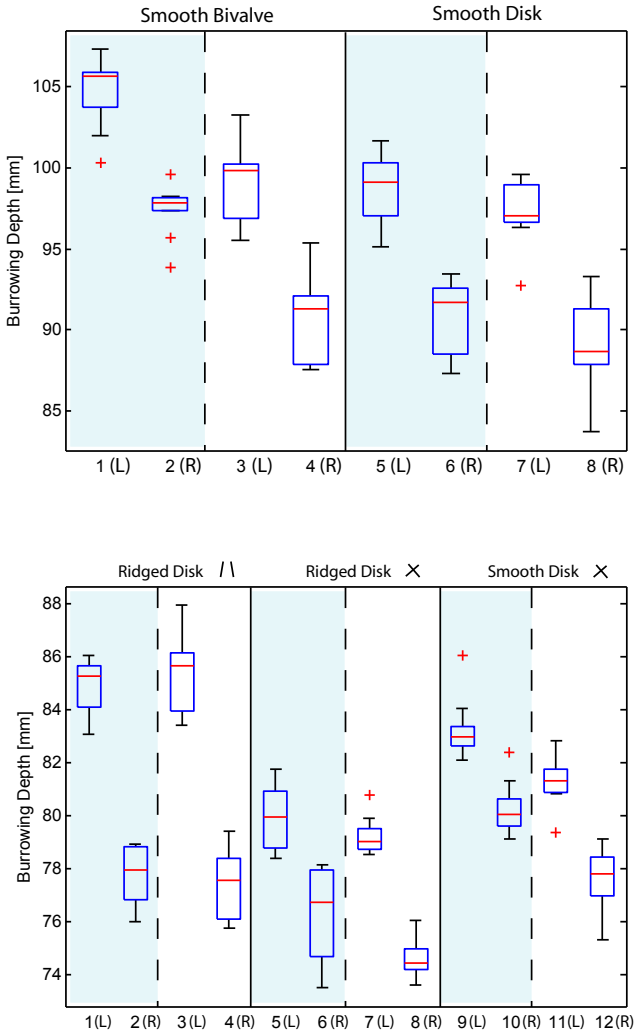

Figure 5: (Top) The left half of this boxplot shows the burrowing depths for the smooth bivalve shape, the right half for the smooth disk shape. (Bottom) Burrowing depths for the ridged and smooth disk shapes. For indices 1-4, the normal uncrossed string configuration was used, for indices 5-12 the crossed string configuration. In both plots, a light blue background stands for activated water expulsion. Odd indices show the results for the left motor, even indices for the right motor. Each set summarises the data of 10 repetitions of the same burrowing experiment. The Matlab [14] boxplot function was used, which plots the median, the 25% and 75% quantiles and the most extreme values that are not outliers as whiskers.

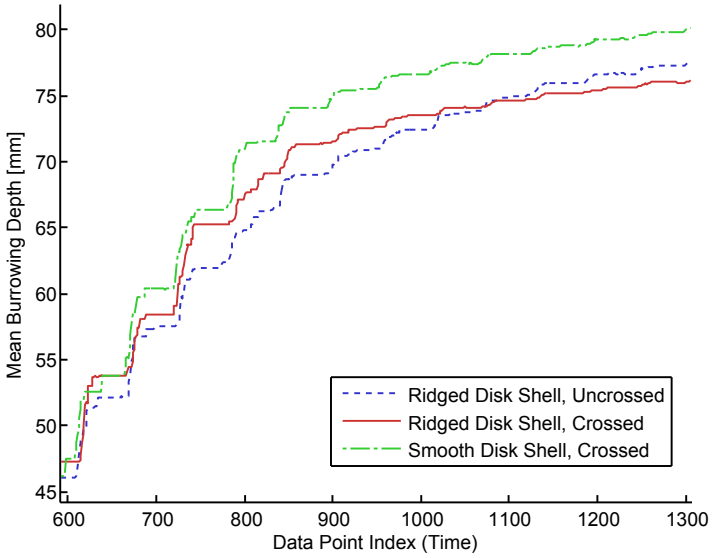

Figure 6: Comparison in burrowing depth of the ridged and smooth disk shells with crossed and uncrossed string configurations. A part of the mean curves for the right motor are shown. Confidence intervals do overlap and are not shown for a better readability. Each mean is computed from 10 data sets, the quantiles in figure 5 (bottom) give an estimation of the respective curve variances.

4 Discussion

4.1 Morphology

According to the data collected so far, the bivalve shape is better suited for burrowing than its crudest approximation, a disk. We did not expect the ridged shape to perform worse than the other two. As sculpture amplitude and grain size are correlated in nature, further experiments using different amplitudes and grain sizes should investigate this issue. Sculpture also has the function of preventing the bivalve from being excavated by water current and buoyancy effects. This cannot be tested easily with the current approach because the strings do not allow the shell to move upwards.

4.2 Water Expulsion

The current method of simulating the water expulsion does not capture an important aspect of the real mechanism: when closing the valves, bivalves do not only eject water, but the shell contraction itself also makes room for liquefied sediment around it.

In the presented experiments, water expulsion was less effective than first test results suggested. This may be due to a design change we made: to avoid the tube holes being blocked by sand grains, we reduced the diameter of the holes below the grain size while increasing the number of holes. It is also possible, that the lack of shell contraction limits the effect because the ejection is not strong enough to displace the compacted sediment around the shell. Future improvements of the shell models including an opening and closing mechanism may shed light on this issue.

4.3 Position control and force control

The controllers prescribing the position were easier to program and to handle, because they correspond to the manner how these industrial motors are normally used. The second kind of controllers that limited the forces, however, turned out to produce more realistic simulations. The increasingly smaller burrowing steps reflect the way natural bivalves burrow much better. The force that bivalve muscles can exert is also limited and probably determines how far it moves in a burrowing cycle. While the force curves in figure 4 are hard to interpret, depth curves like in figure 6 are more readable.

4.4 Pulling angle

Figures 5 (bottom) and 6 show again, that the smooth disk outperforms the ridged disk. However, the second figure shows in addition, that the ranking of the ridged shell is not stable with respect to the crossed and uncrossed configurations. The uncrossed version (smaller rotation angle) is worse a long time until it finally surpasses the crossed version (larger rotation angle). An explanation may be that initially, a large rotation has a similar effect as water expulsion, loosening the sediment and thus reducing penetration resistance. As the shell gets deeper into the sediment and the motion more restricted due to larger friction, this effect is weakened. In this later phase, direct pulling may thus become more effective.

4.5 Sensor Data

As the force is measured indirectly by the current consumed by the motors, it is subject to peaks and fluctuations in the control circuit. The forces react sensitively to small resistance disturbances in order to execute the control program with high precision. This type of fluctuations are not reproducible.

The positions measured by the motors do not reflect the actual burrowing depth perfectly. The length of the strings expands on average by 1.5 mm per kilogram and metre. Also the metal parts the setup is made of do slightly bend. The strings are connected by knots that may tighten slightly when higher forces are applied.

4.6 Sediment

An error source that is hard to handle is the configuration of the sediment. The spatial distribution of grain sizes and the state of compaction are different for every experiment run. The state of compaction of the sediment seems to have a large effect on the burrowing performance. The introduction of a rake for a deeper and more systematic sediment perturbation before a burrowing run increased the burrowing performance of the shells markedly. In order to produce more reliable and less noisy data, an automated standardisation technique should be implemented.

Abrasion of the plastic shells by the sand could not be detected yet. After more than 100 burrowing runs, the front ridges of the ridged disk shell are still intact.

5 Future Work

Although the evaluation of the experiments led to interesting insights into the burrowing mechanism of bivalves and how it may be simulated, the setup has to be improved further to produce more reliable and significant data. It should, e.g. be ensured that the strings are of the same length. As natural bivalves often burrow in a direction lying between anterior and ventral, a shorter right string does not contradict the conditions found in nature, but it makes data evaluation more difficult.

The current geometric model can only produce mixtures of radial and commarginal surface sculpture. As certain types of skew sculpture are considered beneficial for burrowing, they should be integrated into the model.

To overcome the limitations of using only the internal sensors of the motors, we are building shells containing additional force sensors. Optical tracking of the shells will allow more precise burrowing depth measurements and in addition the possibility to also capture the orientation of the shell. Measuring depth and forces redundantly will lead to more precise data, hopefully enabling us to compare differences surface sculptures.

Once morphological changes are expressed in burrowing performance reliably, we will apply the control of an artificial evolutionary system to evolve interesting shapes and shed light on palaeontological questions. Specific recent or fossil specimens may be tested in sediment by using a computed tomography (CT) scanner to generate virtual 3D models and printing them by the 3D printer. Burrowing performance tests in different sediment types may shed light on the mode of life of species with previously unclear habitat.

To further improve and expand the robotic platform, the water expulsion mechanism using rubber tubes will be replaced by and compared to an artificial bivalve featuring a mechanism for opening and closing the valves. The final goal is to construct a mechanically autonomous burrowing robot by adding an artificial foot.

Acknowledgements

Many thanks to A. Koller-Hodac, K. Dietrich, A. Gilgen and P. Brändli from the University of Applied Sciences in Rapperswil (HSR) for their competent contribution in building the setup. We also thank R. Pfeifer, R. Füchslin, M. Hadorn and the other members of the AIlab for their support and the Swiss National Science Foundation for funding the project.

References

[1] Raup D. and Michelson A., Theoretical Morphology of the Coiled Shell, Science, Vol. 147, pp. 1294-1295, 1965.

[2] Fowler D.R., Meinhardt H. and Prusinkiewicz P., Modeling seashells, Computer Graphics, Vol. 26, pp. 379-387, 1992.

[3] Hammer O. and Bucher H., Models for the morphogenesis of the molluscan shell, Lethaia, Vol. 38, pp. 111-122, 2005.

[4] Trueman E.R., Bivalve Mollusks: Fluid Dynamics of Burrowing, Science, New Series, Vol. 152, No. 3721, pp. 523-525, 1966.

[5] Stanley S.M., Why clams have the shape they have: an experimental analysis of burrowing, Paleobiology, Vol. 1, No. 1, pp. 48-58, 1975.

[6] Stanley S.M., Bivalve Mollusk Burrowing Aided by Discordant Shell Ornamentation, Science, Vol. 166, pp. 634-635, 1969.

[7] Savazzi E. and Pan H., Experiments on the frictional properties of terrace sculptures, Lethaia, Vol. 27, pp. 325-336, 1994.

[8] Winter A.G., Hosoi A.E., Slocum A.H. and Deits R.L.H., The Design and Testing of RoboClam: A Machine Used to Investigate and Optimize Razor Clam-Inspired Burrowing Mechanisms for Engineering Applications, Proceedings of the ASME 2009 International Design Engineering Technical Conferences & Computers and Information in Engineering Conference, IDETC/CIE, 2009.

[9] Trimmer B.A., Takesian A.E., Sweet B.M., Rogers C.B., Hake D.C. and Rogers D.J., Caterpillar locomotion, a new model for soft-bodied climbing and burrowing robots, Proceedings of the 7th International Symposium on Technology and the Mine Problem, Monterey, 2006.

[10] Koller-Hodac A., Germann D.P., Gilgen A., Dietrich K., Hadorn M., Schatz W. and Eggenberger Hotz P., Actuated Bivalve Robot – Study of the Burrowing Locomotion in Sediment, IEEE International Conference of Robotics and Automation (ICRA 2010), in press, 2010.

[11] Dimension® 3D printer, model bst 768; CatalystEx, Version 4.0.1, Stratasys Inc.; `www.dimensionprinting.com`

[12] LinMot® linear motors, P01-37x240F/460x660-C; LinMot Talk1100-V3.9, NTI AG; `www.linmot.com`

[13] LabView™, Version 8.6, National Instruments, `www.ni.com/labview/optin/`

[14] Matlab®, Version R2009b, The MathWorks Inc., `www.mathworks.com`

Appendix D

Artificial Bivalves – The Biomimetics of Underwater Burrowing

Reprinted from:

Daniel P. Germann, Wolfgang Schatz and Peter Eggenberger Hotz, *Artificial Bivalves – The Biomimetics of Underwater Burrowing*, Procedia Computer Science, Volume 7, 2011, Pages 169-172, ISSN 1877-0509, 10.1016/j.procs.2011.09.012. http://www.sciencedirect.com/science/article/pii/S1877050911005722

Artificial Bivalves

The Biomimetics of Underwater Burrowing

Daniel P. Germann
Artificial Intelligence Laboratory
University of Zurich
Andreasstrasse 15
8050 Zürich, Switzerland
germann@ifi.uzh.ch

Wolfgang Schatz
Academic Services Centre
University of Lucerne
Pfistergasse 20
6003 Luzern, Switzerland
Wolfgang.Schatz@unilu.ch

Peter Eggenberger Hotz
Mærsk-McKinney-Møller Institute
University of Southern Denmark
Campusvej 55
5230 Odense M, Denmark
eggen@mmmi.sdu.dk

ABSTRACT

Biomimetics is a fruitful combination of biology and engineering, leading not only to technological innovations but also new insights into biological questions. In this ongoing project, embodied artificial intelligence (embodied AI), artificial evolution and palaeontology are combined to investigate the functional morphology of bivalves. This cross-fertilization allows to expand biomimetics from current biological systems to the whole evolutionary history and to apply the synthetic approach common in embodied AI as a method to tackle open palaeontological questions. So far, a robotic platform has been built to mimic the burrowing technique applied by bivalves. First results show interesting insights into underwater burrowing. We plan to build a more complex version of the system and to perform evolutionary robotics experiments.

Keywords

Biomimetics, bionics, artificial evolution, palaeontology, bivalves, burrowing, functional morphology

1. INTRODUCTION

Bionics is recognized as a key discipline for the future. Since biomimetics involves the combination of two disciplines, biology and engineering, there may be an information flow in both directions. The predominant path is to draw inspiration from nature to solve technical problems, but adopting an engineering (synthetic) approach can also contribute to biological knowledge. In our project, we work in a disciplinary and methodical matrix of embodied AI, (evolutionary) robotics, artificial and natural evolution, functional and theoretical morphology and sedimentology.

The bivalve burrowing process is complex partly because of the physical properties of sandy sediment. But morphology and motion can be modelled using only a few parameters, such that they lend themselves well to artificial evolution experiments. Verification is supported by a rich fossil record that documents the evolution of bivalve shell morphology.

The goal of this project is to build increasingly complex models of the burrowing process to investigate (a) correlations in morphology, motion and environment and (b) the evolution of bivalve functional morphology.

[1]Figures 1, 2 and 3 (left) first published in A. Koller-Hodac, D. P. Germann, A. Gilgen, K. Dietrich, M. Hadorn, W. Schatz and P. Eggenberger Hotz, *Actuated Bivalve Robot – Study of the Burrowing Locomotion in Sediment*, Proceedings of 2010 IEEE International Conference on Robotics and Automation (ICRA), 2010.

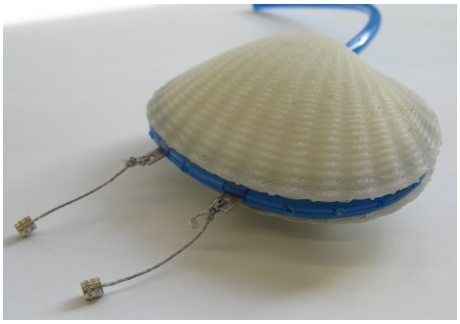

Figure 1: An artificial bivalve shell, generated with a mathematical model and realized by a 3D printer. The model controls the overall shell shape and surface structure (sculpture). A perforated tube along the edge is used to simulate water expulsion (Fig. 2). [1]

2. BACKGROUND

The main components used for burrowing are the overall shell shape, the surface structure (sculpture) and the foot (a tongue-like extension of the soft body). Fig. 2 explains the burrowing process in natural bivalves. Several correlations between shell morphology, burrowing motion and sediment have been reported. For instance, discordant or concentric ridges together with the typical rocking motion may cause a downward force similar to that of a screw turned by a screw-driver [3].

Parameter spaces of mathematical models of morphology (morphospaces, [2]) help to artificially rebuild valves of recent and extinct bivalve specimens but also enable us to explore shapes that have never existed in nature.

In embodied AI, morphology is seen as crucial to producing behaviour. Using a synthetic ("learning by doing") ap-

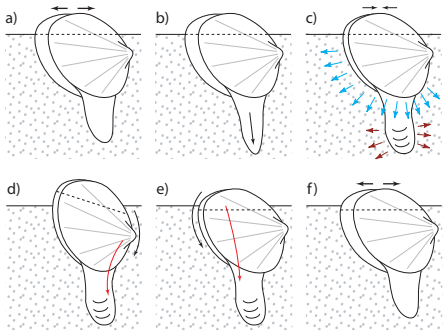

Figure 2: The *burrowing sequence* [4]. (a) The clam is in erect position, partially buried. The valves are open to anchor the shell. (b) The foot probes deeper into the sediment. (c) The valves are adducted to partially close the shell. The thus ejected water liquefies the surrounding sediment to reduce the drag; blood is pressed into the foot, which is inflated and serves as a new anchor. (d) The front side of the bivalve is pulled towards the foot, rotating the shell. (e) The shell is turned back into the erect position. (f) The two rotations around different axes led to a net downward translation, illustrated by the dashed line. In a recreation phase, the valves open again to allow for another burrowing cycle starting at (a). [1]

proach, robots are used to test hypotheses of how behaviour emerges. Evolutionary robotics performs artificial evolution not only in simulation but with real robots, because simulations often do not capture all relevant aspects of reality – like in the case of a granular sediment.

There have been many burrowing robots, based on different principles. Recently, a digging robot inspired by bivalves was built at MIT [5].

3. SETUP AND PRELIMINARY RESULTS

Mathematical models [1] are used to generate bivalve shells in the computer. By changing the parameters either by hand or using evolutionary algorithms it is possible to explore existing and artificial bivalve shapes. Generated morphologies can be used in simulations or turned into real objects using a 3D printer (see Fig. 1).

The printed shell models are used in an experimental setup (Fig. 3) to mimic the burrowing process. Parameters controlling the timing may again be subject to evolutionary algorithms. Preliminary results collected so far suggest that interesting effects on the burrowing efficiency occur and can be investigated, such as the influence of water expulsion (Fig. 2) or a depth-dependent performance of different shapes.

4. CONCLUSION

In this biomimetic project, we propose a robotic setup for simulating the burrowing behaviour of bivalves. We are currently performing more experiments using the existing platform and developing a more sophisticated apparatus more closely mimicking natural bivalves. It will feature a mechanism to open and close the valves and an artificial soft foot to make the bivalve mechanically autonomous. Evolutionary experiments adapting morphology and motion for efficient burrowing will be performed with both setups.

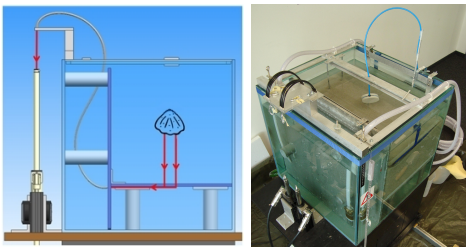

Figure 3: A schematic drawing and a photograph of the current setup. The model of a bivalve shell is set into an tank filled with water and sediment. Two linear motors are vertically attached and pull the model into the sediment via redirected strings. By alternately doing one step after the other, the rocking burrowing motion described in Fig 2 is applied. [1]

By analysing bivalve burrowing, efficient solutions for underwater burrowing may be found. A possible application would be automatic anchoring devices for man-made structures. On the other hand, palaeontological research may profit from a synthetic approach bringing fossil species to life by a robotic device. It is also worth using the platform to further investigate promising ideas such as evolutionary robotics, the co-evolution of morphology and control and the expansion of biomimetics from today's nature to the entire evolutionary history.

5. ACKNOWLEDGMENTS

We would like to thank Rolf Pfeifer, Agathe Koller-Hodac and the Swiss National Science Foundation (SNF).

6. REFERENCES

[1] D. R. Fowler, H. Meinhardt, and P. Prusinkiewicz. Modeling seashells. In E. E. Catmull and B. H. McCormick, editors, *SIGGRAPH '92 conference proceedings*, volume 26.1992,2 of *Computer graphics*, pages 379–387, New York, 1992. ACM Press.

[2] G. R. McGhee. *Theoretical morphology: The concept and its applications*. Perspectives in paleobiology and earth history. Columbia Univ. Press, New York, NY, 1999.

[3] S. M. Stanley. Bivalve mollusk burrowing aided by discordant shell ornamentation. *Science*, 166(3905):634–635, 1969.

[4] E. R. Trueman. Bivalve mollusks: Fluid dynamics of burrowing. *Science*, 152(3721):523–525, 1966.

[5] A. G. Winter, R. L. H. Deits, D. S. Dorsch, A. E. Hosoi, and A. H. Slocum. Teaching roboclam to dig: The design, testing, and genetic algorithm optimization of a biomimetic robot. In *2010 IEEE/RSJ*

University of Zurich[UZH]
Department of Informatics

Artificial Bivalves

ai lab

The Biomimetics of Underwater Burrowing

Daniel P. Germann, Wolfgang Schatz and Peter Eggenberger Hotz

1. Biological Background

Burrowing bivalves use a two-anchor mechanism to dig themselves into sandy underwater sediment.

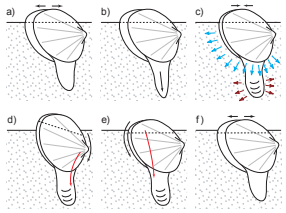

Fig. 1: Bivalve burrowing [1]. (a) erect position, anchored by open valves, (b) foot extends, (c) valves are adducted causing water expulsion and foot expansion (anchoring), (d) front muscle contraction causing forward rotation, (e) back muscle contraction causing backward rotation, (f) valves are reopened now in a deeper position. Another burrowing cycle starts again at (a).

The bivalve functional morphology for burrowing essentially consists of the overall shell shape, the shell surface structure (sculpture) and the shape of the foot.

2. Project Goals

The goal of this ongoing biomimetic project is to build increasingly complex models of the bivalve burrowing locomotion to investigate
a) correlations in morphology, motion pattern and environment
b) the evolution of bivalve functional morphology.

3. Models of Bivalve Morphology

Bivalve shell shapes are generated using a mathematical model [2] based on only a few parameters. It produces an overall shape and a surface structure. Different shapes generated by this model are realized using a 3D printer.

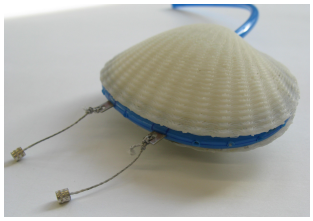

Fig. 2: A printed bivalve model consisting of the shell morphology (white plastic), a perforated rubber tube to simulate water expulsion (blue) and two attachment sites for the actuation strings.

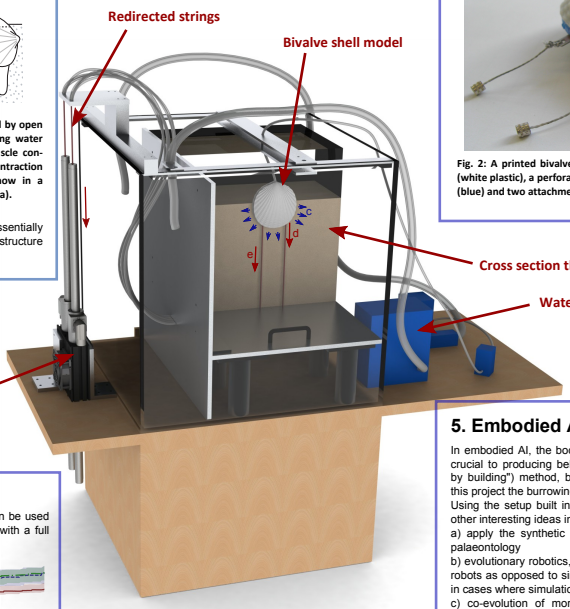

Fig. 4: The setup built to mimic bivalve burrowing. A burrowing motion similar to the one described in fig. 1 is induced by two linear motors attached on the left side. They pull the bivalve model into the sediment by alternately moving one step down. Water expulsion is simulated using a pump and a perforated tube as shown in fig. 2. The letters c-d correspond to the respective steps in fig. 1.

4. Preliminary Results

Proof of concept experiments show that the setup can be used to mimic bivalve burrowing. Systematic experiments with a full statistical analysis have not yet been done.

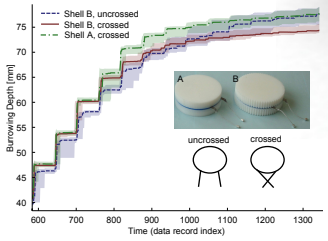

Fig. 3: Graph showing the result of a burrowing experiment to compare three different configurations. The burrowing depth is shown vs. burrowing time. The pulling force was restricted such that higher depth means better burrowing performance. The curves show the median burrowing depth and 0.1/0.9 quantiles of 10 repeated runs for each configuration. The burrowing cycles are clearly visible as steps in the curves. The step size decreases with time like in natural bivalves because the penetration resistance of the sediment increases with burrowing depth. The burrowing performance may not only depend on the configuration but also on burrowing depth.

5. Embodied Artificial Intelligence

In embodied AI, the body morphology of an organism is seen as crucial to producing behaviour. With a synthetic ("understanding by building") method, behaviour is reproduced in real robots; in this project the burrowing behaviour of bivalves.
Using the setup built in this project, it is also possible to pursue other interesting ideas in AI and robotics:
a) apply the synthetic methodology to other diciplines such as palaeontology
b) evolutionary robotics, i.e. artificial evolution performed with real robots as opposed to simulated software agents. This is essential in cases where simulation is difficult, such as in granular materials
c) co-evolution of morphology and controller, instead of only evolving the controller for a fixed robot.

6. Possible Applications

- Locomotion through granular media
- Autonomous underwater burrowing robots
- Automatic anchoring of ships and platforms (see also [3])
- Application as tool in other fields, e.g. palaeontology: identify mode of life of fossil bivalves, compare the rich fossil record of bivalves with results from artificial evolution.

7. Future Work

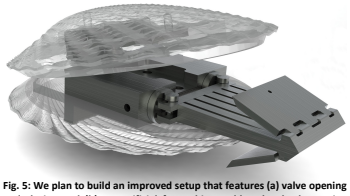

Fig. 5: We plan to build an improved setup that features (a) valve opening and closing and (b) an artificial foot. This would make the burrowing robot mechanically autonomous.
We also plan to perform evolutionary experiments with both setups. This includes (a) reconstruction of the bivalve morphological evolution, (b) tackling palaeontological questions and evolving "optimal" burrowing morphologies and motion patterns.

Acknowledgements

We would like to thank Rolf Pfeifer and the Artificial Intelligence Laboratory as well as Agathe Koller-Hodac from the University of Applied Sciences in Rapperswil (HSR) for their support. We also thank the Swiss National Science Foundation (SNF) for funding this project.

Picture Credits

Fig. 1: This figure is inspired by the figure on page 46 of M. Amler, N. Rogalla and R. Fischer, "Muscheln", ISBN 3-13-118391-8.
Fig. 2: Photo by Alexander Gilgen and Katja Dietrich, HSR.
The CAD parts shown in the images (excluding the shells) were created by Alexander Gilgen, Katja Dietrich (Fig. 4) and Christoph Philipp (Fig. 5) from HSR.
Shell models and renderings by Daniel Germann.

References

[1] E.R. Trueman. Bivalve mollusks: Fluid dynamics of burrowing. Science, 152(3721): 523-525, 1966.
[2] D. R. Fowler, H. Meinhardt and P. Prusinkiewicz. Modeling seashells. In E. E. Catmull and B. H. McCormick, editors, *SIGGRAPH '92 conference proceedings*, volume 26.1992.2 of *Computer graphics*, 379-387, New York, 1992. ACM Press.
[3] A. G. Winter, R. L. H. Deits, D. S. Dorsch, A. E. Hosoi and A. H. Slocum. Teaching roboclam to dig: The design, testing and genetic algorithm optimization of a biomimetic robot. In *2010 IEEE/RSJ International Conference on Intelligent Robots and Systems*, 4231-4235, Piscataway, NJ, 2010. IEEE.

Daniel P. Germann is with the Artificial Intelligence Laboratory, Department of Informatics, University of Zurich, Andreasstrasse 15, 8050 Zürich, Switzerland, *germann@ifi.uzh.ch*
Wolfgang Schatz is with the Academic Services Centre, University of Lucerne, Pfistergasse 20, 6003 Luzern, Switzerland, *Wolfgnang.Schatz@unilu.ch*
Peter Eggenberger Hotz is with the Mærsk-McKinney-Møller Institute, University of Southern Denmark, Campusvej 55, 5230 Odense M, Denmark, *eggen@mmmi.sdu.dk*

Appendix E

Burrowing behaviour of robotic bivalves with synthetic morphologies

Reprinted from:

Daniel P. Germann and Juan Pablo Carbajal, *Burrowing behaviour of robotic bivalves with synthetic morphologies*, Bioinspir. Biomim. 8 (2013) 046009, doi:10.1088/1748-3182/8/4/046009. http://iopscience.iop.org/1748-3190/8/4/046009/

Burrowing behaviour of robotic bivalves with synthetic morphologies

D P Germann[1] and J P Carbajal[2]

[1] Artificial Intelligence Laboratory, Department of Informatics, University of Zürich, Andreasstrasse 15, 8050 Zürich, Switzerland

[2] Department of Electronics and Information Systems, Ghent University, Sint Pietersnieuwstraat 41, 9000 Ghent, Belgium

E-mail: germann@ifi.uzh.ch, juanpablo.carbajal@ugent.be

Abstract. Several bivalve species burrow into sandy sediments to reach their living position. There are many hypotheses concerning the functional morphology of the bivalve shell for burrowing. Observational studies are limited and often qualitative and should be complemented by a synthetic approach mimicking the burrowing process using a robotic emulation. In this paper we present a simple mechatronic set-up to mimic the burrowing behaviour of bivalves. As environment we used water and quartz sand contained in a glass tank. Bivalve shells were mathematically modelled on the computer and then materialized using a 3D printer. The burrowing motion of the shells was induced by two external linear motors. Preliminary experiments did not expose any artefacts introduced to the burrowing process by the set-up. We tested effects of shell size, shape and surface sculpturing on the burrowing performance. Neither the typical bivalve shape nor surface sculpture did have a clear positive effect on burrowing depth in the performed experiments. We argue that the presented method is a valid and promising approach to investigate the functional morphology of bivalve shells and should be improved and extended in future studies. In contrast to the observation of living bivalves, our approach offers complete control over the parameters defining shell morphology and motion pattern. The technical set-up allows the systematic variation of all parameters to quantify their effects. The major drawback of the built set-up was that the reliability and significance of the results was limited by the lack of an optimal technique to standardize the sediment state before experiments.

Keywords: Bivalves, burrowing mechanics, granular media, functional morphology, morphology optimisation

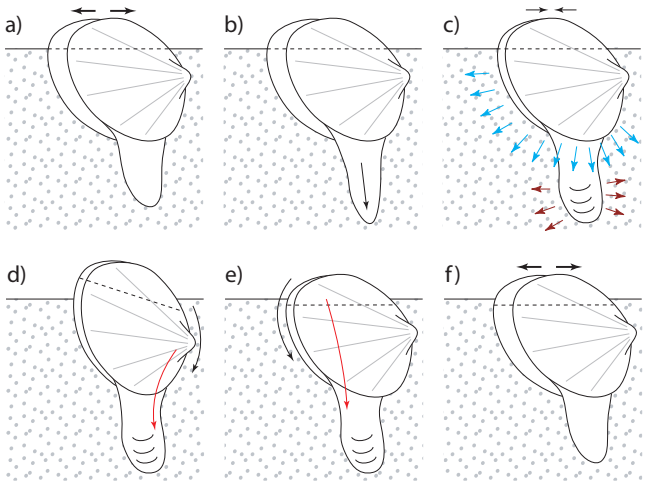

Figure 1: The *burrowing sequence* for bivalves as described by Trueman (1966). (a) The clam is in erect position, partially burrowed in the sediment. The valves are open to anchor the shell, i.e. to prevent back-slippage. (b) The foot probes deeper into the sediment. (c) The adductor muscles contract, partially closing the shell. The water expelled from the cavity liquefies the surrounding sediment to reduce the resistance to penetration. From the soft body inside the shell, blood is pressed into the foot, which is inflated and serves as a new anchor. (d) The anterior retractor muscle (red arrow) pulls the front side of the bivalve towards the foot, leading to a rotation of the shell (black arrow). (e) In the same way, the posterior retractor muscle rotates the shell back into the erect position. (f) The two rotations around different rotation axes led to a net downward translation, as illustrated by the dashed line. The valves open again to allow for another burrowing cycle starting at (a). The figure was inspired by the figure used by Amler et al. (2000, p. 46); reprinted from Koller-Hodac et al. (2010), ©2010 IEEE.

1. Introduction

Bivalve species present a wide variety of modes of life, including lying on the ocean floor, attachment to hard surfaces by their byssus or through cementation, as well as boring and burrowing into soft substrates. There are several reasons for digging into soft substrates: reduction of predation, reduced exposure to sunlight (especially on beaches) and water currents, minimisation of desiccation, and buffering of environmental extremes of temperature, salinity and pH level (Sassa et al., 2011; Watters, 1993).

Bivalves dig into soft sediments using a two-anchor principle as described in figure 1. As anchors they use their shell and a muscular tongue-like expansion of their soft body called *the foot*. The sequential contraction of the anterior and posterior retractor muscles in the foot induces a rocking motion. For *Ensis directus* the retraction force, i.e. the force to pull themselves into the sediment, is known to be up to 10 N (Trueman, 1967).

Bivalves typically dig down to depths 1-3 times their body length (Cox, 1971;

Holland and Dean, 1977; Ziegler, 1983). The time needed to reach the final burrowing depth varies from a few seconds to many minutes (McLachlan et al., 1995; Trueman, 1967; Ziegler, 1983).

Due to the important role of the shell in burrowing, it is believed that its morphology is subject to strong evolutionary pressure. Although it is not entirely clear how the evolutionary process acts on the functional morphology, it seems plausible that there is a need to maximize burrowing speed and the capacity to reach a depth that allows optimal protection (Sassa et al., 2011; Watters, 1993). However, there is also a clear pressure to stay in shallower habitats due to the higher concentration of nutrients (Edelaar, 2000).

The (functional) morphology of bivalve shells can be analysed using different morphometric parameters. The parameter spaces they define are called *morphospaces* (McGhee, 1999). A particular shell morphology can be represented as a point in this space. The *actual* morphospace is constructed by all specimens found in nature, while the *theoretical* morphospace spans all theoretically possible shapes using the given morphometric parameters. In our project we focused on round, inflated shells (*Cardium*, *Venus*) rather than elongated shells (*Ensis*, Winter et al. 2012), because in the former type of bivalve, the rocking motion and shell surface sculpturing are more prominent and therefore the variety of different morphologies and behaviours is greater. While elongated species usually burrow in anterior direction, more compact species may burrow in any direction between anterior and ventral (Kauffman, 1969).

Biological findings are usually achieved by the observation of natural organisms. It is a challenge to quantify aspects of dynamic processes involving living animals. The restriction to existing specimens offers only a sparse representation of the morphological variety and the quantification of their morphological differences is not well-defined, so that generalisations are difficult. In palaeontology, the analysis of bivalve fossils is usually restricted to the shape of the shell and of conserved burrows, and to chemical or physical properties of the sediment. Analyses based on observation of natural specimens can only elucidate the actual morphospace but never the theoretical one.

The synthetic approach to biology, i.e. the construction and analysis of artificial emulations of natural organisms, can help to overcome these difficulties (Pfeifer et al., 2007; Webb, 2000). Due to technical advancements synthetic approaches have recently become more popular and have been successfully applied in fields such as biomimetics, biorobotics and embodied artificial intelligence. It has been widely used to study many different types of locomotion, e.g. legged walking, climbing, undulatory swimming, winged flying, and also locomotion on and within granular media (Jung et al., 2011; Li et al., 2013; Maladen et al., 2011; Mazouchova et al., 2013).

Although there is a large literature about the functional morphology of bivalves, only two examples of application of the synthetic approach to bivalve burrowing are known to the authors, by Stanley (1975, 1977) and Winter et al. (2012).

In his brilliant studies, Stanley produced casts of *Mercenaria mercenaria* (Stanley, 1975) and *Trigoniids* (Stanley, 1977), which he compared to altered copies. In the first case, he tested a shell where the blunt anterior area of *Mercenaria mercenaria*

had been filled up by a more streamlined, sharp cover, in the second case he tested a variant of *Trigonia* with a smooth shell surface instead of the natural sculpture. Stanley reproduced the burrowing process by pushing the cast models into a sandy sediment from above using two rods. In both cases he measured a significant improvement of the natural shapes over the altered ones. He found that the reason were rotation axes shifted outwards to increase the net downward motion. The rocking motion that bivalves use to burrow consists of two rotations induced by the pedal retractors and almost no translation. Neither rotation axis coincides with the centre of gravity of the shell which shows that the shell shape indeed influences the rotational movement. Stanley found that the described morphological features of the tested shells moved the rotation axes further outwards, thus increasing the burrowing efficiency.

A more recent example of a synthetic approach used to study bivalve burrowing is the work by Winter. He identified the fast burrowing bivalve *Ensis directus* as one of the most efficiently burrowing animals (Winter and Hosoi, 2011). He built a robot inspired by this species that used an imitation of the opening and closing valves to fluidize the sediment surrounding the shell and thus reducing the resistance to penetration (Winter et al., 2012). Using this bioinspired technique, the efficiency of previous burrowing and anchoring devices could be greatly improved (Winter and Hosoi, 2011).

Computer simulations often are at the core of the synthetic approach. Sometimes they do not only complement experimental set-ups, but completely replace them. However, it is difficult to computationally simulate bivalve burrowing. While simplified simulations could hardly capture the effects of, e.g., surface sculpture, it would be very labour-intensive to produce a realistic bottom up simulation of the granular media including details such as force chains, fluid-sediment interaction and non-convex grain shapes, even with current state-of-the-art software and algorithms. Therefore, we currently do not see a practicable way to replace a real physical set-up by a simulation for the purpose of studying detailed shell-sediment-water interaction.

In the following, we describe a biomimetic set-up built to apply the synthetic approach to bivalve burrowing. The set-up was designed to mimic the burrowing process using a technical device, that offers new perspectives and ways for the investigation of biological and palaeontological questions, addressing the limitations of observational approaches. After preliminary experiments to test the usability of the set-up, a series of experiments was performed to investigate the effects of cross-sectional area, overall shell shape, sculpture and water expulsion.

2. Materials and Methods

Bivalve burrowing was mimicked using the experimental set-up shown in figure 2a. Bivalve shells were represented by one-piece 3D-printed ABS plastic models. Using a 3D printer, a large variety of different shell morphologies could be tested. The burrowing environment consisted of a tank containing water and quartz sand. The shells were attached to an outside actuation system by two cables that simulated the retractor

muscles of natural bivalves. The set-up did not feature any further representation of the foot. This simplification was done because it would have been technically difficult to build an actuated soft foot of only a few centimetres. Experiments were performed by pulling the artificial shells into the sediment using a rocking motion induced by alternate pulling of the cables. The measurement system was integrated into the control system of the linear motors. A separate system provided a water supply to the shells to simulate water expulsion.

2.1. Shell Models

Bivalve geometries were generated using a method similar to the ones described by Fowler et al. (1992). A planar closed aperture curve was defined using NURBS (non-uniform rational B-splines) and discretized into n points. In $m-1$ discrete growth steps, these points were scaled by a scaling factor and rotated around a fixed axis. The result was a tube-like surface defined by $n \times m$ points. The small end forming the umbo was closed by a simple disc, while the large end forming the aperture and shell edge was closed by a flat disc featuring a structure for easy attachment to the other parts. Using a computer-aided design (CAD) program, this attachment area could be easily adapted to different needs.

The surface sculpture was added in a second step by perturbing the surface in normal direction according to an arbitrary periodic function. We generated shells with radial and commarginal ridges. Using NURBS, it was possible to create ridges with any profile (e.g. jig-saw).

The final closed geometry meshes for the two valves of a shell were printed using a 3D printer. Figure 3 shows the set of shapes that were tested for this study. The layer resolution of the printer was 0.1778 mm; radial ridges converging towards the umbo started to merge at a wavelength of about 0.5 mm. We found that the abrasion of the shells by the sand was negligible ($\leq$ 0.5 mm at the shell front after 280 burrowing runs).

To test generic, simple shapes, we used a circular aperture curve to generate most of the shells shown in figure 3. However, using NURBS, also other shapes could be generated, e.g. the asymmetric shell B-natural. It was also possible to add a translational component along the hinge axis to the coiling of the shell. However, it has to be taken care that whorls of the shell do not separate or overlap in a way that renders the resulting geometry unprintable.

We used a modular approach for the assembly of the shells. The two valves were rigidly fixed to a central stainless steel disc via a bayonet coupling and a locking bolt, as depicted in figures 2b and 4. This mechanism allowed quick replacement of the valves and the minimisation of printer material, since the central part could be reused.

Natural bivalves use their retractor muscles in the foot to pull the shell downwards. Since we had a closed object without mantle cavity, we could not attach the actuating cables inside the shell models. Instead, we used flat rods that protruded from the ventral region of the models to attach the cables, see figure 2b.

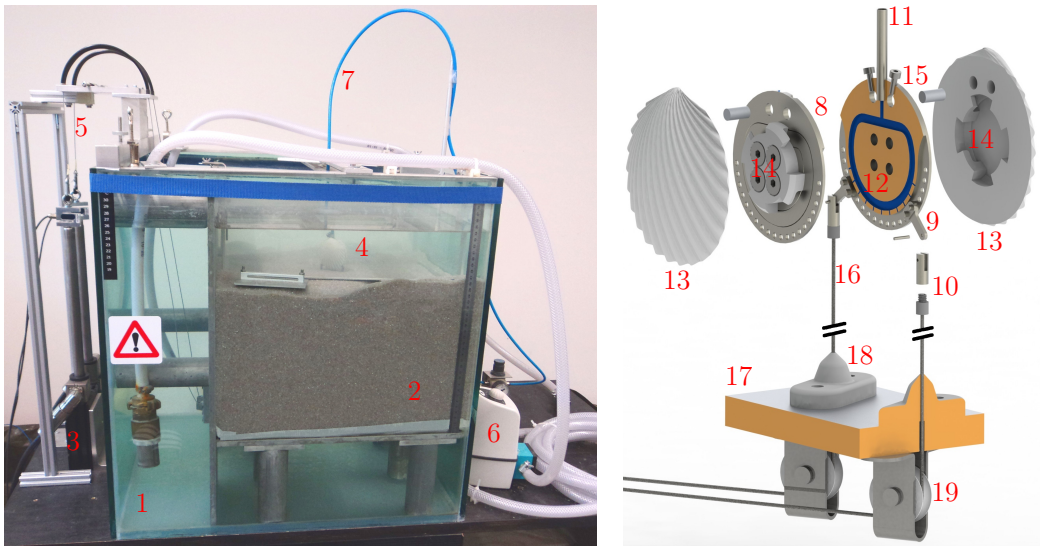

(a) (b)

Figure 2: The experimental set-up used to simulate bivalve burrowing. (a) The experiments were done in a cubic water tank (1) containing a compartment of well-rounded quartz sand (2). Two linear motors (3) vertically mounted on the outside of the tank provided an external actuation of the shell (4). Their force was transmitted by steel cables (5) deviated by pulleys to meet the shell in the sediment from below. The bivalve-like rocking burrowing motion was induced by alternate pulling of the motors. Water for the water ejection was supplied by a pump (6) through a flexible supply tube (7). (b) Details of the modular shell and the cable pulling system: the central part of the shell was a steel disc (8, cut in two halves at the orange area), which was attached to the cables at its cable attachment arms (9). The arms could be fixed at different locations along the lower (ventral) edge of the shell. The shells were attached to the cables by clevises screwed to small cylindrical parts at the end of the cables (10). The flexible supply tube (7) of the water expulsion system was put over a steel duct (11) at the top of the metal disc. From there, the water was pumped through the water expulsion channels (12, blue) out of the shell at the ventral edge. Different valves (13) could be attached to the central disc using a bayonet coupling (14). The valves were locked by bolts (15) fixed by small screws. The cables (16) went through holes in the bottom plate (17, section view, cut at the orange areas). Soft silicone sheaths (18) were used to prevent sand from entering the holes in the bottom plate and abrading the cables. Pulleys (19) were used to deviate the cables and guide them to the linear motors outside the tank.

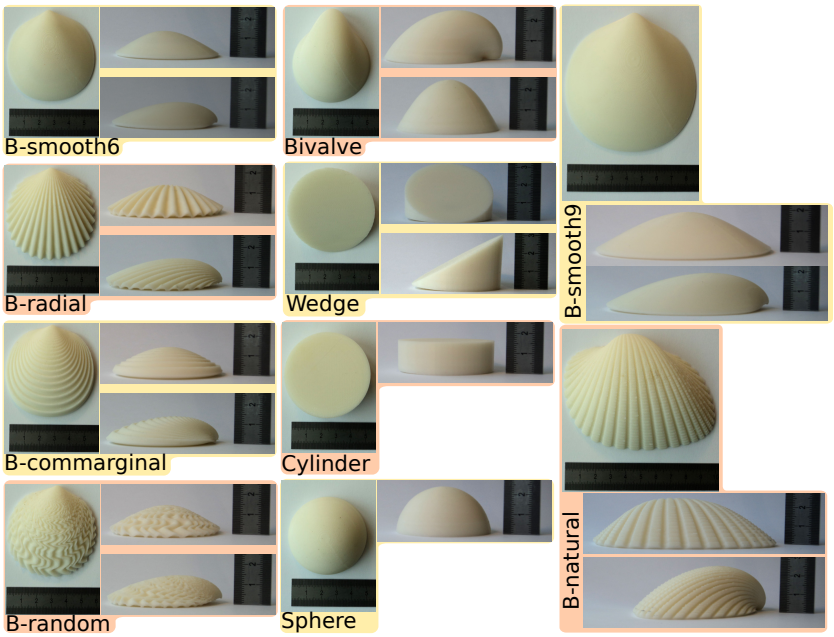

Figure 3: The set of shell shapes used for this study. Only one valve is shown for each. The bivalve-like shapes (starting with "B") were generated using the mathematical model described in section 2.1. Sphere, Cylinder and Wedge were simple geometric shapes of the same volume as Bivalve. The aperture curve of Bivalve was the same circle of 52 mm diameter the three geometric shapes were based on. B-natural was an artificially generated bivalve shape based on the morphology of a bivalve species existing in nature, *Cardium pseudolima*. B-smooth6, B-commarginal, B-radial and B-random did all have the same simple bivalve shape and size, but different sculptures added to their surface: no sculpture, commarginal sculpture (wave length at ventral edge: 5.5 mm, sine-shaped ridge profile), radial sculpture (wave length at ventral edge: 6 mm, terrace shaped ridge profile with the gentle slope towards the burrowing direction), and random sculpture, respectively. The whorl expansion rates (increase in size of the aperture curve after one revolution) are 620 for B-smooth6, B-radial, B-commarginal, B-random and B-smooth9, 30 for B-natural and 12 for Bivalve.

2.2. Water Tank and Sediment

The experiments were done in a cubic water tank (side length 60 cm) containing a compartment (42 ×58 ×24 cm) of well-rounded sorted quartz sand (grain size 0.7 − 1.2 mm, bulk density 1.5 g/cm^3).

To control the initial state of the sediment before each experiment, we manually pressed a small metal plate on the sediment surface to increase its compaction and to undo the loosening caused by retrieving the shell from the previous burrowing run. The height and planarity of the sediment surface was ensured by sliding a metal strip over

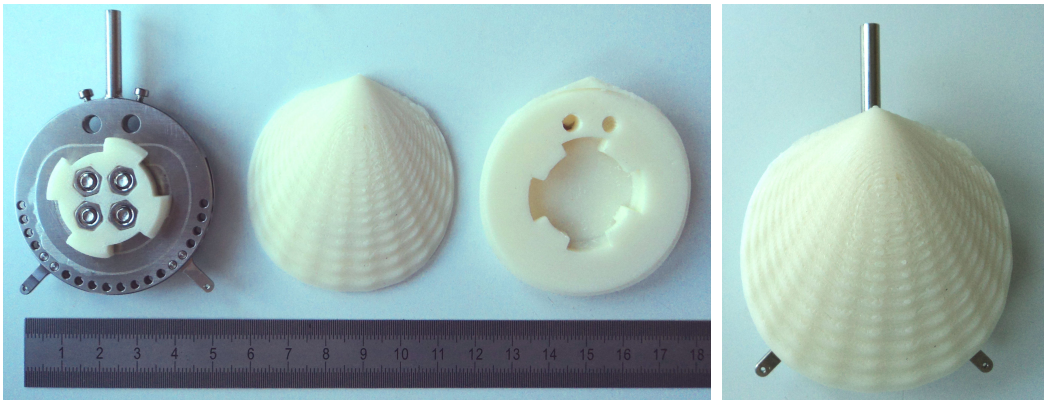

(a) (b)

Figure 4: Modular shell. (a) Central metal disc with male bayonet coupling part, outside of one valve with surface sculpture and inside of the second valve with female coupling part (from left). (b) Assembled shell featuring the cable attachment arms and the water supply duct (cf. figure 2b)

two metal bars horizontally fixed to either side of the sediment compartment. Ensuring a similar state of compaction of the sediment before each experiment was one of the major difficulties of the experiments (see section 4.3).

2.3. Actuation and Measurement System

To transmit the force from the externally mounted linear motors to the shells within the sediment, we used steel cables (Carl Stahl® U 8199512, $8 \times 19 + 7 \times 7$, cable diameter 0.95 mm (steel core) or 1.2 mm (with coating), min. breaking load 850 N). These were each deviated through the set-up using a Bowden cable housing and two pulleys. The cables entered the sediment compartment from below through holes in the aluminium bottom plate. To avoid sand grains from entering the holes and damaging the cables, we added silicone sheaths, see figure 2b.

We used two LinMot® P01-37x240F/460x660-C linear motors with the following characteristics: stroke max.: 660 mm, peak force: 206 N, force constant: 25.8 N/A, max. velocity: 2.6 m/s, position repeatability: ±0.01 mm. B1100-GP-HC controllers provided the proportional-integral-derivative (PID) control of the motors.

For each motor, a force sensor was screwed to the motor slider end and the cable was attached to the sensor. We used ME-Meßsysteme GmbH KD40S sensors with a nominal force range of ±500 N.

At the other end of each cable a screw connector was mounted (see figure 2b). A clevis screwed to the connector added a joint to allow the shell to rotate around a transverse axis and thus perform a rocking motion.

In every experiment, we indirectly measured and recorded the burrowing depth

and retractor pulling forces. To achieve this, the signals from the force sensors and the slider position signals from the linear motor controllers were collected by a National Instruments™ CompactDAQ (data acquisition) device. Because the cables were tight at all times, the burrowing depth could be measured as the displacement of the sliders during the burrowing process.

2.4. Water Expulsion System

Water channels were an additional feature of the central disc (see figure 2b). Their purpose was to allow the ejection of water along the ventral edge to simulate the water expulsion bivalves create when closing their valves.

The pump used for the water supply provided a pressure of 1 bar and a volume flow of 3 l/min. It sucked water from the tank and maintained a constant pressure in a wound up hose from where it could be supplied to the bivalve model through a flexible tube by operating a valve. The valve command signal was generated by one of the controllers of the electrical motors and thus synchronized with the burrowing motion. The amount of water expelled during 500 ms was 15 cm^3. It was therefore comparable to the volumes of the shells ranging from 30 cm^3 (B-smooth6) to 150 cm^3 (B-natural). Water expulsion durations were tested in a realistic range of 0.1 s to 1 s (in nature, durations may go up to several seconds, e.g. in *Mya*, Checa and Cadée 1997).

2.5. Burrowing Motion Control

The open loop control of the actuation system was designed to mimic the rocking burrowing motion of bivalves described in figure 1. The motion pattern was implemented as a sequence of pulling steps as shown in figure 5a, whose timing was similar to the natural case. The measured observables were the tension on the cables f and the displacement of the sliders of the linear motors s. The tension on the cables is a proxy of the force generated in the biological situation by the muscle driving the foot of the bivalve and its interaction with the surrounding sediment. The displacements of the sliders of the linear motors allowed to measure the displacement of the shell within the sediment. In the natural case, this displacement is limited by the maximum length of the foot retractor muscle.

2.6. Experiments

The described set-up was successfully used in a large number of experiments. Figure 3 shows the subset of shell shapes that were tested for this study. For all experiments, the motion pattern and the used pulling force were held constant while the morphology of the shell was changed.

One burrowing process during which the shell moved from its initial position touching the sediment surface to its final position buried in the sediment was called *burrowing run* or *repetition*. An experiment consisted of several repetitions. Between

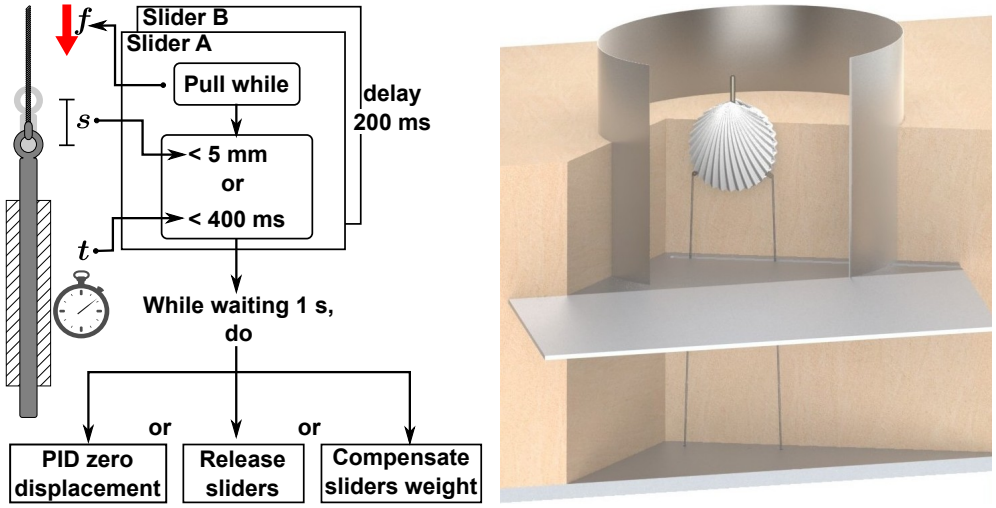

(a) (b)

Figure 5: Artefact testing: (a) Control policy. Scheme of one step of the used control program. A burrowing run consisted of a sequence of such burrowing steps. The second motor connected to the posterior part of the shell executed the same actions as the first motor, delayed by a lag $l = 200$ ms to generate the rocking motion. A constant pulling force f was applied to the motor sliders in the pulling phase. This phase was terminated as soon as either of two conditions was met: 400 ms had elapsed or the sliders had moved over 5 mm. The observed shell displacement values went up to 12.9 mm, the maximum tension observed during our tests was of $f = 200$ N. After a pause of 1 s, the next burrowing step was executed. We tested three different controllers that applied different policies during the pause. The standard controller (1) used PID control to hold the slider position constant during the pause, i.e. to keep the displacement zero. The second controller (2) released the sliders during the pauses, i.e. applied 0 force. The third controller (3) suspended the sliders during the pause by applying a force to compensate for their weight. (b) Sediment confinement. To examine the effect of a confined burrowing area two different cylinder walls (13 cm and 20 cm in diameter) and two different plates (smooth and rough surface) were inserted into the sediment as shown in this cross-sectional view.

experiments, one or several parameters defining shell morphology or motion pattern were changed.

The result plots are based on the measured slider positions, which are denoted as (absolute) burrowing depth. The origin of position was at the sediment surface, with positive values going deeper down into the sediment. The final positions after each burrowing run were averaged between the two motors; repetitions of burrowing runs under identical conditions were summarized by the median of all final burrowing depths. Each box in the depicted boxplots summarizes all repetitions of an experiment.

Final burrowing depth is here defined as the final displacement of the shell, i.e. the distance of the ventral edge to the sediment surface, while in other sources, burrowing depth may mean the distance of the top of the shell to the sediment surface.

The measurements of the slider positions were overestimating the true final burrowing depth due to deformations of the cables and the set-up structure under tension. We measured an increase of $(6.4 \pm 2.2)\%$ (mean $\pm$ standard deviation, $n = 400$) between the depth measured directly by a scale on the water expulsion tube (mean 91.7 mm) and the slider positions (mean 97.6 mm). Since the pulling cables were tight during the burrowing process, the map from the slider positions to the burrowing depth of the shell is monotonic, so that relative comparisons are still valid.

All given p-values are based on a Wilcoxon rank-sum test at a 0.05 significance level to determine the significance of the differences in burrowing depth between different morphologies.

As will be discussed later in section 4.3, there was a memory effect in the sediment that induced a correlation between different experiments. We usually measured a gradual shift of the sediment towards more or sometimes less compaction during the course of a sequence of experiments. Since the sediment standardisation technique described in section 2.2 did not suffice to remove this effect, we did also employ a simple linear model of this drift to alleviate this issue during the evaluation. To this end, the configuration used for the first of a series of experiments was again tested at the end of the series. Because the configurations (i.e. shell morphology and burrowing motion) were identical for the two experiments, their discrepancy provided an estimate of the drift in sediment compaction. By shifting the burrowing depth data of the whole experiment series according to a linear fit through the first and last experiment, the drift could be compensated. Since this procedure modifies the raw data, each of its application is explicitly stated together with the discrepancy of first and last experiment.

2.7. Artefact Testing

Since a new approach to investigate bivalve burrowing was used, several experiments were performed to test the properties of the set-up. Their purpose was to test if the set-up introduced artefacts into the burrowing process that would limit the extent to which the results attained with the set-up can be generalized to other set-ups or to the natural case. Two major aspects were tested, the control policy, i.e. different ways to actuate the shell models, and the sediment confinement, i.e. how a sediment restricted by walls and a bottom plate may be different from an unrestricted, more natural one.

Control policy While in the natural case, bivalves need to anchor their foot to be able to pull themselves deeper into the sediment, the linear motors pulling the shell in our set-up were simply fixed. A natural way to implement the burrowing motion would be to alternately apply a pulling force and no force at all. The control program described in section 2.5 did, instead of applying no force, hold the current position between the

pulling phases. Due to the elasticity of the cables and the set-up structure, the force needed to hold the position increased with burrowing depth. At the point where this holding force reached the magnitude of the pulling force, the shell did not move anymore and the maximal depth was reached. In other words, the linear motors were constantly pulling, with the holding force continuously increasing from 0 to the value of the pulling force. Consequently, the downward motion and the rocking of the shell continuously decreased until they reached 0 at the point where the holding and the pulling forces became equal.

To test if the saturation of the depth curve was an artefact of this set-up dependent effect, we experimented with two alternative controller policies that better reflected the original idea of applying no force between the pulling phases (figure 5a). The first alternative policy did not apply any force between the pulling phases, i.e. completely released the sliders, while the second alternative policy applied a force to compensate the slider weight to set the tension in the cables zero.

Sediment confinement The sediment compartment in the set-up provided only restricted space for the movements of the shell and its surrounding sediment. Objects moving through a granular medium create force chains propagated along touching grains. This effect is called jamming (To et al., 2001; Zhang et al., 2010). In our set-up, sediment jammed against the compartment bottom or walls may have influenced the results of the experiments and explain the saturation behaviour of the depth curve as an artefact of the set-up.

To test the effect of sediment confinement we inserted cylindrical metal walls and horizontal plates into the sediment to change the effective size of the compartment walls (see figure 5b). The two cylindrical walls were of different sizes (13 and 20 cm in diameter). The plates were inserted into the sediment at a depth of 96.4 mm below the sediment surface and provided a 6 mm slit to allow the cables to pass through. To investigate the idea of arcs of sand grains jammed against the bottom plate, we compared the effect of a smooth plate to that of a plate with rough sandpaper attached to its surface. We expected stronger arcs on a rough surface than on a slippery plate. Also, we compared a smooth shell to a radially ridged shell that presumably, together with the rocking motion, would disrupt existing arcs and reduce the jamming effect.

2.8. Basic Shell Morphology Testing

The purpose of the proposed method is to investigate aspects of bivalve burrowing and the functional morphology of bivalve shells. For this study, basic relations were measured: the effect of cross-sectional area of the shell perpendicular to the burrowing direction, and different basic shapes and surface sculptures.

To investigate the influence of shell morphology on the burrowing performance, we separated the shell shape into two levels: overall shape and surface sculpture. The literature suggests that the functional morphology of bivalves has been adapted to

burrowing at both levels (e.g. Alexander et al., 1993; de la Huz et al., 2002; Nel et al., 2001; Savazzi and Huazhang, 1994; Stanley, 1969, 1975, 1977).

Cross-sectional area According to basic soil mechanics, burrowing depth under a given pulling force should inversely correlate with the cross-sectional area of the shell presented to the burrowing direction (Mesri et al., 1996; Sanglerat, 1972). Many bivalves have an elongated shape and burrow with their long axis parallel to the burrowing direction, suggesting that they take advantage of this effect.

To test this basic correlation in our set-up, we analysed burrowing depth measurements from a collection of different experiments using all shells shown in figure 3.

Shell shape To test how bivalve shells compare to other shapes, we measured the performance of four different shapes: a sphere, a disc, a cylinder trunk or wedge-shaped disc, and a bivalve shape ("Sphere", "Cylinder", "Wedge" and "Bivalve" in figure 3). The idea was that the three simple geometric shapes represent different very abstracted versions of bivalve shells. All shapes were smooth, i.e. did not have any sculpture.

All of these shapes had the same volume of 30 cm^3 per valve. This was to make them comparable in an evolutionary sense, i.e. considering the question how evolution would shape the shell given a particular size (volume) of the inner organs of the animal. From a physical point of view, the cross-sectional area perpendicular to the burrowing direction should be kept constant. The pulling force f should be proportional to the density of the sediment ρ, times the gravitational acceleration g, times the cross-sectional area A, times the burrowing depth d (Mesri et al., 1996; Sanglerat, 1972). To compare the experiment results in this respect, we normalized (non-dimensionalized) the measured burrowing depths d by multiplying them with the factor $\rho g A/f$, with $\rho = 1933\ \mathrm{kg/m^3}$, $g = 9.81\ \mathrm{m/s}$, $f = 200\ \mathrm{N}$ and using the computed cross-sectional areas that were also used for figure 7.

The same shape may lead to different burrowing depths depending on its orientation. Relative to the umbo and hinge axis of their shell, bivalves burrow in different directions, covering about 90° from ventral to anterior (Kauffman, 1969). To test the effect of different burrowing directions, in addition to the standard experiments in ventral direction, we performed an experiment with B-smooth6, B-radial and B-natural, where the shells were rotated by 90°, such that they entered the sediment in anterior direction.

Surface sculpture To test the effect of surface sculpture, we measured the performance of four shells that had all the same shape and size but different sculpture types added to their surface: radial ridges, commarginal ridges, random ridges (all of the same amplitude) and no sculpture at all. Radial and commarginal ridges are the basic elements of bivalve sculpture and many burrowing species feature either of them or a mixture of both. To separate the effects of sculpturing per se and its

pattern, we also tested a random sculpture with radial ridges sampled from a Gaussian process (Rasmussen and Williams, 2006).

3. Results

In all burrowing experiments, burrowing depth as a function of burrowing time followed a curve similar to the ones shown in figure 6a. It featured discrete staircase-like steps corresponding to the burrowing steps. These steps decreased in size during the course of a burrowing run, i.e. the curve saturated and asymptotically converged to a maximal burrowing depth. All three control policies described in figure 5a exhibited this saturation.

Figure 6b shows the burrowing depth dependent on the different configurations described in figure 5b. The cylindrical walls clearly decreased the burrowing depth, the smaller one by 3.5 cm (37%), the bigger one by 1.6 cm (17%). The plates did not have any clear effect. Although the differences between the configurations using plates are significant, they are only a few millimetres and therefore not clearly distinguishable from fluctuations in the compaction of the sediment. Radial ridges on the shell or sandpaper covering the plate did not introduce major differences either.

Figure 7 shows the depths reached by the different shape models of figure 3. The depth shows roughly a linear relationship with cross-sectional area of the shapes perpendicular to the burrowing direction.

A comparison of the bivalve shell shape Bivalve with the three abstracted shapes Sphere, Wedge and Cylinder is shown in figure 8. Bivalve reached the maximum absolute depth and Cylinder the minimal one, while the other two shapes ranged in between at comparable depths. While the three simple geometric shapes did not protrude out of their ground circle, the umbo of the bivalve shape did, i.e. it was higher than the other three shapes. When considering the relative burrowing depth, i.e. the burrowing depth divided by the shape height, the bivalve shape had a lower performance and ranked even behind the cylinder. In the third plot showing normalized depth, Bivalve has yet another rank, while the ranking of the three other shapes is stable.

For B-smooth6 and B-radial, burrowing in anterior direction led to a depth 2.9 mm lower than when burrowing in ventral direction. For B-natural, the turn towards anterior led to an improvement in burrowing depth of 8.9 mm (see figure 7). However, if again relative depths are computed, the ranking is reversed: B-natural reached a relative depth of 0.69 in the ventral case and of 0.60 in the anterior case. All differences were significant (p-values $\leq 3{\times}10^{-5}$).

Figure 9 shows a comparison between the different tested sculptures. The sculptured shells did not reach larger depths than the smooth shell. Only when comparing normalized depths, B-commarginal had a similar performance as B-smooth6.

We continuously tested the differences between experiments with and without water expulsion. We collected data from 14 pairs of experiments comparing a set-up configuration with and without water expulsion (a total of 175 burrowing runs

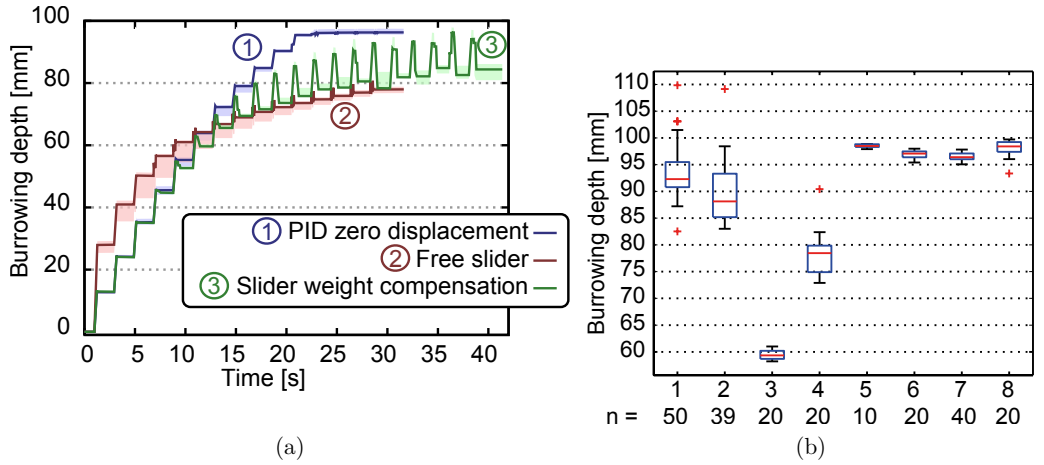

(a) (b)

Figure 6: Artefact testing results. (a) Comparison of the three different controllers (1), (2) and (3) as described in figure 5a. The x-axis shows the experiment (burrowing) time, the y-axis the final burrowing depth reached by the shell. The single burrowing steps are visible as steps in the curves. As the shell penetrates deeper into the sediment the steps gradually diminish, showing a saturation effect for all three controllers. The curves were averaged over 20, 10 and 5 repetitions, respectively. The shaded area contains 100% of the data, the solid line depicts the median. The number of burrowing steps in each experiment was 15, 15 and 20, respectively. The experiments were done using B-smooth6 and identical pulling phases. (b) A boxplot of the results of the confinement tests described in figure 5b. The final burrowing depths are shown for different configurations: (1) B-smooth6, no wall, (2) B-radial, no wall, (3) B-smooth6, small cylindrical wall, (4) B-smooth6, big cylindrical wall, (5) B-smooth6, smooth plate, (6) B-radial, smooth plate, (7) B-smooth6, rough plate, and (8) B-smooth6, rough plate and big cylindrical wall. All other parameters, including the burrowing control were identical. The difference between the experiments 5 and 8 is not significant ($p = 0.91$), the difference between experiments 6 and 7 is barely significant ($p = 0.049$). All other p-values are ≤ 0.003.

each). The used water expulsion duration was 500 ms. We measured a change in burrowing depth of (mean $\pm$ standard deviation) 0.23 ± 2.65 mm or (0.22 ± 2.94)%, i.e. no difference. Only in 7 out of the 14 pairs, the water expulsion led to an improvement.

4. Discussion

The presented set-up was successfully used to perform bivalve burrowing experiments. While shell morphology and burrowing pattern were close to natural bivalves, the necessary pulling force of 200 N is one order of magnitude larger than in the natural case (10 N, *Ensis*). We suspect that this difference is mainly due to dynamic aspects of the natural burrowing process that are missing in our set-up, like a movable soft foot

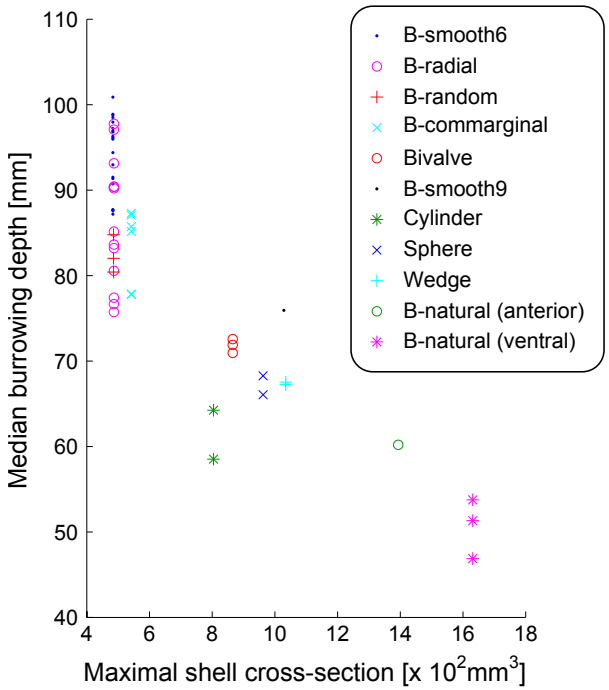

Figure 7: Median burrowing depth dependent on the maximal shell cross section. Every point in this plot shows the result of one of 56 burrowing experiments, each summarising usually 10 repeated burrowing runs (644 burrowing runs in total). All shells shown in figure 3 were evaluated. The x-axis represents the maximum cross-sectional area, perpendicular to the burrowing direction, for one valve of each shell. For B-natural, the results for two burrowing directions are shown, ventral and anterior.

and the opening and closing motion of the valves. However, our simplified set-up allows a systematic analysis of shell morphology and rocking motion.

To our knowledge, Stanley (1975, 1977) was the first and so far only one to manufacture replicas of bivalve shapes to experimentally test how the shell morphology influences the burrowing process. This study builds on his work and tries to expand it in several directions. For instance, by using a pulling mechanism, we were more closely mimicking the foot retractor muscles, and the linear motors could be precisely controlled, while Stanley pushed his models manually or using weights. Also, using computational models of bivalve shell shapes and a 3D printer, a larger number of different shapes can be tested, including artificial shapes, and the experiments are more reproducible, since the shapes are defined exactly. On the other hand, Stanley did an analysis of the rotation axes, which was not possible with the data collected in our experiments (see section 4.4).

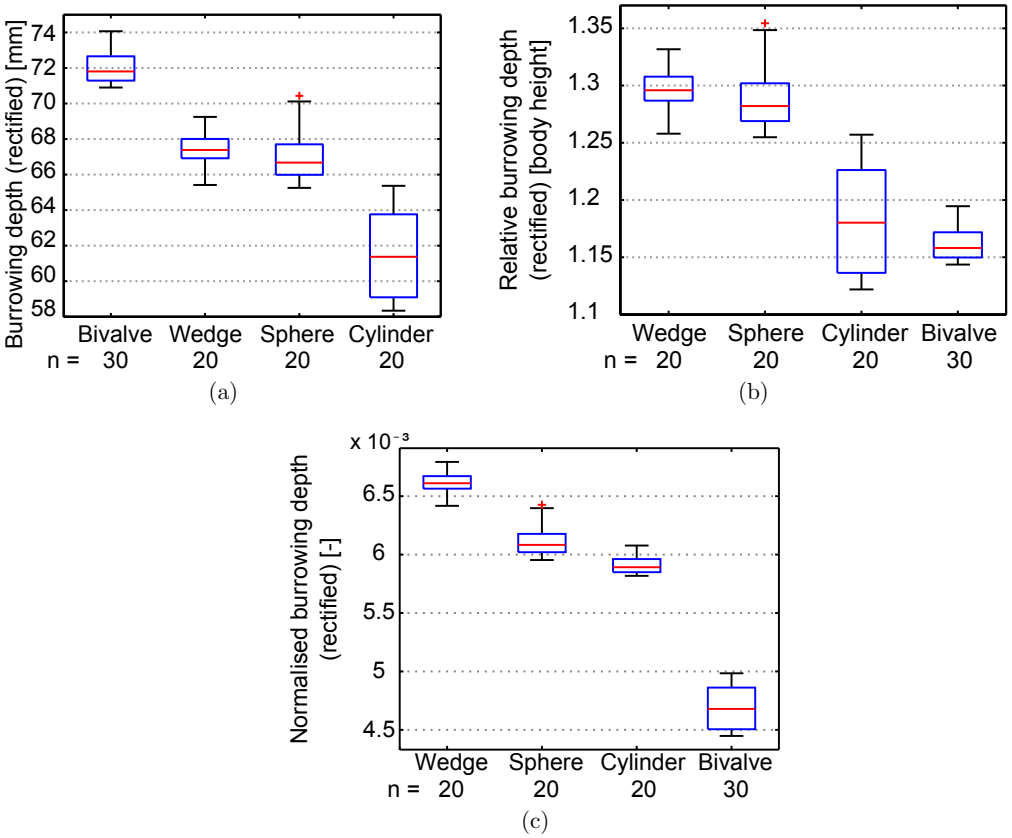

Figure 8: Burrowing depth dependent on shape. The following shell shapes are compared: Bivalve, Sphere, Cylinder and Wedge (cf. figure 3). (a) Absolute burrowing depths. (b) Relative burrowing depths. (c) Normalized burrowing depths (see section 2.8). The data for these plots was linearly shifted; the discrepancy between first and last experiment in this case was 2.5 mm.

4.1. Set-up Artefacts

The set-up was tested for artefacts it may introduce into the experiment results, i.e. effects that reflect the way the set-up works rather than general aspects of bivalve-like burrowing. No significant disturbing effects caused by the motion controllers or by the sediment confinement were found.

Control policies The hypothesis that the saturation behaviour was only due to the increasing position holding forces and therefore an artefact of the set-up was not supported by the data shown in figure 6a. The saturation in the depth curve was present in all control policies suggesting that it was due to the interaction between shell morphology and sediment. The final burrowing depths of the three controllers

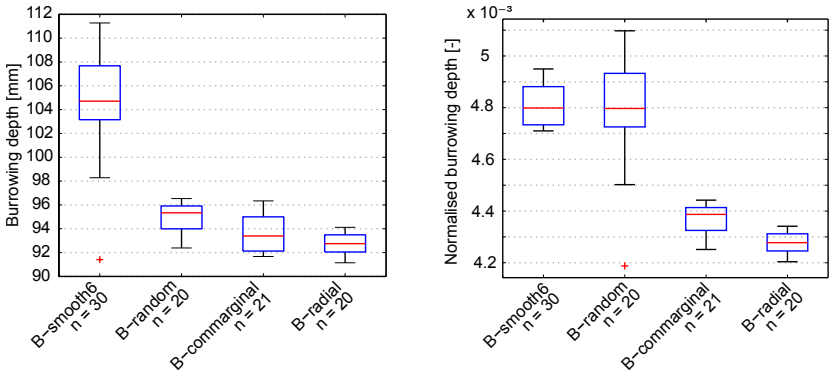

(a) (b)

Figure 9: Burrowing depth dependent on sculpture. The following shell shapes are compared: B-smooth6, B-radial, B-commarginal, B-random, cf. figure 3. (a) Absolute burrowing depths. The difference between B-commarginal and B-radial is not significant ($p = 0.12$). All other differences are significant with $p < 0.0072$. (b) Normalized burrowing depths. The difference between B-commarginal and B-smooth is not significant ($p = 0.92$), all others are significant ($p \leq 3{\times}10^{-5}$).

are consistent with each other. The standard controller (1) reached a depth of almost 100 mm. Controller (2) moved the shell deeper into the sediment in the beginning due to the released sliders that continued pulling by their weight after the actual pulling phase. In the later burrowing phase, the short bursts of the sliders could hardly move the shell anymore. In contrast to the constantly pulling controller (1), the final depth was therefore smaller. The third controller (3) started in a similar way as controller (1), but later oscillated between the final depths of the other two controllers. The reason is that after the pulling phase, the suspended sliders were pulled back up by the tension in the cables and the structure of the set-up. Controller (3) therefore illustrates that the difference between controllers (1) and (2) is due to the motors distorting the set-up rather than a real displacement of the shell in the sediment.

The non-holding controller variants tended to damage the set-up because of the more sudden movements. Since all three controllers led to a saturation process, we consistently used the variant holding the position in all experiments.

Sediment confinement It can be seen immediately from the results in figure 6b that the plates reduced the variance of the measured burrowing depths, but not their absolute values. In the plot, the depth of the plates may be estimated at 100 mm, which deviates by 3.6% from the true value of 96.4 mm. This can be explained by the difference between the slider position and the actual burrowing depth of about 6.4% mentioned earlier.

The cylinder wall of diameter 13 cm decreased the burrowing depth by 3.5 cm and the cylinder wall of diameter 20 cm by 1.6 cm. If fitting a line through these points,

the influence would decrease to zero at a cylinder wall diameter of 26 cm. Even if assuming a very long-tailed curve, the influence of the sediment compartment wall (compartment diameter $\geq$ 42 cm) does not measurably influence the result anymore and should therefore not be distinguishable from an unrestricted sediment.

The results do also show that the sediment was pushed mainly laterally and not downwards. Considering the pulling direction and given that the models used in the experiments did not laterally open the valves, this was unexpected. While we argued above that our sediment compartment was large enough to avoid artefacts due to wall effects, bivalves burrowing in a narrow space between two glass walls may be helpful for the visualisation but not for the investigation of the process.

The results did not show evidence that the radial ridges in connection with the rocking motion or the rough plate influenced the burrowing depth and did therefore not support our hypothesis that these features influence the occurrence or strength of arcs of jammed sand grains. This was unexpected. It seems to follow that jamming is a local effect among the sand grains laterally around the shell.

Another unexpected result was the apparent difference between experiments 4 and 8 (in figure 6b). While the big cylindrical wall clearly reduced the burrowing depth, a plate added to the cylindrical wall removed this effect completely. We cannot offer an explanation for this effect other than a potential error due to the sediment state (see section 4.3).

4.2. Bivalve Burrowing

Burrowing curve In all experiments, a saturation of the burrowing depth in the course of time was measured. While the successive compaction of the sediment may be a general explanation for this, the detailed mechanics are unclear and reducing the phenomenon to a few parameters is not straightforward (cf. paragraph on sculpture below). As we described in the previous section, we did not find artefacts of the set-up influencing the burrowing process. We therefore conclude that the fast convergence to the maximal burrowing depth is an inherent characteristic of the burrowing process and caused by local interactions of shell, water and sand grains.

Cross-sectional area The trend visible in figure 7 is consistent with the basic expectation that larger cross-sectional areas perpendicular to the burrowing direction decrease the burrowing depth. It can, however, be seen that morphology (Cylinder vs. B-smooth9) and sediment fluctuations (B-radial) caused considerable variation in the burrowing depth at fixed values of cross-sectional area. This suggests that by changing their shell shape, bivalves may optimize burrowing depth even if the cross-sectional area is kept constant.

Note that maximum cross-sectional area may change significantly depending on the sculpture details. In particular, B-commarginal may have a larger cross-sectional area than e.g. B-radial, because one of the ridges longitudinally intersects the cross-section.

Shape The results in figure 8 show a stable ranking of Wedge, Sphere and Cylinder, while the performance of Bivalve depends on the measure used. According to these results, a bivalve shape should be more similar to a wedge or a sphere than to a cylinder to increase its burrowing performance. A difference between absolute and relative burrowing depth was also found in the case of burrowing direction. While the absolute burrowing depth of B-natural could be improved by turning it from ventral to anterior and thus reducing the cross-sectional area perpendicular to the burrowing direction, the relative burrowing depth decreased.

Sculpture The results on surface sculpture in figure 9 were unexpected. They suggest that sculpture does not increase burrowing efficiency. If the burrowing depth is normalized by cross-sectional area (figure 9b), B-commarginal performs as well as B-smooth. However, as stated above, maximum cross-sectional area may not be a very stable measure for this type of sculpture.

The results did not support our hypothesis that ridges together with a rocking motion may disrupt jamming in the sediment to increase burrowing depth. Since the literature strongly suggests that sculpture improves the burrowing ability of bivalves (e.g. de la Huz et al., 2002; Savazzi and Huazhang, 1994; Stanley, 1969, 1977), more specific combinations of sculpture (e.g. discordant ridges), burrowing motion and sediment grain size should be tested in future studies. Stanley (1969), e.g., described how ridges rotated into the sediment at a small angle transport grains upwards and the shell downwards.

The results also highlight the difficulty of simulating sculpture-sediment interactions using numerical models, since these models would have to include details at the scale of the sculpture (i.e. three orders of magnitude smaller than the burrowing depth) and of the grain dynamics. Though effective models based on coarse-graining (McComb, 2007; Sahimi, 2003) of granular media dynamics could be suitable to study sculpture-sediment interactions and should be tried, it has been shown that fundamental breakdowns on simple models could render the dynamics not renormalisable (Du et al., 1995; Jaeger et al., 1996) leaving detailed models as the main, if not only, numerical resource to study bivalve burrowing (Herrmann and Luding, 1998; Pöschel and Schwager, 2005).

Water expulsion We did not measure a significant effect of the water expulsion. It is possible that the difficulties with the sediment (see next section) were hiding the (subtle) differences due to the water expulsion. The difficulties with the sediment themselves are a strong argument that bivalves actually do manipulate the sediment state to burrow deeper or faster. We therefore suspect that the explanation for the missing difference is the incomplete representation of water expulsion in our set-up. While our set-up only expels water into the sediment, in the real case, the shells do also close, leading to a volume reduction of the animal and an increased empty space around the shell that can be filled with liquefied sediment.

4.3. Limitations

Synthetic approaches can never capture all aspects of the real process. The focus in the presented set-up lay on the shell morphology and the rocking motion pattern. Depending on the goals of further research, it may be desirable to add more aspects of the natural burrowing process, such as valve motion or an artificial foot or to add a more powerful measurement system (see section 4.4).

A major drawback of the set-up was the lack of an effective method to standardize the state of compaction of the sediment before each experiment. We could not avoid a memory effect, i.e. a dependence of experiments on previous experiments. We measured an approximate compaction state by placing a weighted vertical thin rod on the sediment and observing how far it sank in. The method we applied (section 2.2), did not lead to satisfactory results. However, it was still the most effective method among several tested alternatives. Due to the technical efforts that would have been necessary, we did not implement the mechanism suggested in section 4.4.

The differences between two experiments were often highly significant. However, without satisfactory sediment standardisation, it is difficult to separate the effect of the morphological difference from the effect of the sediment state difference.

We often observed a drift of the state of the sediment to a higher degree of compaction over time. As mentioned in section 2.6, a linear model may be used to remove this drift from the evaluated data. This method was applied to the results shown in figure 8. The number of usually 10 repetitions per experiment was found to be a reasonable compromise between a large sample size for high significance and a compact sequence of experiments where the sediment state did not drift too far away from previous experiments.

Our difficulties with the sediment standardisation are not well reflected in the literature. In his similar study, e.g., Stanley did only mention this issue in one single sentence: “The sediment was packed firmly between experiments.” (Stanley, 1975, p. 53).

In our study, we used burrowing depth as a performance measure. However, as mentioned in the introduction, there is no clear evolutionary pressure for bivalves to maximize burrowing depth. In our experiments, the shells were usually buried to a depth of 0.5 to 1.5 body heights. We may argue that it is a safe assumption that there is an evolutionary pressure to at least cover the whole shell and that we are therefore still in a reasonable range to use depth as a performance measure. Other measures such as burrowing speed or the burrowing rate index (BRI, Stanley 1970) could be used. However, they directly depend on time. Since the temporal pattern of the burrowing process is fixed by the controllers, time cannot be used as a measure. Nevertheless, if a model of the burrowing process was available, other parameters of this model beside the saturation depth could be used. In particular, the change in depth associated with each rocking step (effectively a rate of burrowing) would account for both, maximum depth and speed of burrowing without the explicit use of time measurements.

4.4. Future Work

As possible technical improvements of the set-up we suggest: (1) a better sediment standardisation; based on our experience, we would recommend an automated procedure to first loosen the sediment by pumping in high pressure water and to then vibrate the whole sediment compartment – this should minimize residual structures in the sediment from previous experiments, (2) a more robust structure to be able to test more sudden movements, (3) the automation of the experimentation process (retrieval of the shell, sediment standardisation and initialisation of the shell position and orientation before each experiment), (4) more sensors to gather more detailed information about the burrowing trajectory, and (5) a more sophisticated mechanism for sculpture generation could be used to also test skew and asymmetric sculptures. Also, depending on the goal of future studies, additional aspects of the original process may be implemented, such as movable valves connected by a hinge or an artificial soft foot.

The set-up may then be used to investigate additional shapes, motion patterns and sediment types and to reproduce and expand on the work by Stanley (1975, 1977). In collaboration with biologists and palaeontologists open questions of bivalve functional morphology may be studied and evolutionary experiments may be performed to optimize shell morphology and burrowing motion.

4.5. Conclusion

The synthetic methodology is useful to systematically study the functional morphology of natural processes. In bivalve burrowing and in locomotion through granular media in general, this approach has scarcely been applied. In this paper, we presented a simple mechatronic set-up to mimic the burrowing behaviour of bivalves. Using two linear motors and a system of deviated steel cables, the rocking motion applied by many bivalve species was simulated. We systematically investigated the influence of the shell morphology on the burrowing performance.

We found that the digging motion saturates towards a fixed maximum depth dependent on the morphology. The pressure of the shell against the sediment seems to propagate predominantly in horizontal as opposed to vertical direction, since a cylindrical wall around the burrowing shell reduced the burrowing depth significantly, while a plate inserted into the sediment had almost no influence. It was found that the presented method did not introduce artefacts into the burrowing process.

Using the set-up to test different morphologies, it was found that a wedge is a more efficient burrowing shape than a sphere, which in turn is more efficient than a cylinder. Depending on how the performance is measured, a bivalve shape can have a performance similar to either of the three abstract shapes. In our experiments, sculpture did not increase the burrowing efficiency.

In his study, Stanley (1975, 1977) was restricted in his technical possibilities to test many different morphologies, since he had to manufacture a cast of each shape. He compared a natural shape to an artificially altered version missing a particular

morphological feature (blunt anterior area or surface sculpture). Applying geometrical models and modern 3D manufacturing techniques, in contrast, allows the continuous variation of any modelled parameter and a more precise quantisation of its effect on burrowing performance.

Applying a synthetic approach to study bivalve functional morphology therefore has a large potential. In particular, we see the following advantages: (1) extensive control over the bivalve shell morphology and the applied burrowing motion pattern, (2) the controlled variation of single parameters allows systematic comparisons of morphological traits, (3) effects of shell morphology and burrowing pattern can be easily measured and quantified, (4) no natural shells need to be collected or bought, all shapes can be manufactured by a 3D printer, (5) simplified comparison between shapes because their geometries are well-defined, (6) generation of any shell form, even if it does not exist in nature, i.e. no limitation to the actual morphospace, but potential coverage of the whole theoretical morphospace, (7) shells can be produced in larger quantities; this does not only allow replacing broken shells by another exact copy, increasing the degree of reproducibility, but also gives rise to the possibility of performing evolutionary robotics experiments, (8) 3D printing techniques will be cheaper, faster and more accurate in the future and offer even more possibilities to investigate (functional) morphologies, and (9) there are no ethical issues (as for keeping living bivalves).

Acknowledgments

The authors would like to thank Steven M. Stanley and the people from the MOLLUSCA mailing list for the discussions, Peter Eggenberger Hotz and Wolfgang Schatz for initiating and accompanying this research, Kurt Bösiger from the workshop for his services and Rolf Pfeifer for providing the AILab infrastructure.

We would like to thank the Swiss National Science Foundation [113934, 129900] for funding this project.

Author contributions **DPG** carried out the experiments and data analysis. **JPC** contributed to the experiment design and data analysis. Both authors contributed equally to the writing of this paper.

References

Alexander, R. R., Stanton, R. J. J., and Dodd, J. R. Influence of sediment grain size on the burrowing of bivalves; correlation with distribution and stratigraphic persistence of selected Neogene clams. *Palaios*, 8(3):289–303, 1993.

Amler, M., Fischer, R., and Schröder-Rogalla, N. *Muscheln*, volume 5 of *Haeckel-Bücherei*. Enke im Georg Thieme-Verlag, Stuttgart, 2000. ISBN 3-13-118391-8.

Checa, A. G. and Cadée, G. C. Hydraulic burrowing in the bivalve Mya arenaria linnaeus (Myoidea) and associated ligamental adaptations. *Journal of Molluscan*

Studies, 63(2):157–171, 1997. doi: 10.1093/mollus/63.2.157. URL http://mollus.oxfordjournals.org/content/63/2/157.full.pdf#page=1&view=FitH.

Cox, L. *Mollusca 6: Bivalvia*, volume Part N of *Treatise on invertebrate paleontology*. Geological Society of America, Boulder, Colorado, USA, 1971. ISBN 0-8137-3026-0.

de la Huz, R., Lastra, M., and López, J. The influence of sediment grain size on burrowing, growth and metabolism of Donax trunculus L. (Bivalvia: Donacidae). *Journal of Sea Research*, 47(2):85–95, 2002. ISSN 13851101. doi: 10.1016/S1385-1101(02)00108-9.

Du, Y., Li, H., and Kadanoff, L. P. Breakdown of Hydrodynamics in a One-Dimensional System of Inelastic Particles. *Phys. Rev. Lett.*, 74(8):1268–1271, 1995. doi: 10.1103/PhysRevLett.74.1268. URL http://link.aps.org/doi/10.1103/PhysRevLett.74.1268.

Edelaar, P. Phenotypic plasticity of burrowing depth in the bivalve Macoma balthica: experimental evidence and general implications. *Evolutionary biology of the bivalvia*, 177:451–458, 2000.

Fowler, D. R., Meinhardt, H., and Prusinkiewicz, P. Modeling Seashells. In Catmull, E. E. and McCormick, B. H., editors, *SIGGRAPH '92 conference proceedings*, volume 26.1992,2 of *Computer graphics*, pages 379–387, New York, 1992. ACM Press. ISBN 0201515857.

Herrmann, H. and Luding, S. Modeling granular media on the computer. *Continuum Mechanics and Thermodynamics*, 10(4):189–231, 1998. ISSN 0935-1175. doi: 10.1007/s001610050089. URL http://link.springer.com/10.1007/s001610050089.

Holland, A. F. and Dean, J. M. The biology of the stout razor clam Tagelus plebeius: I. Animal-sediment rlationships, feeding mechanism, and community biology. *Chesapeake Science*, 18(1):58, 1977. ISSN 00093262. doi: 10.2307/1350364.

Jaeger, H., Nagel, S., and Behringer, R. Granular solids, liquids, and gases. *Reviews of Modern Physics*, 68(4):1259–1273, 1996. ISSN 0034-6861. doi: 10.1103/RevModPhys.68.1259. URL http://link.aps.org/doi/10.1103/RevModPhys.68.1259.

Jung, S., Winter, A. G., and Hosoi, A. Dynamics of digging in wet soil. *International Journal of Non-Linear Mechanics*, 46(4):602–606, 2011. ISSN 00207462. doi: 10.1016/j.ijnonlinmec.2010.11.007.

Kauffman, E. G. Form, function, and evolution. In Cox, L. R., editor, *Mollusca 6: Bivalvia*, Treatise on invertebrate paleontology Part N N 0028639. The Geological Society of America, 1969.

Koller-Hodac, A., Germann, D. P., Gilgen, A., Dietrich, K., Hadorn, M., Schatz, W., and Eggenberger Hotz, P. Actuated Bivalve Robot: Study of the Burrowing Locomotion in Sediment. In *IEEE International Conference on Robotics and Automation (ICRA), 2010*, pages 1209–1214, Piscataway, NJ, 2010. IEEE. ISBN 9781424450381.

Li, C., Zhang, T., and Goldman, D. I. A Terradynamics of Legged Locomotion

on Granular Media. *Science*, 339(6126):1408–1412, 2013. ISSN 0036-8075. doi: 10.1126/science.1229163.

Maladen, R. D., Ding, Y., Umbanhowar, P. B., Kamor, A., and Goldman, D. I. Mechanical models of sandfish locomotion reveal principles of high performance subsurface sand-swimming. *Journal of The Royal Society Interface*, 8(62):1332–1345, 2011. ISSN 1742-5689. doi: 10.1098/rsif.2010.0678.

Mazouchova, N., Umbanhowar, P. B., and Goldman, D. I. Flipper-driven terrestrial locomotion of a sea turtle-inspired robot. *Bioinspiration & Biomimetics*, 8(2):026007, 2013. ISSN 1748-3182. doi: 10.1088/1748-3182/8/2/026007.

McComb, W. D. *Renormalization Methods: A Guide For Beginners*. OUP Oxford, 2007. ISBN 9780199236527.

McGhee, G. R. *Theoretical morphology: The concept and its applications*. Perspectives in paleobiology and earth history. Columbia Univ. Press, New York, USA, 1999. ISBN 0231106173.

McLachlan, A., Jaramillo, E., Defeo, O., Dugan, J., Ruyck, and Coetzee, P. Adaptations of bivalves to different beach types. *Journal of Experimental Marine Biology and Ecology*, 187(2):147–160, 1995. ISSN 0022-0981. doi: 10.1016/0022-0981(94)00176-E. URL http://www.sciencedirect.com/science/article/pii/002209819400176E.

Mesri, G., Terzaghi, K., and Peck, R. B. *Soil mechanics in engineering practice*. Wiley, New York, third ed. edition, 1996. ISBN 9780471086581. URL http://sfx.ethz.ch/sfx_locater?sid=ALEPH:EBI01&genre=book&isbn=978-0-471-08658-1.

Nel, R., McLachlan, A., and Winter, D. P. E. The effect of grain size on the burrowing of two Donax species. *Journal of Experimental Marine Biology and Ecology*, 265 (2):219–238, 2001. ISSN 0022-0981. doi: 10.1016/S0022-0981(01)00335-5. URL http://www.sciencedirect.com/science/article/pii/S0022098101003355.

Pfeifer, R., Lungarella, M., and Iida, F. Self-Organization, Embodiment, and Biologically Inspired Robotics. *Science*, 318(5853):1088–1093, 2007. ISSN 0036-8075. doi: 10.1126/science.1145803.

Pöschel, T. and Schwager, T. *Computational Granular Dynamics: Models and Algorithms*. SCIENTIFIC COMPUTATION. Springer, 2005. ISBN 9783540214854.

Rasmussen, C. E. and Williams, C. K. *Gaussian processes for machine learning*. Adaptive computation and machine learning. The MIT Press, Cambridge, 2006. ISBN 978-0-262-18253-9. URL http://www.gaussianprocess.org/gpml/chapters.

Sahimi, M. *Heterogeneous Materials II: Nonlinear and Breakdown Properties and Atomistic Modeling*. Heterogeneous Materials. Springer, 2003. ISBN 9780387001661. URL http://books.google.be/books?id=Fcvxa7UfjgAC.

Sanglerat, G. *The penetrometer and soil exploration: Interpretation of penetration diagrams-theory and practice*, volume 1 of *Developments in geotechnical engineering*. Elsevier, Amsterdam, 1972. ISBN 978-0-444-40976-8.

Sassa, S., Watabe, Y., Yang, S., Kuwae, T., and Thrush, S. Burrowing Criteria and Burrowing Mode Adjustment in Bivalves to Varying Geoenvironmental Conditions in Intertidal Flats and Beaches. *PLoS ONE*, 6(9):e25041, 2011. ISSN 1932-6203. doi: 10.1371/journal.pone.0025041.

Savazzi, E. and Huazhang, P. A. Experiments on the frictional properties of terrace sculptures. *Lethaia*, 27(4):325–336, 1994. ISSN 0024-1164. doi: 10.1111/j.1502-3931.1994.tb01583.x.

Stanley, S. M. Bivalve Mollusk Burrowing Aided by Discordant Shell Ornamentation. *Science*, 166(3905):634–635, 1969. ISSN 0036-8075. doi: 10.1126/science.166.3905.634.

Stanley, S. M. *Relation of shell form to life habits of the Bivalvia (Mollusca)*, volume 125 of *Memoir / The Geological Society of America*. The Geological Society of America, Boulder, Colorado, USA, 1970. ISBN 05854216.

Stanley, S. M. Why Clams have the Shape they Have: An Experimental Analysis of Burrowing. *Paleobiology*, 1(1):48–58, 1975.

Stanley, S. M. Coadaptation in the Trigoniidae, a remarkable family of burrowing bivalves. *Palaeontology*, 20:869–899, 1977.

To, K., Lai, P.-Y., and Pak, H. Jamming of Granular Flow in a Two-Dimensional Hopper. *Physical Review Letters*, 86(1):71–74, 2001. ISSN 0031-9007. doi: 10.1103/PhysRevLett.86.71.

Trueman, E. R. Bivalve Mollusks: Fluid Dynamics of Burrowing. *Science*, 152(3721):523–525, 1966. ISSN 0036-8075. doi: 10.1126/science.152.3721.523.

Trueman, E. R. The dynamics of burrowing in Ensis (bivalvia). *Proceedings of the Royal Society of London. Series B, Biological Sciences*, 166(1005):p 459–476, 1967. ISSN 00804649. URL http://www.jstor.org/stable/75643.

Watters, G. T. Some Aspects of the Functional Morphology of the Shell of Infaunal Bivalves (Mollusca). *Malacologia*, 35(2):315–342, 1993.

Webb, B. What does robotics offer animal behaviour? *Animal Behaviour*, 60(5):545–558, 2000. ISSN 00033472. doi: 10.1006/anbe.2000.1514.

Winter, A. G. and Hosoi, A. E. Identification and Evaluation of the Atlantic Razor Clam (Ensis directus) for Biologically Inspired Subsea Burrowing Systems. *Integrative and Comparative Biology*, 51(1):151–157, 2011. ISSN 1540-7063. doi: 10.1093/icb/icr038.

Winter, A. G., Deits, R. L. H., and Hosoi, A. E. Localized fluidization burrowing mechanics of Ensis directus. *Journal of Experimental Biology*, 215(12):2072–2080, 2012. ISSN 0022-0949. doi: 10.1242/jeb.058172.

Zhang, J., Majmudar, T. S., Sperl, M., and Behringer, R. P. Jamming for a 2D granular material. *Soft Matter*, 6(13):2982, 2010. ISSN 1744-683X. doi: 10.1039/c000147c.

Ziegler, B. *Spezielle Paläontologie: Protisten, Spongien und Coelenteraten, Mollusken*, volume 2/3 of *Einführung in die Paläobiologie / Bernhard Ziegler*. Schweizerbart'sche Verlagsbuchhandlung, Stuttgart, 1 edition, 1983. ISBN 3-510-65036-0.

Appendix F

Artificially evolved functional shell morphology of burrowing bivalves

Reprinted from:

Daniel P. Germann, Wolfgang Schatz, and Peter Eggenberger Hotz, *Artificially evolved functional shell morphology of burrowing bivalves*, Palaeontologia Electronica, vol. 17, issue 1, 2014. http://palaeo-electronica.org/content/2014/649-artificial-bivalves

Artificially evolved functional shell morphology of burrowing bivalves

Daniel P. Germann

Artificial Intelligence Laboratory, Department of Informatics, University of Zürich, Andreasstrasse 15, 8050 Zürich, Switzerland

Corresponding author. Email: germann@ifi.uzh.ch

Wolfgang Schatz

Academic Services Centre, University of Lucerne, Pfistergasse 20, 6003 Luzern, Switzerland

Peter Eggenberger Hotz

Mærsk-McKinney-Møller Institute, University of Southern Denmark, Campusvej 55, 5230 Odense M, Denmark

ABSTRACT

The morphological evolution of bivalves is documented by a rich fossil record. It is believed that the shell shape and surface sculpture play an important role for the burrowing performance of endobenthic species. While detailed morphometric studies of bivalve shells have been done, there are almost no studies experimentally testing their dynamic properties. To investigate the functional morphology of the bivalve shell, we employed a synthetic methodology and built an experimental setup to simulate the burrowing process. Using an evolutionary algorithm and a 3D printer, the first ever artificial evolution of a physical bivalve shell was performed. The result was a vertically flattened shell occupying only the top sediment layers. Insufficient control of the sediment was the major limitation of the setup and restricted the significance of the results. Nevertheless, it is demonstrated that systematic palaeontological research may substantially profit from synthetic methods. We suggest investigating functional morphologies not only by emulating the dynamical processes but also evolutionary pressure using evolutionary algorithms.

Keywords burrowing bivalves; functional morphology; artificial evolution; evolutionary pressure; biomechanics, morphospaces

1 INTRODUCTION

Bivalves constitute about a ninth of the known fossil record (Amler et al., 2000). Periods of fast radiation and drastic morphological changes, e.g. due to the appearance of siphons in the post-Palaeozoic or to the transition from hard to soft substrates, alternated with periods of only minor modifications to the shell (Seilacher, 1984; Stanley, 1968). It has been repeatedly shown that the shell morphology is adapted to effective locomotion through the sediment (Stanley, 1975a), e.g. by becoming more streamlined and elongated (Seilacher, 1984; Watters, 1993), by reducing back-slippage and forward friction using terrace-shaped commarginal ridges (Savazzi and Huazhang, 1994; Seilacher, 1984), by using discordant ridges (Stanley, 1969) or by adjusting the sculpture to the sediment grain size (de la Huz et al., 2002; Savazzi and Huazhang, 1994).

To burrow themselves into the sediment, bivalves use a two-anchor system. The shell and the foot – a muscular part of the soft body ventrally protruding out of the shell – alternately anchor the bivalve in the sediment, while the other one is moved forward. Anchoring is done by increasing the size: the shell is opened and presses against the sediment, the foot swells through an increase in blood pressure. By the anterior and posterior retractor muscles the shell is pulled closer to the anchored foot. The sequential contraction of these muscles leads to a characteristic rocking motion of the shell. The rotation around two separate rotation axes leads to a net downward motion. When the valves are contracted to release anchoring and to inflate the foot, water is expelled from the mantle cavity between the valves loosening the sediment and thus decreasing the resistance to penetration. The whole process is called “burrowing sequence” and was first described by Trueman (1966).

The (functional) morphology of bivalves may be analysed using different approaches (e.g. Crampton, 1995). Often, morphometric analyses are based on landmarks, i.e. salient points of the shell morphology such as the beak, valve adductor muscle scars etc. (Adams et al., 2004; Bookstein, 1997; Dryden and Mardia, 1998).

Another approach uses virtual growth processes to generate shell geometries. They use the fact that bivalve shells – as the shells of gastropods – have a convoluted shape following a logarithmic spiral due to an accretionary growth process. One of the first attempts to mathematically model this process was done by Raup and Michelson (1965), where also the term “theoretical morphology” was introduced. Since then, many different approaches have been suggested, most of which are based on a simple growth

process that produces a sequence of closed profile curves of increasing size that travel along a three-dimensional helicospiral (Fowler et al., 1992; Hammer and Bucher, 2005; Okamoto, 1988). With these approaches, only few parameters are needed to generate realistic virtual shell shapes.

To systematically analyse and compare different shell morphologies, a *theoretical morphospace* can be constructed from the morphological parameters. The theoretical morphospace is a multidimensional space where the dimensions correspond to the parameters and each individual shape is represented as a point (McGhee, 1999). While the theoretical morphospace spans the whole space of possible morphologies using a given set of parameters, the *actual morphospace* is the set of points representing specimens actually found in nature (McGhee, 1999).

While morphometric measures can be extracted from fossils, it is not possible to adequately assess the function of the morphological traits since no living specimens can be observed. Conclusions may be drawn by analogy from similar recent species, but these studies are restricted to the available specimens and may not properly reflect the details of the fossil morphology. To adequately assess the function of the morphological traits, it would be necessary to watch the fossil species in action.

In this paper we present an experimental platform to test different bivalve shell morphologies in terms of their burrowing performance. A synthetic methodology is followed by generating arbitrary artificial shell shapes and materializing them using a 3D printer. They are then tested in an artificial burrowing environment to better understand the function of the morphological traits. We also report the results of the first ever experiment to evolve physical shell morphologies based on burrowing performance. We propose artificial evolutionary systems as a tool to study evolutionary pressure on functional morphology.

The synthetic approach has been increasingly productive in fields such as biomimetics, biorobotics and artificial life (Langton, 1989; Webb, 2000). Also the emulation of evolution has proved both insightful and useful in many areas (Bäck, 1997; Fogel, 1998). Evolutionary algorithms have been used to optimize technical systems (Bentley, 1999; Rechenberg, 1973, 2000) or to evolve controllers of robots (Floreano et al., 2008). Also morphologies of artificial organisms have been evolved in software (Eggenberger Hotz, 2003; Sims, 1994) or, as manufacturing processes become faster and cheaper, hardware (Lipson and Pollack, 2000).

Two examples of the synthetic approach applied to study bivalve burrowing are described by Stanley (1975b) and Winter et al. (2012). Stanley used a cast of *Mercenaria mercenaria* to demonstrate the effect of the blunt anterior area of its shell. By decreasing back-slippage, it moved the rotation axes of the rocking motion outwards and thus increased the downward motion of the shell. Winter built a technical drilling device inspired by the bivalve *Ensis directus* and demonstrated its reduced energy consumption compared

to traditional devices. He also investigated the localized fluidization of the sediment around the shell due to valve contraction.

Most biomimetic research has two aspects: a) to draw inspiration from nature to build better technical artefacts; and b) to use a synthetic approach to better understand natural phenomena and organisms. Often the focus lies on the first aspect, especially in the case of artificial evolution that is used as a bio-inspired optimization tool. In this paper we focus on the second aspect and suggest expanding the synthetic methodology by using evolutionary algorithms to study the evolutionary pressure on the functional morphology of burrowing bivalves.

In this paper, we describe the experimental setup including the morphological shell model and the evolutionary algorithm. We also present the results of a morphological evolution experiment performed with the setup.

2 MATERIALS AND METHODS

The setup consisted of an environment of underwater sandy sediment, models of bivalve shells and an external actuation system that induced a rocking burrowing motion on the shells. During the evolutionary experiment, the morphology of the shells changed according to a fitness function based on the burrowing performance. A more detailed description of the setup used in this study was published in Germann and Carbajal (2013). Compared to an earlier version of the setup (Koller-Hodac et al., 2010), it featured technical improvements like a modular approach to switch bivalve shell models or an improved control program that used force control instead of position control (Germann and Carbajal, 2013) to make the burrowing process more realistic.

2.1 Setup

Bivalve burrowing was mimicked using the experimental setup shown in Figure 1. The cubic water tank (side length 60 cm) contained a compartment with well-rounded quartz sand (grain size $0.7 - 1.2$ mm, bulk density 1500 kg/m^3).

Bivalve shells were assembled from two 3D-printed ABS (acrylonitrile butadiene styrene) plastic valves and a central metal disc. Depending on the type of feature, the resolution of the printer was between 0.1 and 0.5 mm. We found that the abrasion of the ABS-shells by the sand was negligible (< 0.5 mm at the shell front after more than 280 burrowing runs).

Using a 3D printer allowed the materialization of any shell morphology generated by the evolutionary algorithm. To create one valve of a shell, an outer shell surface was combined with an inner attachment structure featuring a bayonet coupling mechanism (Figure 1.3). This mechanism allowed the attachment to a central metal disc. The disc had two attachment sites

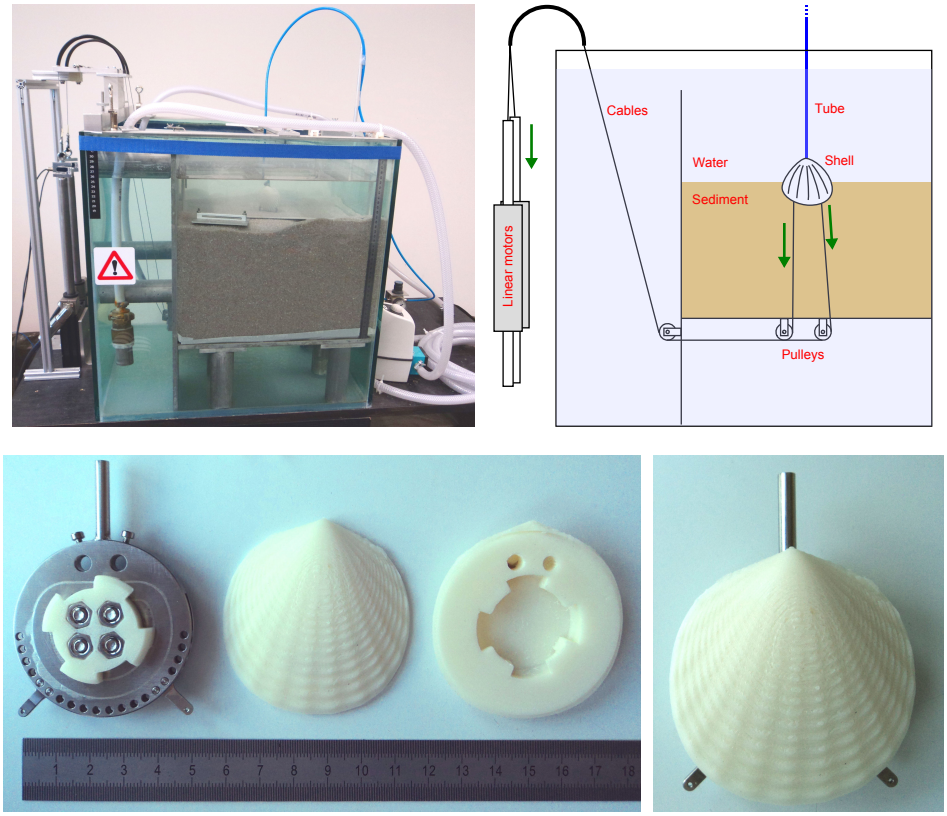

Figure 1: The experimental setup. 1.1 Picture of the water tank containing the burrowing environment. 1.2 Scheme of the setup. Shell models were placed at an initial position touching the sediment surface and then pulled in by two linear motors mounted vertically at the outside of the tank. The force was transmitted to the shell by two steel cables deviated by pulleys. By alternately pulling, the linear motors induced the typical rocking motion employed by burrowing bivalves. 1.3 Central metal disc and two 3D printed valves, outer and inner side. The valves were fixed to the metal disc by a bayonet coupling mechanism. The cables were attached to the shell at the two attachment arms of the metal disc. 1.4 Assembled shell. Pictures 1.1, 1.3 and 1.4 reprinted from Germann and Carbajal (2013).

for the actuation mechanism at the bottom and a water supply duct at the top (Figure 1.2–1.4). Water pumped into the shell and ejected through holes along the ventral edge could be used to imitate water expulsion. However, in this study, the water expulsion system was not used. The water supply tube was still attached to all shells to maintain comparability to other experiments and to ensure an erect standard orientation of the shells at the beginning of the experiments.

The shells were attached to the outside actuation system by two coated steel cables (diameter 1.2 mm) that simulated the force of the foot retractor muscles of natural bivalves. One cable was attached to the anterior part of the shell, one to the posterior part. The setup did not feature any further representation of the foot. Experiments were performed by pulling the artificial shells into the sediment using a rocking motion induced by alternate pulling of the cables. These were deviated through the sediment via pulleys and attached to two linear motors mounted vertically at the outside of the tank (Figure 1.2).

The burrowing process was simulated by an open-loop control program on the controllers of the linear motors. Each motor executed a sequence of single burrowing steps. By adding a short time lag for the second motor a rocking motion of the shell was induced, which rotated the shell first in anterior and then in posterior direction. A burrowing step consisted of a pulling and a waiting phase. During the pulling phase, a fixed pulling force was applied to the cable. During the waiting phase, the position of the motor sliders and therefore of the shell was held constant by PID (proportional-integral-derivative) control. A maximal step size was maintained by switching to the waiting phase early as soon as a predetermined limit was reached. The total step duration was held constant by adapting the waiting phase duration.

For the experiments of this study, we used the following configuration: applied pulling force: 130 N (with measured peaks up to 200 N), pulling phase duration: 400 ms, maximal step size: 12 mm, waiting phase duration: 1 s, number of steps: 15, time lag of the second motor: 200 ms. Burrowing depth as a function of burrowing time saturated, i.e. the actually performed steps became smaller with increasing depth until the shell did not move any more (Germann and Carbajal, 2013).

The internal slider position signals of the motors and signals from force sensors inserted between the slider ends and the cables were recorded for all experiments. The slider positions were systematically overestimating the burrowing depth by $(6.4 \pm 2.2)\%$ (mean $\pm$ standard deviation, $n = 400$) due to deformations of the setup under cable tension, but did not change the relative performance of the different shells. Throughout this paper we use "burrowing depth" to mean "slider position".

Parameters determining the configuration of the setup for each experiment can be divided into a) environmental parameters (such as grain size); b) motion parameters (as mentioned above); and c) morphological parame-

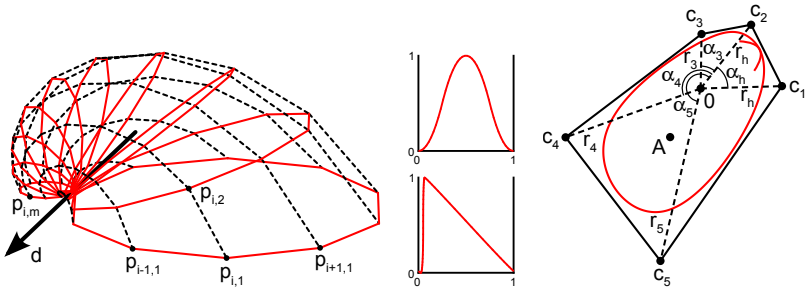

2.1 2.2 2.3

Figure 2: Geometrical model to generate artificial shell morphologies. 2.1 Illustration of the generation of a shell mesh, with $n = 10$ segments (black, dashed) and $m = 10$ growth steps (red, solid). The aperture curve was repeatedly scaled and rotated around axis $\boldsymbol{d}$ to generate the shell surface. 2.2 The sculpture profiles δ_r and δ_c used to generate radial (top) and commarginal ridges (bottom, ventral to the right). 2.3 Aperture curve of a shell (individual 6 in Figure 8), generated from parameters 1-8 in Table 1. The parameters define the polar coordinates of five points $\boldsymbol{c}_1$-$\boldsymbol{c}_5$ in the plane that span a control polygon (black) and define a NURBS curve (red). The aperture curve consists of a discretization of this curve into n points as in 2.1. The red arc denotes the position of the umbo and point $\boldsymbol{A}$ the position of the incircle of the aperture curve, where the attachment structure was placed (see text).

ters. Experiments reported here did only vary the morphological parameters of the shell.

2.2 Morphological Model

Bivalve geometries were generated using a simple method similar to the ones mentioned in the introduction (Fowler et al., 1992). A planar closed aperture curve was defined using NURBS (non-uniform rational B-splines) and discretized into n aperture points (Figure 2). In $m-1$ discrete growth steps, the aperture points were scaled by a scaling factor $\frac{1}{\lambda} < 1$ and rotated around a fixed axis $\boldsymbol{d} \in \mathbb{R}^3$ lying in the same plane as the aperture curve. λ determined the inflation of the shell. A value of 1 would lead to a torus, slightly larger values to inflated shells and large values to very flat shells (cf. Figure 3.9–3.10). Instead of starting at the umbo, we created the desired final aperture curve and generated the shell backwards toward the umbo, in reverse biological growth direction:

$$\hat{\boldsymbol{p}}_{i,j} = \frac{1}{\lambda}\mathbf{R}_{\boldsymbol{d},\varphi}\hat{\boldsymbol{p}}_{i,j-1}, \text{with } i = 1..n, j = 2..m,$$

where $\hat{\boldsymbol{p}}_{i,j} \in \mathbb{R}^3$ is the surface point i of growth step j, λ is the scaling factor and $\mathbf{R}_{\boldsymbol{d},\varphi} \in \mathbb{R}^{3\times3}$ the rotation matrix around the rotation axis $\boldsymbol{d}$ by angle φ. The points $\hat{\boldsymbol{p}}_{i,1}$ were initialized by the aperture curve. The points $\hat{\boldsymbol{p}}_{i,m}$ constituted the umbo.

The surface sculpture was added in a second step by perturbing the surface in normal direction according to a scalar sculpture function $\delta(i,j) \in [0,1]$:

$$\boldsymbol{p}_{i,j} = \hat{\boldsymbol{p}}_{i,j} + \delta(i,j)\boldsymbol{n}_{i,j},$$

where the points $\boldsymbol{p}_{i,j} \in \mathbb{R}^3$ are the final surface points including surface sculpture and $\boldsymbol{n}_{i,j} \in \mathbb{R}^3$ is the normal vector at point $\hat{\boldsymbol{p}}_{i,j}$. We used a sculpture function of the following structure:

$$\delta(i,j) = a\, w(j) \left[q\ \delta_r \left(\frac{i-1}{n} f_r \right) + (1-q) \right] \left[(1-q)\, \delta_c \left(\frac{j-1}{m} f_c \right) + q \right],$$

where $a \in [0,1]$ is an overall sculpture amplitude parameter, $w(j)$ is the maximal width or wavelength of a ridge (radial or commarginal) at the ventral edge at growth step j, $q \in [0,1]$ is a parameter balancing radial and commarginal ridges, the functions $\delta_r, \delta_c : [0,1] \to [0,1]$ are the radial and commarginal profile curve, respectively, and f_r and f_c are frequency parameters determining how many radial and commarginal ridges, respectively, should be distributed over the whole shell. The parameter q allowed a gradual mixture of the sculpture from its radial and commarginal components. A value of 0 led to purely commarginal ridges, 1 to purely radial ridges. A value of 0.5 led to a mixture of equal parts of radial and commarginal ridges, i.e. a rectangular pattern. For a high flexibility in defining the profile curves δ_r and δ_c for the ridges, again NURBS were used. For the evolutionary experiment, we used a symmetric smooth function with one peak for radial ridges and a jig-saw-shaped profile for commarginal ridges, as shown in Figure 2.2.

The result was a tube-like surface defined by $n \times m$ points $\boldsymbol{p}_{i,j}$ (Figure 2.1). To get a closed printable mesh, the small end forming the umbo was closed by a simple disc, while the large end forming the aperture and shell edge was closed by a flat disc featuring a bayonet coupling cavity for easy attachment to the other parts (see Figure 1.3).

We used a resolution of $n = 400$ by $m = 720$ and a rotation angle $\varphi = 0.25°$ per growth step. This led to a valve covering $719 \times 0.25° \approx 180°$ or half a whorl. We stopped there, because the shells tapered fast towards the umbo and after 180° would cross the aperture plane, bending into the space occupied by the other valve.

To perform the morphological evolution experiments, we defined the aperture by a NURBS curve of order 4 with five control points $\boldsymbol{c}_k$, $k = 1..5$

(Figure 2.3). To define the shape of an aperture curve it would be possible to give the Cartesian (x, y)-coordinates of its control points. However, a continuous change of these coordinates would not lead to "natural" changes in the aperture curve. We therefore decoupled changes in tangential (commarginal) and radial direction by using polar coordinates instead of Cartesian coordinates. Two control points were summarized in one hinge segment. The aperture curve was therefore defined using four pairs of polar (r, α)-coordinates. The hinge angle α_h defined the angle between the two first control points, the hinge radius r_h the distance of both points to the origin. The aperture curve was aligned such that the hinge axis, i.e. the line through the first two control points, was parallel to the rotation axis $\boldsymbol{d}$ and the origin touching the discretized aperture curve. This ensured compact and printable geometries but allowed orthogyrate shells only (see also section 4.3). The angle of the full circle not occupied by the hinge was partitioned into three sectors according to the three remaining control point angles α_3-α_5.

Since natural bivalve shells are often tilted towards anterior when burrowing, we introduced an angle parameter $\vartheta \in [0°, 90°]$ to determine this rotation. It ranged from 0°, where the hinge axis was horizontal and the umbo at the top, to 90°, where the anterior part of the shell pointed downwards and the hinge axis was vertical. Technically, this parameter rotated the bayonet coupling at the inside of the valves such that they were rotated relative to the central disc. The coupling structure was generated using computer-aided design (CAD) and was always placed at the incircle centre of the aperture curve.

As the purpose of this study was to investigate the shell shape, the volume of the shells was held constant. All shells were scaled such that the volume of one valve was 25 cm^3.

Table 1 shows a complete list of the 14 parameters used to generate the shells. Since the parameters span a morphospace, we may call them morphological parameters. However, they do also represent a genotype, which is, using a virtual growth process, translated into a shell geometry, i.e. a phenotype. We therefore also call them genetic parameters. Figure 3 shows a set of sample shells illustrating how the genetic parameters affect the final shell shape.

2.3 Evolutionary Algorithm

Bivalve shell morphologies as defined above were subjected to an artificial evolutionary process in a series of experiments. Following the common terminology for evolutionary algorithms, we use the terms "genome" and "genetic" in an abstract sense to refer to a set of parameters defining the properties of an individual (in our case a bivalve shell morphology). This section explains how the parameters were encoded in an artificial genome,

	Variable	Range	Parameter description
1	α_h	$[30°, 120°]$	hinge angle
2	r_h	$[0, 1]$	hinge radius
3	α_3	$[0°, 360° - \alpha_h]$	angle of 3$^{\text{rd}}$ control point
4	r_3	$[0, 1]$	radius of 3$^{\text{rd}}$ control point
5	α_4	$[0°, 360° - \alpha_h]$	angle of 4$^{\text{th}}$ control point
6	r_4	$[0, 1]$	radius of 4$^{\text{th}}$ control point
7	α_5	$[0°, 360° - \alpha_h]$	angle of 5$^{\text{th}}$ control point
8	r_5	$[0, 1]$	radius of 5$^{\text{th}}$ control point
9	λ	$[1.00339, 1.04086]$	growth scaling factor
10	ϑ	$[0°, 90°]$	shell rotation towards anterior
11	q	$[0, 1]$	radial/commarginal mixture
12	a	$[0, 1]$	sculpture amplitude
13	f_r	[10..100]	radial ridge frequency
14	f_c	[18..180]	commarginal ridge frequency

Table 1: Genetic parameters from which the shell morphology was generated. Parameters 1-10 defined the overall shape of the shell, parameters 11-14 the surface sculpture. The shape of the aperture curve used 8 parameters, see Figure 2.3. For the effect of parameters λ, q, f_r and f_c, see Figure 3. By reducing parameter a from 1 to 0, the sculptures of the sculptured examples in Figure 3 would be linearly reduced to a smooth surface.

how that genome was adapted during evolution and how the experiments were performed.

2.3.1 Genome Encoding

The genome consisted of 15 real numbers $\in [0, 1]$; the first 14 were mapped to the genetic parameters shown in Table 1, the last one encoded a mutation rate, see section 2.3.3. The values from the genome were directly used or linearly scaled to the appropriate range except for λ.

Shell inflation is a highly non-linear function of λ. To ensure a smooth linear change of the morphology as a response to a change in the genome, we therefore used a special mapping in this case. The value on the genome was used to encode the ratio of the width of one valve (distance from the aperture plane to the most distant point on the umbo) and the height (dorsal-ventral diameter of the aperture curve). This ratio was limited to $[0.04, 0.39]$. A value of 1 would imply a torus (and $\lambda = 1$). The value of λ was then determined such that the shell satisfied the given ratio.

To maintain an order of increasing angles for the control points $\boldsymbol{c}_3$ to $\boldsymbol{c}_5$, the corresponding parameter pairs (r_3, α_3)-(r_5, α_5) were first sorted according to the angle and then assigned to the control points in ascending order (i.e. the indices 3-5 of the control points and the parameter pairs may not

match).

Despite the considerations above to find a natural encoding, it was still necessary to specifically test for invalid shells, i.e. shells that were not printable because their surface was self-intersecting or had too thin features. We employed the following criteria to detect invalid shells: a) crossing segments of the control polygon; b) an aperture with an incircle smaller than the metal disc (diameter 50 mm); c) an outside shell surface intersecting the inner attachment structure; d) a length-height ratio $\notin [\frac{1}{5}, 5]$; and e) angles between segments of the control polygon below 10°, leading to too thin structures.

2.3.2 Fitness Function

For each shell morphology, a fitness value was computed from the experimental results. It was used to measure the ability of the shell to vanish and hide below the sediment surface. We computed the fitness value F based on the final burrowing depth, as a sum of two volumes, $F = V_b + V_c$, where V_b was the part of the volume of one valve buried below the sediment surface and V_c was a virtual volume of sediment covering a completely buried shell.

For partially buried shells, V_c was 0. For completely buried shells (where V_b was equal to the full valve volume), V_c was computed as $V_c = dA$, where d was the distance of the top of the shell to the sediment surface and A was the average cross section of a valve with volume 25 cm^3, i.e. $A = (25\,000\ \text{mm}^3)^{\frac{2}{3}} \approx 855\ \text{mm}^2$. A fitness value of 0–25 000 mm^3 did therefore signify partial burial, while each additional 855 mm^3 meant one more millimetre below sediment surface.

Both values, V_b and V_c, were computed from the burrowing depth measured by the linear motors. From the initial position and orientation of the shell, touching the sediment surface, and the displacement of both sliders, a final position and orientation of the shell was computed, assuming that the shell was moving in its sagittal plane and that the disc centre stayed in the same vertical line. These are reasonable assumptions due to the convergent nature of pulling motions. Visual observations of the final state of the shells at the end of the burrowing run were in accordance with the computed results. The main reason to compute the fitness value of a shell from the volumes V_b and V_c – rather than directly using the burrowing depth – was to avoid pathological cases such as shells with long thin ventral spikes. Using these, a shell could have just "fallen over" to get a high fitness, i.e. move down by rotating away the spike without actually entering the sediment.

2.3.3 Evolution Strategy

A (2+3) evolution strategy (ES) was used for the experiments (Schwefel, 1995). This means that from a generation of shell morphologies, two were selected, which then produced three child morphologies; from all five mor-

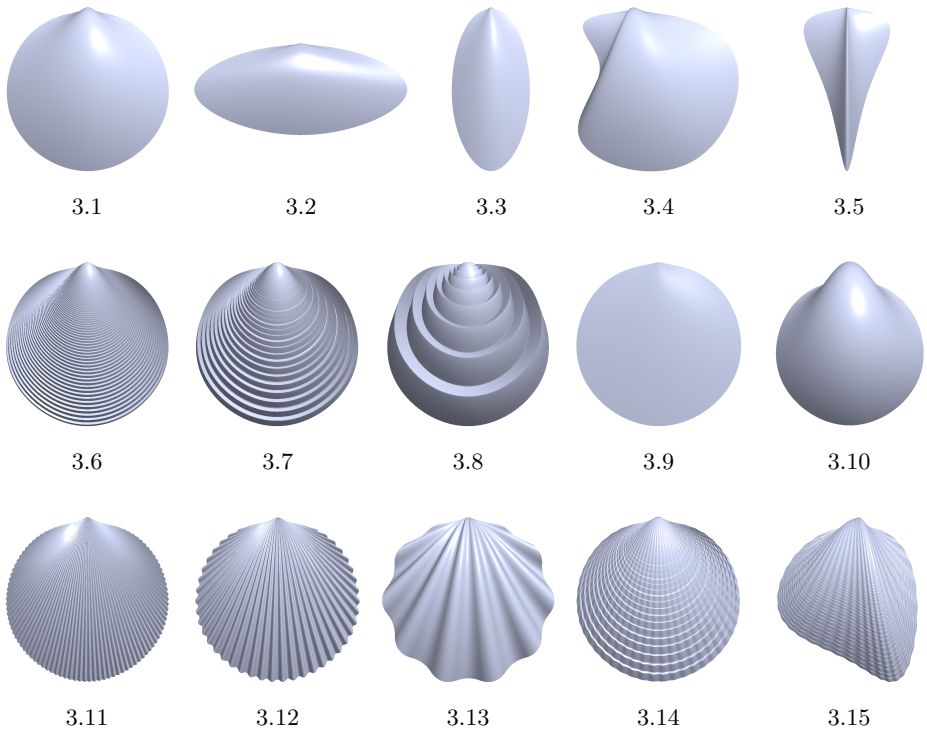

Figure 3: Example shell morphologies: 3.1 neutral, with a round aperture curve, intermediate values for all parameters and no sculpture ($a = 0$), 3.2 long aperture curve, 3.3 high aperture curve, 3.4 featuring an ear, using an aperture curve with a large indentation, 3.5 featuring a sharp arrow shape, 3.6 with maximal commarginal frequency, 3.7 with medium commarginal frequency, 3.8 with minimal commarginal frequency, 3.9 flat, with $\lambda = 1.02069$, 3.10 inflated, with $\lambda = 1.00339$, 3.11 with maximal radial frequency, 3.12 with medium radial frequency, 3.13 with minimal radial frequency, 3.14 with a radial-commarginal mixture, 3.15 with an arbitrary shape. Note that the scale is not the same for all shells.

phologies, again two were selected for the next generation. We used a "+"-strategy as opposed to a ","-strategy (i.e. applied selection to the offspring and parents instead of only to the offspring, Schwefel, 1995), because we wanted to avoid the risk of losing good morphologies. The number of children was limited to three because of the size of the 3D printer; six was usually the maximum number of valves of the given volume that could be printed by the 3D printer in one job. Considering the long printing times (see section 2.4), it was decided to set the offspring size accordingly.

From the full population of five different shell morphologies, the two with the highest fitness values were chosen. This kind of selection operator is called elitism and commonly used in evolutionary algorithms.

The reproduction operators were mutation and uniform crossover. Each of the two parents was mutated and a third child was generated by crossover + mutation. A self-adaptation scheme was used for the mutation rate (Beyer and Schwefel, 2002; Schwefel, 1995). Each genome $\boldsymbol{g}_i$ of generation i stored a value σ_i as its mutation rate. The mutated genome was then generated as follows:

$$\begin{aligned} \sigma_{i+1} &= \sigma_i e^{N(0,\tau^2)} \\ \boldsymbol{g}_{i+1} &= \boldsymbol{g}_i + \boldsymbol{N}(0, \sigma_{i+1}^2), \end{aligned}$$

where $N(0, \tau^2)$ is a scalar normally distributed around 0 with variance τ^2 and $\boldsymbol{N}(0, \sigma_{i+1}^2)$ is a vector of length 14 of values normally distributed around 0 with variance σ_{i+1}^2. First, the mutation rate itself was changed using the parameter τ, then the rest of the genome was mutated using the new mutation rate. The genomes of the first generation $\boldsymbol{g}_1$ were initialized randomly with values uniformly distributed in $[0, 1]$. As an initial mutation rate, we set $\sigma_1 = 0.1$ for all genomes. For τ we used a value of 1. This is higher than the standard value of 0.3 proposed by the literature (Beyer, 1995), because we decided to allow for a faster adaptation of the mutation rate due to the small number of children and generations.

Uniform crossover was done by randomly and independently choosing each value of the genome either from the first or second parent, with equal probability (Syswerda, 1989). Because we could only perform a small number of generations, it was important to be able to combine successful traits of different individuals.

As explained in section 2.3.1, some genomes led to invalid shell geometries. During the reproduction phase, we therefore discarded any invalid morphology and generated new genomes until one was valid. This led to an artificial reduction of the mutation rate, as the probability to be valid was higher for offspring close to the valid parent. To counteract this effect, we generated three versions of each generation and chose the one with the highest diversity.

2.3.4 Experiments

For the experiments, the following steps were repeated for each generation: 1. print the three new shells, 2. evaluate them and re-evaluate the two individuals selected from the last generation, 3. from the five shells, select the two with the highest fitness, 4. use them to generate three new shells by mutation and crossover.

Before each burrowing run, the sediment was treated to establish a standardized configuration. This was done by manually pressing a small metal plate on the sediment surface to increase its compaction and to undo the loosening caused by retrieving the shell from the previous burrowing run. The height and planarity of the sediment surface was ensured by sliding a metal strip over two metal bars horizontally fixed to either side of the sediment compartment. As explained in section 4.2, we could not avoid a memory effect of the sediment, i.e. a dependence of the sediment state on earlier experiments. Usually, the sediment became more compacted in the course of the experiments.

To deal with the fluctuations in the sediment, each burrowing run was repeated 10 times. The fitness value for a morphology was therefore based on 10 successive evaluations of the shell. Also, already evaluated and selected parent individuals were re-evaluated in each generation.

To evaluate the different morphologies, only the valves were exchanged, the central metal disc and all other parts of the setup were re-used for all experiments. The computer program did not only execute the evolution strategy and generate the new shell morphologies but did also automatically adapt the control programs of the linear motors. To ensure a consistent initial position of the different shell morphologies, touching the sediment surface, it was necessary to adjust the initial position of the sliders.

2.4 Phenotypic Parameters

In addition to the genetic (or morphological) parameters used to generate the shells, we computed a set of derived phenotypic (or morphometric) parameters to describe the shell morphology in more detail and to test for correlations with the fitness. Because the exact geometries of all shells were known, the phenotypic parameters could be computed exactly as well. Table 2 shows a list of the derived parameters. Note that the evolutionary algorithm modified the genetic parameters, while the phenotypic parameters were computed afterwards from the resulting shell geometries.

Length L, height H and width W are the standard shell dimensions used in biology. Since we allowed the shell to rotate towards anterior by adding the parameter ϑ, the two dimensions L and H may rotate with respect to the environment. We therefore introduced measures perpendicular to the coordinate system of the environment. The tallness T measured the shell

	Variable	Unit/Range	Parameter description
1	L	[mm]	length, dimension parallel to hinge axis
2	H	[mm]	height, dimension orthogonal to length
3	B	[mm]	broadness, dim. orth. to burrowing direction
4	T	[mm]	tallness, dim. parallel to burrowing direction
5	J	[mm]	major axis length, largest diameter
6	N	[mm]	minor axis length, dim. orth. to major axis
7	W	[mm]	width, dim. orth. to aperture plane (over both valves)
8	l_A	[mm]	aperture curve length, circumference of aperture
9	A_A	[mm^2]	aperture area
10	γ	$[0, 1]$	non-convexity, part of aperture area bending inwards
11	p_u	$[0, 1]$	relative umbo position (along L)
12	p_c	$[0, 1]$	relative centre position (along L)
13	S_1	$[0, 1]$	streamlining, (Watters, 1993, based on L and H)
14	S_2	$[0, 1]$	streamlining, (Watters, 1993, based on B and T)
15	S_3	$[0, 1]$	streamlining, average angle between faces and burrowing direction

Table 2: Phenotypic (morphometric) parameters. In addition to the parameters listed in Table 1 that were used to generate the shells, we used this set of phenotypic parameters computed from the final shells to find possible correlations with the fitness.

dimension along the burrowing direction, i.e. perpendicular to the sediment surface. The broadness B measured the dimension perpendicular to T, i.e. parallel to the sediment surface. Finally, we also computed the largest overall dimension J of the shell and the dimension parallel to it, N. All these additional measures lay in the sagittal plane of the shell, while the third direction was always measured by W (which in our case covered both valves and the central metal disc). See Figure 4 for an illustration of the different dimensions.

The other morphometric measures included the length l_A and area A_A of the aperture curve and the ratio $\gamma = (A_c - A_A)/A_c$, where A_c is the area of the convex hull of the aperture curve. If γ is 0, the aperture curve itself is convex, the higher γ becomes, the more indentations there are in the aperture curve, leading to ears as in Figure 3.4, or shells with more than one spine, e.g. shell 11 in Figure 8. We also computed the relative positions of the umbo (average of all surface points $\boldsymbol{p}_{i,m}, i = 1..n$) and the centre (of the incircle of the aperture curve, where the attachment structure was placed) and three different measures of streamlining.

Streamlining is a value assessing the average alignment of the shell surface with the burrowing direction. Shapes with a large flat area opposing (perpendicular to) the burrowing motion have values close to 0, while shapes with a small front but a large lateral area have values close to 1. Because

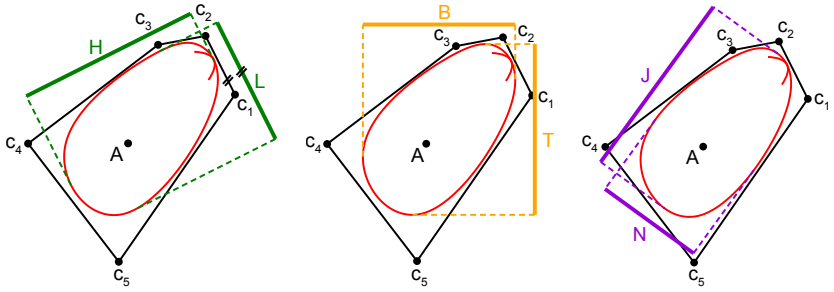

4.1 4.2 4.3

Figure 4: Different shell dimensions. While the width W is always defined as the dimension orthogonal to the aperture plane, the other two dimensions may be defined in different ways, cf. Table 2. The burrowing direction is downwards. 4.1 Length L and height H. Length is parallel to the hinge axis. 4.2 Tallness T and broadness B. Tallness is parallel to the burrowing direction, i.e. vertical. 4.3 Major axis length J and minor axis length N. J is along the largest diameter of the shell.

it is difficult to compute an exact value from given natural bivalve shells, Watters (1993) defined an approximation for streamlining as

$$S_1 = \exp\left(\frac{H \cdot W}{L^2}\right)^{-1},$$

where H, W and L are height, width and length, respectively, as defined in Table 2. For the formula, Watters assumed the length to be the dimension in burrowing direction. Since in our case, we actually know the burrowing direction for each shell, we can define a second measure of streamlining, S_2 using the same formula but computed from broadness B, width W and tallness T, instead of H, W and L, respectively.

Since we knew both the orientation of the shells with respect to the burrowing direction and the shell geometry, it was possible to compute an exact measure of streamlining, S_3. The angles between the shell mesh faces (the rectangular facets in Figure 2.1) and the burrowing direction were scaled to $[0, 1]$ (with 0 = perpendicular to the burrowing direction and 1 = parallel to the burrowing direction), weighted using the corresponding face areas and aggregated to compute an average. Very flat shells (small W) tended to have values close to 1, while highly inflated shells tended to have values close to 0.5. Values close to 0 were not possible with our geometric model.

3 RESULTS

Using the described setup and evolution strategy, 20 generations of ar-

tificial evolution were performed. The number of printed shells was 60. On average, one generation needed a printing time of 20 h and 139 cm^3 of printing material.

3.1 Burrowing Depth, Fitness and Sediment

Figure 5 shows the burrowing depths that were measured during the course of the evolution. They continuously decreased by about 14 mm over the 20 generations. In an evolutionary experiment, it should be expected that fitness, which in our experiments was indirectly linked to the burrowing depth, increases during the course of evolution. In the case of a "+"-strategy it is even guaranteed that the best fitness does not decrease from generation to generation, provided the same individual is always mapped to the same fitness value. This requirement is not met in cases where the fitness value is based on a physical measurement. In this study, fitness did not only depend on the morphology but also on the state of the sediment. From previous experiments (Germann and Carbajal, 2013), we know that the state of the sediment has a large influence on the burrowing process, see also section 4.2. There was a memory effect, i.e. a burrowing run was not independent of previous burrowing runs. Over the period of several experiments, the compaction of the sediment usually increased continuously. This counteracted the effect of more adapted shell morphologies that evolved.

The variance of the burrowing depth within the 10 repetitions of an evaluation is in most cases small enough to allow comparisons in burrowing performance. Outliers or large variances can usually be explained by accidents like connectors that broke loose from the shell and that had to be retrieved from within the sediment (e.g. shell 1 in generation 3 or shell 47 in generation 17). When testing the differences between the five individuals within a generation using a Wilcoxon ranksum test at a 0.05 confidence level, 81% of all differences are significant. However, we cannot reliably determine how much of this difference is indeed caused by the shell morphology and how much by fluctuations in the state of the sediment.

Because of the sediment fluctuations we re-evaluated selected shells in each generation. In the ideal case, morphology would be the only factor influencing the burrowing depth, and the re-evaluated individuals would reach exactly the same depth as in all previous evaluations. Figure 6.1 shows a plot of all burrowing depths, with identified repetitions. It is possible to compute a correction vector that shifts the data points vertically to make the repetitions match. However, there is no unique solution, so although such a correction vector helps to correct the repetitions, it cannot reveal the true global course of the curve, i.e. the curve we would have gotten if we could return the sediment in the exact same state before each burrowing run. In Figure 6.2–6.3, we show two solutions for a correction. For the first correction, "shift 1", we computed a shift vector for each repeated individual

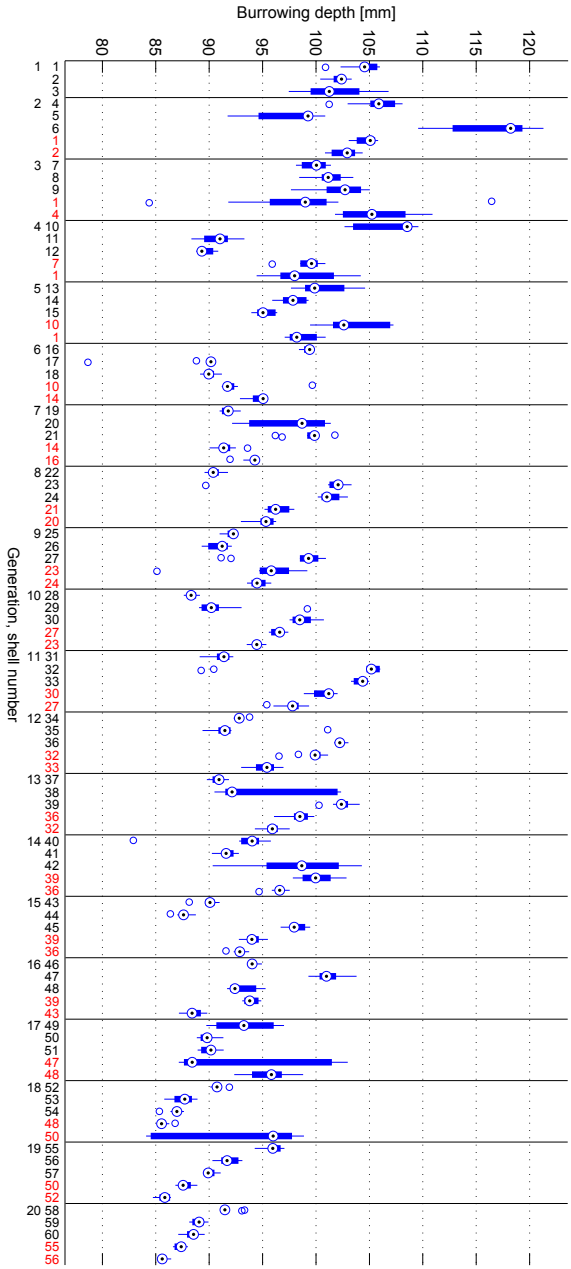

Figure 5: Burrowing depth boxplot. 20 generations of shells were generated. In each generation, the three new shells were evaluated and the two parents of the previous generation were re-evaluated (red labels). Each evaluation of a shell consisted of 10 repeated burrowing runs of which the final burrowing depths were measured. One box in the plot summarizes these 10 repetitions. The labels of the x-axis give the generation number (1-20) and the shell number (1-60).

that assumed that the shift value for the last repetition stayed the same for the following experiments (i.e. that the compaction of the sediment up to this point in time was irreversible). This led to a strongly increasing depth curve shown in 6.2. For the alternative correction "shift 2" shown in 6.3, the shift vector was adjusted such that the linear regression line through the resulting depth curve was horizontal. The shift vectors for both types of correction are shown in Figure 6.4.

Figure 7.1 shows a comparison of the original fitness values and two versions corrected using an analogous method as for the depth. The fitness values of the different individuals are summarized by areas covering all (bright area) and only the selected individuals (dark area). According to our experience with the behaviour of the sediment, we suspect that the curve would lie between the two corrections, but closer to the shift 2 correction, if we could perform experiments with a perfectly standardized sediment. In the rest of this section, we therefore show results based on the original data or of the shift 2 correction.

Figure 7.2 shows the same kind of range evolution plot for the mutation rate. It decreased quickly from the initial value of 0.1 and then fluctuated around a tenth of this value.

3.2 Phylogeny

Figure 8 shows the complete phylogenetic tree of the evolutionary experiment. The number of occurrences of the two types of reproduction, mutation and crossover + mutation, does not indicate any advantage of one over the other. In the fittest individuals, the ratio is 7:5, in the selected individuals 16:8, i.e. the ratios do not deviate from the overall ratio of 2:1. Among selected individuals, crossover was mainly present in generations 7-13.

All individuals from generation 3 onwards were descendants of shell 1. Together with the decreasing mutation rate, this led to a high similarity among the shells of the remaining generations. While the shell shape moderately changed towards taller shells and back to shells with a lower tallness, the shell sculpture basically stayed constant, featuring commarginal ridges of an intermediate frequency and amplitude.

The comparison of different shells reveals the important role of tallness. Based on the original data, shell 58 was the best shell of the final generation (see Figure 8). Overall, shell 10 in generation 4 was the best (fittest) individual, followed by shell 1 in generation 2. All of these shells had a low or moderate tallness. Shell 5 in generation 2 was the worst individual, followed by shell 9. These were also the tallest shells. Shell 6 had the greatest burrowing depth but was very tall, which led to a low fitness. These rankings are similar but not identical in the corrected versions of the data.

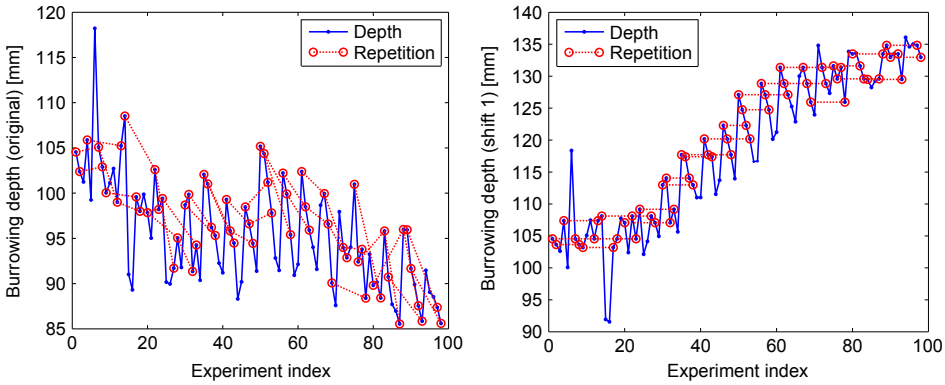

6.1 6.2 6.3 6.4

Figure 6: Depth correction. 6.1 Original depth data (blue, corresponds to the sequence of medians shown in Figure 5). The repeated evaluations are marked by red circles and connected by dashed lines. 6.2 Shift 1: depth data shifted such that repetitions match under the assumption that compaction is irreversible. 6.3 Shift 2: depth data shifted such that repetitions match and the final depth curve has a horizontal regression line. 6.4 The shift vectors shift 1 and shift 2 added to the original data to generate the corrected versions in 6.2 and 6.3.

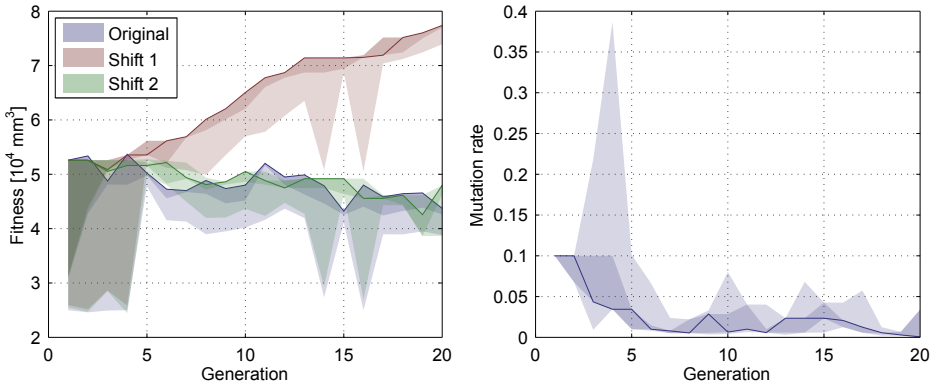

7.1 7.2

Figure 7: Fitness and mutation rate. 7.1 The plot shows the range of fitness values for each generation. The solid line follows the best individual of each generation. The dark shaded area covers the best two individuals, i.e. the selected ones, the bright shaded area covers all individuals. The original data is compared to two versions corrected in analogy to the depth values in Figure 6. 7.2 The same kind of range evolution plot for the mutation rate.

3.3 Correlation of Parameters with Fitness

Because the rotation angle ϑ was virtually always close to 90° and most shells had their largest diameter perpendicular to the hinge axis, the dimension measures strongly correlate. Length correlates (Pearson) with tallness by $r = 0.92$ (p-value = $2{\times}10^{-25}$) and with the major axis length by $r = 0.55$ (p-value = $7{\times}10^{-6}$). Height correlates with broadness by $r = 0.90$ (p-value = $3{\times}10^{-22}$) and with the major axis length by $r = 0.34$ (p-value = 0.008). While the major and minor axes are sometimes misaligned, length is basically equivalent to tallness and height to broadness. Figure 4 shows the measures for individual 6, which is an exception in the sense that the measures do not align.

Figure 9 shows the evolution of the genetic parameters over the generations. After a quick convergence during the first three to five generations, most values stayed virtually constant. Some parameters show a slight change around generation 15. It can be seen that the parameter values of invalid shells cover a larger interval than those of valid shells.

To investigate the distribution of invalid shells, we generated a sample of 10 000 random individuals. Fourteen percent of these were valid, while in the evolutionary experiment, 56% of the generated shells were valid. In the sample, the valid shells were evenly distributed throughout the parameter space except for λ, r_h and the angles α_3-α_5. Valid shells were restricted to an interval of about [0.1,0.8] in λ. Also, there were more valid shells for

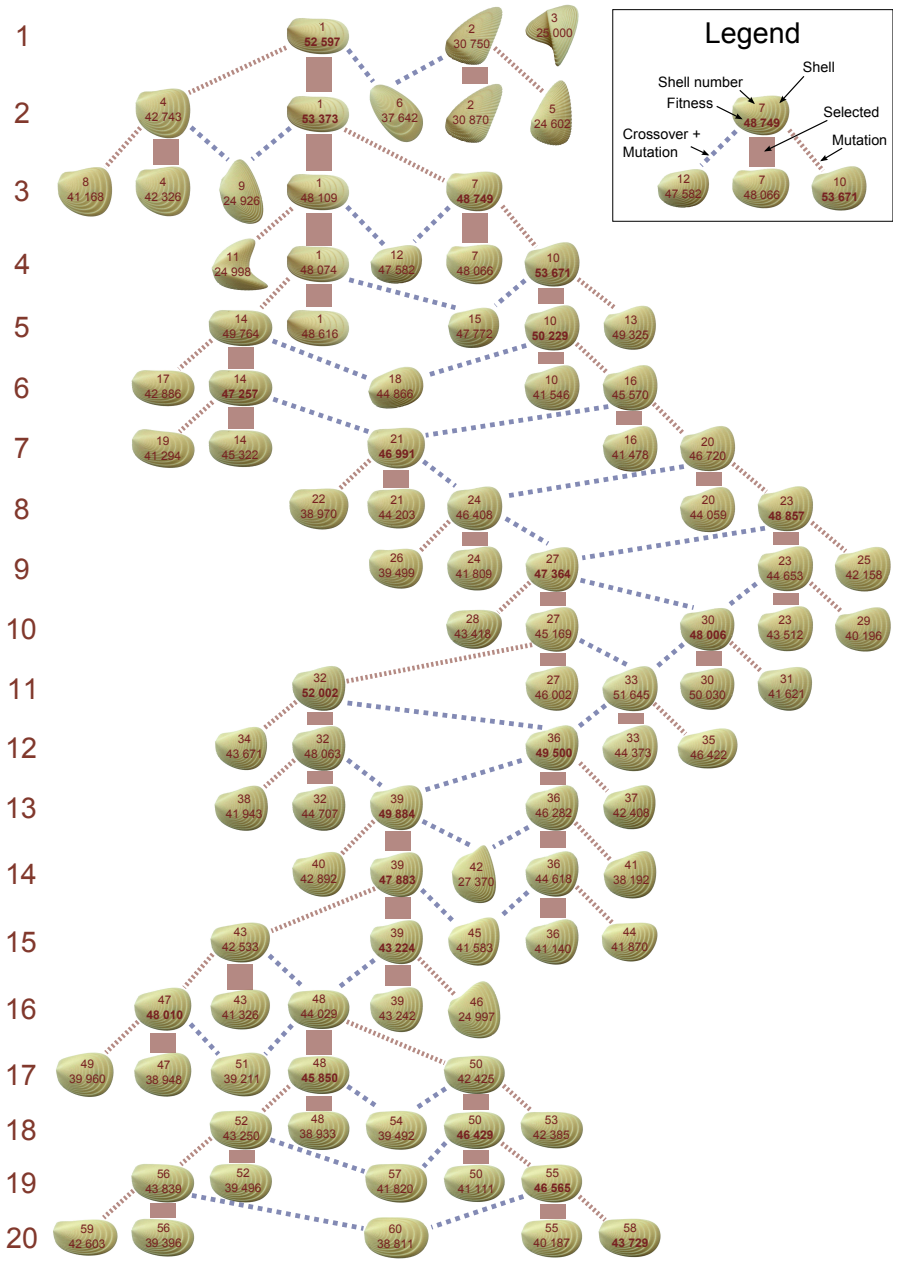

Figure 8: Phylogenetic tree. Each row corresponds to a generation. A generation contains three new individuals generated by reproduction and two re-evaluated individuals selected in the last generation. As reproduction operators, mutation (red dotted lines) and crossover + mutation (blue dashed lines) were used.

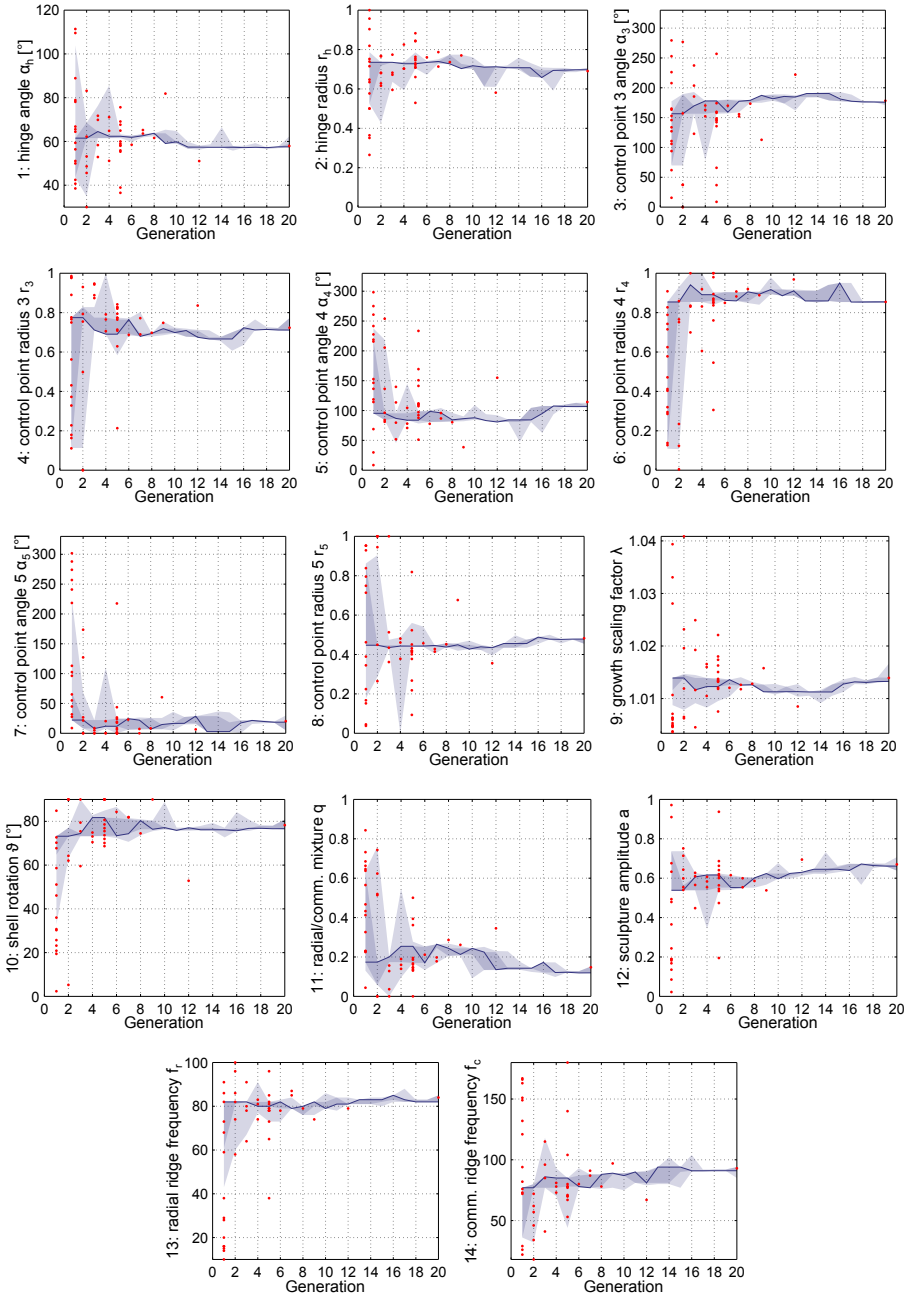

Figure 9: Parameter range evolution. The plots show how the parameters changed during evolution. The solid line follows the best individual, the dark shaded area covers the selected individuals, the bright shaded area covers all individuals. The red dots represent shells that were generated but discarded because they were invalid, i.e. because they did not result in printable shell morphologies. The range of the y-axis corresponds to the range of the respective parameter.

higher values of r_h. There were less valid shells in the regions where two of the angles α_3-α_5 had a similar value.

Figure 10 shows how the computed phenotypic parameters changed over the course of evolution.

Correlations of the genetic and the phenotypic parameters and the burrowing depth D with the fitness are listed in Table 3. The table is sorted according to the p-value of the Pearson correlation. The order is similar for the original fitness measure and the one corrected by "shift 2". The shift 2 correction of the fitness values often increases the correlation coefficients, e.g. from -0.68 to -0.73 for the tallness.

4 DISCUSSION

In this paper we presented an experimental setup to simulate the burrowing behaviour and morphological evolution of bivalves. Using evolutionary algorithms, the first ever artificially evolved bivalve shapes were created. While the used method as such has many advantages, the system suffered from two main drawbacks. Because of the lack of an optimal mechanism to standardize the sediment, fluctuations in the sediment state disturbed the performance measure of the different individuals. And due to geometrical restrictions of the valves used to assemble the shells, many created geometries were invalid, increasing the brittleness of the evolutionary system.

4.1 Evolution Results

As seen in Figure 5, depth decreased during the course of the evolutionary experiments. The difference between the median depth in the first generation and the median depth in the last generation is 13.8 mm. As the fitness and with it the burrowing depth would be expected to increase during evolution, it can be assumed that this difference is due to the increasing compaction of the sediment. A similar value is observed in the repeated evaluations of individuals in Figure 6.1. The maximal range of different measurements for one single individual is 16.8 mm.

In contrast, the difference between all possible pairs within all generations is 5.1 mm $\pm$ 3.6 mm (mean $\pm$ standard deviation). Therefore, the influence of the sediment by far overweighs the effect of the shell morphology. This indicates that there may be a large pressure on bivalves to manipulate the sediment state, which they actually do by expelling water and moving the foot and the valves.

In this study, however, we were only concerned with the influence of the shell morphology on the burrowing performance. Although the repeated evaluations of individual shells gave a hint at how the state of the sediment changed, they did not suffice to remove the noise of the sediment. We therefore do not know the true depth curve, i.e. the depths that would have

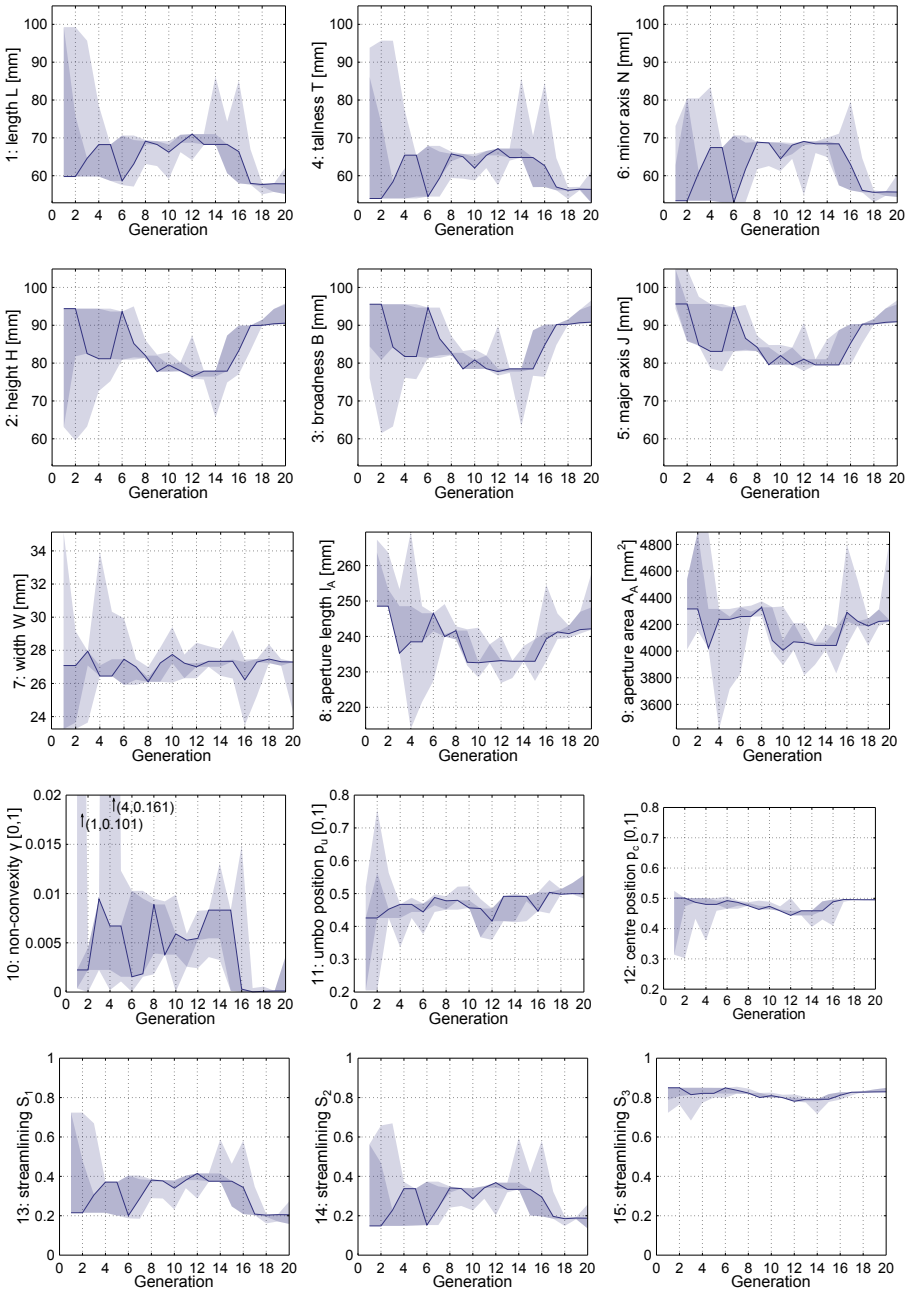

Figure 10: Phenotypic parameter range evolution. The plots show how the phenotypic parameters changed during evolution. The solid line follows the best individual, the dark shaded area covers the selected individuals, the bright shaded area covers all individuals.

	Pearson correlation				Spearman correlation			
	Fitness (orig.)		Fitness (shift 2)		Fitness (orig.)		Fitness (shift 2)	
Variable	p-value	r	p-value	r	p-value	r	p-value	r
$D-T$	3e-40	0.92	4e-29	0.85	0	0.84	6e-8	0.52
T	2e-14	-0.68	0	-0.73	5e-3	-0.28	5e-3	-0.28
L	3e-10	-0.58	7e-12	-0.62	0.14	-0.15	0.18	-0.14
S_2	6e-10	-0.57	2e-11	-0.62	9e-3	-0.26	9e-3	-0.26
l_A	4e-8	-0.52	2e-9	-0.56	2e-4	-0.37	1e-4	-0.38
p_c	5e-8	0.52	8e-10	0.57	0.30	0.11	0.30	0.10
f_r	6e-8	0.51	6e-9	0.55	0.55	0.06	0.93	0.01
S_1	9e-7	-0.47	1e-7	-0.50	0.19	-0.13	0.21	-0.13
α_5	1e-6	-0.47	2e-8	-0.53	0.06	-0.19	0.03	-0.22
α_4	2e-6	-0.46	2e-8	-0.53	0.01	-0.26	2e-3	-0.31
S_3	5e-6	0.44	2e-6	0.46	0.25	0.12	0.15	0.15
r_4	2e-5	0.42	7e-7	0.48	0.38	0.09	0.17	0.14
γ	5e-5	-0.40	5e-6	-0.44	0.06	0.19	0.02	0.24
r_h	1e-4	0.37	2e-6	0.46	2e-3	0.31	4e-6	0.45
α_3	4e-4	0.35	3e-5	0.41	0.44	-0.08	0.37	-0.09
J	5e-4	-0.35	2e-4	-0.37	3e-3	-0.30	2e-3	-0.31
B	1e-3	0.33	5e-4	0.35	0.48	0.07	0.49	0.07
H	1e-3	0.33	5e-4	0.35	0.68	0.04	0.76	0.03
q	4e-3	-0.29	8e-4	-0.33	0.07	0.18	3e-3	0.30
r_3	6e-3	0.28	2e-3	0.31	0.86	0.02	0.72	-0.04
λ	0.02	0.24	0.01	0.25	0.45	-0.08	0.23	-0.12
D	0.03	0.23	0.01	0.26	7e-7	0.48	2e-4	0.37
a	0.03	-0.22	0.02	-0.24	2e-4	-0.37	1e-6	-0.47
ϑ	0.04	0.21	6e-3	0.28	0.46	-0.08	0.39	-0.09
A_A	0.04	-0.21	0.04	-0.21	0.03	-0.22	0.04	-0.20
N	0.08	-0.18	0.05	-0.20	0.41	-0.08	0.41	-0.08
α_h	0.22	-0.13	0.30	-0.11	0.28	0.11	0.04	0.21
r_5	0.24	-0.12	0.26	-0.11	0.02	-0.23	0.03	-0.22
p_u	0.27	0.11	0.20	0.13	0.02	-0.24	3e-3	-0.30
f_c	0.38	0.09	0.18	0.14	0.20	-0.13	0.06	-0.19
W	0.48	-0.07	0.42	-0.08	0.12	0.16	0.11	0.16

Table 3: Correlations of genetic and phenotypic parameters and the burrowing depth D with fitness (original and shift 2, see Figure 6). We computed Pearson and Spearman correlation. The p-values and the correlation coefficients r are given.

resulted if the sediment could be put into an identical state before each burrowing run.

The burrowing depth and indirectly the shell tallness were the two basic components of the fitness. This fact is reflected by the high correlation of the depths D minus tallness T with fitness shown in Table 3. The next highest correlations were found for tallness and length, which basically mean the same. A lower tallness improves the ability of the shell to vanish below the sediment surface and thus increases the fitness. While the burrowing depth decreased over the course of evolution due to the increasing sediment compaction, tallness may have been the main variable for evolution to optimize. This is supported by the fact that the correlation between tallness T and fitness is much higher than between burrowing depth D and fitness. Also, tallness had a larger variance than the burrowing depth: the overall burrowing depth was 95.6 mm $\pm$ 5.9 mm (mean $\pm$ standard deviation), i.e. varied by 6.2%, the overall tallness was 65.1 mm $\pm$ 10.5 mm varying by 16.2%. This indicates that it was easier to maximize fitness by a low tallness than by further penetrating into the sediment. The shell was therefore "spread" horizontally to occupy the top sediment layer where penetration was much easier than in deeper layers.

Since tallness was not controlled by one single parameter, the aperture curve had to be changed accordingly, involving eight aperture parameters as well as ϑ and λ. The latter does not change the ratio of the dimensions but, via the constant volume, the absolute size of the dimensions. In our experiments, we may have had a trade-off for λ between a small width W and a small tallness T. This may explain the low correlation of λ with fitness. For a fitness function only based on burrowing depth, we would probably have seen a significant decrease of W (increase of λ) over time.

Following tallness and length, streamlining S_2 had the next largest correlation with fitness. Note that the correlation coefficient of the streamlining S_3 has the opposite sign of that of S_2 and S_1. Fitness decreased with increasing streamlining S_2 but increased with increasing S_3. The assumption behind S_1 and S_2 is that streamlining grows with increasing vertical elongation of the shell and decreasing cross-sectional area perpendicular to the burrowing direction. However, the diverging results for the different measures show that the approximated value can be very different from a computation based on the actual shell geometry.

In our experiments, the effect of the overall shape was more important than the sculpture, which essentially stayed constant. There is only one sculpture parameter in the first half of Table 3, radial sculpture frequency f_r. However, since radial ridges were basically not expressed due to a low q parameter, it is likely that this parameter was coupled to another successful trait but did not increase fitness by itself. A reason for the low impact of the shell sculpture on fitness may also be that in our setup its function is limited to supporting the burrowing process. Most sculptural elements of

the shell are interpreted as barbs (Seilacher, 1981). Their function is to reduce the buoyancy of the shell during the digging. In our experimental setting, the steel cables simulating the pulling force of the foot muscles are under tension during the entire experiment and thus prevent the shell from floating up.

The fitness curve (Figure 7.1) did not feature major jumps, i.e. there was no instance of an innovative morphological feature significantly increasing fitness. As long as shell 1 stayed in the population, it produced a set of distinct shell morphologies (shells 4, 6, 9 and 11, see Figure 8), which, however, had all a low fitness. Later shells were all very similar due to the decreased mutation rate. More differing shells like 42 and 46 were penalized with a low fitness (drops in generations 14 and 16 in Figure 7.1).

As can be seen in the genetic parameter range evolution plot (Figure 9), the range of possible values was not covered and the values stayed relatively stable during the whole evolution. The phenotypic parameter range evolution plot (Figure 10) shows that there were still two minor transitions, separating the evolution into three phases, at generations 5-7 and 14-16. In the middle phase, shells were relatively tall, returning to a low tallness in the transition to the third phase.

Compared to the realized parameters, the parameters that were tried but resulted in invalid shells covered a larger interval (Figure 9). This indicates that invalidity may account for the stability of the values during evolution. Because the probability of hitting a valid shell was larger close to an already realized valid shell, evolution reduced the mutation rate leading to a stagnating pool of shell morphologies. The procedure of generating three new generations and choosing the one with the largest variation did not suffice to counteract this effect.

To summarize, our experiments led to a clear ranking of factors in terms of the effect size on burrowing performance: 1. sediment state, 2. overall shape, 3. sculpture. It is interesting to note that in both our experiment and in nature, elongated shells evolved (Kauffman, 1969). However, in our experiments, due to the restriction to a rigid morphology, there was an evolutionary pressure for elongation in horizontal direction to avoid deeper and harder layers of sediment. In nature, bivalves can take advantage of water ejection and valve motion to manipulate the sediment state, which enables them to reach deeper layers and makes an elongation in burrowing direction more beneficial.

4.2 Limitations

No biomimetic setup is able to imitate all aspects of the original process in nature. The impact of the experiments depends on how well the setup manages to simulate the components essential to the research question. In this study we examined the influence of the shell morphology on burrowing

performance in bivalves using a rocking burrowing motion. Some aspects of bivalve burrowing were omitted, e.g. water expulsion.

The major limitation of the presented setup was the lack of an effective method to standardize the sediment before each burrowing run. Pressing a metal plate onto the sediment did not provide a satisfactory reduction of the memory effect. The noise thus introduced into the fitness reduces the comparability of different morphologies because the effect of the sediment cannot be clearly separated from the effect of the morphology. Since the differences between individuals usually decrease during evolution, the result of selection will be increasingly random.

Brittleness is the probability that a small change in the parameters will have a large effect on the fitness, e.g. lead to a sharp drop in fitness or even to an invalid individual that cannot be evaluated (Ronald, 1997). In the applied evolutionary algorithm, the major drawback was the increased brittleness due to invalid shells. Small changes in the parameters were able to render a well performing shell invalid. Still, we found that shells closer to a valid shell were more likely to be valid as well. This led to a fast decrease in the adaptive mutation rate. To counteract this effect, we employed a mechanism that generated three versions of a new generation and then manually chose the one with the highest variety. This whole procedure is not satisfactory. For future experiments, the morphological shell model, its encoding and the geometrical restrictions due to the coupling mechanism should therefore be revised to avoid invalid shells.

According to Arnold (1983), the mapping from morphology to fitness can be separated into the mapping from morphology to performance and the mapping from performance to fitness. Our study is based on two simplifying assumptions or restrictions that need to be considered when interpreting the results: 1) it is assumed that there is only one performance variable, namely burrowing performance; and 2) it is assumed that fitness is proportional to burrowing performance.

Both assumptions are not generally true. The shell morphology does, e.g., also influence the overall fitness by its performance in anchoring within the sediment or in protection against predators. Also, it is not entirely clear if there is an evolutionary pressure to go as deep into the sediment as possible, since several other factors like the concentration of oxygen or nutrients influence burrowing depth as well (da Silva Cândido and Brazil Romero, 2007; Edelaar, 2000; Marsden and Bressington, 2009; Schwalb and Pusch, 2007; Stanley, 1970). We assume that there is nevertheless a pressure to hide the shell within the sediment by at least burying the whole shell, and that therefore it is reasonable to assume a linear relationship between burrowing performance and fitness in the depth ranges covered in this study. While the two assumptions restrict the generality of the reported results, they help focus on a practicable and relevant subset of the natural phenomenon.

Another drawback of the experiments is the large required effort in time

and resources. As a result, only a small population and a small number of generations could be simulated. This increases the probability to get stuck in local optima of the fitness landscape.

4.3 Future Work

The experiments in this study may be repeated under both the same and different conditions (esp. fitness function, initial population) to get a better understanding of general evolutionary pressures working on the functional morphology of burrowing bivalves. To perform efficient experiments, the execution of repeated burrowing runs should be automated.

Any study trying to repeat experiments of a similar kind as described here should implement an improved method to standardize the sediment between burrowing runs. We suggest using a combination of sediment loosening, e.g. by a high pressure water supply in the bottom plate, and subsequent uniform sediment compaction, e.g. by vibrating the whole sediment compartment.

While in evolutionary robotics usually only the controller of a robot is evolved (Floreano et al., 2008), our setup can easily be used to co-evolve the shell morphology and burrowing motion pattern. It would be interesting to study the interaction of morphology and control in evolution.

The mathematical model of the shell morphology may be replaced or extended to capture a larger variety of overall shell shapes. In particular, the evolved shells were all orthogyrate, while many burrowing bivalve species have prosogyrate shells. This condition is known to be beneficial for burrowing (Stanley, 1975b).

The surface sculpture in this study was limited to radial and commarginal ridges and mixtures of them. Findings of Stanley (1969) suggest that skew ridges may improve the burrowing performance. To test this, a method that can generate a larger variety of surface patterns, including skew ridges, should be used. We would suggest to apply a reaction-diffusion system similar to the one described by Meinhardt and Klingler (1987).

The setup may be used to test the properties of fossil shapes. Using a computed tomography (CT) scanner, a fossil may be digitized and after the necessary modifications 3D printed as plastic valves. The shape could then be compared to other shapes, e.g. from recent related species. By testing the fossil shape in different types of sand, one could learn more about the possible habitats of the fossil species. Also, using artificial evolution, it may be possible to identify the most suitable burrowing motion for a given fossil.

4.4 Conclusion

To our knowledge, we were the first to perform an experiment to evolve physical bivalve shell morphologies using an evolutionary algorithm. We

combined well established components like geometric models for generating bivalve shell shapes, evolutionary algorithms and 3D printing devices. The experiments were done in a tank containing water and sand, the rocking burrowing motion typical for bivalves was applied to the printed shells by an external actuation system.

The results show that the influence of the sediment state is a main – and so far underestimated – factor for the effectiveness of bivalve burrowing. Granular media show highly complex dynamics that are still not well understood (Jaeger and Nagel, 1992; Losert et al., 2000; Sassa et al., 2011; To et al., 2001; Umbanhowar and Goldman, 2010). As long as there are no reliable and detailed computer simulations available, only physical experiments can deliver realistic results. When just considering shell morphology and ignoring the influence of the valve and foot motion, shells with a small vertical diameter are best suited to vanish within the sediment, confirming the high resistance of deeper sediment layers and the necessity for the manipulation of the sediment compaction state to burrow deeper. Commarginal and radial shell sculpture plays a minor role in the effectiveness of burrowing, if we can exclude buoyancy.

While the synthetic approach is used in biomimetic projects to emulate a large variety of recent organisms and animal behaviour, it is not common in palaeontology. However, we suggest it is well suited to complement analytical studies, e.g. by testing the morphological features of fossil species in an experimental setup like the one presented here. Moreover, it is insightful to not only emulate the dynamics of behaviour, but also evolutionary pressure. This is the main idea of the described method. While evolutionary algorithms are commonly used as bio-inspired optimization techniques, we believe that the reverse way is just as fruitful: using them as a tool to identify and study evolutionary pressure on the functional morphology of organisms.

Evolutionary algorithms contrast to other models of evolution, common in palaeontology, which are based on statistics, population means and empirically determined rates of evolution (Arnold et al., 2002; Lande, 1976; Polly, 2004). While those approaches quantify evolutionary change by statistically analysing large data sets of phenotypic characters of natural species, the approach using evolutionary algorithms actively simulates the process of evolution and is based on an artificial genome that is used to generate different specific morphologies that are tested using a specific fitness function. We do not suggest to replace any method by the proposed method, but we believe it is a valuable additional tool that is particularly suited to test specific hypotheses and to generate and compare morphologies that do not exist in nature. A disadvantage of the proposed method may be that it is more difficult to relate the results to natural species and that only small population sizes and generation numbers are possible due to the resources and time needed to build the physical setup, to print the shells and

to perform the experiments.

Although the presented setup had drawbacks, we believe that the method has a large potential for future studies. In particular, we see the following advantages of our method: 1) In addition to standard morphometric analyses of fossilized shapes, the functional morphology can be tested in action; 2) Tests are more realistic using a physical setup than a computer simulation, especially for sandy sediments that are still hard to simulate in the computer; 3) Factors that may have exerted an evolutionary pressure on functional morphology may be isolated; 4) Optimal burrowing morphologies can be generated under different conditions (fitness functions); 5) Using morphological models and 3D printers, the whole theoretical morphospace can be covered, there is no restriction to the shapes of available specimens; 6) Innovations in functional morphology can be identified by analysing jumps or other transitions in the artificial evolution; 7) The bivalve shell morphology and the applied burrowing motion pattern can be completely controlled, which allows systematic experiments or the application of evolutionary algorithms; 8) The burrowing performance can be quantified using different sensors; 9) Due to the full access to the detailed geometry of all shells, morphometric measures such as streamlining can be computed exactly; 10) The exact definition of the shell morphologies increases the repeatability of experiments; 11) several aspects of the method, like the mathematical shell model, the burrowing motion or the fitness function, can be easily changed to reflect the purpose of future experiments; 12) 3D printing techniques will be cheaper, faster, more accurate and possibly extend to other materials in the future and offer even more possibilities to investigate (functional) morphologies.

ACKNOWLEDGEMENTS

The authors would like to thank R. Pfeifer for providing the AILab infrastructure including the 3D printer. We would also like to thank the Swiss National Science Foundation for funding this research (projects 113934 and 129900).

REFERENCES

Adams, D.C., Rohlf, F.J., and Slice, D.E. 2004. Geometric morphometrics: Ten years of progress following the " revolution". *Italian Journal of Zoology*, 71:5–16.

Amler, M., Fischer, R., and Schröder-Rogalla, N. 2000. *Muscheln*, volume 5 of *Haeckel-Bücherei*. Enke im Georg Thieme-Verlag, Stuttgart. ISBN 3-13-118391-8.

Arnold, S., Pfrender, M., and Jones, A. 2002. The adaptive landscape as

a conceptual bridge between micro- and macroevolution. In A. Hendry and M. Kinnison (eds.), *Microevolution Rate, Pattern, Process*, volume 8 of *Contemporary Issues in Genetics and Evolution*, pp. 9–32. Springer Netherlands. ISBN 978-1-4020-0108-6. doi: 10.1007/978-94-010-0585-2_2.

Arnold, S.J. 1983. Morphology, performance and fitness. *Integrative and Comparative Biology*, 23:347–361. ISSN 1540-7063. doi: 10.1093/icb/23.2.347.

Bäck, T. 1997. *Handbook of evolutionary computation.* Oxford University Press, New York. ISBN 0750303921.

Bentley, P.J. 1999. *Evolutionary design by computers.* Morgan Kaufmann Publishers, San Francisco, CA. ISBN 978-1558606050.

Beyer, H.G. 1995. Toward a theory of evolution strategies: Self-adaptation. *Evolutionary Computation*, 3:311–347. ISSN 1063-6560. doi: 10.1162/evco.1995.3.3.311.

Beyer, H.G. and Schwefel, H.P. 2002. Evolution strategies – a comprehensive introduction. *Natural Computing*, 1:3–52. ISSN 15677818. doi: 10.1023/A:1015059928466.

Bookstein, F.L. 1997. *Morphometric tools for landmark data: Geometry and biology.* Repr. edition. Cambridge University Press, Cambridge. ISBN 9780521585989.

Crampton, J.S. 1995. Elliptic fourier shape analysis of fossil bivalves: some practical considerations. *Lethaia*, 28:179–186. ISSN 0024-1164. doi: 10.1111/j.1502-3931.1995.tb01611.x.

da Silva Cândido, L.T. and Brazil Romero, S.M. 2007. A contribution to the knowledge of the behaviour of anodontites trapesialis (bivalvia: Mycetopodidae). the effect of sediment type on burrowing. *Belgian Journal of Zoology*, 137:11–16.

de la Huz, R., Lastra, M., and López, J. 2002. The influence of sediment grain size on burrowing, growth and metabolism of donax trunculus l. (bivalvia: Donacidae). *Journal of Sea Research*, 47:85–95. ISSN 13851101. doi: 10.1016/S1385-1101(02)00108-9.

Dryden, I.L. and Mardia, K. 1998. *Statistical shape analysis.* Wiley series in probability and statistics. Wiley & sons, Chichester. ISBN 978-0471958161.

Edelaar, P. 2000. Phenotypic plasticity of burrowing depth in the bivalve macoma balthica: experimental evidence and general implications. *Evolutionary biology of the bivalvia*, 177:451–458.

Eggenberger Hotz, P. 2003. Genome-physics interaction as a new concept to reduce the number of genetic parameters in artificial evolution. In *IEEE Congress on Evolutionary Computation, CEC '03*, pp. 191–198. IEEE. ISBN 0-7803-7804-0. doi: 10.1109/CEC.2003.1299574.

Floreano, D., Husbands, P., and Nolfi, S. 2008. Evolutionary robotics. In B. Siciliano and O. Khatib (eds.), *Springer handbook of robotics*. Springer, Berlin. ISBN 978-3-540-23957-4.

Fogel, D.B. 1998. *Evolutionary Computation: The Fossil Record*. 1 edition. Wiley-IEEE Press. ISBN 0780334817.

Fowler, D.R., Meinhardt, H., and Prusinkiewicz, P. 1992. Modeling seashells. In E.E. Catmull and B.H. McCormick (eds.), *SIGGRAPH '92 conference proceedings*, volume 26.1992,2 of *Computer graphics*, pp. 379–387. ACM Press, New York. ISBN 0201515857.

Germann, D.P. and Carbajal, J.P. 2013. Burrowing behaviour of robotic bivalves with synthetic morphologies. *Bioinspiration & Biomimetics*, 8:046009. ISSN 1748-3182. doi: 10.1088/1748-3182/8/4/046009.

Hammer, Ø. and Bucher, H. 2005. Models for the morphogenesis of the molluscan shell. *Lethaia*, 38:111–122. ISSN 0024-1164.

Jaeger, H.M. and Nagel, S.R. 1992. Physics of the granular state. *Science*, 255:1523–1531. ISSN 0036-8075. doi: 10.1126/science.255.5051.1523.

Kauffman, E.G. 1969. Form, function, and evolution. In L.R. Cox (ed.), *Mollusca 6: Bivalvia*, Treatise on invertebrate paleontology Part N N 0028639. The Geological Society of America.

Koller-Hodac, A., Germann, D.P., Gilgen, A., Dietrich, K., Hadorn, M., Schatz, W., and Eggenberger Hotz, P. 2010. Actuated bivalve robot: Study of the burrowing locomotion in sediment. In *IEEE International Conference on Robotics and Automation (ICRA), 2010*, pp. 1209–1214. IEEE, Piscataway, NJ. ISBN 9781424450381.

Lande, R. 1976. Natural selection and random genetic drift in phenotypic evolution. *Evolution*, 30:314. ISSN 00143820. doi: 10.2307/2407703.

Langton, C.G. 1989. *Artificial life: The proceedings of an Interdisciplinary Workshop on the Synthesis and Simulation of Living Systems held september, 1987, in Los Alamos, New Mexico*, volume 6 of *Santa Fe Institute studies in the sciences of complexity. Proceedings*. Addison-Wesley, Redwood City Calif. ISBN 0201093464.

Lipson, H. and Pollack, J.B. 2000. Automatic design and manufacture of robotic lifeforms. *Nature*, 406:974–978. ISSN 00280836. doi: 10.1038/35023115.

Losert, W., Géminard, J.C., Nasuno, S., and Gollub, J. 2000. Mechanisms for slow strengthening in granular materials. *Physical Review E*, 61:4060–4068. ISSN 1063-651X. doi: 10.1103/PhysRevE.61.4060.

Marsden, I.D. and Bressington, M.J. 2009. Effects of macroalgal mats and hypoxia on burrowing depth of the new zealand cockle (austrovenus stutchburyi). *Estuarine, Coastal and Shelf Science*, 81:438–444. ISSN 0272-7714. doi: 10.1016/j.ecss.2008.11.022.

McGhee, G.R. 1999. *Theoretical morphology: The concept and its applications*. Perspectives in paleobiology and earth history. Columbia Univ. Press, New York, USA. ISBN 0231106173.

Meinhardt, H. and Klingler, M. 1987. A model for pattern formation on the shells of molluscs. *Journal of Theoretical Biology*, 126:63–89.

Okamoto, T. 1988. Analysis of heteromorph ammonoids by differential geometry. *Palaeontology*, 31:35–52.

Polly, P.D. 2004. On the simulation of the evolution of morphological shape: multivariate shape under selection and drift. *Palaeontologia Electronica*, 7:1–28.

Raup, D.M. and Michelson, A. 1965. Theoretical morphology of the coiled shell. *Science*, 147:1294–1295. ISSN 0036-8075. doi: 10.1126/science.147.3663.1294.

Rechenberg, I. 1973. *Evolutionsstrategie: Optimierung technischer Systeme nach Prinzipien der biologischen Evolution*, volume 15 of *Problemata*. Frommann-Holzboog, Stuttgart-Bad Cannstatt. ISBN 3772803733.

Rechenberg, I. 2000. Case studies in evolutionary experimentation and computation. *Computer Methods in Applied Mechanics and Engineering*, 186:125–140. ISSN 00457825. doi: 10.1016/S0045-7825(99)00381-3.

Ronald, S. 1997. Robust encodings in genetic algorithms: a survey of encoding issues. In *Proceedings of 1997 IEEE International Conference on Evolutionary Computation (ICEC '97)*, pp. 43–48. IEEE. ISBN 0-7803-3949-5. doi: 10.1109/ICEC.1997.592265.

Sassa, S., Watabe, Y., Yang, S., Kuwae, T., and Thrush, S. 2011. Burrowing criteria and burrowing mode adjustment in bivalves to varying geoenvironmental conditions in intertidal flats and beaches. *PLoS ONE*, 6:e25041. ISSN 1932-6203. doi: 10.1371/journal.pone.0025041.

Savazzi, E. and Huazhang, P.A. 1994. Experiments on the frictional properties of terrace sculptures. *Lethaia*, 27:325–336. ISSN 0024-1164. doi: 10.1111/j.1502-3931.1994.tb01583.x.

Schwalb, A.N. and Pusch, M.T. 2007. Horizontal and vertical movements of unionid mussels in a lowland river. *Journal of the North American Benthological Society*, 26:261–272. ISSN 0887-3593. doi: 10.1899/0887-3593(2007)26[261:HAVMOU]2.0.CO;2.

Schwefel, H.P. 1995. *Evolution and optimum seeking*. Sixth-generation computer technology series. Wiley, New York. ISBN 978-0471571483.

Seilacher, A. 1981. Konstruktionsmorphologie von muschelgehäusen. In W.E. Reif (ed.), *Funktionsmorphologie*, Paläontologische Kursbücher Band 1 1 0015798. Paläontologische Gesellschaft Selbstverlag.

Seilacher, A. 1984. Constructional morphology of bivalves: Evolutionary pathways in primary versus secondary soft-bottom dwellers. *Palaeontology*, 27:207–237.

Sims, K. 1994. Evolving 3d morphology and behavior by competition. *Artificial Life*, 1:353–372. ISSN 1064-5462. doi: 10.1162/artl.1994.1.4.353.

Stanley, S.M. 1968. Post-paleozoic adaptive radiation of infaunal bivalve molluscs: A consequence of mantle fusion and siphon formation. *Journal of Paleontology*, 42:214–229. ISSN 00223360.

Stanley, S.M. 1969. Bivalve mollusk burrowing aided by discordant shell ornamentation. *Science*, 166:634–635. ISSN 0036-8075. doi: 10.1126/science.166.3905.634.

Stanley, S.M. 1970. *Relation of shell form to life habits of the Bivalvia (Mollusca)*, volume 125 of *Memoir / The Geological Society of America*. The Geological Society of America, Boulder, Colorado, USA. ISBN 05854216.

Stanley, S.M. 1975a. Adaptive themes in the evolution of the bivalvia (mollusca). *Annual Review of Earth and Planetary Sciences*, 3:361–385. ISSN 0084-6597. doi: 10.1146/annurev.ea.03.050175.002045.

Stanley, S.M. 1975b. Why clams have the shape they have: An experimental analysis of burrowing. *Paleobiology*, 1:48–58.

Syswerda, G. 1989. Uniform crossover in genetic algorithms. In J.D. Schaffer (ed.), *Proceedings of the 3rd International Conference on Genetic Algorithms, George Mason University, Fairfax, Virginia, USA, June 1989*, pp. 2–9. Morgan Kaufmann. ISBN 1-55860-066-3.

To, K., Lai, P.Y., and Pak, H. 2001. Jamming of granular flow in a two-dimensional hopper. *Physical Review Letters*, 86:71–74. ISSN 0031-9007. doi: 10.1103/PhysRevLett.86.71.

Trueman, E.R. 1966. Bivalve mollusks: Fluid dynamics of burrowing. *Science*, 152:523–525. ISSN 0036-8075. doi: 10.1126/science.152.3721.523.

Umbanhowar, P. and Goldman, D.I. 2010. Granular impact and the critical packing state. *Physical Review E*, 82. ISSN 1063-651X. doi: 10.1103/PhysRevE.82.010301.

Watters, G.T. 1993. Some aspects of the functional morphology of the shell of infaunal bivalves (mollusca). *Malacologia*, 35:315–342.

Webb, B. 2000. What does robotics offer animal behaviour? *Animal Behaviour*, 60:545–558. ISSN 00033472. doi: 10.1006/anbe.2000.1514.

Winter, A.G., Deits, R.L.H., and Hosoi, A.E. 2012. Localized fluidization burrowing mechanics of ensis directus. *Journal of Experimental Biology*, 215:2072–2080. ISSN 0022-0949. doi: 10.1242/jeb.058172.

Appendix G

Additional Methods and Materials

We followed an entirely synthetic approach in this project. This section describes the experimental setup and how we used it to mimic bivalve burrowing behaviour. The setup has been built and improved over several years. Therefore also some of the history of these improvements and their benefits are reported.

It is clear that an experimental setup can only capture a part of the real process and has to omit elements that are technically hard to reproduce or irrelevant for the purpose of the study. One objective in evaluating the results was to assess if the chosen elements suffice to reproduce a satisfying bivalve burrowing simulation.

The setup described here used models of bivalve shells that were manufactured using a 3D printer. The rocking burrowing motion was applied to the model by an external actuation mechanism. The controlled parameters covered the shell morphology, the pulling force, the step sizes and the timing schedule of the motion.

It is seen as good practice to develop in parallel a physical robotic simulation and a virtual computer simulation of the phenomenon of interest. We therefore searched for a suitable simulation software for granular media and implemented a version of such a simulation using the PhysX SDK (PhysX SDK). Finally, however, we found it was not possible to work both on a sophisticated simulation and on a physical setup within the limits of this project. We decided the robotic setup and the experiments to be more important than the simulation and stopped our efforts to implement one. See section 3.2.3 for a description of the implemented prototype.

We did also build a second, more complicated setup that more closely emulated the burrowing sequence described in Figure 2.2. The bivalve in that setup had four degrees of freedom and could move the valves and an artificial foot using a hydraulic system. In contrast to the previous setup it was therefore "mechanically autonomous", i.e. it was not actuated externally. The energy (i.e. pressured oil) was still supplied from outside. While the hydraulic shell has been tested for its functionality, the hydraulic setup as a whole has not been finished and tested. We therefore do not report any results from this setup and describe it in the future work section (3.3).

G.1 The Experimental Setup

The setup consisted of the following main elements: 1) models of bivalve shells, 2) a burrowing environment, 3) an actuation system, 4) a water expulsion system and 5) a measurement system. Shells in this setup were one-piece objects that could not open and close the valves. Using a 3D printer, a large variety of different shell morphologies could be manufactured (Figure G.1 and

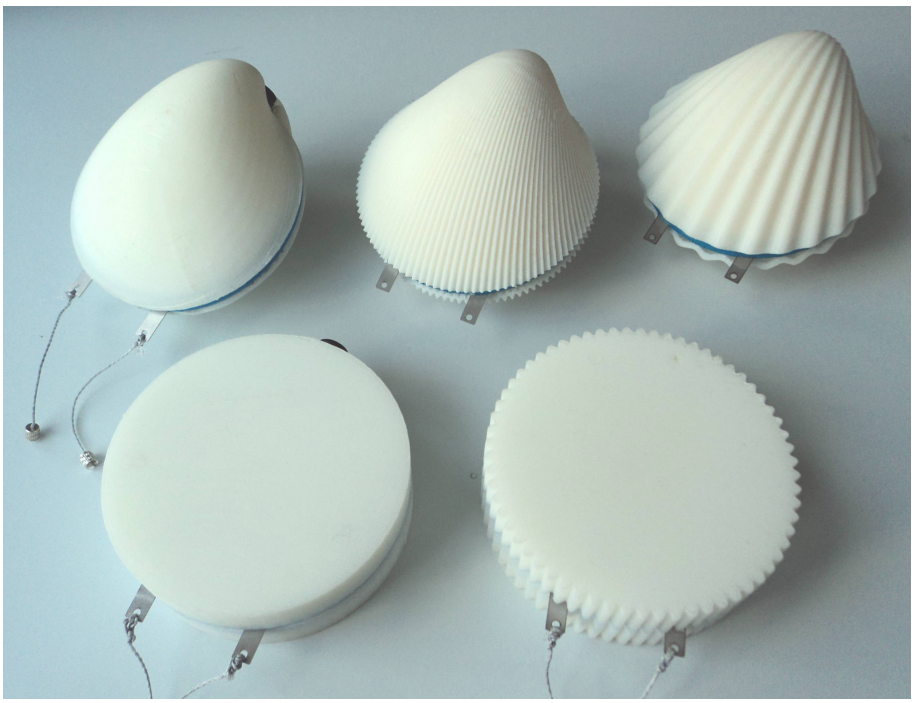

Figure G.1: Shell collection. These are five example shells that were printed. From top left to bottom right: BB-smooth, BB-radial1, BB-radial2; D-smooth, D-cogged. The circular aperture curve was the same for all shells, it had a diameter of 8 cm. This picture shows shells built using the U-shaped metal piece and the rubber tube for water expulsion. Cf. the modular shells shown in the pictures in chapter E.

pictures in chapter E). The burrowing environment consisted of an aquarium containing water and quartz sand. The shells were actuated by two external linear motors that pulled them into the soil via strings that were guided through the sediment and that exited the aquarium at the top. By alternately pulling, the motors could induce a rocking motion of the shell similar to the burrowing sequence described in Figure 2.2. The measurement system was integrated into the control system of the linear motors. Another separate system provided a water supply to the shells to simulate water expulsion.

G.1.1 Shells

During the project a large variety of different shell models have been created and tested, see Figure G.1 for five examples. The shells were manufactured using a 3D printer (Dimension 3D printer) and usually assembled from their two valves, which were printed separately. Valves had two sides: the outer side, i.e. the actual shell morphology, and the inner side, which in the natural case would house the soft animal body, but was used in our case to contain structural elements. Bivalve shell models were created by gluing the two halves together (older versions used in chapters B, C and D) or by attaching them to a central metal disc by a bayonet coupling (newer versions used in chapters E and F). In the second case, the bivalves were thus modular, i.e. the valves could be easily replaced to test different morphologies.

To generate the bivalve shell shapes (the outer side of the valves), a virtual growth process

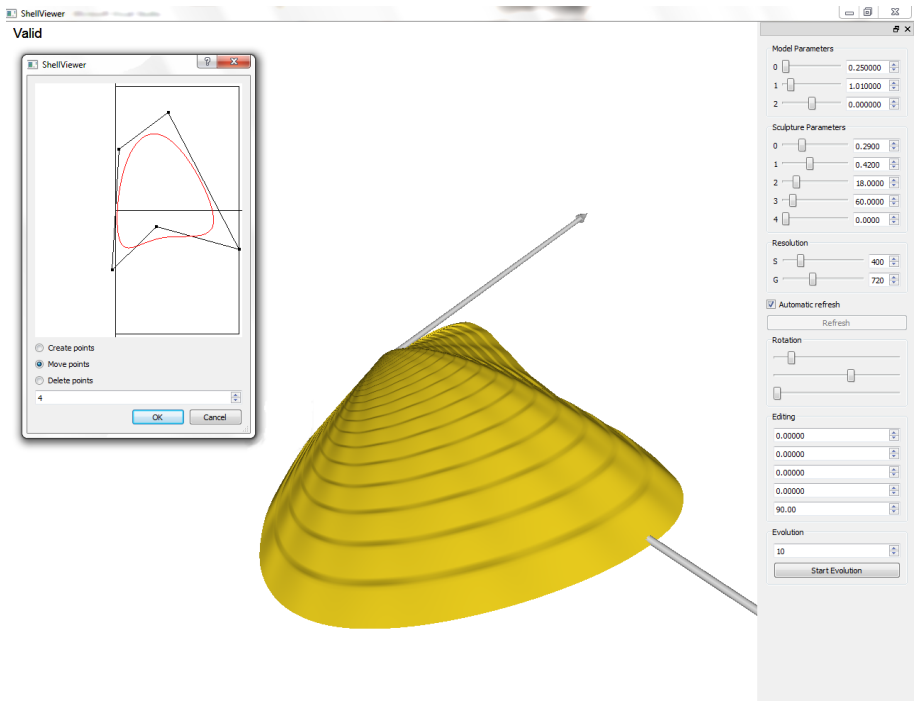

Figure G.2: ShellViewer screenshot. The picture shows the program used to visualize and edit shell morphologies based on parameters defining the overall shape and the surface sculpture. Using the panel on the right the parameters could be modified interactively. The smaller window on the left shows the aperture curve and its control polygon.

was used (see section 2.1.2 and chapter F). Figure G.2 shows a screenshot of the "ShellViewer", a program that was written in C++ and using Qt (Qt) to visualize the shells generated from different parameters.

The shells featured two additional components: cable attachment arms and water expulsion channels (see Figure G.3). The attachment arms ventrally protruded from the shell and were connected to the two cables actuating the shell. For the shells consisting of two glued valves, a U-shaped metal piece was inserted between them into a milled cutout (Figure G.3, left). When using the metal disc, the attachment location could be adjusted by pinning the arms to different holes (Figure G.3 right). The pins were then held in place by the attached valves.

In the glued shells, the water channels consisted of perforated rubber tubes held between the valves along the ventral shell edge (Figure G.3, left). The metal disc featured integrated water channels that were milled and drilled into it (Figure G.3, right). Water was then supplied to these channels from an external pump, which maintained a constant pressure of $1\ \mathrm{bar}$ in a reservoir. The valve controlling the flow from the reservoir to the shell was operated by the same controllers as the actuation system (section G.2).

G.1.2 Burrowing Environment

The experimental environment for the artificial bivalves was contained in a water tank. We used a cubic aquarium with an overall side length of $60\ \mathrm{cm}$ and a pane thickness of $1\ \mathrm{cm}$. The content volume was therefore $198.5\ \mathrm{l}$.

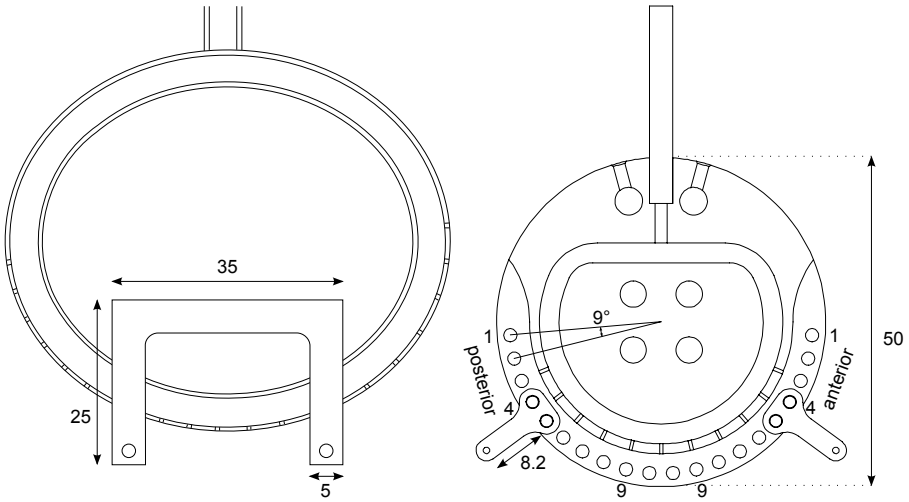

(a) (b)

Figure G.3: Cable attachment arms and water channels. A cross section along the sagittal plane is shown. Water could be supplied to both variants through a tube attached at the top. Water pumped through the channels was then expelled through the holes along the ventral edge. (a) fixed arm pair as used in sections B, C and D). (b) Adjustable arm pair used for the modular valves used in sections E and F. The attachment locations were adjusted by pinning the arms to different hole pairs. The arms in the picture are pinned to the hole pair 4.

We used de-ionized laboratory water to fill the tank, because we wanted to minimize scales and because it reduced the corrosion of the aluminium plates. Earlier experiments had been performed in tap water. In addition to the sediment and the metal parts inside the water tank, an amount of about $120\ \mathrm{l}$ of water was needed to fill the tank.

The area containing the sediment was restricted by two aluminium plates, one vertical and one horizontal (chapters E and F). The dimensions of the sediment area were $42\ \mathrm{cm} \times 58\ \mathrm{cm} \times 24\ \mathrm{cm}$ (width $\times$ length $\times$ height, $58.5\ \mathrm{l}$).

As sediment, we used well-rounded sorted quartz sand with grain sizes between 0.7 and $1.2\ \mathrm{mm}$. Note that due to the interaction of the shells with the sediment, the grains were ground, leading to smaller particles. The sand had a bulk density of $1500\ \mathrm{kg/m^3}$.

To avoid air bubbles and holes in the sediment, we filled it in when it was entirely dry and added the water afterwards. Another method was to gradually fill in the water and sediment in a synchronized fashion such that the wet sediment was evenly distributed and free of air and holes.

G.1.3 Actuation

To actuate the shells, we used two LinMot® P01-37x240F/460x660-C linear motors (LinMot) with the following characteristics: stroke max.: $660\ \mathrm{mm}$, peak force: $8\ \mathrm{A}$ or $206\ \mathrm{N}$, force constant: $25.8\ \mathrm{N/A}$, max. velocity: $2.6\ \mathrm{m/s}$, position repeatability: $\pm 0.01\ \mathrm{mm}$.

The motors were vertically mounted outside the water tank and connected to the shell by two steel cables as described in sections E and F. Carl Stahl® U 8199512 steel cables were used. They had a diameter of $1.2\ \mathrm{mm}$, or $0.95\ \mathrm{mm}$ without coating, a strand configuration of $8 \times 19 + 7 \times 7$ and a min. breaking load $850\ \mathrm{N}$, (Carl Stahl Technocables)). The cables were connected to the shells using necklace screws and clevises (E).

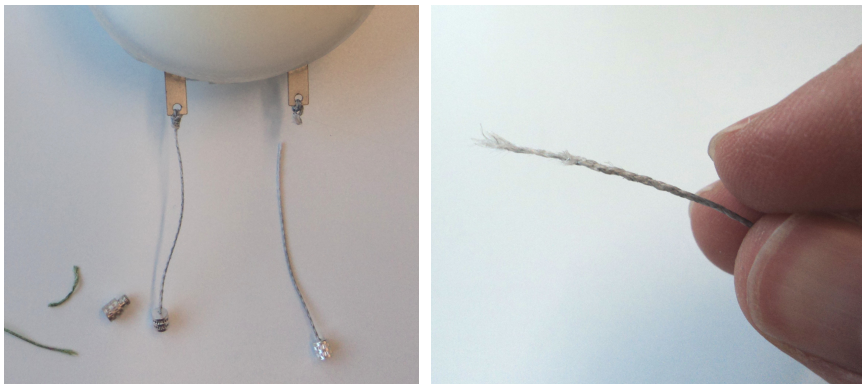

Figure G.4: Strings torn by the sediment. Bursts happened usually where the strings went through the holes in the bottom plate or close to the shells.

For early experiments (chapters B, C and D), we had used fishing lines ((Rapala Sufix Advanced Superline)) instead of steel cables. Although the breaking load was around $45\ \mathrm{kg}$, which is beyond the forces generated in the setup, these strings kept tearing (Figure G.4). The reason were small sand particles entering the holes in the bottom plate and abrading the strings. Torn strings had to be replaced, which originally had only been possible by removing water, sediment and bottom plate. Later, we devised the procedure described in Figure G.5. With this, the replacement of a string could be done in about an hour. Nevertheless, a part of the sediment had to be removed to replace a torn string. After refilling, the sediment was always in a loosened state, which disturbed the experiments (see section H.2). Other disadvantages of the fishing lines were creep and the gradual fastening of knots that led to an increased need to recalibrate the starting position of the shells. The expansion of the strings was found to be 0.1-$0.3\ \mathrm{mm}$ per burrowing run. There was also a trade-off for the smoothness of the string surface, because a smoother string was better to prevent abrasion but worse for robust knots.

The problem of sand particles entering the bottom holes was alleviated for the steel cables by adding a silicone sheath on top of the bottom holes (section E).

G.2 Motion Control

The linear motors connected to the shells were controlled by LinMot® B1100-GP-HC (LinMot) controllers. They could be configured and programmed using the software LinMot® Talk 4.3 and provided PID (proportional-integral-derivative) control and could execute sequence of instructions called the command table. We used the control program shown in Figure G.6 to induce a burrowing motion similar to the one described in Figure 2.2. The valve controlling the water expulsion was operated by this program as well (see also section G.1.1).

For an explanation of the control program, see also chapter E. We used two controllers, one for each motor. They were synchronized by a shared switch to start the execution of the program. The two controllers essentially executed the same program, up to their individual starting position and a time lag that delayed the second motor that was connected to the posterior part of the shell. Thus the motors alternated in pulling to induce the rocking motion.

To employ a natural control scheme mimicking the bivalve retractor muscles, we limited the pulling force and the step size. A constant force could be applied by setting a constant current, since the force exerted by the linear motors was proportional to the applied current. In the pulling

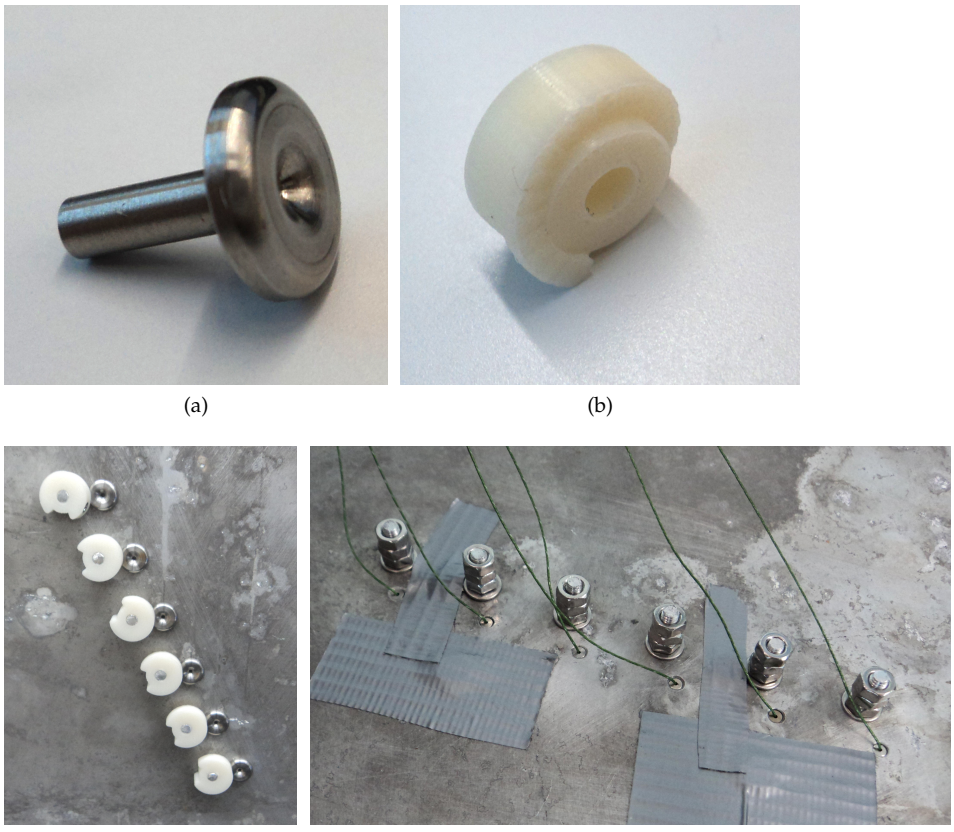

(a) (b)

(c) (d)

Figure G.5: String guides for the horizontal plate. The fishing lines ran through eyelets as the one shown in (a). These were put loosely into holes in the bottom plate only held by holders as the one shown in (b). The bottom side of the plate with inserted and fixed eyelets is shown in (c), the top side with the protruding axles to which the holders were fixed is shown in (d). A torn string was replaced by the following procedure: 1) a cylinder wall (a cut PET bottle) was inserted into the sediment above the hole in the bottom plate through which the torn string had run, 2) the sediment within the cylinder wall was removed, 3) when turning the axle, the holder unlocked of the eyelet, which fell into a bucket below the plate and could be retrieved from there, 4) the new string was put through the eyelet and the rest of the guiding structure of the setup 5) the eyelet was prevented from gliding off the string by a knot that could only be opened by pulling the motor end of the string, 6) the shell end of the string was inserted into the hole of the bottom plate using a needle and a telegripper, 7) the string and because of the knot the eyelet could be pulled through the hole, 8) the eyelet was fixed by turning the axle, 9) the knot was removed by pulling the motor string end, 10) the cylinder wall was removed.

phase of a burrowing step, a constant force was applied until the maximal step size or a time limit was reached. The pulling phase was followed by a waiting phase in which the current position was held until the beginning of the next burrowing step.

We tested a number of different controller policies until we decided to use the one described above. The first policy controlled the position of the linear motors using commands such as 'Go to position x' (see chapter B). This is a standard way to use the motors in industrial settings. The motors will use PID control to move to the target position using the desired speed and any available force necessary. The disadvantages of this scheme were: (1) While the given target positions (step sizes) were followed precisely, the only measurable output parameter to assess the performance of the shell was force (or current). Since the force was a result of PID control, it contained high fluctuations and was hard to interpret (e.g. results in chapter B). (2) This type of motion is unnatural, since bivalves do not have unlimited strength and do not follow a precise trajectory. We therefore switched to force control policies, where force was controlled and position (burrowing depth) was the output parameter to assess the burrowing performance.

The first version of force control we tested was using force sensors inserted between the slider ends and the cables. PID control was then used to keep the signals from the sensors constant during the pulling phase. This led to a more realistic behaviour. However, we did not find PID control parameters leading to a satisfying behaviour. The controller was either unstable or too slow to reach the desired force within the time period of a pulling phase. Also a combination of first setting a fixed force close to the desired force and then switching to PID control using the force sensor signal did not remove all oscillations.

After testing several variants, we then finally came up with the controller version shown in Figure G.6 that applied a fixed force and had two stopping criteria: step size and pulling phase duration. The disadvantage of this controller was that different friction characteristics of the motors and sliders led to differences in the tension of the two cables. We therefore calibrated the applied current to match the resulting tensions in the cables, but since the friction of the sliders

Figure G.6 *(following page)*: Control program (simplified pseudo-code), as used in chapters E and F. The controllers of the linear motors could execute a command table of a maximum of 31 instructions. Two variables v1 and v2 could be used. The captions on the left denote the general phases of the program. Variables that were changed for different configurations but were explicitly set in the control program for an experiment are in italic font. Instructions 1-5 initialized the program and moved the sliders to their initial positions p, such that that shell was touching the sediment and the cables were tight. For the posterior motor, the waiting period d_i included the lag with respect to the anterior motor. Instruction 6 looped over the burrowing steps (e.g. $n = 15$ burrowing steps). Since the number of variables was restricted to two, the counter had to be saved in instruction 7. Instructions 8-10 turned on and off water expulsion of duration d_w by sending a signal to the valve. Instructions 11-14 retrieved the current position and time and added the desired limits for step size s and pulling phase duration d_s. Instruction 15 switched from PID control to the application of a constant force F that had been set by instruction 3. Instructions 16-19 polled the current position and time to stop the pulling phase once one of the two limits was reached. For this diagram, instructions 18 and 19 have been omitted. They were necessary on the "no"-path from instructions 16 and 17 due to technical reasons but did not execute any operation. Instructions 20-22 turned off the constant force and switch back to PID control to hold the current position. Instructions 23-24 ensured a consistent step duration. This was necessary because the pulling phase could be switched off by reaching either the step size or the step duration limit. Instructions 26-28 retrieved the counter and waited for the duration given by d_p for the next burrowing step. Instructions 29-31 moved the sliders back to their home position and ended the program.

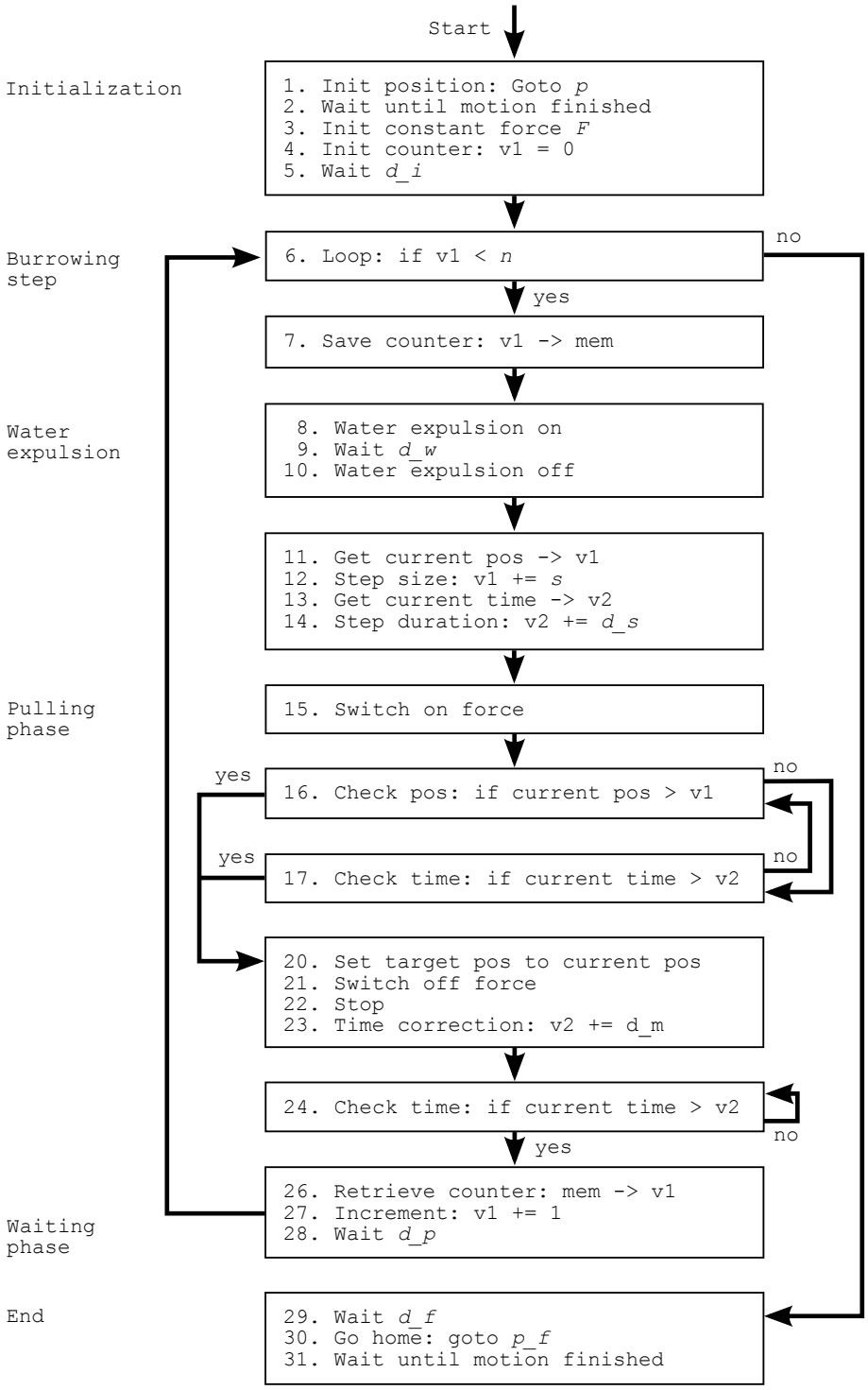
Start
Initialization
1. Init position: Goto p
2. Wait until motion finished
3. Init constant force F
4. Init counter: v1 = 0
5. Wait d_i
Burrowing step
6. Loop: if v1 < n
no
yes
7. Save counter: v1 -> mem
Water expulsion
8. Water expulsion on
9. Wait d_w
10. Water expulsion off
11. Get current pos -> v1
12. Step size: v1 += s
13. Get current time -> v2
14. Step duration: v2 += d_s
Pulling phase
15. Switch on force
yes
16. Check pos: if current pos > v1
no
yes
17. Check time: if current time > v2
no
20. Set target pos to current pos
21. Switch off force
22. Stop
23. Time correction: v2 += d_m
24. Check time: if current time > v2
no
yes
Waiting phase
26. Retrieve counter: mem -> v1
27. Increment: v1 += 1
28. Wait d_p
End
29. Wait d_f
30. Go home: goto p_f
31. Wait until motion finished

depended on the motion speed, it was not possible to achieve an identical behaviour of both motors. Usually, the tension in the posterior motor was a bit higher.

In the pause between successive pulling phases, PID control was used to maintain the current position of the shells. As the shell went deeper into the sediment, the tension in the cables increased so that an increasing force was necessary to hold the position in the waiting phases. Once this tension reached the level of the fixed pulling force, the shell did not move anymore. See chapter E for a discussion of this problem.

G.3 Experiments

G.3.1 Reproducibility

To unambiguously attribute a difference in burrowing performance to a difference in a factor of interest, all other factors – the shell model, the environment and the motion pattern – should be exactly the same for each experiment. In this section, factors that might have an influence on the burrowing process are listed together with our procedure to control them, if any.

Sediment State

It is obviously impossible to return to a state where the whole set of sand grains attain the same position and orientation as in a previous experiment. Nevertheless, the state of the sediment should be controlled as precisely as possible to achieve reproducible results. A rough measure for the compaction of the sediment can be gained by placing a weighted stick on the sediment surface and see how far it sinks in. Even when only considering this rough estimation of the sediment state, we could not achieve a satisfactory sediment standardisation, see section 3.2.

The finally used procedure was manually pressing a metal plate on the sediment surface to compact the sediment and to then slide a metal stripe along two metal bars mounted horizontally at either side of the sediment compartment to establish a sediment surface that was planar and always at the same height level.

We had also tried the following methods to control the sediment state (see Figure G.7):

Loosening with a rake The first procedure was to loosen the sediment by stirring it with a rake. The rake was attached by strings to a bar above the sediment compartment to make sure that its reach was constant. Nevertheless, the burrowing depths were very sensitive to how deeply the sediment was loosened (see Figure H.5). Also, we anticipated more significant results for water expulsion in compacted sediment. We therefore switched from loosening to compacting methods.

Compacting with a vibrating plate We tested a plate that could be placed on the sediment surfaces and vibrated using an electric motor rotating an excentric weight. However, this did not have any measurable influence on the sediment. Also adding thin walls to the plate that were inserted into the sediment did not change this result.

Compacting with a cylinder wall In tests with a round plastic bucket we had found that shaking it by rotational oscillation around its vertical axis was well suited to compact the sediment. We therefore tested a cylinder wall inserted into the sediment of the setup and manually shaken in the same manner. However, rotating the cylinder wall did not lead to more stable sediment conditions but introduced rotational jamming patterns into the sediment and also rotated the cables, resulting in a twisted motion of the shells during the burrowing process.

Waiting While small particles suspended in the water sink to the ground within hours or days, there are only minor events of collapsing cavities in the sediment if there is no interaction over a longer period of time. The compaction state does not substantially change, therefore waiting was not a valid option as a standardization technique. (Losert et al., 2000)

Starting position and orientation

The starting orientation of the shells was always upright and was held until the start of the burrowing process by the water supply tube (see E). The starting position was calibrated (i.e. the parameter p of the control program in Figure G.6 was adjusted for both motors) at the beginning of each experiment set (steel cables) or set of repetitions (fishing lines) such that the lowest point of the shell was touching the sediment surface. This was done using a metal bar placed on the bars mounted at the sediment compartment walls, with a precision of about $1\ \mathrm{mm}$.

Temperature

We did not control water temperature, because we did not assume it had any significant effect. However, it often changed considerably during an experiment series due to friction and to the absorption of body heat during manual interaction with the shells.

Water Level

We did not control the water level, except that we made sure that the shell was completely covered by water at all times during an experiment. The water level and thus the pressure in the sediment compartment could theoretically influence the burrowing process. Evaporation and the transport of water out of the tank by manual interaction made it necessary to replace the lost water regularly. Also, water expulsion increased the water level within the sediment compartment relative to the water level outside the compartment, where the water was sucked out by the pump. It took a few hours until the levels were balanced again.

G.3.2 Measurements

To assess the result of an experiment, two kinds of sensors were used: position sensors and force sensors. To measure the position, the internal sensors of the linear motors were used that measure the current position of the sliders very precisely ($\ll 1\ \mathrm{mm}$). To measure the applied force, force sensors were inserted between the slider ends and the cables. We used ME-Meßsysteme GmbH KD40S sensors with a nominal force range of $\pm 500\ \mathrm{N}$. The signals of the two position and two force sensors were collected by a National Instruments™ (NI) compactDAQ (data acquisition) device (National Instruments compactDAQ) and recorded using an NI LabView™2011 (National Instruments LabView) program on a computer. The recorded data for one burrowing run was therefore a sequence of 5-tuples containing a timestamp, the current position of both sliders and the current force measured by the force sensors. The sampling rate was $1613\ \mathrm{Hz}$.

In earlier experiments (including those reported in chapter C), we had used an RS232 connection directly from the motor controllers to a computer to record the data internally measured in the motors. These were the current position and current. The current could be translated into pulling force by multiplication with the force factor and adding the slider weight. This did not work well due to the slow and asynchronous serial communication. Replacing this connection by the NI cDAQ system brought the following advantages: 1) no invalid data (loss of information), 2) regular sampling, 3) higher sampling rate ($1613 Hz$ vs. 10–$100 Hz$), 4) synchronization of both

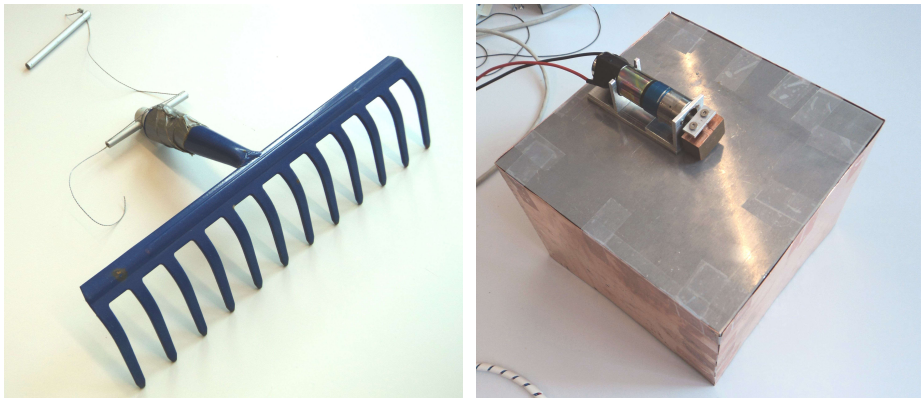

(a) (b)

(c) (d)

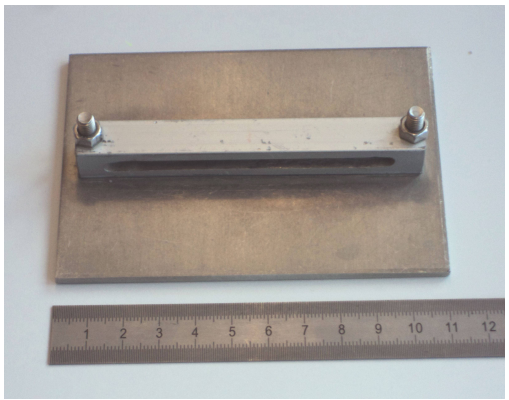

(e)

Figure G.7: Sediment standardisation techniques. (a) Rake used to stir the sediment. (b) Vibrating plate with walls. (c) Cylinder wall for rotational shaking. (d) The same cylinder wall inserted into the sediment. (e) The plate finally used.

motors. There was one disadvantage: it was not possible to record the current, because this signal could not be output from the controllers. It would have been possible to record this signal by using the old RS232 connection in parallel to the cDAQ. However, this would have undone some of the advantages of the new measurement system.

The measurements recorded from the position and force sensors were limited in two ways. First, they did not collect rich information about the burrowing process, such as the orientation of the shell, but only one-dimensional depth values. Second, the sensors did only indirectly measure the state of the shell. Due to the deformation of the setup and the cables under tension, the slider position systematically overestimated the true burrowing depth. To test the size of this effect, we added a scale onto the water supply tube to manually measure the displacement of the shell. See Figure H.3 for a comparison of the two depth measurements. Since the mapping of burrowing depth to cable tension and from cable tension to overestimation error is monotonous, we consider relative comparisons between burrowing depths of different experiments still valid. However, when comparing results on burrowing depth and absolute dimensions such as shell sizes, this overestimation error should be kept in mind.

G.3.3 Data collection and evaluation

A standard experiment was executed according to the following protocol:

1. Edit the motion parameters and choose the shell according to the goal of the experiment
2. Attach the shell to the cables and water supply tube and calibrate the starting position
3. Return the sediment into its standard state (following the procedure described in section G.3.1
4. Start the measurement
5. Execute the control program to perform a burrowing run
6. Stop the measurement
7. Repeat steps 3-6 until enough data is collected (usually 10 repetitions)

The collected data was cut before the first and after the last burrowing step. The repeated burrowing runs using the same configuration were synchronized to start at the same location. Average curves for depth as a function of time were then computed by first averaging over the anterior and posterior motor and then computing the median over all repetitions (cf. plots in section H. The final burrowing depth was defined as the latest value of this average depth curve. In this thesis "burrowing performance" is usually used as a synonym of "final median burrowing depth".

The term "experiment" is used to denote series of repeated burrowing runs (often called "repetitions") with identical parameter settings. Several experiments performed in a row used to compare different parameter settings are called "experiment set" or "experiment series" in this thesis. Any p-values given in the results were computed using a Wilcoxon ranksum test and assessing the difference between two experiments.

Appendix H

Additional results

This chapter reports additional experimental results not described in chapters B–F. While chapters E and F focus on the influence of the shell morphology, this chapter focuses on the influence of burrowing motion. Also, more results about the details of the burrowing process are provided.

We distinguish parameters that define the shell morphology (spatial or static parameters) from parameters that define the burrowing motion (temporal or dynamic parameters). This separation cannot be done in a strict way, because some parameters influence both morphology and motion pattern. For example, the location of cable attachment at the shell is a morphological parameter, but directly influences the rocking motion, since more distant attachment locations increase the rotation during the rocking motion. Also, the amount of water that natural bivalves can expel depends on their morphology (volume enclosed by the valves). But also dynamic aspects such as the timing of valve adduction and subsequent foot retraction are important.

As described in section G.3.2, we measured the slider positions and the pulling forces for each experiment. For evaluation, the curve of these values as a function of time may be analysed. Often, we reduce all repetitions of an experiment to one value giving the median final burrowing depth.

Because of the fluctuations of the sediment (section G.3.1), it is sometimes difficult to separate the effect of shell morphology or motion pattern from random effects. In some cases, we employed simple calculations to correct the data, i.e. to remove part of the error introduced by sediment fluctuations. These computations are always clearly declared. In all other cases, the original data was used.

H.1 Characteristics of the Burrowing Process

Figure H.1 shows the course of a typical burrowing run. If force control is used (section G.2), the steps become smaller with increasing depth like in real bivalves. There usually is a point at which the step size abruptly becomes almost zero (at $15\ \mathrm{s}$ in Figure H.1a). The reason for this transition probably is the force accumulation caused by the controller, as discussed in E. We also saw that alternative force controllers did remove the abrupt transition but not the existence of the saturation in general. They led to a similar final burrowing depth.

Figures H.1c andH.1d show example depth and force curves for the case of position control. Here, the step size was constant. Also note that the duration of the steps was constant. This is due to the fixed schedule of the control program.

We used fishing lines in early experiments and steel cables in later experiments. Figure H.2 shows a comparison of the two variants. The transition to vanishing step sizes is sharper for

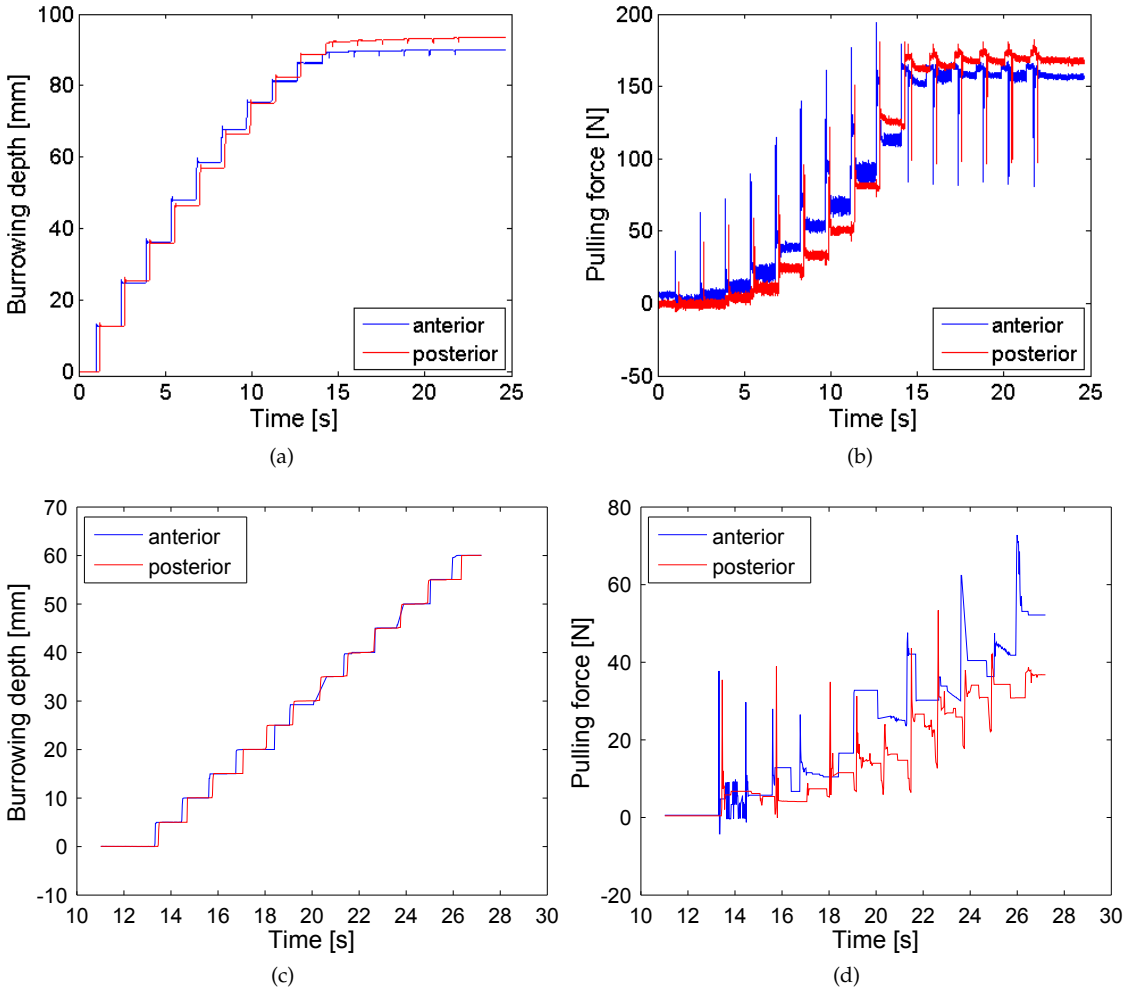

Figure H.1: Depth and force curves. These plots visualize a typical burrowing run, showing burrowing depth and force as functions of time. (a) Depth curve. This plot shows the burrowing depth (slider position) as a function of time. 15 burrowing steps were performed. They can be clearly seen as steps in the curves. As in natural bivalves, the step size continuously decreased as the resistance of the sediment increased the deeper the shell penetrated. As was often the case, the posterior motor ended at a slightly higher depth than the anterior motor. The shown data is from the evaluation of shell 5 in the morphological evolution (chapter F). (b) Force curve. This plot shows the pulling force (as measured by the force sensors at the end of the sliders) as a function of time. It can be seen that the peaks in the pulling phases become stronger as the resistance increases. As described in section G.2, the same constant force was applied in each step. However, the force measured by the sensors and plotted here does not exhibit equal peaks. This is because in the early steps, the maximal step size is reached very quickly, such that the pulling force is switched off before the tension in the cables reaches its maximum. In the saturation phase (starting at 15 s), there are peaks in the other direction. They are caused by the high tension in the strings pulling the sliders upwards, decreasing tension, before the PID control stabilizes their position. (c) Depth curve with position control. The steps do all have equal sizes. The irregularities in the plot are due to the suboptimal data acquisition (see section G.3.2). This experiment was still done with sediment standardization by loosening and fishing lines. (d) Force curve with position control. This force was not measured by the force sensors but computed from the current applied by the motor (by multiplication with the force factor 25.8 N/A and adding the slider weights of 17.3 N).

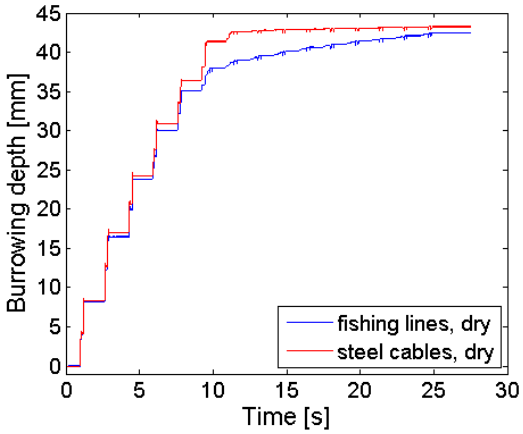

Figure H.2: String comparison. Fishing lines and steel cables led to a similar burrowing behaviour. The only difference was that fishing lines continued to expand throughout the burrowing run, while steel cables transitioned more abruptly to a fully saturated state. The data shown is from the first repetition of the first experiment in Figures H.7a (fishing lines) and H.7b (steel cables).

steel cables than for fishing lines. The reason is probably that the fishing lines expand more with increasing tension, while the shells do not actually move deeper.

Due to the expansion of the strings under tension, the slider positions did not exactly measure the actual burrowing depth of the shells. To test the size of this disparity, we added a scale onto the water expulsion supply tube and recorded the starting and end position of this tube. The absolute precision of this measurement is disturbed by lateral and rotational movements of the shell and may thus be several millimetres. The relative error compared to the other measurements should not be larger than ± 2 mm. A comparison of the two measurements for an experiment with 400 repetitions is shown in Figure H.3.

An important question is how much energy is consumed by burrowing. However, from a technical setup it is difficult to compute a realistic value comparable to the natural case. Since we measured position and force at a relatively high sample rate of 1613 Hz, energy could be computed using the formula $E = \int F \mathrm{d}s$. Figure H.4 shows the plots of two large data sets. Note that applied force that does not lead to a displacement does not contribute to the energy if it is computed in this way. Total consumed energy is plotted against the final burrowing depth. From the slopes an energy consumption of 0.084 J/mm and 0.175 J/mm can be derived. This is considerably more but still comparable in terms of order of magnitude to the value of 0.021 J/mm for *Ensis directus* reported by Winter et al. (2012).

If water expulsion is used, the energy for it would have to be added. However, it is not straightforward to compute the energy needed to expel water. Using technical data such as power consumption of the pump or provided pressure would lead to a massive overestimation of the energy consumed in the natural case.

H.2 Influence of the Environment

Ideally, the sediment would be returned into a standard state that is identical for each burrowing run. However, with the setup we used it was not possible to establish a reasonably similar state. The sediment therefore introduced a memory effect into each series of experiments. The

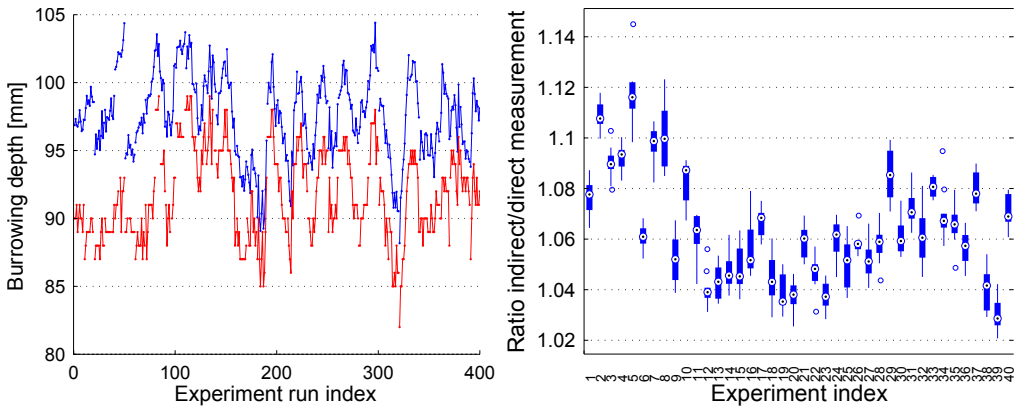

(a) (b)

Figure H.3: Slider positions vs. direct manual depth measurements, shown for the data from the second evolutionary experiment described in section H.4.2. (a) burrowing depth as measured by the motor sensors based on slider position (blue) and manually measured burrowing depth using a scale on the water expulsion tube (red). (b) The ratio between the two measurement techniques, summarized in a boxplot with one box for each individual (10 repetitions). The slider position was between 2% and 12% bigger than the direct measurement due to string expansion and setup deformation.

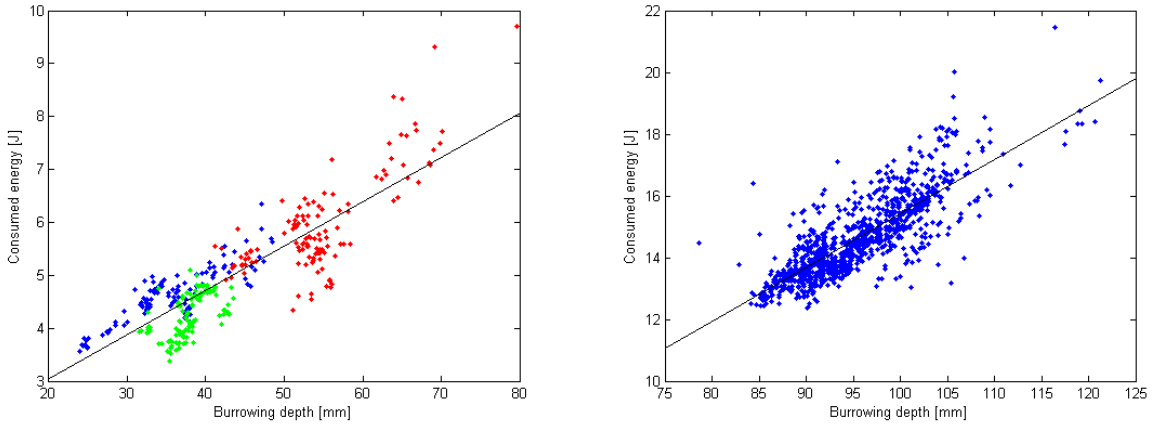

(a) (b)

Figure H.4: Energy consumption. (a) Consumed energy vs. burrowing depth of the three data sets in Figure H.7 (blue, green and red, respectively). Parameters of the line ($y = Ax + B$): $A = 0.084$, $B = 1.36$. (b) Consumed energy vs. burrowing depth of the individuals evaluated in the morphological evolution (chapter F). Parameters of the line: $A = 0.18$, $B = -2.07$.

performance of a given configuration (set of morphological and motion parameters) was thus additionally influenced by events of previous experiments such as (1) sediment standardization process, (2) previous burrowing runs, (3) retrieval of the shell from the previous burrowing runs, (4) particular events such as the manual retrieval of loose string ends after a string burst. Figure H.5 shows two data sets that illustrate how the sediment state was influenced by different events.

We found that these events tended to either increase or decrease the compaction of the sediment. From the sediment standardization techniques (point 1 above), described in section G.3.1, one loosened the sediment, while all others were used to compact the sediment. Burrowing runs (2) could influence following burrowing runs in both directions, towards more or less compaction. Small burrowing steps, fast burrowing (short pulling durations and pauses) and small time lags tended to compact the sediment. Water expulsion and distant attachment sites (larger rotation angles) tended to loosen the sediment. Retrieval of the shell (3) and of other objects (4) usually loosened the sediment. Depending on the mixture and strength of the above events, the sediment was more or less compacted over time.

Figure H.5a shows 60 repeated burrowing runs using the same configuration. It can be seen that even after these 60 repetitions, the drift of the sediment towards more compaction is not saturating. It has to be assumed that the comparability of two experiments decreases as the number of burrowing runs performed between them increases (up to a certain limit, since compaction will not increase endlessly). We found that 10 repetitions was a reasonable compromise between this effect and a sample size large enough to smooth out short term fluctuations.

As illustrated in the 60 repetitions in Figure H.5a, the drift towards more or less compaction over a series of similar experiments was often close to linear, except after events (4) that involved a strong loosening of the sediment.

String bursts could be avoided in later experiments using steel cables instead of fishing lines. The linear part of the sediment drift was in some experiment series computationally corrected. To do this, the first experiment of the series was repeated at the end. In the evaluation of the experiment series, a line was fitted through the first and last experiment. By adding a linear correction to the data, the line could be made horizontal. This method is illustrated in Figure H.6. A slightly more complicated method to correct depth data was used in chapter F.

A number of experiments was performed in the setup without water, i.e. in dry sediment. In the comparison of the dry to the underwater case shown in Figure H.7 the water increased the burrowing depth by ca. 50%. Wall effects were analysed in chapter E. We did not test different sediments, i.e. different grain sizes.

H.3 Influence of the Burrowing Motion

H.3.1 Motion parameters

The parameters defining the burrowing motion pattern are shown in Table H.1.

When we were using the fishing lines, we had six of them instead of two. We used them in pairs and called them the "inner", "middle" and "outer" string pair. The holes in the bottom plate were arranged in steps of $2\ \mathrm{cm}$ along the width (direction towards and away from the motors) and $1\ \mathrm{cm}$ along the length of the water tank. The distances between the holes for the inner, middle and outer string pair were therefore $22.4\ \mathrm{mm}$, $67.1\ \mathrm{mm}$ and $111.8\ \mathrm{mm}$, respectively. The steel strings were always in the middle hole pair. Their distance at the plate was therefore slightly larger than the distance between the attachment locations when both arms were in hole 1 ($h_a = 1$ and $h_b = 1$).

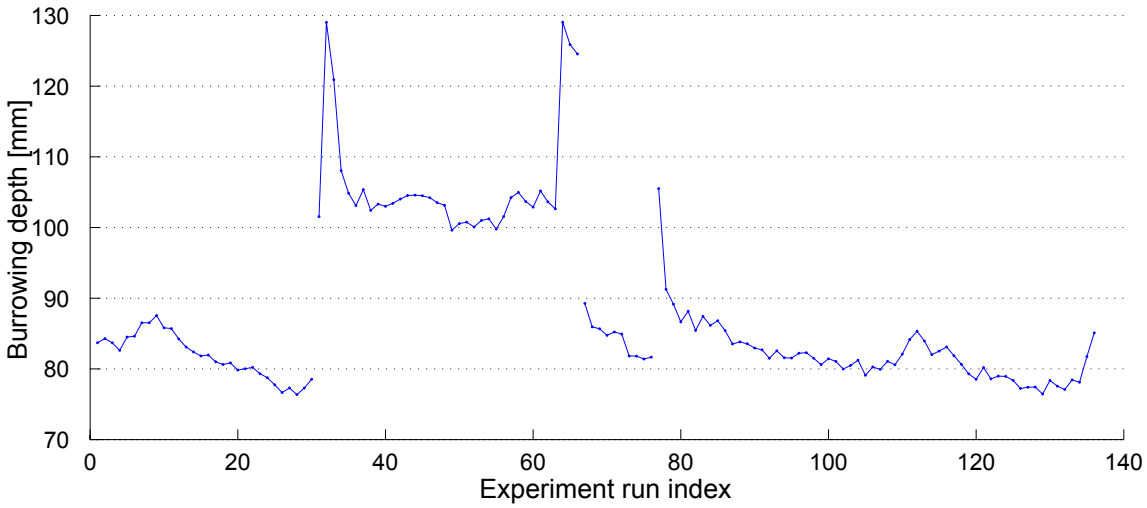

(a)

(b)

Figure H.5: Memory effect of the sediment. (a) Sediment standardization and drift. The first three experiments were with BB-radial2 and $F_a = F_p = 4.5$ A, the last with B-mixed, shown in Figure 2 in chapter E, and $F_a = F_p = 3$ A. The four segments are sequences of 30, 36, 10 and 60 repetitions. Loosening was used in the second experiment, the first and last three burrowing runs were done with deep loosening. The difference is clearly visible. Compaction was used in the other experiments. This chart shows that we still have drift even after 60 repetitions. (b) String bursts. The plot shows the depth evolution of a first evolutionary experiment, where six generations of three individuals with 10 repetitions each were performed ($6 \times 3 \times 10 = 180$ burrowing runs). The experiment was performed in dry sediment, fishing lines and using the loosening technique to standardize the sediment (section G.3.1). The ideal plot would have plateaus of length 10, and there should not be any connection between the successive experiments except a general trend towards higher fitness (burrowing depth). There were two string bursts that happened before the indices 85 and 141 (arrows). The disruption of the experiment due to string retrieval and the associated loosening of the sediment is clearly visible as an abrupt increase in burrowing depth.

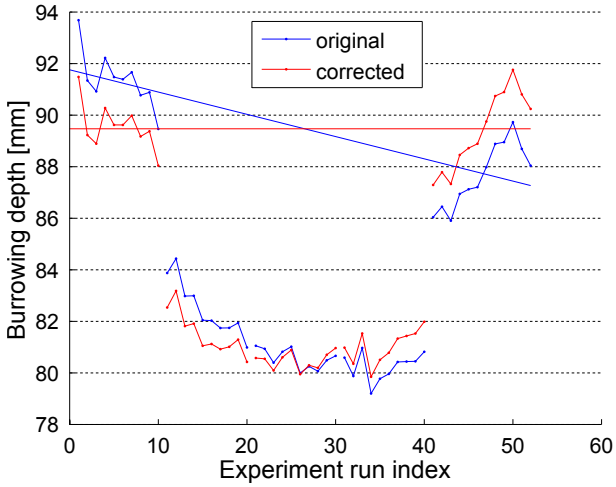

Figure H.6: Linear depth correction. The plot shows the depth evolution of a series of experiments (blue). The last experiment (last 10 repetitions) was a repetition of the first experiment (first 10 repetitions). With an ideal sediment standardization, the reached depths of these two experiments would match. To correct the data, a line may be fitted through the two experiments and used to linearly correct the data (red). Note that this changes the absolute burrowing depth. The difference between the median depth of the first and the last experiment in this case is 3.7 mm. The shells used were B-smooth, B-random, B-radial, B-random and B-smooth (see chapter E), the forces $F_a = F_p = 4$ A.

	Variable	Range/Unit	Parameter description
1	h_a	[1..9]	anterior attachment location
2	h_p	[1..9]	posterior attachment location
3	F_a	[A] or [N]	pulling force anterior motor
4	F_p	[A] or [N]	pulling force posterior motor
5	s	[mm]	step size limit
6	d_s	[ms]	pulling phase duration limit
7	d_w	[ms]	water expulsion duration
8	d_p	[ms]	waiting phase (pause) duration
9	l	[ms]	lag between the motors
10	n	$\mathbb{N}$	number of burrowing steps

Table H.1: Parameters to define the burrowing motion. The default values we used for many experiments were $h_a = 5$, $h_p = 5$, $F_a = 5$ A, $F_p = 4.6$ A, $s = 5$ mm, $d_s = 400$ ms, $d_w = 500$ ms (if used), $d_p = 1000$ ms, $l = 200$ ms and $n = 15$. Deviating values are explicitly given in the Figure captions. Parameters 1 and 2 determine the cable attachment location in terms of the hole number defined in Figure G.3. Parameters 3-10 are directly used in the program shown in Figure G.6. The force was set in the controllers in Ampère A. Using the force constant 25.8 N/A, a force in Newton can be computed. The force measured by the force sensors was usually higher because of the additional slider weight and the dynamics of the actuation system.

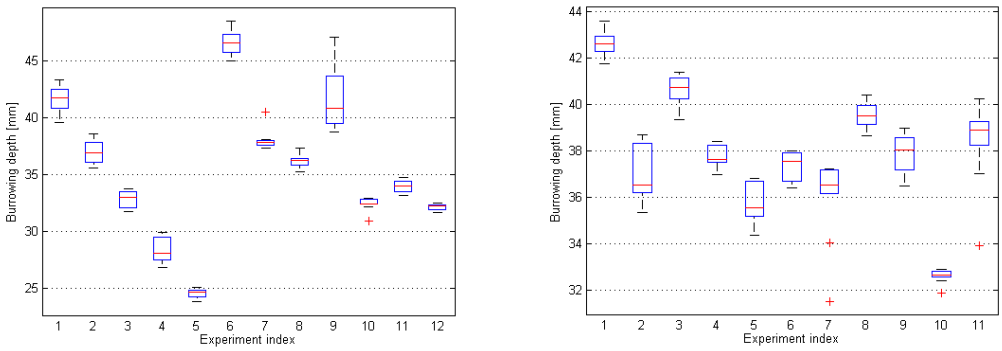

(a)

(b)

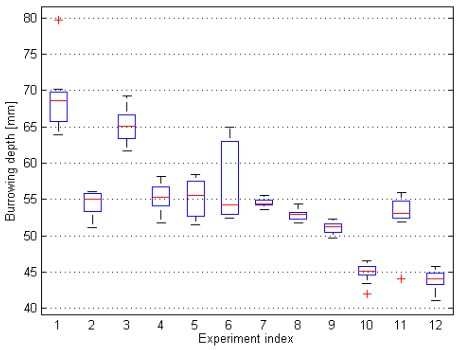

(c)

Figure H.7: Effects of different parameters and the sediment. The same sequence of experiments was done three times: (a) in dry sediment and with fishing lines, (b) in dry sediment and with steel cables and (c) in water and with steel cables. The other parameters used were: Test-shell (experiments 1-8), BB-smooth (9-10), BB-radial2 (11), no water expulsion, $F_a = 2.6$ A, $F_p = 2.8$ A, the number of steps and the step sizes were sequentially set to the values $(n = 15, s = 5\ \mathrm{mm})$, $(35, 1\ \mathrm{mm})$, $(12, 10\ \mathrm{mm})$, $(15, 5\ \mathrm{mm})$, $(25, 2\ \mathrm{mm})$, $(15, 5\ \mathrm{mm})$, $(15, 5\ \mathrm{mm})$, and $(15, 10\ \mathrm{mm})$ for the remaining experiments. Lag and pause were $l = 200$ ms and $d_p = 1000$ ms except for experiment 5, where $(20\ \mathrm{ms}, 0\ \mathrm{ms})$ was used. In experiments 7,8 and 10, the cables were crossed. In the case of the fishing lines, the inner string pair was used for experiments 1-5 and the outer string pair for the other experiments. The overall burrowing depth in the first experiment was 35.6 ± 6.0 mm, in the second experiment 37.8 ± 2.7 mm and in the third experiment 54.7 ± 7.2 mm. The first is an increase by 6%, the second by 45%. The difference in the first case is significant with a p-value of 2e-004, in the second case with a p-value of 5e-039 (Wilcoxon ranksum test).

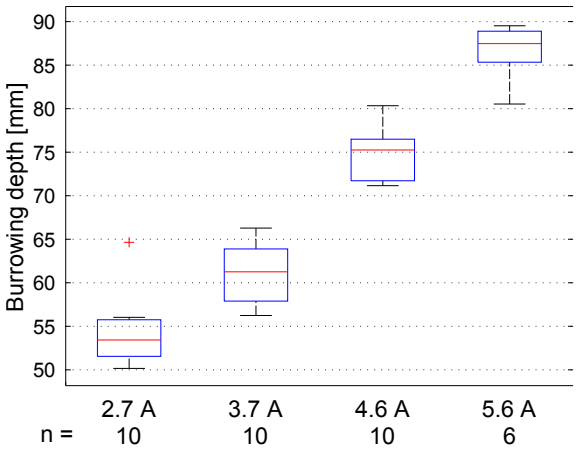

Figure H.8: Effect of the pulling force. Burrowing depths at different forces in dry sediment. Test-shell. $d_s = 500$ ms.

H.3.2 Pulling Force

Figure H.8 shows the result of an experiment testing different forces in dry sediment. In the measured interval, the relation was linear, i.e. the burrowing depth reached was proportional to the applied force. The highest of the applied forces, 5.6 A resulted in a measured peak tension in the cables of 245 N. Tensions in this region tended to damage the glass panes of the setup. We therefore kept the applied forces below 5 A or 200 N.

An experiment in water and also considering the shell size was reported in chapter E.

H.3.3 String Attachment Location

This morphological change also influences the burrowing motion, because closer string attachment locations lead to a smaller rocking motion.

The first shells that were used before the modular version with the central metal disc had just one standard metal piece to attach the strings (Figure G.3a). The attachment location was therefore the same for all shells. To test different angles at which the pulling force is applied to the shell, we therefore performed experiments with crossed strings. This means that we turned the shell by 180°around its vertical axis, without re-attaching the strings. The motors swapped their role as anterior and posterior retractor. The results of these experiments are shown in sections C and D.

Using the central metal disc, the attachment locations could be changed by pinning the arms to different holes, see Figure G.3b. Figure H.9 shows the results of an experiment testing the difference between hole 1 and hole 9 of the disc, i.e. between the closest and the most distant attachment locations.

The different angles of the cables were considered for the experiments, i.e. the pulling force was slightly increased in the case of hole 9 to ensure the same magnitude of pulling force pointing downwards. However, the friction of the cables in the sediment were not accounted for in the experiment. We therefore did a second experiment where we attached a thin metal strip to the cables instead of the shell. It had holes with the same distances as the attachment arms. Figure H.9b shows the difference in pulling force needed to pull the strip to the same depth. The difference was similar to the difference measured in the previous experiment between the holes 1 and 9. The difference measured between the two holes may therefore be due to the cable friction.

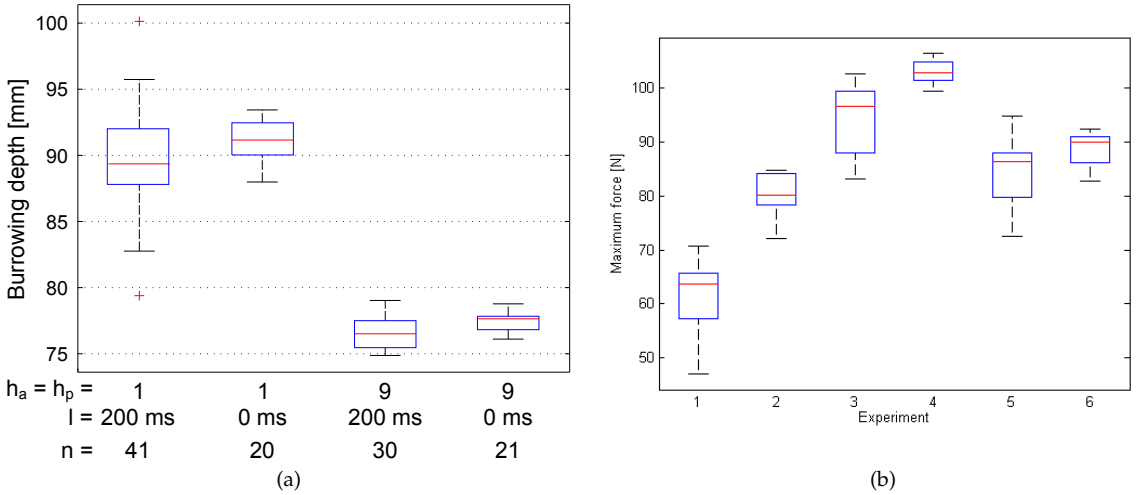

Figure H.9: Effect of the attachment location. (a) B-mixed, h_a and h_p varied as indicated (p-value = 1e-019, 16.9% increase), $F_a = F_p = 3.5$ A, no water expulsion, $d_p = 1000$ ms, $l = 200$ ms. Starting position and pulling forces are adapted according to the used attachment sites. Lag varied as indicated. (p-value = 0.40). (b) Forces necessary to pull down only the strings and a small horizontal aluminium strip. The aluminium strip had holes at distances of 16 mm and 64 mm (according to holes 9 and 1 of the metal disc attachment arms). Repetitions: 10, 10, 11, 10, 10 and 10. The holes with distance 64 mm were used in the experiments 1, 2, 5 and 6, the holes with distance 16 mm in the experiments 3 and 4. A pulling speed of 0.1 m/s was used in the experiments 1, 3 and 5, a pulling speed of 0.01 m/s in experiments 2, 4 and 6. There was a quite strong compaction during the first experiments. When considering experiments 3-6, the smaller distance increased the necessary force by 11.9% (faster speed) and 14.2% (slower speed).

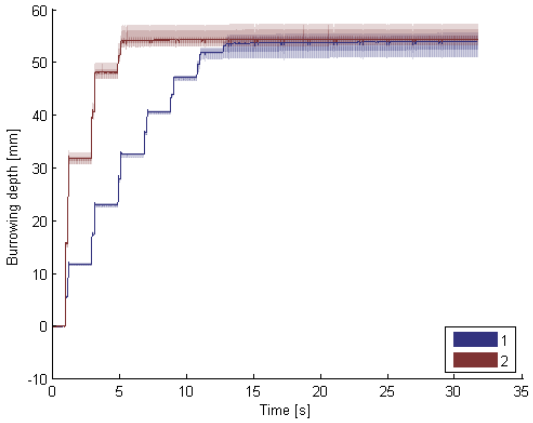

Figure H.10: Effect of the step size. B-natural, $F_a = F_p = 4$ A, $s = 5$ mm in the first experiment and $s = 15$ mm in the second experiment, 10 and 9 repetitions were done. The difference between the step sizes is not significant ($p = 0.1186$).

H.3.4 Step Size

Larger burrowing steps tended to have a positive effect on burrowing performance, see Figure H.7. However, the results were not conclusive. Figure H.10 shows two experiments using B-natural (see picture of the shells in chapter E) with two different step sizes. Though the different step sizes led to a different burrowing speed, the final depth was not significantly different.

The actually performed step sizes were larger than the programmed maximal step size due to the time it took for the PID control to stop the sliders. The overshoot was up to about 70% in the experiment shown in Figure H.5b (fishing lines).

H.3.5 Timing

Figure H.11 shows the result of an experiment testing varying values for the lag between the motors. Note the two very different results for the experiments with the value 400 ms. This again illustrates the difficulties with the sediment as discussed in section H.2.

There is a trade-off between a doubled force and the rocking motion. A lag of 0 ms means that both motors pulled synchronously for a pulling duration of 400 ms, doubling the pulling force with respect to just one motor. A lag of 400 ms means that the posterior motor started pulling at the moment when the anterior motor stopped pulling, leading to a "strict" rocking motion. An intermediate lag of 200 ms led to an overlap of 200 ms, where both motors were pulling but still resulted in a rocking motion.

We did not find any connection of the burrowing performance with the pause duration.

H.3.6 Water Expulsion

The effect of water expulsion of varying duration is shown in Figure H.12. Longer water expulsion tended to have a positive effect on burrowing performance, although there seemed to be a maximum from which a longer duration was counterproductive.

The water expulsion holes were bigger in the first shells used in chapter B, which may explain the stronger results there. Later, we reduced the size of the holes to smaller diameters than the

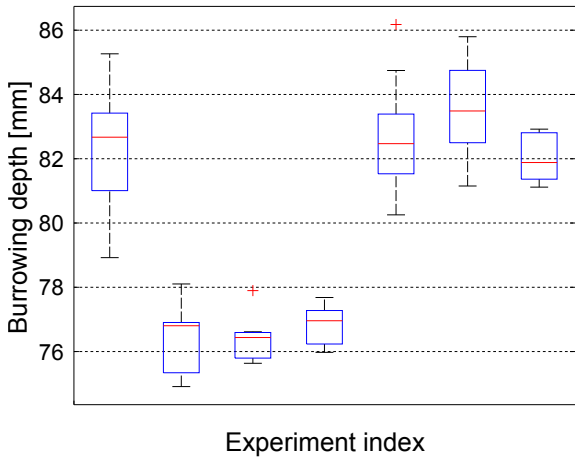

Figure H.11: Effect of the lag. B-mixed, $f_a = f_p = 3$ A. 10, 10, 10, 11, 10, 10 and 10 repetitions. The lag l was 0 ms in experiments 1, 5 and 7; 200 ms in experiments 2 and 4; and 400 ms in experiments 3 and 6. A linear depth correction of 7.4 mm was done. Note the large difference between the two experiments with $l = 400$ ms.

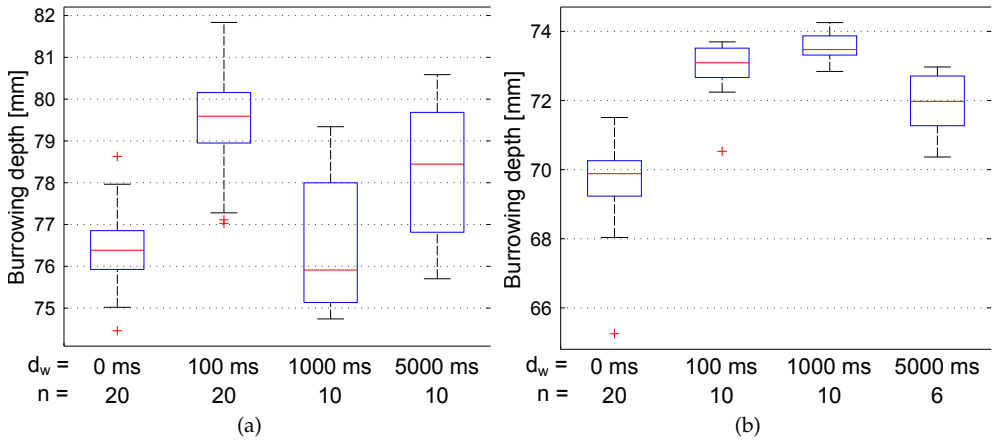

Figure H.12: Effect of water expulsion. (a) B-mixed, $f_a = f_p = 3$ A. (b) BB-radial2, $f_a = f_p = 5$ A.

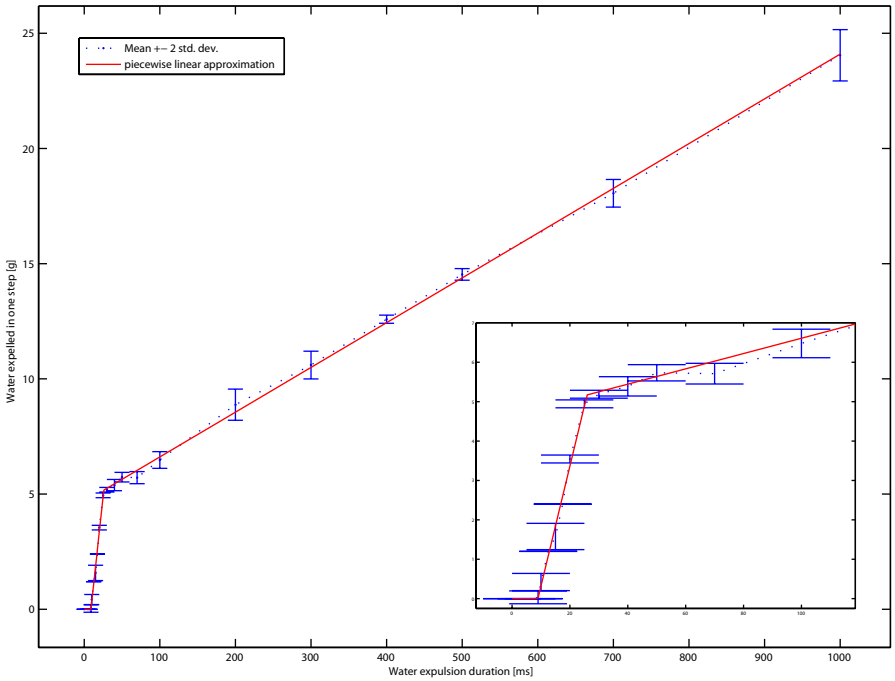

Figure H.13: Amount of water expelled. The central metal disc was put into a bucket while a reduced burrowing experiment with 15 burrowing steps was executed. The amount of water expelled was weighed after each step. The precision of the scales was $1\ \mathrm{g}$. The amount of expelled water was smaller but still comparable to the volume of the shells. A shell had a volume between $30\ \mathrm{cm}^3$ (B-smooth6) and $150\ \mathrm{cm}^3$ (B-natural).

grains to avoid congestion in the tubes. Figure H.13 shows the amount of water expelled through the channels of the metal disc.

H.4 Artificial Evolution

The setup was used to perform evolutionary experiments. Because of the very large difference in terms of effort and resources, we divided the parameters into morphological parameters and parameters determining the motion pattern. The morphology of the shell could be changed by generating a new geometry using the desired parameters and the mathematical model and printing it with the 3D printer (chapter F). Due to the relatively large effort to print shells for each new morphology, we only performed one experiment evolving the shell morphology. It is described in chapter F.

We also performed three evolutionary experiments only changing the motion pattern, i.e. using the same shell, B-smooth, throughout the experiment. The first one was a test; the resulting depth evolution curve is shown in Figure H.5b. The results of the other two experiments are reported in the next two sections.

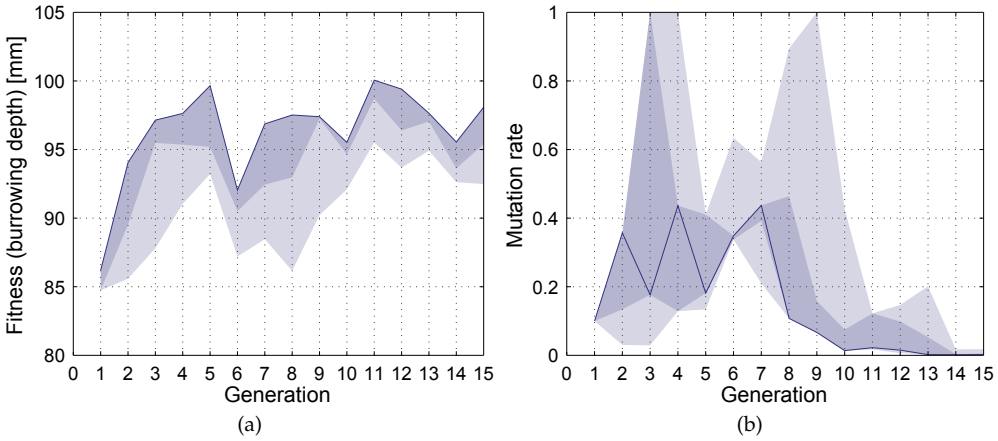

Figure H.14: Fitness and mutation rate of the first evolutionary experiment. (a) This plot shows the evolution of the fitness. Fitness is plotted against the generation. The light shaded area covers the fitness values of all individuals (4 per generation), the dark shaded area of those selected (2 per generation). The dark line follows the best individual. (b) Plot of the mutation rate. We stopped the experiment after it became very small (0.01).

H.4.1 Motion pattern evolution 1

In the first evolutionary experiment to evolve the motion pattern the genome contained eight values. Seven were encoding motion parameters and the eighth encoded the mutation rate. The encoded parameters were (1) water expulsion duration d_w, 0–1000 ms, (2) maximal step size s, 1–10 mm, (3) maximal step duration d_s, 100–1000 ms, (4) pause duration d_p, 0–1000 ms, (5) time lag of the posterior with respect to the anterior motor l, 0–1000 mm], (6) anterior hole index $h_a \in [1..9]$, and (7) posterior hole index $h_p \in [1..9]$ (see table H.1). The values on the genome were in the range $[0, 1]$ and were linearly mapped onto the ranges of the parameters. To compute the lag, the maximal step duration was multiplied by the value on the genome for the lag to ensure that the pulling phase of the posterior motor did not start later than at the end of the pulling phase of the anterior motor. The number of steps was computed from the step size by another linear map with the end points $(1\text{ mm}, 50\text{ steps})$ and $(10\text{ mm}, 10\text{ steps})$.

A (2, 4)-ES (evolution strategy) was used. From the best two individuals from the last generation, four children were produced by mutating each parent once and by using uniform crossover and mutation to generate another two children. Selection was done on the children only (“,”-strategy instead of “+”-strategy). The mutation rate was initialized with 0.1 in the first generation and then adapted before each mutation. The final burrowing depth was used as fitness. For a more detailed description of how we performed evolutionary experiments, see chapter F.

Figure H.14a shows the resulting fitness curve over the generations. The experiment was stopped after 15 generations, when the mutation rate became small (Figure H.14b). In this time the fitness values increased from 86 mm to 98 mm, i.e. by 12 mm. Ranges of the 10 repetitions reached from 2 mm to 15 mm, i.e. the noise of the sediment had the same size as the overall increase in fitness.

Figure H.15 shows how the parameters changed over the generations. Often, the values tended towards extreme values in a scale. The water expulsion duration increased to the maximum value of 1 s. The maximal step size increased but did not settle around the maximum of 10 mm but around 7 mm. The step duration dropped towards the minimum of 100 ms. This is un-

Variable	p-value	r
d_w	1e-06	0.59
h_a	1e-06	-0.59
d_s	2e-06	-0.58
l	2e-05	-0.53
s	3e-05	0.52
n	4e-05	-0.51
h_p	0.009	-0.34
d_p	0.09	-0.22

Table H.2: Correlations (Pearson) of the motion parameters (Table H.1) with fitness. The p-values and the correlation coefficients r are given.

expected, since one would assume that longer pulling phases increase the burrowing depth. The break at the end of a burrowing step tended towards 0 ms. This combination of minimal durations (short pulling phase, short pause) led to an almost uninterrupted water expulsion, because the closing of the valve was slightly delayed, before it was opened almost immediately for the next step. The lag tended towards 0 ms, the attachment hole indices towards 1, meaning a larger distance between the attachment arms.

Table H.2 lists the correlations of the eight parameters with the fitness (burrowing depth). All correlations except the last (d_p) are significant on an $\alpha = 0.05$ significance level. The influence of the water expulsion duration was most significant.

H.4.2 Motion pattern evolution 2

Due to the almost uninterrupted water expulsion resulting in the previous evolution experiment, a second experiment was performed without water expulsion. The same parameters were used except the water expulsion duration d_w. The ranges were the same as well, except for the number of burrowing steps. After two generations, the maximal number of steps was increased from 50 to 60, because 50 steps were not enough to reach saturation in the burrowing depth.

As initial population, four instead of two individuals were used. In contrast to the previous experiment, efficiency was used as fitness. It was computed by dividing the burrowing depth by the energy consumed for the burrowing (see section H.1). All other parameters were the same as in the previous evolutionary experiment.

Figure H.16 shows how the fitness, the burrowing depth and the mutation rate changed over the generations. Note the drop in fitness after generation 2. This is due to the change in parameterization from a maximum of 50 burrowing steps to 60 burrowing steps. Because the burrowing efficiency decreased towards the end of a burrowing run, the overall fitness decreased as well, so that the best fitness in generation 2 was never reached again in later generations. Also, in the ratio between burrowing depth and consumed energy, an increase in burrowing depth was more than compensated by the increase in energy to reach that depth. The fitness function therefore turned out to be a bad choice. We computed the correlations of all parameters with fitness and with burrowing depth. None of them was significant on an $\alpha = 0.05$ significance level.

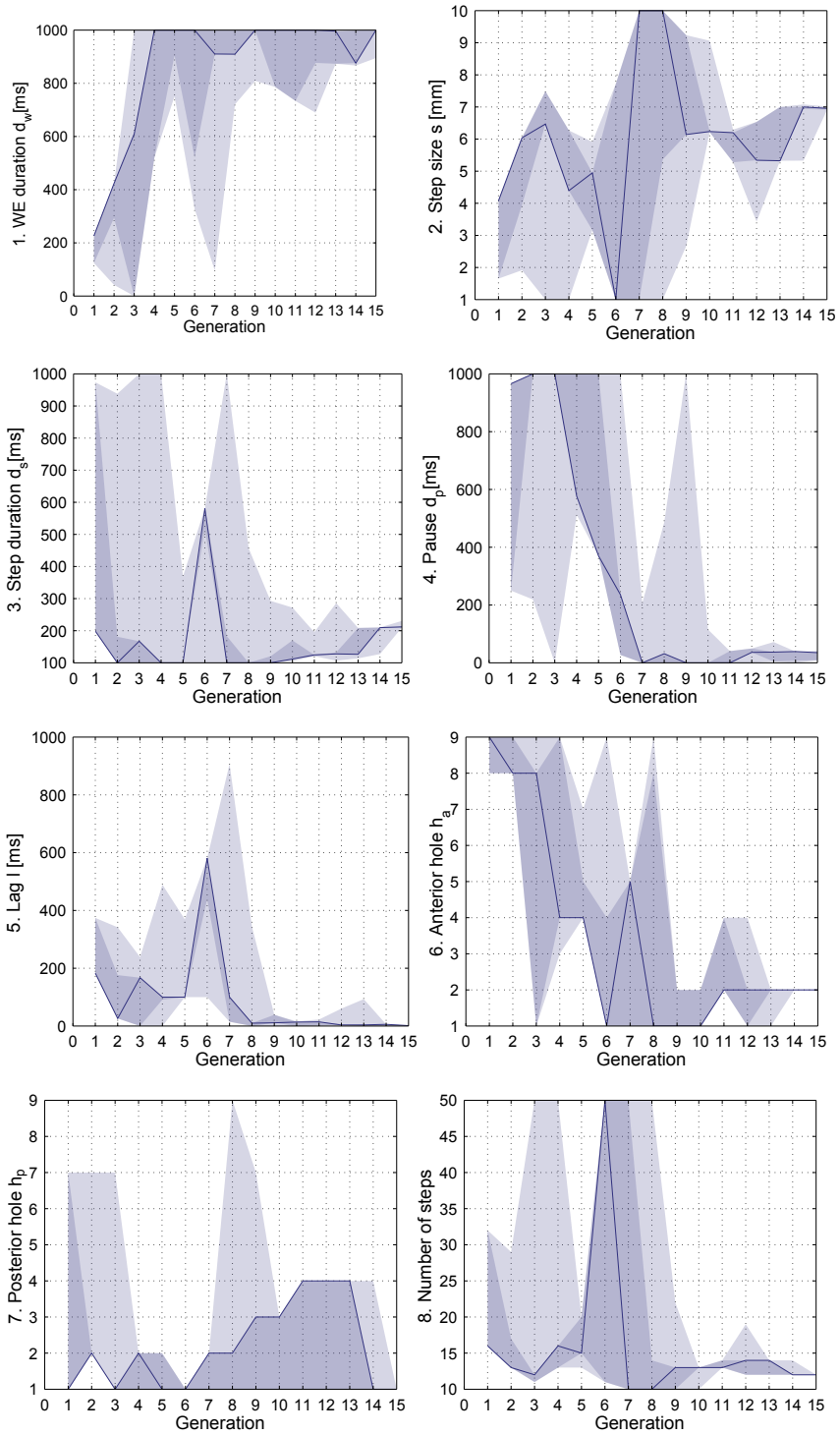

Figure H.15: Range plots of the first evolutionary experiment. There was a clear trend towards longer water expulsion, while the pulling phase and pause became shorter.

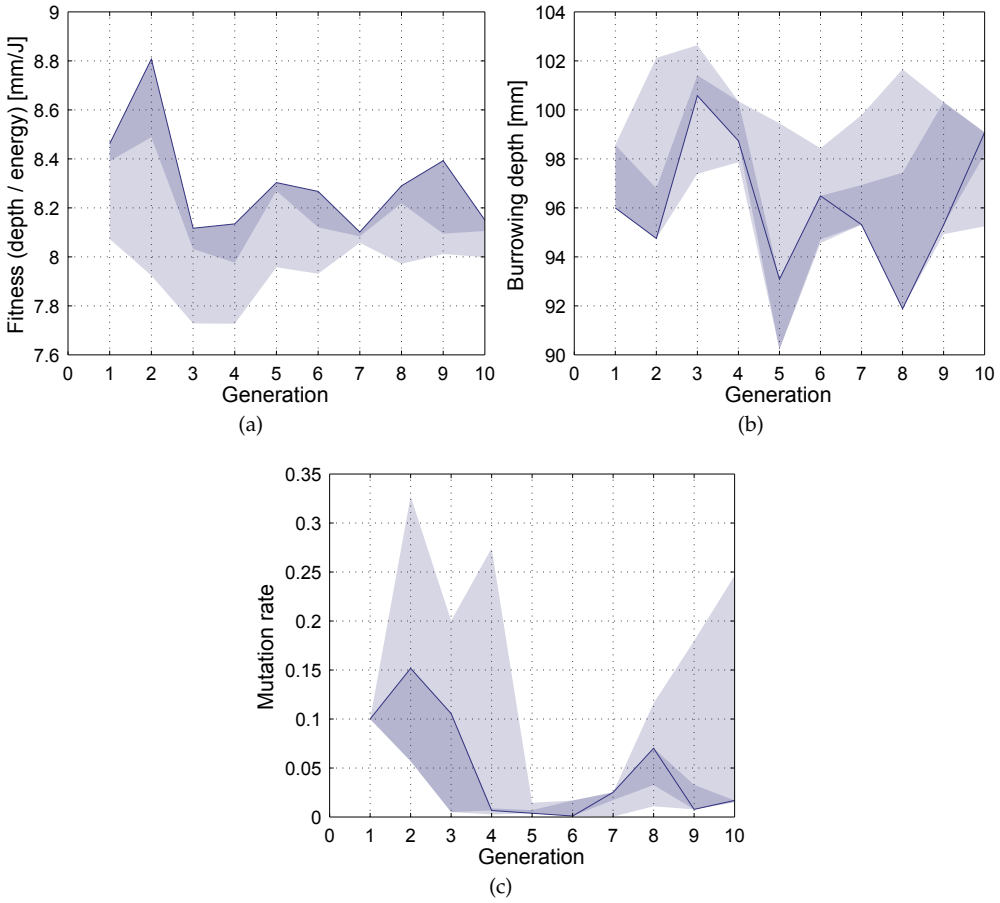

Figure H.16: Fitness, depth and mutation rate of the second evolutionary experiment. (a) This plot shows the evolution of the fitness. Fitness is plotted against the generation. The light shaded area covers the fitness values of all individuals (4 per generation), the dark shaded area of those selected (2 per generation). The dark line follows the best individual. (b) Burrowing depth over the generations. (c) Plot of the mutation rate over the generations.

H.4.3 Influence of the Shell Size[1]

This section is taken from an earlier draft of the article in chapter E. It was not part of the published version. Originally, it complemented the experiment about the influence of the cross-sectional area of the shell. This section is coauthored by Juan Pablo Carbajal.

In a second, similar experiment, the size of a shell was not defined as cross-sectional area perpendicular to the burrowing direction but by scale. Again, the burrowing depth under a given pulling force should inversely correlate with size. However, since a larger shell does also provide more space for a larger animal and therefore larger muscles, different shell sizes should be studied together with varying pulling forces.

We therefore generated two shells of the same shape but of different scales: B-smooth9 had a height of $92\ \mathrm{mm}$, B-smooth6 of $61\ \mathrm{mm}$, i.e. the first shell was 1.5 times bigger than the second shell. Note that the central metal disc was the same for both shells, i.e. the length of the levers of the cable attachment arms did not change. We then tested both shells at four different force levels separated by the same factor of 1.5.

The results are shown in figure H.17. In addition to the absolute burrowing depths, also the relative burrowing depths are given. These were computed by dividing the absolute burrowing depths by the heights of the shells (diameter along the burrowing direction). It can be seen immediately, that the smaller shell consistently reached larger depths when using the same pulling force. The abscissae in the plots show the measured maximal pulling forces. The forces were generated with currents sent to the motors separated by a factor of 1.5. Because of the deformation of the set-up, the factors between the measured forces are $[1.4, 1.4, 1.5]$ starting from the smallest force. Considering this, the big shell needed a pulling force ≈ 1.4 times higher to reach the same absolute depth as the small shell. It needed a pulling force ≈ 2.7 times higher to reach the same relative depth.

The variation between shell shapes was excluded in the experiments using B-smooth6 and B-smooth9. Still, the bigger shell required bigger forces than the smaller shell to reach the same absolute depth (figure H.17), which is in agreement with the previous results. However, this case is more interesting, since it allows a more detailed analysis of the size aspect.

Consider two opposing effects: on one hand, a bigger shell volume increases the resistance of the sediment to penetration and therefore reduces the burrowing depth; on the other hand, a bigger body volume allows bigger muscles and therefore bigger maximal retraction forces for digging. The question is which effect is stronger. Assume that maximal muscle force (F) increases proportionally to the cross-sectional area (A) of the muscle, i.e. $F \propto A$. For the muscle forces produced by two shells, where one is a scaled version of the other with scale factor r, we get

$$\frac{F_b}{F_s} \propto \frac{A_b}{A_s} \propto r^2,$$

since their areas scale with the square of the length scaling factor (subindices b and s standing for big and small, respectively). In our case r was 1.5, leading to a theoretical muscular strength in the big shell $1.5^2 = 2.25$ times higher than in the small shell. Figure H.17 shows that the bigger shell consistently required a force approximately 1.4 times bigger to reach the same absolute depth, and a force approximately 2.7 times bigger to reach the same relative depth. According to these results, bigger shells are better to reach a larger absolute depth, while smaller shells may be better to reach a larger relative burrowing depth. One may argue that relative depth is more important, since it measures how well a bivalve can hide in the sediment. However, larger bivalves may be better protected by their size and strength.

The findings of Stanley (1970, pp. 71, 165) suggest that the smaller juvenile venerids normally live at greater relative or even absolute depths than the bigger adults. While our results offer an

[1] Coauthored by Juan Pablo Carbajal

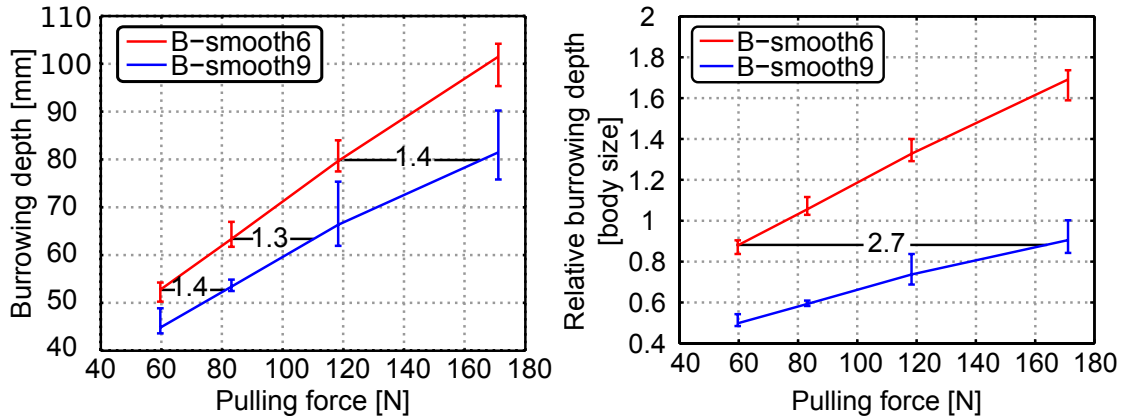

(a) (b)

Figure H.17: Burrowing depth dependent on shell scale and pulling force. (a) Burrowing depths reached of two shells of identical shape but different scale, B-smooth6 and B-smooth9, for different pulling forces. (b) The same plot but showing relative burrowing depth instead of absolute burrowing depth. The relative burrowing depth was computed by dividing the absolute burrowing depth by the height (diameter in burrowing direction) of the respective shell (61 mm for B-smooth6 and 92 mm for B-smooth9). The numbers on the black lines indicate the factors between the different pulling forces for the two shells to reach a comparable burrowing depth. For each point, 20 repetitions were performed. The data was linearly shifted for this plot as described at the beginning of section **??**. In this way, a gradual drift of the sediment towards more compaction was compensated. The discrepancy between first and last experiment in this case was 3 mm.

explanation for a greater relative depth, a greater absolute depth of juveniles may indicate that adults do not use their potential to go deeper although they could. If this turns out to be the case, burrowing depth may not be the most relevant trait for selection and shell morphology may be selected under other criteria, e.g. efficiency of burrowing (force per unit length) or holding grip force.

Appendix I

Student Theses

The project was supported by several student's theses. There were two bachelor and one term theses by four students from HSR (Hochschule für Technik Rapperswil) and one internship by a student from ETH Zurich. The students from HSR were supervised by Prof. Dr. Agathe Koller-Hodac and Daniel Germann. Thomas Vasileiou from ETH was supervised by Daniel Germann.

1. Alexander Gilgen and Katja Dietrich, "Entwicklung eines grabenden Muschelroboters", Bachelor thesis, SS 2009, supervised by Prof. Dr. Agathe Koller-Hodac
2. Pascal Brändli, "Muschelroboter", Bachelor thesis, WS 2009, supervised by Prof. Dr. Agathe Koller-Hodac
3. Christoph Philipp, "Development of an Autonomous Bivalve Robot", Term Paper, WS 2010, supervised by Prof. Dr. Agathe Koller-Hodac
4. Thomas Vasileiou, "Recording the 2D trajectory of a bivalve robot using an IMU (inertial measurement unit)", Internship project report, winter 2011/2012, supervised by Daniel Germann

The abstracts of the theses done at HSR are accessible on the Internet: http://www.hsr.ch/Dozierende.5626.0.html?&tx_icscrm_pi4[content]=16313&tx_icscrm_pi4[id_person]=1269, "Betreute Arbeiten".

Appendix J

Media Coverage

The bivalve project was mentioned in the following media contributions:

1. Daniel Germann, "Muschelroboter als Versuchstier", HSR Magazin, magazine of the University of Applied Sciences in Rapperswil (Hochschule für Technik Rapperswil, HSR), issue 2-2010, p. 26-27, accessible online under http://www.hsr.ch/HSR-Magazin.8552.0.html.

2. Nicola Nosengo, "Zoobotics", The Economist, print edition July 9th-15th 2011, p. 70-71, online version under http://www.economist.com/node/18925855.

3. Laura Chaparro, "Zoorobots", Redes, http://www.redesparalaciencia.com/tag/revista-redes, accessible online under http://lis2.epfl.ch/media/gallery2/d/1705-1/Zoorobots.pdf.

4. "Innovation: zoom sur les robots", TV footage on RTS Info (Radio Télévision Suisse), broadcast on 20 July 2012, accessible online under http://www.rts.ch/g/HPNo

Appendix K

SNF Application Summary

This research was funded by the Swiss National Science Foundation (SNF). The next page shows the summary of the research project application.

2.1. SUMMARY OF RESEARCH PLAN

Goal

To functionally correlate bivalve (shell) forms and (shell) sculptures with sediment types and burrowing techniques, evolutionary computation, robotics, paleontology, neontology, and sedimentology are combined to develop a burrowing simulation as well as an autonomously burrowing robot.

Background

Under the direction of Pfeifer, the Artificial Intelligence Laboratory of the University of Zurich acquired knowledge in the development of different kinds of robotic applications and the simulation of real-world processes. In the field of evolutionary computation, Eggenberger further investigated biological mechanisms that enable a modular robotic system to assemble and repair itself. In paleontology, Schatz was able to provide new insights into taphonomy, morphology, numeric systematics, biostratigraphy, paleobiogeography, paleoecology, and evolution of Mesozoic mollusks. One focus of his research lay on the interaction of functionality and morphogenesis of mollusk shells, shell structures and environment. Eggenberger and Schatz have established a successful collaboration between evolutionary computation and paleontology by elaborating a morphogenesis simulation. They gathered experience in dealing with the modeling of a (fossil) organism, the physical modeling of a granular medium, and a genetic regulatory network, whose parameters are evolved by an artificial evolutionary system and control modeled cellular mechanisms. This collaboration has improved our understanding of evolutionary processes, optimized computer simulations in the field of genetic regulatory networks, and yielded the possibly first metazoan sexual dimorphism in the history of life.

Project summary

The knowledge acquired in the previous collaboration is transferred to the development of a bivalve burrowing simulation and an autonomously burrowing robot. The burrowing simulation consists of models of recent and fossil bivalve species, a model of a granular medium (sandy sediment), a model of the bivalve-sediment interactions, and a burrowing simulation controlled by a genetic regulatory network and evolved by an artificial evolutionary system. The autonomously burrowing robot is used to test the physical adequacy of the bivalve-sediment-interaction model and to calibrate its physical properties. After testing the biological significance of the burrowing simulation, we investigate the functional correlations between (shell) forms and (shell) sculptures with sediment types and burrowing techniques. The resulting correlations are then used to investigate the paleoecology of the modeled fossil bivalve species based on their shell morphologies.

Importance

Models of bivalve shells and sandy sediments as well as burrowing robots exist already – but have never been combined. The models of bivalve shells so far focus on morphogenesis, ontogeny, and pigmentation patterns. The burrowing robots are used to investigate the influence of the shell morphology on burrowing. In this project, we propose to increase the complexity of these different jigsaw pieces and to combine them in an integral whole. By combining the modeled bivalves with the modeled sandy sediment generating a bivalve-sediment-interaction model, by testing its physical adequacy, and by calibrating its the physical properties by using real-world data acquired using an autonomously burrowing robot, the reciprocal coherence of the model and the real world could be investigated. Finally, we will be able to investigate the functional interaction between (shell) sculptures, sediment types, and burrowing techniques by using the burrowing simulation. This will broaden our understanding of shell functionality and (paleo-) eocology of bivalves and of burrowing organisms in general. By investigating the functionality of aberrant shell forms and sculptures of extinct species, we could extend the field of bionics. In addition, geologists gain a tool to bypass diagenetical shortcomings of sediments (e.g. sorting processes, particle solutions, compaction, cementation) and to reconstruct the primary sediment conditions (e.g. water saturation, grade of compaction) of lithological units bearing endobenthic fossils. We expect that the investigated effects of different shell forms and sculptures on moving the shell through the sediment and anchoring the shell in the sediment could obtain importance in engineering by yielding new insights into drilling and anchoring in soft sediments. For evolutionary computation, this type of interdisciplinary collaboration will lead to a refinement of the methods used in artificial evolution, especially in the subfield of embryogenic evolution. By validating the biological significance of the simulations in artificial evolution with real-world data found in recent as well as fossil bivalve species, the current embryogenic methods will be improved. Further, the collaboration with specialists in natural evolution will give an important feedback for the improvement of control methods of modular robots. Based on the results generated in this project, further projects could focus on the evolutionary constraints the bivalves faced in phylogeny or the matching of trace and body fossils.

Keywords and phrases

Evolutionary computation, robotics, paleontology, neontology, sedimentology, burrowing sculptures, experimental biology, biomechanics, interdisciplinarity, functionality, morphology, autonomously burrowing robots, models of bivalves, hard parts, soft parts, model of a well sorted quartz sand, burrowing simulation, genetic regulatory network, artificial evolutionary system, functional correlation of (shell) forms and (shell) sculptures with sediment types and burrowing techniques

Curriculum Vitae

Curriculum Vitae

Daniel Peter Germann
MSc ETH in Computer Science

Address | Adam Zeltner-Weg 1
4600 Olten
Switzerland

Home Phone | +41 (0)62 534 58 45
Mobile | +41 (0)79 740 33 16

Email UZH | germann@ifi.uhz.ch
Email private | daniel@dataway.ch

Date of Birth | 7th June 1982

Marital Status | married to Tabitha Germann-Müntener, Dr. med. vet., Dipl. ECVP

Citizenship | Swiss

Working Experience

since 01/04/2008 | **Ph. D. Program in Informatics**
Where: Artificial Intelligence Laboratory, Department of Informatics, University of Zurich, Switzerland (http://ailab.ifi.uzh.ch/)
Function: Ph.D. student
What: Interdisciplinary robotics project that investigates the burrowing behaviour and morphological evolution of bivalves

01/05/2007 – 31/12/2010 | **Dybuster AG**
Where: Dybuster AG (ETH spin-off company, http://www.dybuster.ch/ch/)
Function: Software engineer
What: Development of a software tool for therapists (addition to the main software), software maintenance, customer support, shipping
After 13 months the position was reduced to 20% due to the Ph.D.

SS 2006 | **ETH Zürich**
Where: Department of mechanical and process engineering, ETH Zürich
Function: Student assistant
What: Assistance for the lecture course “Informatik I” by Dr. Volker Roth

18/10/2004 - 07/01/2005 | **NovodeX AG**
Where: NovodeX AG in Zürich (today known as Nvidia PhysX)
Function: Intern, software engineer
What: Development of a prototype for continuous collision detection

WS 2003/04 | **ETH Zürich**
Where: Department of computer science, ETH Zürich
Function: Student assistant
What: Assistance for the lecture course “Informatik III” (Programming III) by Prof. David Basin and Prof. Robert Stärk

Publications

Daniel P. Germann, Wolfgang Schatz, and Peter Eggenberger Hotz, "Artificially evolved functional shell morphology of burrowing bivalves", Palaeontologia Electronica, Vol 17, Issue 1, 2014.

Daniel P. Germann and Juan Pablo Carbajal, "Burrowing behaviour of robotic bivalves with synthetic morphologies", Bioinspir. Biomim. 8 (2013).

Daniel P. Germann, Wolfgang Schatz and Peter Eggenberger Hotz, "Artificial Bivalves – The Biomimetics of Underwater Burrowing", Proceedings of the 2nd European Future Technologies Conference and Exhibition 2011 (FET 11), Procedia Computer Science, Vol 7, pp. 169–172, 2011.

Daniel P. Germann, Wolfgang Schatz and Peter Eggenberger Hotz, "Bivalve burrowing robots: correlating shell morphology and movement pattern with burrowing efficiency", Design and Nature V, WIT Transactions on Ecology and the Environment, Vol 138, pp. 389-402, June, 2010.

Agathe Koller-Hodac, Daniel P. Germann, Alexander Gilgen, Katja Dietrich, Maik Hadorn, Wolfgang Schatz and Peter Eggenberger Hotz, "Actuated Bivalve Robot – Study of the Burrowing Locomotion in Sediment", Proceedings of 2010 IEEE International Conference on Robotics and Automation (ICRA), May 3-8, 2010, Anchorage, Alaska, USA.

Daniel Germann, Wolfgang Schatz, Maik Hadorn, Andreas Fischer and Peter Eggenberger Hotz, "Correlation between morphology, behaviour and habitat – bivalve burrowing in simulation and robotics", Abstracts of the 6th Swiss Geoscience Meeting, 2008.

Academic Education

2003 – 2007 **Advanced study**
Computer science at ETH Zürich (pilot-master programme)
Main topics: 3D graphics, simulation, artificial intelligence, machine learning, computer vision, software engineering
Major: computational sciences
Minor: artificial intelligence

Master Thesis:
"Top-Down Collision Detection with Multilevel Deformable Models"
at the Computer Graphics Laboratory (CGL) at ETH
Supervisor: Miguel A. Otaduy
Professor: Markus Gross

Semester Thesis (major):
work on the project OpenOpal, an open framework for optimization and learning written in Java
Supervisor: Stefan Kern
Professor: Petros Koumoutsakos

Semester Thesis (minor):
work on a class library in C++ for the simulation of artificial evolution and a genetic regulatory network; AIlab, University of Zurich
Supervisors: Dominik Langer, Pascal Kaufmann
Professor: Rolf Pfeifer

2001 – 2003	**Basic study** Computer science at ETH Zürich (1. and 2. "Vordiplom", similar to a bachelor)
	Additional Education
31/01/2005 - 25/02/2005	English language courses at the St Giles Language School, Highgate, London
WS 2003/04	Didactics courses for student assistants in the department of computer science at ETH Zürich
2002 – 2011	Member of the Swiss Students Foundation (Schweizerische Studienstiftung), attendance of several seminars and courses
	Basic Education
1995 – 2001	Secondary school: Friedberg High-School, Gossau SG Focus subject: Latin Supplementary focus: applied mathematics Final examination paper: "Altruismus ist gesund" ("Altruism is healthy") includes a Delphi-program for the simulation of the iterated "prisoner's dilemma"
1989 - 1995	Primary school in Schwarzenbach
	Languages
	German: native language English: proficiency level French: intermediate level Spanish: beginner
	Programming Languages
	Extensive experience: C, C++, Matlab, Java Some experience: IA32 Assembler, SPARC Assembler, C#, Oberon, Haskell, SML, Prolog, VHDL, Power Basic, Pascal, Delphi, Maple Libraries: OpenGL/GLU/GLUT, Qt
	IT Experience
	Operating systems: Windows, Linux, Unix Programming: MS Visual Studio, Eclipse, Dev-C++ CAD: SolidWorks Image processing: Gimp